Lire la première partie
de la thèse

Chapter 7

Exploration with 2-by-2 experiments

Contents

7.1 Introduction

7.1.1 What are 2-by-2 experiments ?

The idea of 2-by-2 experiments is the following. After a first work of development, a new system (denoted by a function f, such as in figure 6.1) is built and a sensitivity analysis is desired. The first phase of development usually provides a set of values for the input parameters for which the system globally works and a guess on the range in which they belong. The sensitivity analysis will explore the influence of the input parameters when they browse this range.

Sensitivity indices (such as Sobol indices) provide a quantification of the influence of an input by a single value, without any assumption on the system. But a single value is a very

short summary of the influence. The form of the function f is a much more fertile knowledge on the system because it can be interpreted.

So called "One-At-Time" (OAT) methods are very informative about the form of f. Using the nominal values and the range of variations provided by the development phase, OAT methods make one input vary while the others are set to a nominal value. By doing so, it is possible to draw the evolution of outputs when this input varies. But this method looses the effect of interactions between inputs (Saltelli and Annoni, 2010) and there is a chance that the nominal value of another input hinders the effects of the moving input.

On another hand, let all the inputs vary is the good method to catch all variations, as we have seen in sensitivity analysis. But the shape of f is not accessible when all inputs are moving. Only projections can be drawn, and they are poisoned by the variations of others parameters.

Let 2 inputs vary is a compromise to keep the drawing capacity of OAT and the possibility to take interactions into account. Such experiments are denoted as *2-by-2 experiments*. It is a way to check the main features pointed out by the sensitivity analysis. The expected result is to find the mechanism at the origin of the influence in order to control it (to reduce uncertainty or to tune the system to various situations). The total experimental plan is summarized in the table 7.1, but the resulting figures are too numerous to be all included in the main matter. To make browsing easier, hyperlinks to the appendix are inside the table 7.1. The experimental plan can also be represented by a graph: vertices are input parameters and edges exists between two inputs for which a 2-by-2 experiment has been carried out. The resulting graph of the present experimental plan is shown figure 7.1. For each edge of the graph 7.1, the five outputs have been computed. The inputs connected by the edge are the only ones to move, the others stay at their nominal value. Both nominal values and ranges of variation are recap in the table 7.2.

	C_0	C_1	ℓ	N	σ^{add}	σ^{obs}	σ^V	σ^X	τ
C_0		p.303	p.306						
C_1	p.303								
ℓ	p.306			p.312	p.315	p.318			
N			p.312		p.321	p.324			p.327
σ^{add}			p.315	p.321		p.330			p.333
σ^{obs}			p.318	p.324	p.330			p.336	p.339
σ^V								p.342	
σ^X						p.336	p.342		
τ				p.327	p.333	p.339			

Table 7.1 – Couples of inputs experimented: results are on the indicated page (hyperlink). This table is a copy of C.3.

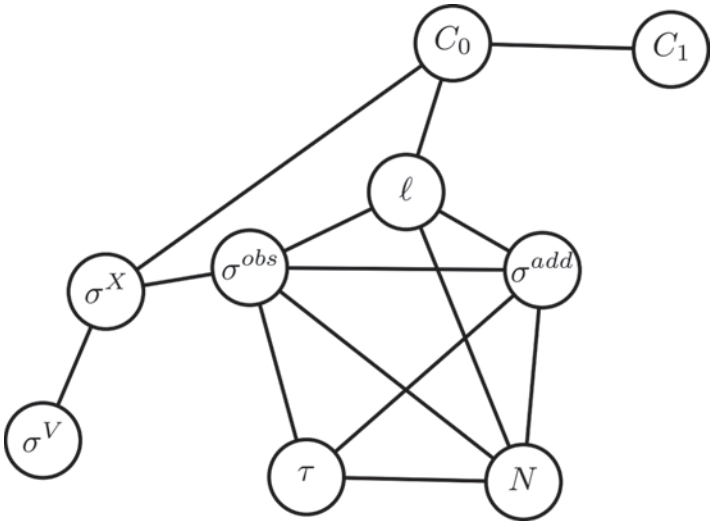

Figure 7.1 – Graph of 2-by-2 experiments: vertices are input parameters and edges exist between inputs involved in a common 2-by-2 experiment. The annotated numbers are the degree of the vertices.

Input	**Min**	**Max**	**Nominal value**	**Unit**
C_0	0.3	2.5	2.1	none
C_1	0	2.5	0.9	none
ℓ	3	100	10	m
N	400	2500	700	none
σ^{add}	0.1	2.1	0.5	$\mathrm{m{\cdot}s^{-1}}$
σ^{obs}	0.1	2.1	0.5	$\mathrm{m{\cdot}s^{-1}}$
σ^V	0	1.1	0.1	$\mathrm{m{\cdot}s^{-1}}$
σ^X	0	11.1	1.0	m
τ	5	30	10	min

Table 7.2 – Range of variation and nominal value for each input.

7.1.2 Link with global sensitivity analysis

For global sensitivity analysis, the computer code is seen as a function of all the parameters. The Hoeffding decomposition of this function allows to attribute the variance on the output to a group of parameters.

$$Y = f(X) = \sum_{\mathbf{u} \in I} f_{\mathbf{u}}(X_{\mathbf{u}}) \tag{7.1}$$

For a 2-by-2 experiment, we look at the same function but with only two parameters moving. The others are fixed to their nominal value. The 2 parameters varying are denoted X_i and X_j. It is also possible to write the Hoeffding decomposition on this new model, which

has only 3 terms :

$$\tilde{Y} = \tilde{f}(X_i, X_j) = \tilde{f}_i(X_i) + \tilde{f}_j(X_j) + \tilde{f}_{i,j}(X_i, X_j) \tag{7.2}$$

The two models are linked by the fixation of the parameters $X_{\overline{i,j}} = \{X_k,\, k \in [\![1, p]\!], k \neq i, j\}$ to their nominal value $x_{\overline{i,j}}$.

$$\mathcal{L}(\tilde{Y}) = \mathcal{L}(Y | X_{\overline{i,j}} = x_{\overline{i,j}}) \tag{7.3}$$

Because the Hoeffding decomposition is unique, one can identify the terms :

$$\tilde{f}_i(X_i) = \sum_{\mathbf{u} \in I, i \in \mathbf{u}} f_{\mathbf{u}}(X_i, x_{\mathbf{u} \setminus i}) \tag{7.4}$$

$$\tilde{f}_{i,j}(X_i, X_j) = \sum_{\mathbf{u} \in I, \{i,j\} \in \mathbf{u}} f_{\mathbf{u}}(X_i, X_j, x_{\mathbf{u} \setminus \{i,j\}}) \tag{7.5}$$

But this relationship are not exploitable without additional assumptions. The main interest of 2-by-2 experiments is to allow a visualization of the response surface and thus to infer about the shape of the function f.

7.2 Validation of the tuning strategy

The conclusions of the sensitivity analysis presented in the previous chapter sustain the possibility to reduce the system to only 3 informative outputs and 3 influential inputs. The reduced system has two degrees of freedom: σ^{add} (which is unknown in practice) and the affordable time of execution T_{exe}. It states a tuning strategy for the 3 main inputs which ensures the reconstruction is then performing well. The tuning strategy consists in setting σ^{obs} with the wind spectrum slope and then to set N by a trade-off between the affordable time of execution T_{exe} and the desired precision r_V.

7.2.1 Setting σ^{obs} with wind spectrum slope

We have seen is the chapter 1 (REF +précise), that the wind spectum has a characteristic -5/3 slope in log-log scale (see figure 5.32 for an illustration). This output has been shown to be affected by the inputs σ^{add} and σ^{obs}, mainly. It is poorly affected by interactions so that it is a useful output to tune the inputs. The input σ^{add} is the error made by the instrument, which is unknown in practice. Conversely, σ^{obs} is the guess of this error, and it is the parameter used in the algorithm instead of σ^{add}. We can expect the system to perform the best when the guess σ^{obs} is equal to the true value σ^{add}.

Figure 7.2 shows the result of the 2-by-2 experiment when σ^{obs} and σ^{add} are the only input moving. The displayed output is the wind spectrum slope b. One can see the clear influence of both variable. The red plan in the middle of the figure stands for the theoretical -5/3 value. The black line represents the equality of the two inputs. In the area where $\sigma^{obs} < \sigma^{add}$ (right hand side of the figure, where the ground is red), the wind spectrum slope is higher than the expected value. Indeed, the true observation noise (σ^{add}) is higher than its guess (σ^{obs}) thus the filter let some noise left in the estimation. Conversely, in the area where $\sigma^{obs} > \sigma^{add}$ (left hand side of the figure, where the ground is blue), the wind spectrum slope is lower than the expected value. There, the filter overestimates the amount of noise and removes to much power in the highest frequencies. The sensitivity analysis and this response surface show the wind spectrum slope is very sensitive to this setting. One can see that the response surface seems to cross the -5/3 value when σ^{obs} and σ^{add} are equal. This feeling is confirmed by a look at the cross-sections in figures 7.3 and 7.4.

Figure 7.3 shows the evolution of the output b against σ^{add}, for different values of σ^{obs}. Each solid curve corresponds to a different value of σ^{obs} (precised in the key). The -5/3 value is the horizontal dashed line. The vertical dashed lines are where σ^{add} is equal to one of the value of σ^{obs} displayed. One can see that the solid lines cross the horizontal dashed line when $\sigma^{obs} = \sigma^{add}$ (it is less clear for small values of σ^{obs}). The observation is the same for the figure 7.4 which displays the evolution of the output b against σ^{obs}, for different values of σ^{add}. It sustains that the output b has the expected value when $\sigma^{obs} = \sigma^{add}$.

It also confirms the tuning strategy. For a given instrument, σ^{add} is fixed. The parameter σ^{obs} should be set the same value. The strategy consists in drawing the output b against σ^{obs}

and to pick the value of σ^{obs} which gives the wind spectrum slope the closest to -5/3.

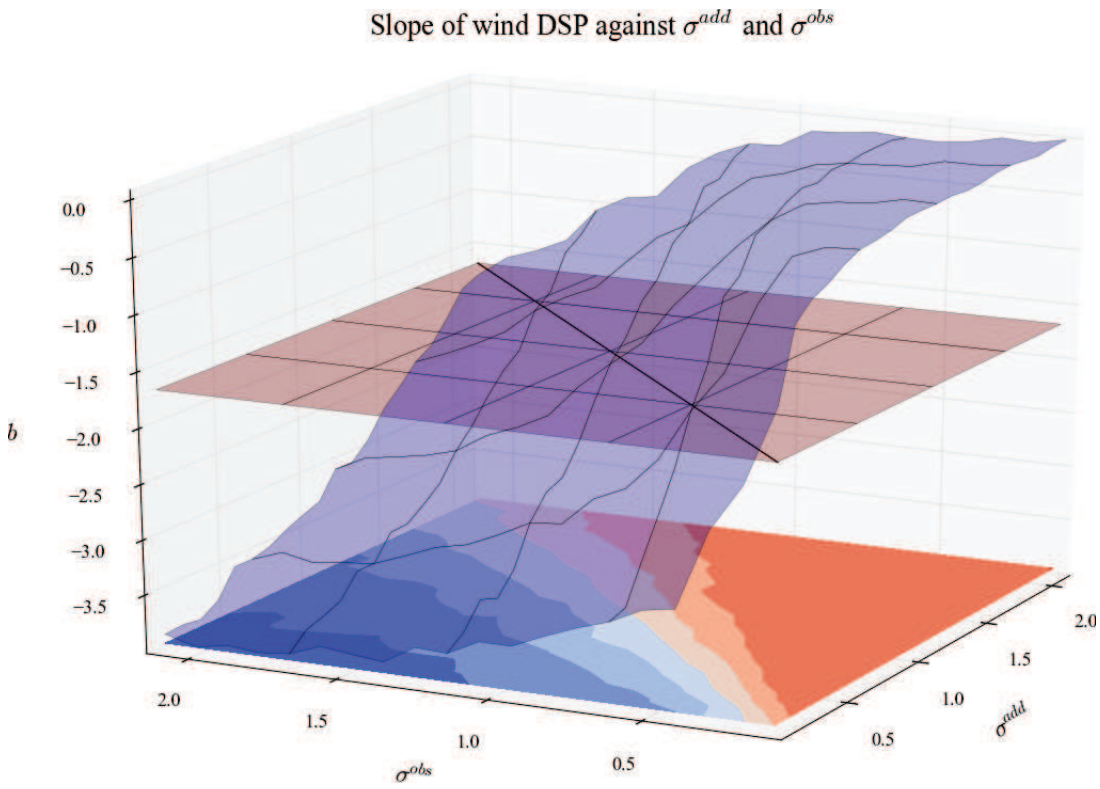

Figure 7.2 – Evolution of b when only σ^{add} and σ^{obs} vary. The sampling grid has 20 values of σ^{obs} and 20 values of σ^{obs} (400 points in total). The red plan is at the level $b = -5/3$ (theoretical expected value).

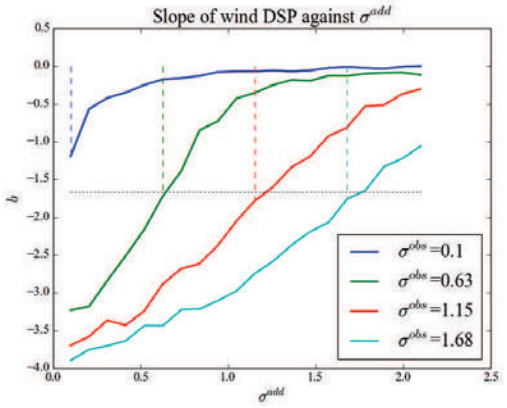

Figure 7.3 – Evolution of b when σ^{add} vary, for different values of σ^{obs}. Horizontal dotted line is $b = -5/3$. Vertical dashed lines signalize when $\sigma^{add} = \sigma^{obs}$ for each value of σ^{obs}.

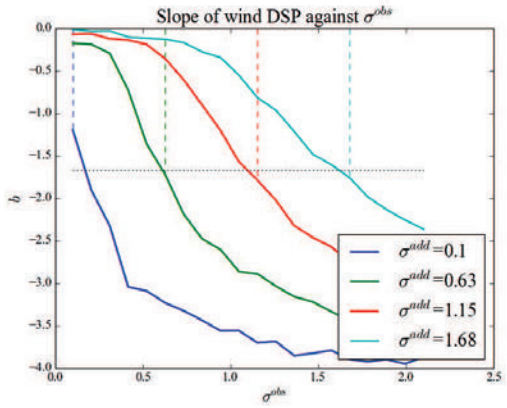

Figure 7.4 – Evolution of b when σ^{obs} vary, for different values of σ^{add}. Horizontal dotted line is $b = -5/3$. Vertical dashed lines signalize when $\sigma^{add} = \sigma^{obs}$ for each value of σ^{add}.

7.2.2 Variations of the wind RMSE against the main inputs

Among the 5 outputs, the TKE RMSE and the number of null potential have been dismissed because of their complex variations, unsuitable to a tuning strategy. The execution time depends only on N and the wind spectrum slope is exploited to set σ^{obs} equal to σ^{add}. The wind RMSE is thus the only relevant score to assess the wind retrieval with reconstruction. It has been shown that this score depends mostly on the first group of parameters: N, σ^{add} and σ^{obs}. Since it also have been shown that the influence of these inputs could be complex because of interactions, the 2-by-2 experiments will be fully exploited here. Three 2-by-2 experiments are required to completely visualize the influence and the interactions of these three main inputs. The figure 7.5 (respectively 7.6 ; 7.7) shows the variations of the wind RMSE when only N and σ^{add} (repectively N and σ^{obs} ; σ^{add} and σ^{obs}) are moving.

In the figure 7.5, one can see the wind RMSE steadily decreases with N, whatever the value of σ^{add}. The theorem 5.1 predicts a $1/\sqrt{N}$ decrease of r_V, which look confirmed here, independently from σ^{add}. The effect of σ^{add} is to increase the RMSE. But one can see that this increase is not linear. As long as $\sigma^{add} < 0.5$, the RMSE does not increase and then increases rapidly (the increasing speed depends on N). The 0.5 threshold is interesting because it is the nominal value of σ^{obs}.

In the figure 7.6, one can see the effect of N is the same as in figure 7.5. The effect of σ^{obs} is interesting. It shows a minimum around the value $\sigma^{obs} = 0.5$ which corresponds to the nominal value of σ^{add}. It sustains that the reconstruction is performing the best when $\sigma^{obs} = \sigma^{add}$.

Figure 7.7 crosses the effects of σ^{obs} and σ^{add} already observed. Two areas are to consider: when $\sigma^{obs} < \sigma^{add}$ and $\sigma^{obs} > \sigma^{add}$. As long as $\sigma^{add} < \sigma^{obs}$, there is no effect of σ^{add} on

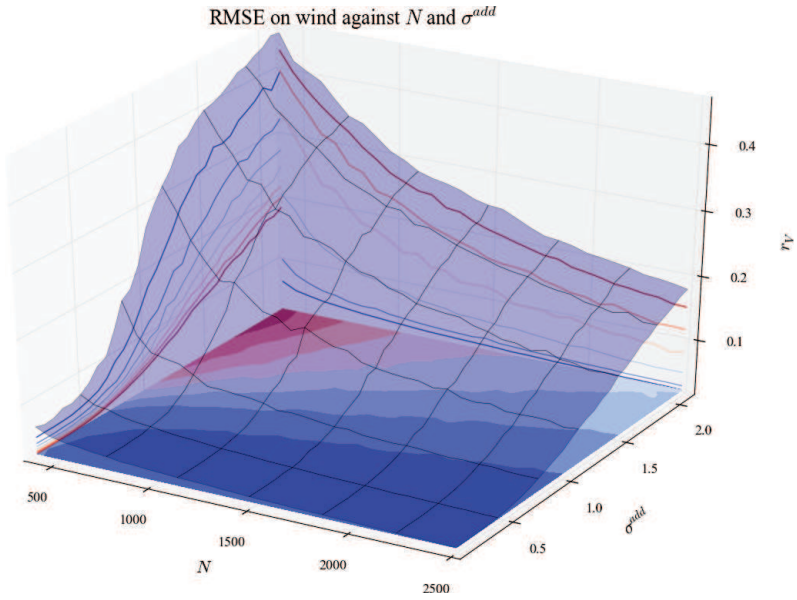

Figure 7.5 – Evolution of r_V when only N and σ^{add} vary.

the RMSE and σ^{obs} makes it increase linearly. When $\sigma^{obs} > \sigma^{add}$, the evolution of the wind RMSE is much more complex. It fastly increases with σ^{add}. The effect of σ^{obs} is in two stages: for very small σ^{obs} the RMSE increases and reaches a maximum and then decreases up to the point where $\sigma^{obs} = \sigma^{add}$ (after what it increases again, as mentioned previously). In any case, there is a low on the line $\sigma^{obs} = \sigma^{add}$.

The best choice for σ^{obs} is thus to be equal to σ^{add}. We have seen this can be obtained quite safely by the tuning with the wind spectrum slope. Once this setting has been made, one can see the evolution of wind RMSE against σ^{add} and N in figure 7.8. The RMSE increases linearly with the observation noise and decreases as $1/\sqrt{N}$, as the regressions in figure 7.9 show. Hence the wind RMSE can be approached by the relation (7.6) when the input σ^{obs} is correctly set.

$$r_V = K\frac{\sigma^{add}}{\sqrt{N}} \tag{7.6}$$

The constant K is estimated by ordinary least squares on the points of the surface 7.8 The resulting value is $K = 2.33$. One can see in the figure 7.9 that the wind RMSE is always lower that the input σ^{add}, even for very low N. For example, if one has a lidar making a error $\sigma^{add} = 1.19$ m·s^{-1} (middle line in figure 7.9), the error on the wind at the output of the filter is below 0.2 m·s^{-1}, even with only 500 particles. It reduces the noise about 83% for the lowest N tested and rate raises up to 93% with $N = 2500$. It shows the efficiency of the wind retrieval with the reconstruction. Even for an instrument quite noisy, the filter lessens strongly the inaccuracy on the wind.

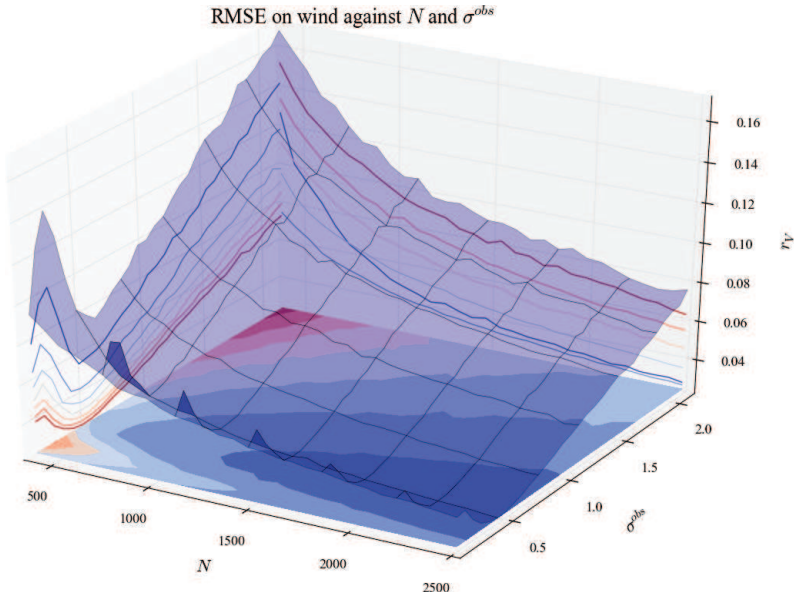

Figure 7.6 – Evolution of r_V when only N and σ^{obs} vary.

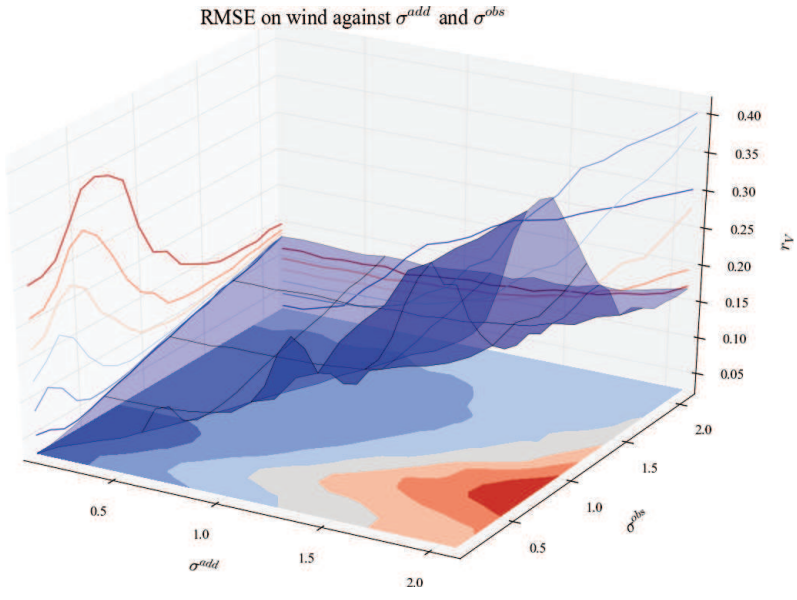

Figure 7.7 – Evolution of r_V when only σ^{add} and σ^{obs} vary.

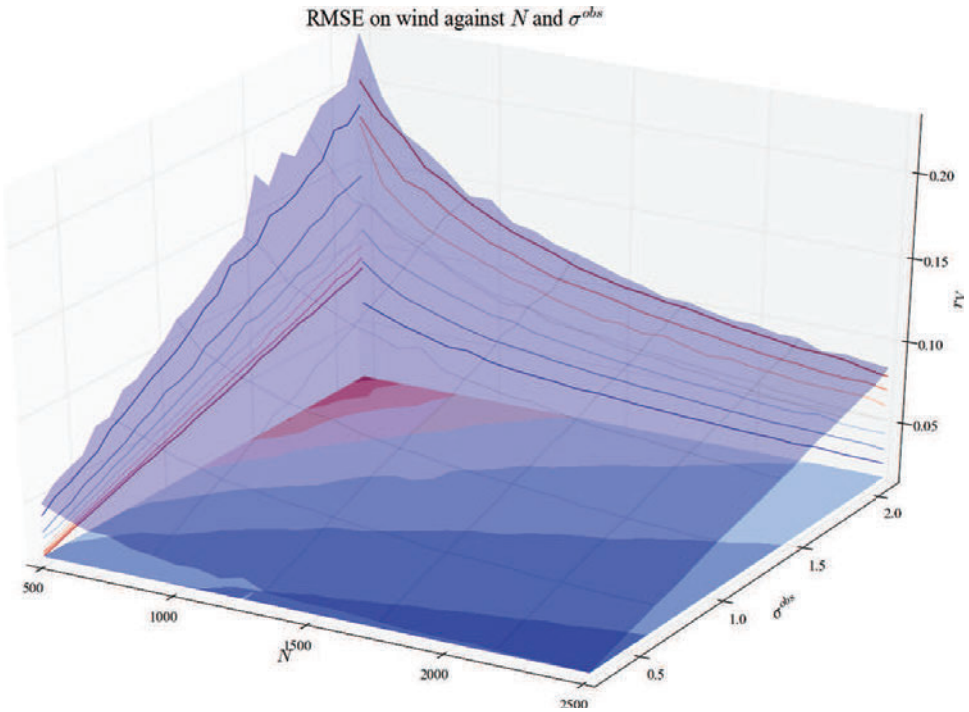

Figure 7.8 – Well set case: evolution of r_V when only N and σ^{obs} vary with $\sigma^{obs} = \sigma^{add}$.

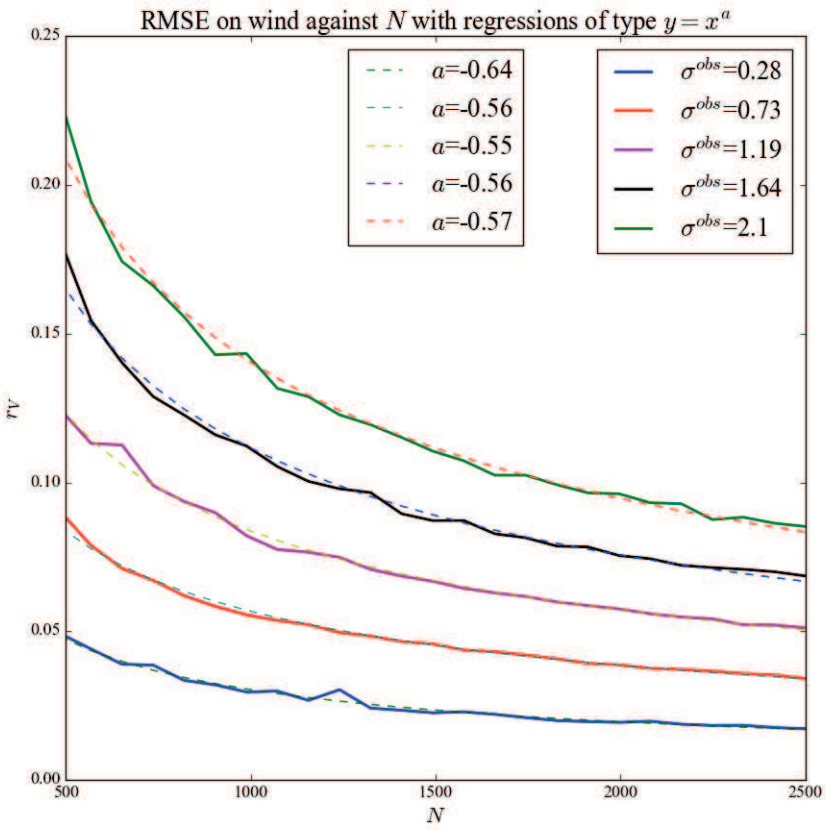

Figure 7.9 – Evolution of r_V with N when $\sigma^{obs} = \sigma^{add}$. Regressions (dashed lines) show the observed decrease is close the square root, as predicted by the theory.

7.2.3 Effect of N on the execution time

The number of particles is the only parameter to have an influence on the execution time T_{exe}. The 2-by-2 experiments confirm this claim (see the results for T_{exe} in the appendix, page 361). By regression, as shown in the figure 7.10, the rate of increase seems to be a power law:

$$T_{exe} = N^a \tag{7.7}$$

The parameter a is estimated by ordinary least squares is $a = 1.75$. According to this relation, twice the number of particles multiply by 3.36 the execution time. The other regression tested is exponential ($T_{exe} = 2^{N/a}$), but it seems less in agreement with the observations. Nevertheless, according to the exponential relationship, the time of execution should double each 515 particles. They are key figures to dimension numerical experiments.

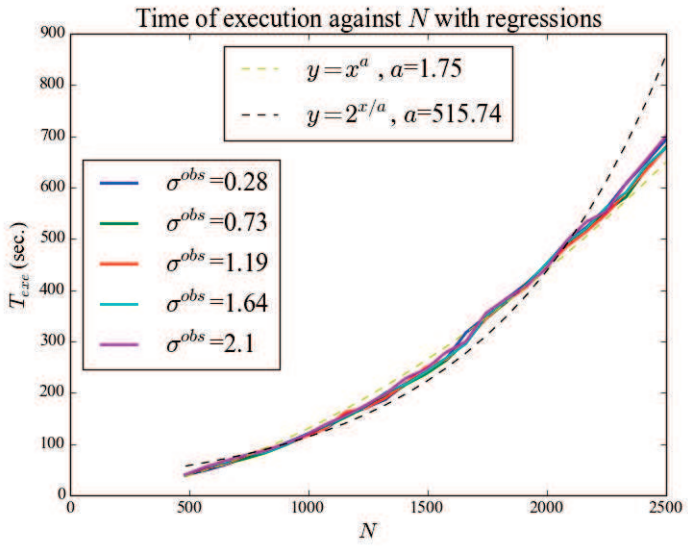

Figure 7.10 – Evolution of T_{exe} with N for different values of σ^{obs}. Regressions (dashed lines) show the best fit is a power function.

7.2.4 Tuning strategy for the reconstruction

The best wind retrieval is thus obtained with the following three inputs values:

- σ^{add} the smallest,
- σ^{obs} equal to σ^{add},
- N the highest.

Although σ^{add} is fixed by the instrument, this result helps to assess which precision is affordable for a given instrument. Even for inaccurate instrument, the resulting error is much lower

than the raw error. The number of particles is bounded by the affordable time of execution. Examining these results, the following tuning strategy seems to be the most appropriate:

1. Set N to a low value, such that T_{exe} is really small.
2. For σ^{obs} ranging around the a priori accuracy of the instrument, calculate the wind spectrum slope b.
3. Set σ^{obs} to the value which gives b the closest to -5/3. σ^{obs} is then almost equal to σ^{add}.
4. Set N to the maximum affordable value. The error on wind retrieval is now minimum, estimated by $K\frac{\sigma^{obs}}{\sqrt{N}}$ with $K = 2.33$

7.3 Other interesting results

7.3.1 On the bad construction of the score r_k

After the sensitivity analysis, the output r_k (TKE RMSE) have been shown to have very complicated behaviour, including high order interactions. As a consequence, it cannot be used to tune the output. We will see at the examination of the 2-by-2 experiments that the interpretation of the score r_k itself is also complex, which makes it an irrelevant score.

Figure 7.11 depicts the surface response when only ℓ and σ^{add} vary. σ^{add} is the most influential input. Although its interaction with ℓ does not have a high Sobol index, one can see in the figure 7.11 that they are clearly interacting. The effect of σ^{add} depends on the value of ℓ. The shape of the response surface is complex and no clear interpretation can explain it. When ℓ is large, the local average is no longer local and converges to a spatial average. When ℓ is large, the RMSE r_k reaches a minimum when $\sigma^{add} = 0.9$. The value of σ^{add} where this minimum is reached increases when ℓ decreases. One of the unclear interpretations about this could be that RMSE on TKE is the lowest when the instrument has a variance of error comparable to the ambient turbulence. This could be checked by changing the reference wind in the system, but it has not been done here. The effect of ℓ is due to the local average used to compute the TKE. By using another TKE estimator, for example the STKE defined in the section 1.4, one should retrie the same evolution as ℓ is maximum.

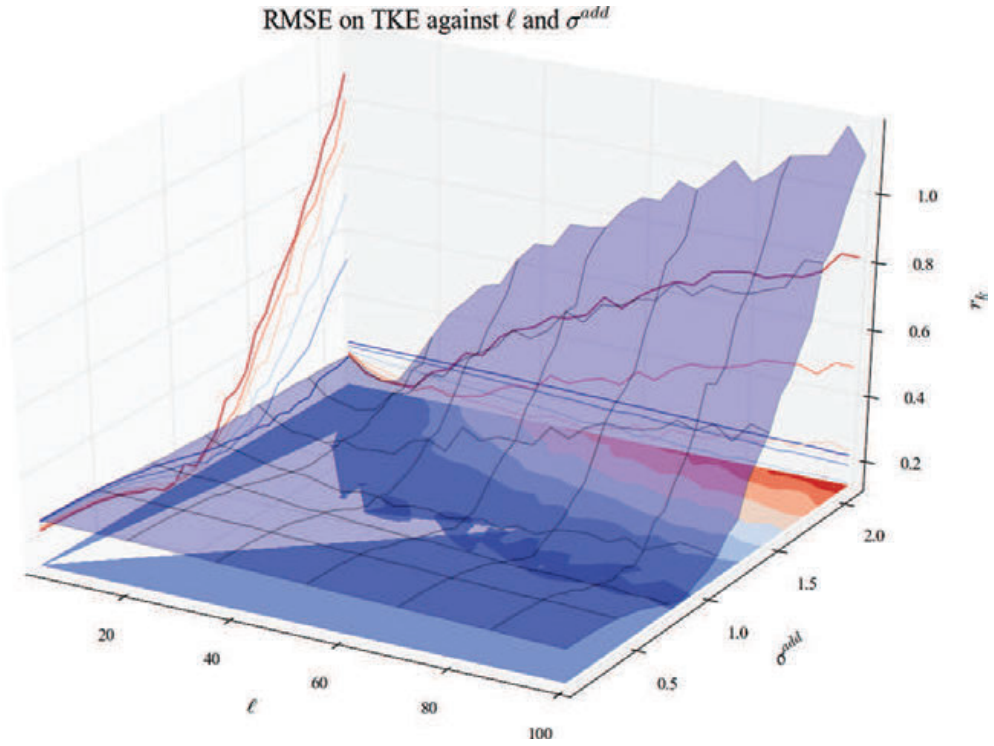

Figure 7.11 – Evolution of r_k when only ℓ and σ^{add} vary.

Figure 7.12 is the response surface when only N and τ vary. Both have quite small Sobol

indices, but τ showed an asymmetric influence on the cobweb plot 6.25. In the figure 7.12 one can see that τ does have an influence, while N has no influence at all. The non influence of N is retrieved in the others 2-by-2 experiments in the appendix. The weird effect of τ is confirmed as well by others 2-by-2 experiments in the appendix. This effect is due to the construction of the score r_k. The time average operator introduce some threshold effect that is visible here. This effect makes difficult the interpretation of the score.

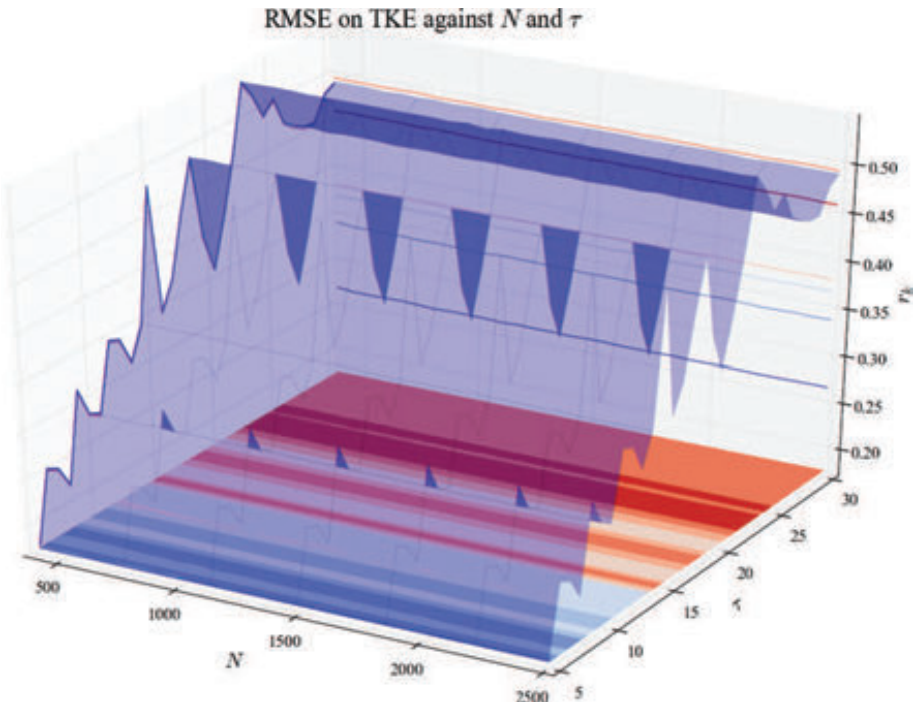

Figure 7.12 – Evolution of r_k when only N and τ vary.

Finally, the figure 7.13 shows the response surface r_k against σ^{add} and σ^{obs}. r_k is minimum when $\sigma^{add} = 1.6$ and σ^{obs} is not too small. When σ^{obs} is not too small, this minimum disappears. There is no low on the line $\sigma^{obs} = \sigma^{add}$, as for the wind RMSE. It tells that knowing perfectly the instrument error does not help to improve r_k. Whatever, is the guess of the instrument error σ^{obs}, if the real σ^{add} is not at the good value (related to ℓ as seen in 7.11 and probably related to the ambient turbulence), the TKE retrieval will not work. This is a very bad issue for this score because it depends on arbitrary parameters (ℓ) or uncontrollable (ambient turbulence) or unknown (if the previous reasoning are wrong). In any case, this output is hardly useful in practice.

The 2-by-2 experiments give more insight about the variations of r_k. But they are complex and there is no satisfying interpretations for them. Unverified interpretations could be that the score r_k depends on the balance between the instrument error σ^{add} and the ambient turbulence, and not on the balance between σ^{add} and its guess σ^{obs}. Hence, the conclusion of this analysis is that the score r_k is not well constructed and is not very informative about the system.

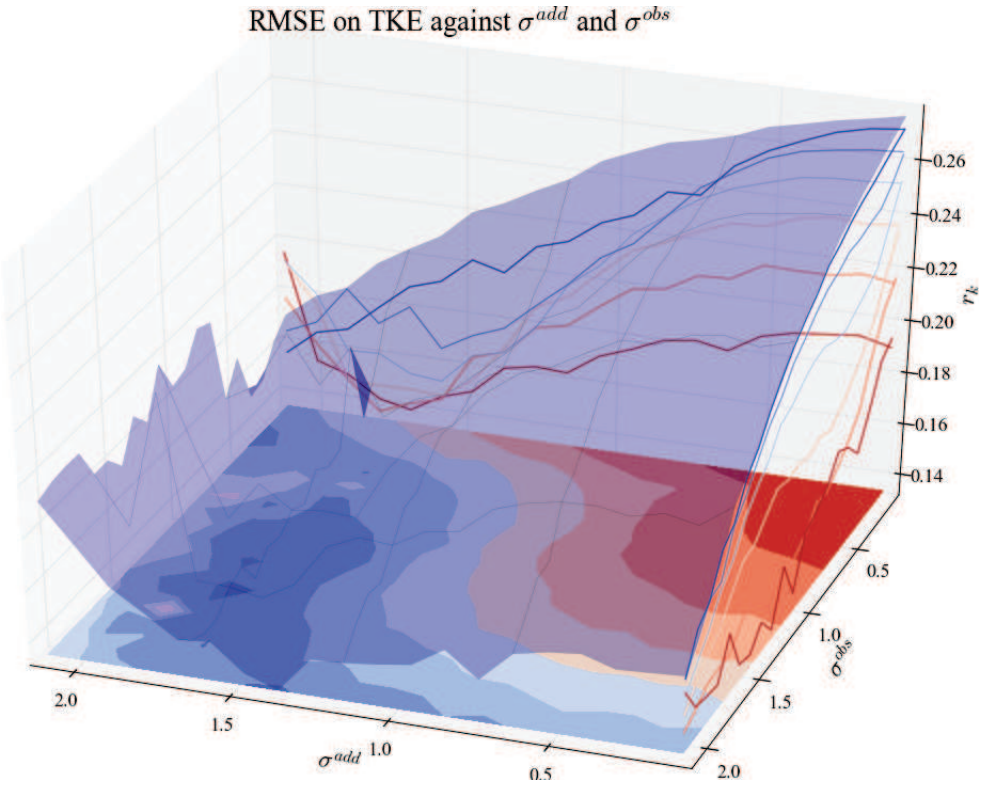

Figure 7.13 – Evolution of r_k when only σ^{add} and σ^{obs} vary.

7.3.2 Influence of C_0 and C_1

The inputs C_0 and C_1 have been put in the second group of influence in the last chapter. They have a notable influence but the interaction share was the argument to put them out of the first group. Another argument was that turbulence modelling provide estimation of them. In particular, Pope (1994) proposes the relationship $C_1 = \frac{1}{2} + \frac{3}{4}C_0$ with the value $C_0 = 2.1$. Nevertheless, the 2-by-2 experiments can give more insight about their influence and check if such relationship is visible in the outputs.

On the output b (wind spectrum slope) they were mentioned to be influential. Figure 7.14 shows the evolution of b when only C_0 and C_1 vary. One can see the response surface crosses the -5/3 value around the thick line, which has for equation $C_1 = \frac{1}{2}C_0$. The dashed line has the equation suggested by Pope $C_1 = \frac{1}{2} + \frac{3}{4}C_0$. The black dot is where the nominal values have been chosen. The equation suggested by Pope looks wrong in this figure because it has been designed for 3D flows while this one is only 1D. The nominal values are close to optimal line.

On the output N_{G0} (number of null potential), C_0 and C_1 were spot as influential (respectively second and third total Sobol index in figure 6.3). In the figure 7.15 is displayed the evolution of N_{G0} against C_0 and C_1. Although the sensitivity analysis let think that N_{G0} has complex variations when C_0 and C_1 vary (because of interactions), the response surface is

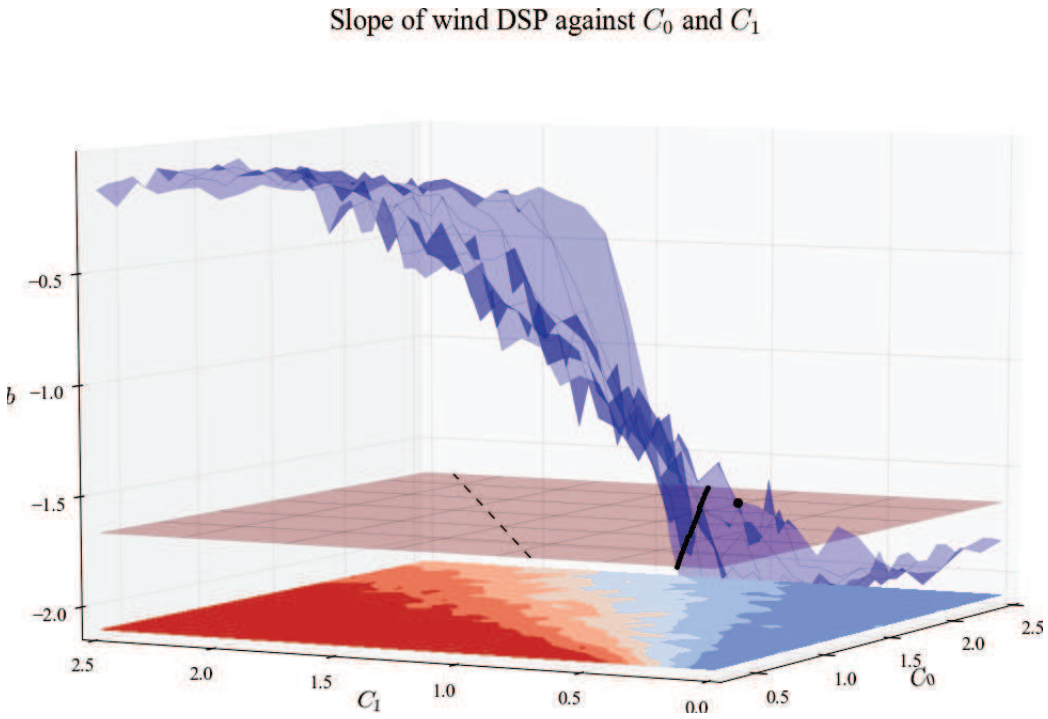

Figure 7.14 – Evolution of wind spectrum slope when only C_0 and C_1 vary. The black dotted line are the points where $C_1 = \frac{1}{2}C_0$. The dashed line has for equation $C_1 = \frac{1}{2} + \frac{3}{4}C_0$. The dot denote the nominal values.

very smooth. One can see that a range of values are admissible (they give no null potential) and another is not. The same lines as in the previous figures are plotted ($C_1 = \frac{1}{2} + \frac{3}{4}C_0$, Pope's result, is the dashed line ; $C_1 = \frac{1}{2}C_0$, the convenient equation for the wind spectrum, is solid dotted). The line that was admissible for the wind spectrum ($C_1 = \frac{1}{2}C_0$, solid dotted) is admissible here too. The line given by Pope for 3D flows ($C_1 = \frac{1}{2} + \frac{3}{4}C_0$, dashed) is not very convenient according to this score neither. The nominal values ($C_0 = 2.1$, $C_1 = 0.9$) are in the admissible area too, close to the dotted line.

On the output r_V (wind RMSE), they are also in good position in figure 6.21. The figure 7.16 displays the evolution of wind RMSE when only C_0 and C_1 vary. The same lines as in the two previous figures are plotted. As for the two previous figures, the line $C_1 = \frac{1}{2}C_0$ is admissible (it gives low RMSE) while the line $C_1 = \frac{1}{2} + \frac{3}{4}C_0$ is not. The results are thus consistent among the 3 exploitable outputs. One more thing about the figure 7.16: it shows the extreme value $C_1 = 0$ always gives the lowest RMSE, which is strange, because it suggests the model is better without the fluctuation term.

On the output r_k the inputs C_0 and C_1 have a contrary effect, as shows the figure 7.17. The line $C_1 = \frac{1}{2}C_0$ gives the highest TKE RMSE, while the line $C_1 = \frac{1}{2} + \frac{3}{4}C_0$ gives lower values (still not minimum). The influence of C_0 and C_1 on r_k is antagonist to the influence on r_V. But the sensitivity analysis raised many questions on the reliability of the score r_k. It has been shown to be influenced in a complex way. Moreover, the range of the variations due

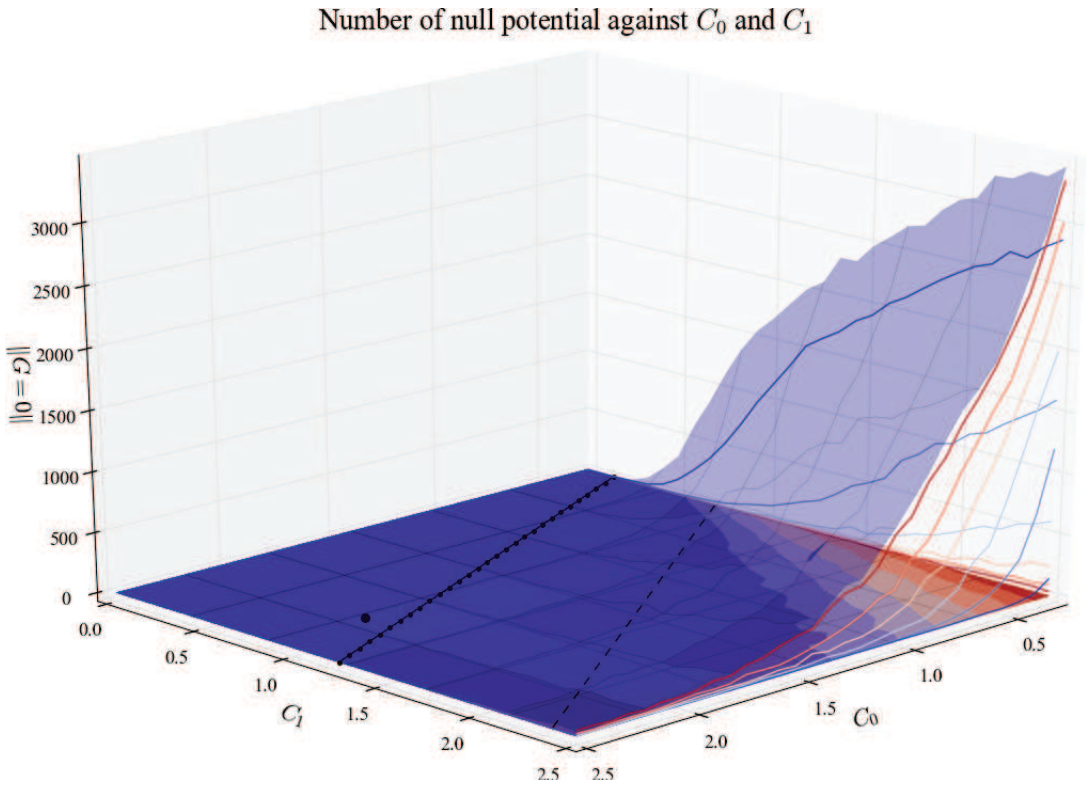

Figure 7.15 – Evolution of N_{G0} when only C_0 and C_1 vary. The black dotted line are the points where $C_1 = \frac{1}{2}C_0$. The dashed line has for equation $C_1 = \frac{1}{2} + \frac{3}{4}C_0$. The bullet denotes the nominal values.

to C_0 and C_1 is not as broad as other inputs can give. Hence, to set C_0 and C_1, the choice is made to choose the effect on r_V rather than the effect on r_k.

Further examination of the influence of parameters C_0 and C_1 with 2-by-2 experiments confirm the influence that was suspected with Sobol indices. The response surfaces are smoother than what was expected according the interactions in which they are involved. The wind spectrum gives the sharpest criterion to choose C_0 and C_1. By visual examination, the relation $C_1 = \frac{1}{2}C_0$ should be fulfilled to have a -5/3 spectrum slope. This criterion is valid for the output N_{G0} and r_V too. However, it appears to be the worst choice for the output r_k. But this output suffers from many weakness in its construction. Hence, the effect of r_k is ignored. Thus, the 2-by-2 experiment concludes that C_0 and C_1 must fulfil the relation $C_1 = \frac{1}{2}C_0$ to be well set. The nominal point ($C_0 = 2.1$, $C_1 = 0.9$) does not fulfil exactly, it should be improved easily.

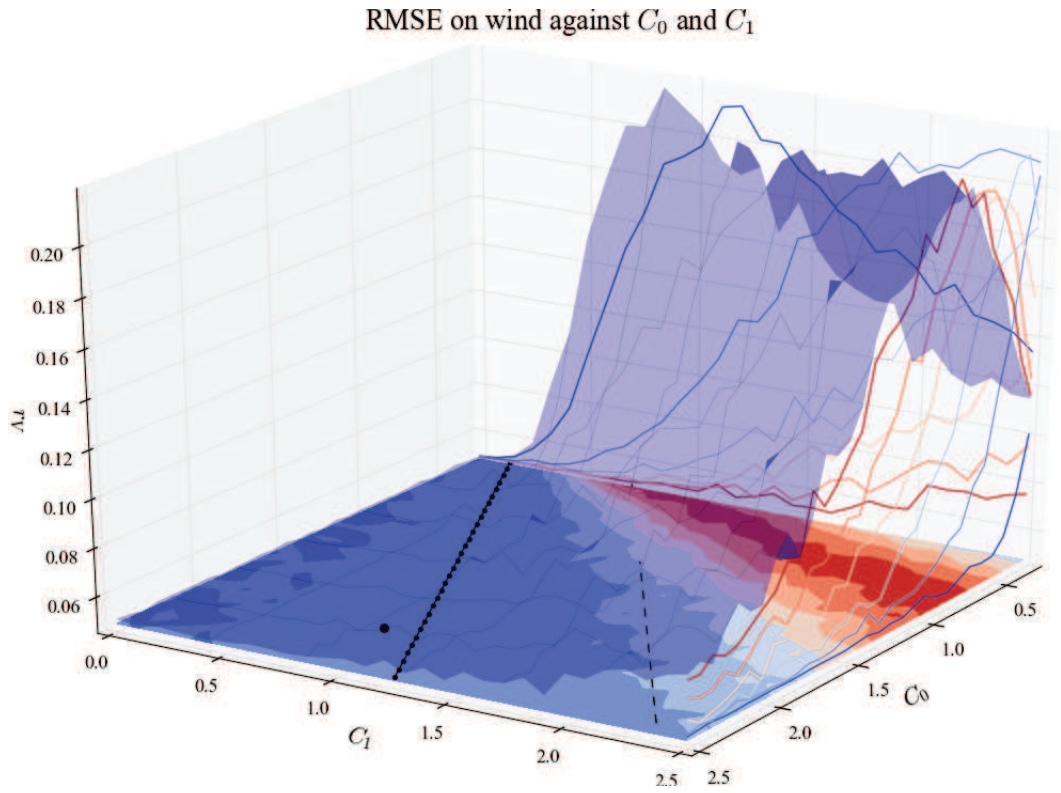

Figure 7.16 – Evolution of wind RMSE when only C_0 and C_1 vary. The black dotted line are the points where $C_1 = \frac{1}{2}C_0$. The dashed line has for equation $C_1 = \frac{1}{2} + \frac{3}{4}C_0$. The bullet denotes the nominal values.

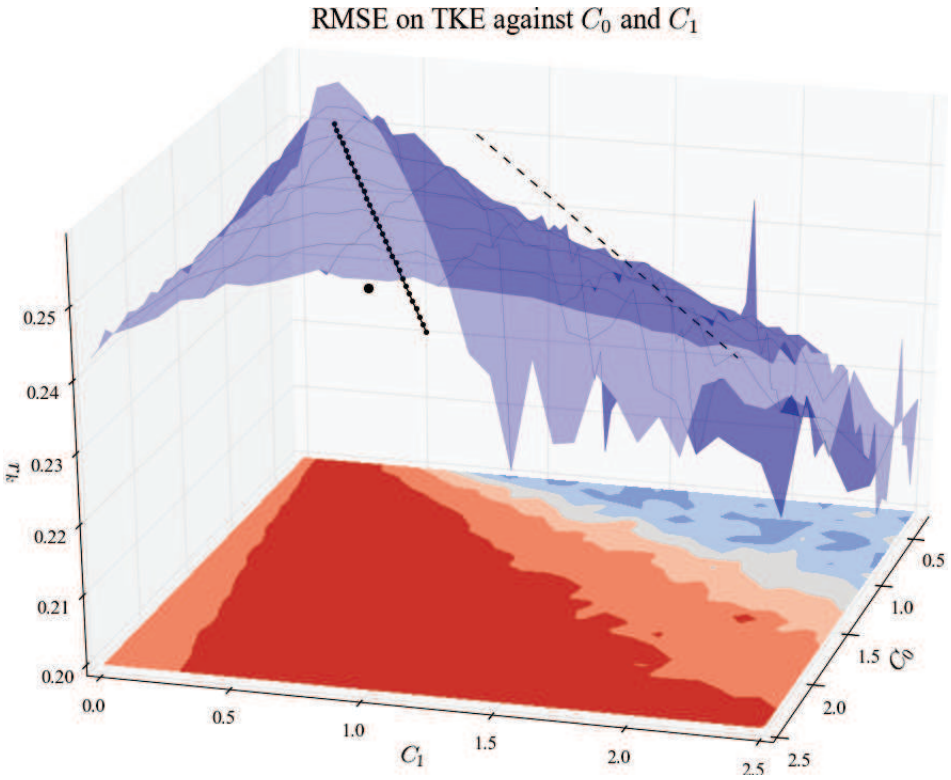

Figure 7.17 – Evolution of TKE RMSE when only C_0 and C_1 vary. The black dotted line are the points where $C_1 = \frac{1}{2}C_0$. The dashed line has for equation $C_1 = \frac{1}{2} + \frac{3}{4}C_0$. The bullet denotes the nominal values.

7.3.3 Retrieval of known variations of N_{G0}

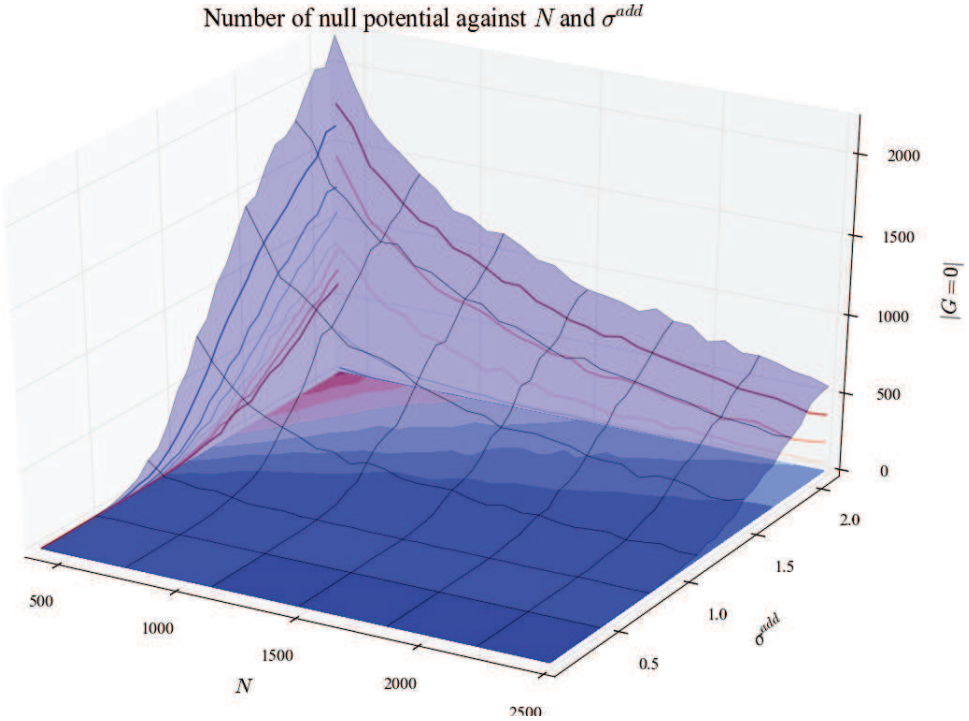

Figure 7.18 – Evolution of N_{G0} when only N and σ^{add} vary.

The influence of N, although not visible in the Sobol indices (both in figures 6.3 and 6.41), is quite clear in figures 7.18 and 7.19. It shows a regular decrease of N_{G0} as N is rising. We retrieve the behaviour predicted by the theorem 5.2 which states an exponential decrease of N_{G0} with N.

The influence of σ^{add} and σ^{obs} is described by the theorem 5.3. This theorem gives an upper bound for the average number of null potential. This upper bound is displayed in figure 7.21. One can see this bound is very low in a large corner of the figure. The actual number of null potential, obtained when only σ^{add} and σ^{obs} vary, is displayed in figure 7.20. One can see the same large corner of very low values. This corner is delimited by the black line.

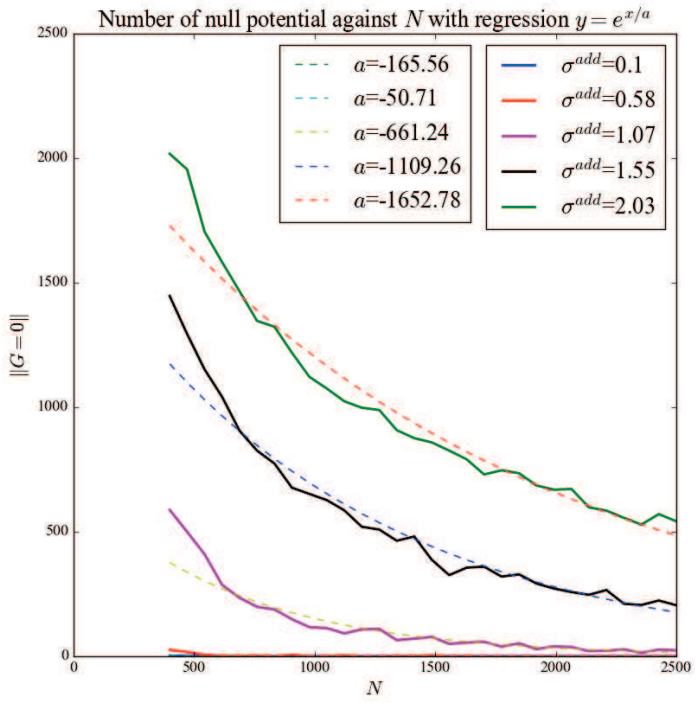

Figure 7.19 – Evolution of N_{G0} with N. Regressions show an exponential decrease.

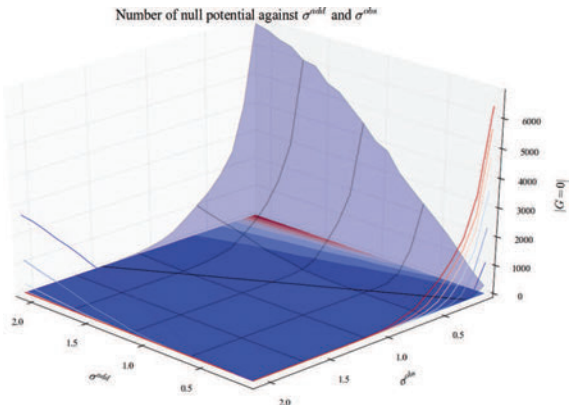

Figure 7.20 – Evolution of N_{G0} when only σ^{add} and σ^{obs} vary.

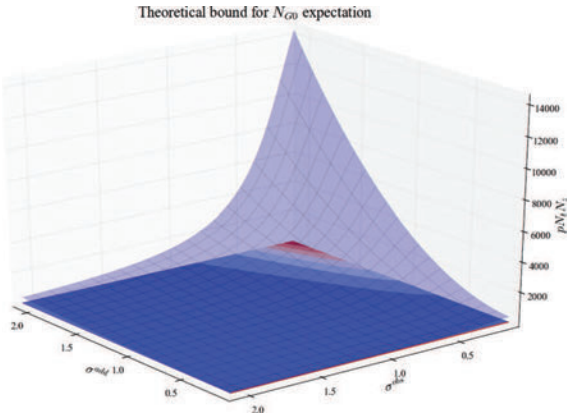

Figure 7.21 – Theoretical average for the N_{G0} output against σ^{add} and σ^{obs}.

7.4 Conclusion

So-called 2-by-2 experiments are the computation of the surface response when only 2 inputs vary and the others are kept to their nominal values. It allows visualizations of the surface response which are not possible in higher dimensions and thus help to find the shape of the response function f. Such visualizations have been used to confirm the tuning strategy coming out of the sensitivity analysis. Only few 2-by-2 experiments are necessary, thanks to the ranking of importance made by the sensitivity analysis. The surface response of wind spectrum slope and wind RMSE have been commented and confirm the following tuning strategy:

1. Set N to a low value, such that T_{exe} is really small.
2. For σ^{obs} ranging around the a priori accuracy of the instrument, calculate the wind spectrum slope b.
3. Set σ^{obs} to the value which gives b the closest to -5/3. σ^{obs} is then almost equal to σ^{add}.
4. Set N to the maximum affordable value. The error on wind retrieval is now minimum, estimated by $K\frac{\sigma^{obs}}{\sqrt{N}}$ with $K = 2.33$.

Beside, some results of the 2-by-2 experiments have been used to check remarkable points. From these additional examinations, it comes out that

- The score r_k has been shown to be not very well constructed because it is not very informative on the system.
- The inputs C_0 and C_1 have been left apart from the tuning strategy, they are explored with 2-by-2 experiments. It yields that the setting fulfilling the relation $C_1 = \frac{1}{2}C_0$ gives the best results.
- The influence of N on N_{G0} is in agreement with the theorem 5.2, although not visible in the Sobol indices.

The full results of 2-by-2 experiments have not been commented all, but they are let available to the curious reader in the appendix C, page 301.

Chapter 8

Penalised regression to estimate the Sobol indices

Contents

8.1 Sobol indices estimated by regression

8.1.1 Motivation

In the chapter 4, several estimators for Sobol indices have been presented. They are all based on a different way to estimate the average operator in the Sobol index. For example, Sobol (2001) compares 2 estimators (though denoted λ and μ in the paper, here the notations of the previous chapter are kept):

$$\widehat{D_{\mathbf{u}}}^{MC1} = \frac{1}{N}\sum_{i=1}^{N} f(X^i) f(Z^i_{\mathbf{u}}, X^i_{\bar{\mathbf{u}}}) - \left(\frac{1}{N}\sum_{i=1}^{N} f(X^i)\right)^2 \tag{8.1}$$

$$\widehat{D_{\mathbf{u}}}^{MC2} = \frac{1}{N}\sum_{i=1}^{N}\left(f(X^i) - f(Z^i_{\mathbf{u}}, X^i_{\tilde{\mathbf{u}}})\right)^2 \tag{8.2}$$

He shows that $\widehat{D_{\mathbf{u}}}^{MC2}$ has a smaller variance to estimate total Sobol indices, while $\widehat{D_{\mathbf{u}}}^{MC1}$ has a smaller variance to estimate main effect Sobol indices. Moreover, $\widehat{D_{\mathbf{u}}}^{MC2}$ is always positive, which avoid the estimation to be negative when indices are small. Saltelli et al. (2010) makes a broader comparison focused on the estimation of first order Sobol indices, and proposes another Monte Carlo estimator:

$$\widehat{D_{\mathbf{u}}}^{MC3} = \frac{1}{N}\sum_{i=1}^{N} f(X^i)\left(f(Z^i) - f(Z^i_{\mathbf{u}}, X^i_{\tilde{\mathbf{u}}})\right) \tag{8.3}$$

Owen (2013) also makes a comparison of several estimation strategies and proposes a new estimator with the concern of improving the estimation of small Sobol indices.

Among all these estimators, the estimation method of $V(\mathbb{E}[Y|X_{\mathbf{u}}])$ is modified to improve its efficiency (smaller variance, more efficient calculation) or to retrieve valuable properties (positivity, asymptotic normality). In this section, we present another type of estimation, based on a linear regression. When sensitivity analysis comes to the user, a complete set of Sobol indices is not always informative. The interpretation of the highlighted sensitivity is the final result of the sensitivity analysis. Only few coefficients are relevant to describe the contribution of variance. Poorly influential groups are not taken into account in the interpretation of the Sobol indices, even though their Sobol index is not exactly zero. Using a linear regression opens to all feature selection techniques and makes the final result easier to interpret. It also gives an alternative way to get estimators with good properties. In addition, the optimisation formulation of regression takes profit of many efficient off-the-shelves algorithms to make the minimization. Three estimators are presented and compared:

- The least squares estimator : $\widehat{S_{\mathbf{u}}}^{ls}$
- The Lasso estimator : $\widehat{S_{\mathbf{u}}}^{l1}$
- The best subset estimator : $\widehat{S_{\mathbf{u}}}^{l0}$

First, the Sobol index estimation with regression is stated in a general way. Then, the properties and the relationship among the three considered estimators are reviewed. A strategy to set the penalty is also given. Next, a small scale numerical experiment is carried out on the case of turbulent medium reconstruction.

8.1.2 Linear model statement

The notation will be the same as in the chapter 4:

- $[\![1,p]\!] = \{1,\dots,p\}$
- I is the collection of all subset of $[\![1,p]\!]$ (thus of cardinal 2^p).
- $\mathbf{u}$ is an element of I.
- $|\cdot|$ the cardinal of the set "$\cdot$". For example, $|\mathbf{u}|$ is the number of indices in $\mathbf{u}$; and $|I|$ is the number of groups of indices in I ($|I| = 2^p$).
- $I' \subset I$ is the number of subsets considered. $d = |I'| \leqslant 2^p$ is its cardinal. For example, if one is interested in first and second order Sobol indices only, one will have $I' = [\![1,p]\!] \cup \{(i,j) \in [\![1,p]\!]^2\}$.
- For all $\mathbf{u} \in I$, it is denoted $\bar{\mathbf{u}} = [\![1,p]\!] \setminus \mathbf{u} = \{i \in [\![1,p]\!], i \notin \mathbf{u}\}$
- $X = (X_1, ..., X_p)$ is the vector of random inputs (inputs are assumed independent).
- $Z = (Z_1, ..., Z_p)$ is an independent copy of X.
- $Y = f(X) = (X_1, ..., X_p)$ is the output (also random).
- $X_{\mathbf{u}} = (X_i)_{i \in \mathbf{u}}$ is the vector of random inputs in $\mathbf{u}$.
- $Z_{\mathbf{u}} = (Z_i)_{i \in \mathbf{u}}$ is an independent copy of $X_{\mathbf{u}}$.
- $Y_{\mathbf{u}} = f(Z_{\mathbf{u}}, X_{\bar{\mathbf{u}}})$ is the output when the inputs in $\mathbf{u}$ are taken from another independent realisation.

The aim is to estimate $S_{\mathbf{u}} = \frac{\mathrm{cov}(Y, Y_{\mathbf{u}})}{V(Y)}$. It is the coefficient of the slope of the linear regression between Y and $Y_{\mathbf{u}}$:

Lemme 8.1. *For any set* $\mathbf{u}$ *of indices (*$\mathbf{u} \in I'$*), when*

$$(a_{\mathbf{u}}, b_{\mathbf{u}}) = \underset{(a,b)}{arg\min} \left\{ \mathbb{E}\left[(Y - aY_{\mathbf{u}} - b)^2 \right] + \mathbb{E}\left[(Y_{\mathbf{u}} - aY - b)^2 \right] \right\} \tag{8.4}$$

then

$$a_{\mathbf{u}} = S_{\mathbf{u}}$$

Proof is in the appendix B.3.1.

The lemma 8.1 shows the best coefficient to predict the total variance from the predictor $Y_{\mathbf{u}}$ is the Sobol index $S_{\mathbf{u}}$. The coefficient $a_{\mathbf{u}}$ in the linear model of the lemma is equal to the Sobol index even if $\mathbb{E}[Y] \neq 0$. The $b_{\mathbf{u}}$ coefficient is not interesting to interpret the variance. Hence, **in the following, we will suppose that the output Y is centred**: $\mathbb{E}[Y] = 0$. The variance of the output can be explained with the linear model (8.5).

$$Y = a_{\mathbf{u}} Y_{\mathbf{u}} + \epsilon_{\mathbf{u}} \tag{8.5}$$

The statistical model (8.5) answers the following question: if the output Y has to be explained with $Y_{\mathbf{u}}$ (the same code with the input parameters $X_{\mathbf{u}}$ frozen), how much variance is it possible to explain? The best approximation of Y as a function of $Y_{\mathbf{u}}$ is $\mathbb{E}[Y|Y_{\mathbf{u}}]$ (it can be seen as the projection of Y onto $Y_{\mathbf{u}}$). The assumption stated by the linear model is that $\mathbb{E}[Y|Y_{\mathbf{u}}] = a_{\mathbf{u}}Y_{\mathbf{u}}$. As a consequence, the error ϵ of such model is a centred and the coefficient $a_{\mathbf{u}}$ is chosen to minimize its variance. The variance of $\epsilon_{\mathbf{u}}$ when it is minimum is denoted $\sigma^2_{0\mathbf{u}}$.

The statistical model (8.5) can be used to estimate only the Sobol index $S_{\mathbf{u}}$. The aim is to get all Sobol indices at once. The vector of all slopes is denoted $\mathbf{a} = (a_{\mathbf{u}}, \mathbf{u} \in I')$. The vector of all Sobol indices is denoted $\mathbf{S} = (S_{\mathbf{u}}, \mathbf{u} \in I')$. These vectors are of dimension $d = |I'|$. Finally, the minimization problem (8.4) is changed into (8.6).

$$\mathbf{S}^{ls} = \arg\min_{\mathbf{a}} \left\{ \sum_{\mathbf{u}\in I'} \mathbb{E}\left[(Y - a_{\mathbf{u}}Y_{\mathbf{u}})^2\right] + \mathbb{E}\left[(Y_{\mathbf{u}} - a_{\mathbf{u}}Y)^2\right] \right\} \tag{8.6}$$

The minimization of (8.6) benefits then from the advances in linear regression. In particular, we will focus on two penalties to select the most relevant coefficients: the L^1 penalty (problem 8.7, Lasso method) and the L^0 penalty (problem 8.8, best subset method).

$$\mathbf{S}^{l1} = \arg\min_{\mathbf{a}} \left\{ \sum_{\mathbf{u}\in I'} \mathbb{E}\left[(Y - a_{\mathbf{u}}Y_{\mathbf{u}})^2\right] + \mathbb{E}\left[(Y_{\mathbf{u}} - a_{\mathbf{u}}Y)^2\right] + \lambda\|\mathbf{a}\|_1 \right\} \tag{8.7}$$

with the L^1 norm $\|\mathbf{a}\|_1 = \sum_{\mathbf{u}\in I'} |a_{\mathbf{u}}|$.

$$\mathbf{S}^{l0} = \arg\min_{\mathbf{a}} \left\{ \sum_{\mathbf{u}\in I'} \mathbb{E}\left[(Y - a_{\mathbf{u}}Y_{\mathbf{u}})^2\right] + \mathbb{E}\left[(Y_{\mathbf{u}} - a_{\mathbf{u}}Y)^2\right] + \lambda\|\mathbf{a}\|_0 \right\} \tag{8.8}$$

with the L^0 norm $\|\mathbf{a}\|_0 = \sum_{\mathbf{u}\in I'} \mathbf{1}_{a_{\mathbf{u}}\neq 0} = |\{\mathbf{u},\, a_{\mathbf{u}} \neq 0\}|$.

8.2 Properties and links among estimators

The theoretical Sobol indices from penalized regression have been defined: least squares (8.6), Lasso (8.7), best subset (8.8). Now we focus on their estimation. The problem is to find an estimation of the coefficients in the linear model (8.5) from the following data:

$$Y = \begin{pmatrix} y^1 \\ \vdots \\ y^N \end{pmatrix} \qquad Y_{\mathbf{u}} = \begin{pmatrix} y^1_{\mathbf{u}} \\ \vdots \\ y^N_{\mathbf{u}} \end{pmatrix}$$

for all $\mathbf{u} \in I'$. The samples Y and $Y_{\mathbf{u}}$ are denoted the same way as the random variables Y and $Y_{\mathbf{u}}$ they are sampling.

Moreover, the random variables Y and $Y_{\mathbf{u}}$ are assumed centred: $\mathbb{E}[Y] = \mathbb{E}[Y_{\mathbf{u}}] = 0$ which has for consequence $\sum_{i=1}^{N} y^i = \sum_{i=1}^{N} y^i_{\mathbf{u}} = 0$. Since the random variables Y and $Y_{\mathbf{u}}$ follow the same law, we have $\mathbb{E}[Y^2] = \mathbb{E}[Y_{\mathbf{u}}^2] = \sigma^2$ and so $\sum_{i=1}^{N}(y^i)^2 = \sum_{i=1}^{N}(y^i_{\mathbf{u}})^2 = \hat{\sigma}^2 \simeq \sigma^2$. The variance of the noise in the linear model (8.5) is denoted $\sigma^2_{0\mathbf{u}} = V(Y - a_{\mathbf{u}} Y_{\mathbf{u}})$.

8.2.1 The least squares estimator

The coefficients of the linear model (8.5) can be estimated with ordinary least squares. The problem to solve in theory (8.6). In estimation, it is (8.9):

$$\widehat{\mathbf{S}}^{ls} = \arg\min_{\mathbf{a}} \left\{ \sum_{\mathbf{u}\in I'} \|Y - a_{\mathbf{u}} Y_{\mathbf{u}}\|_2^2 + \|Y_{\mathbf{u}} - a_{\mathbf{u}} Y\|_2^2 \right\} \tag{8.9}$$

For any $\mathbf{u} \in I'$, the solution is given by (8.10):

$$\widehat{S}^{ls}_{\mathbf{u}} = (Y_{\mathbf{u}}^T Y_{\mathbf{u}})^{-1} Y_{\mathbf{u}}^T Y = \frac{\sum_{i=1}^{N} y^i y^i_{\mathbf{u}}}{\sum_{i=1}^{N} (y^i_{\mathbf{u}})^2} \tag{8.10}$$

The least squares estimator is known to be the BLUE: Best Linear Unbiased Estimator. Its bias is zero and its variance is minimum among all estimators of the form AY with $A \in \mathbb{R}^{d\times N}$ (Gauss-Markov theorem, (Saporta, 2006) section 17.2).

$$\mathbb{E}\left[\widehat{S}^{ls}_{\mathbf{u}}\right] = S_{\mathbf{u}} \tag{8.11}$$

$$V\left(\widehat{S}^{ls}_{\mathbf{u}} | Y_{\mathbf{u}}\right) = (Y_{\mathbf{u}}^T Y_{\mathbf{u}})^{-1} \sigma_0^2 = \frac{\sigma_0^2}{\sigma^2} \tag{8.12}$$

Its expression is the same as the Monte Carlo estimator $\widehat{D_{\mathbf{u}}}^{MC1}$. Janon et al. (2014) already pointed out the equality of such estimators (remark 1.3 of the paper) and they proved their asymptotic normality (proposition 2.2 of the paper). Moreover, the asymptotic variance of the estimator given by Janon (denoted σ^2_{MC1}) and the variance given by Gauss-Markov theorem (equation (8.12)) are the same. Indeed, when Y is centred, σ^2_{MC1} is written

$$\begin{aligned}
\sigma^2_{MC1} &= \frac{V(Y(Y_{\mathbf{u}} - S_{\mathbf{u}} Y))}{V(Y)^2} && \text{From Janon et al. (2014)} \\
&= \frac{V(Y_{\mathbf{u}} - S_{\mathbf{u}} Y)}{V(Y)} && \text{because } \mathbb{E}[Y_{\mathbf{u}} - S_{\mathbf{u}} Y] = \mathbb{E}[Y] = 0 \text{ and } (Y_{\mathbf{u}}, Y) = (Y, Y_{\mathbf{u}}) \\
&= \frac{\sigma_0^2}{\sigma^2}
\end{aligned}$$

In conclusion, the least squares method gives the same estimator as crude Monte Carlo. This estimator is unbiased but asymptotically Gaussian: if the samples Y and $Y_{\mathbf{u}}$ are too small or for small Sobol indices, the variance is high and negative estimations are possible.

8.2.2 Lasso versus least square

The Lasso method (Least Absolute Shrinkage and Selection Operator) aims to solve a least squares problem while pushing some coefficients to be exactly 0. It is thus a valuable tool when the vector of coefficient is sparse (van de Geer, 2016). Having several coefficients equal to zero makes the statistical model more informative and more easily interpreted: predictors with a coefficient to 0 are dismissed. The Lasso method was first introduced by Tibshirani (1996). The principle is to solve the least square problem with a L^1-penalty in the function to minimize.

The use of a L^1-penalty is what make some coefficients to be exactly zero. Indeed, the admissible area has a very different shape with the L^1 norm and the L^2 norm. This is visible in the figure 8.1: an illustration with $p = 2$ is presented. On the right hand side, the admissible area for the L^2 norm is a circle. On the left hand side, the admissible area for the L^1 norm is a square with angle on the axis. The solution of the unconstrained problem (8.6) is denoted $\widehat{\beta}^{LS}$ in the figure 8.1 and the lines of equal cost are drawn in red. The solution of the constrained problem is the point in the admissible area the closest to $\widehat{\beta}^{LS}$ according to the cost lines in red. For the L^2 norm (right panel), the solution is on a circle. Both coefficients are likely to be non-zero. For the L^1 norm (left panel), the solution is likely on one of the corner of the square. On any corner, one the coefficient will be exactly zero.

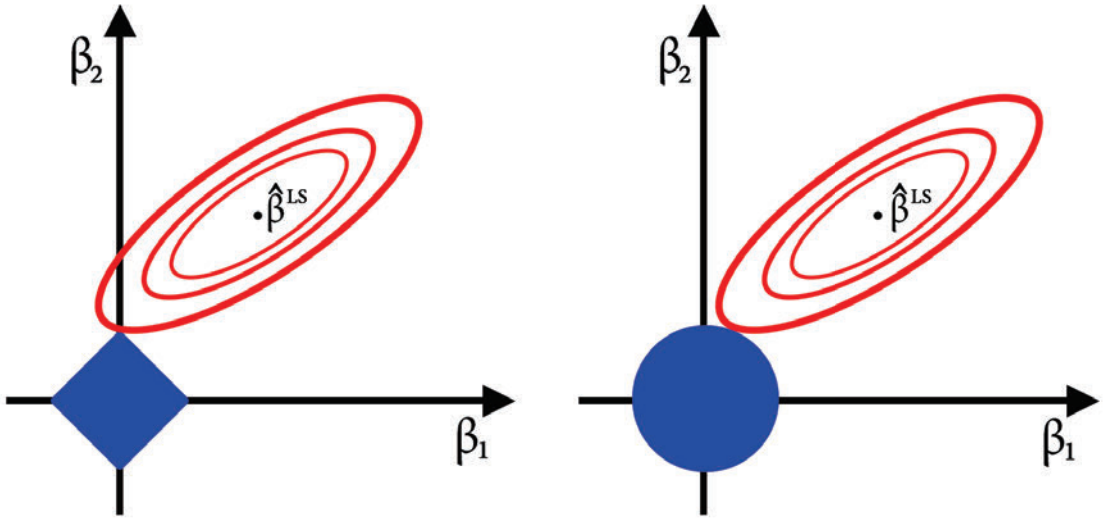

Figure 8.1 – Illustration of admissible area with L^1 and L^2 norms. The extreme points are located on an axis for the L^1 norm, thus one of the coefficient is null.
Credit: Par LaBaguette — Travail personnel, CC BY-SA 4.0, https://commons.wikimedia.org/w/index.php?curid=48816401

The Lasso is written only for the Sobol indices estimation problem. The problem to solve

is (8.13) and the solution is given by the proposition (8.1).

$$\widehat{\mathbf{S}}^{l1} = \arg\min_{\mathbf{a}} \left\{ \sum_{\mathbf{u}\in I'} \|Y - a_{\mathbf{u}} Y_{\mathbf{u}}\|_2^2 + \|Y_{\mathbf{u}} - a_{\mathbf{u}} Y\|_2^2 + \lambda_1 \|\mathbf{a}\|_1 \right\} \tag{8.13}$$

Proposition 8.1. *For any $\mathbf{u} \in I'$, the Lasso and least squares estimators are related according to the following formula:*

$$\widehat{S}_{\mathbf{u}}^{l1} = \max\left(\widehat{S}_{\mathbf{u}}^{ls} - \varepsilon_1, 0\right)$$

with $\varepsilon_1 = \frac{\lambda_1}{2\sigma^2}$.

Proof is in the appendix B.3.2, page 296.

The Lasso method gives an estimator that has a direct relationship with the least squares estimator. To get the Lasso estimator, the least square estimator is shrunk of $\varepsilon_1 = \lambda_1/(2\sigma^2)$. When the least squares estimator is smaller that the shrunk, the Lasso estimator is exactly zero.

From a Bayesian point of view, the penalty is equivalent to give a prior distribution to the coefficients $\mathbf{a}$. The L^1-penalty imposes an absolute exponential prior distribution: $\forall a \in \mathbf{a}$, $\mathbb{P}(a) \propto \exp(-\lambda_1 |a|)$. Maximizing the likelihood gives the least squares estimator. Maximizing the posterior probability with an absolute exponential prior gives the Lasso estimator.

The hard part to take profit of the Lasso is to correctly set the penalty λ_1. When $\lambda_1 \to 0$, the estimator tends to the ordinary least squares estimator and there is no benefit to use the Lasso. When $\lambda_1 \to +\infty$, the penalty unrealistically shrinks the coefficients to estimate. Good predictors will be dismissed, leading to too simple models.

8.2.3 Best subset versus least square

The so-called best subset method (mentioned in (Tibshirani, 1996; Breiman, 1995; Lin et al., 2010)) adds a L^0 penalty to the least square problem (equation (8.8)):

$$\widehat{\mathbf{S}}^{l0} = \arg\min_{\mathbf{a}} \left\{ \sum_{\mathbf{u}\in I'} \|Y - a_{\mathbf{u}} Y_{\mathbf{u}}\|_2^2 + \|Y_{\mathbf{u}} - a_{\mathbf{u}} Y\|_2^2 + \lambda_0 \|\mathbf{a}\|_0 \right\}$$

with the L^0 norm $\|\mathbf{a}\|_0 = |\{i,\, a_i \neq 0\}|$ denoting the number of non-zero components in $\mathbf{a}$.

Proposition 8.2. *For any* $\mathbf{u} \in I'$*, the best subset and least squares estimators are related according to the following formula:*

$$\widehat{S}^{l0}_{\mathbf{u}} = \widehat{S}^{ls}_{\mathbf{u}} \mathbf{1}_{\widehat{S}^{ls}_{\mathbf{u}} > \varepsilon_0}$$

with $\varepsilon_0 = \sqrt{\frac{\lambda_0}{\sigma^2}}$.

Proof is in the appendix B.3.3, page 298.

The best subset estimator gives also an estimator directly linked with the least square estimator. When the least square estimator is smaller than the threshold $\varepsilon_0 = \sqrt{\lambda_0}/\sigma$, the best subset estimator is exactly zero. Otherwise, least square and best subset estimators are equal. The shrinkage is not systematic, conversely to the Lasso. As for the Lasso, the difficulty is to correctly choose the penalty λ_0.

The best subset estimator is optimal in terms of information loss. Indeed, it minimizes the Akaike information criterion. The Akaike information criterion (AIC) is a metric of the information loss due to the model (original publication in 1973, republished in the collection (Akaike, 1998)). The model $Y = a_{\mathbf{u}} Y_{\mathbf{u}} + \epsilon_{\mathbf{u}}$ is imperfect and the AIC quantifies the benefit of adding a new predictor. It is defined by

$$AIC = 2k - 2\log(L(\mathbf{a}))$$

where k is the number of coefficients to estimate and L is the likelihood function. In our case, k is the number of non-zero Sobol indices and the likelihood function is given by

$$\log(L(\mathbf{a})) = \log(\mathbb{P}(Y|\mathbf{a})) \propto \sum_{\mathbf{u} \in I} \|Y - a_{\mathbf{u}} Y_{\mathbf{u}}\|_2^2$$

Hence, the AIC for our problem is exactly the function of $\mathbf{a}$ to minimize in the best subset problem (8.8).

Unfortunately, the minimization with a L^0 penalty is a NP-hard problem (Natarajan, 1995). As a consequence, only greedy algorithms can perform the minimisation of (8.8). For example, in (Tibshirani, 1996), they are estimated using the so-called *leaps and bounds* procedure (Furnival and Wilson, 1974).

8.2.4 Lasso versus best subset

Lasso and best subset estimators are both related to the least squares estimator. Transitively, they are related to each other. The property 8.1 tells the Lasso is *soft threshold* of the least square estimator, while property 8.2 tells the best subset is a *hard threshold* of the least square estimator. The threshold of Lasso is said soft because it is continuous, while the hard threshold is not. Shapes of both threshold functions are displayed in figures (8.2) and (8.3).

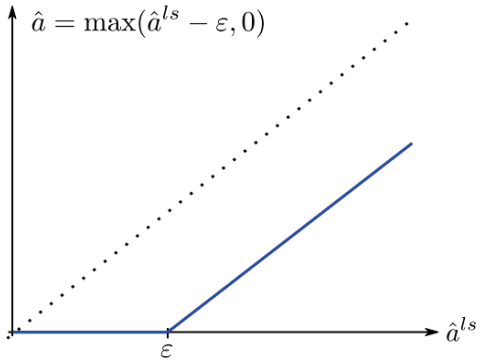

Figure 8.2 – Soft threshold: link between the Lasso estimator and the least square estimator.

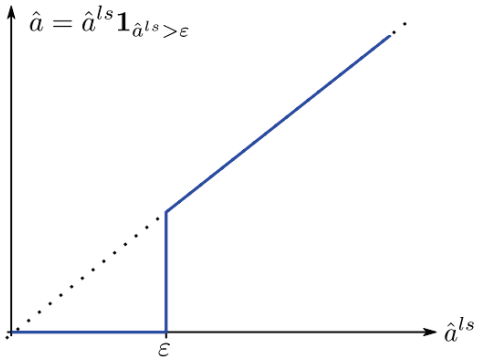

Figure 8.3 – Hard threshold: link between the best subset estimator and the least square estimator.

To have the same threshold $\varepsilon = \varepsilon_1 = \varepsilon_0$, we need to have the following relation between the penalty:

$$\lambda_1 = 2\sigma\sqrt{\lambda_0} \tag{8.14}$$

In this case, the relationship between $\widehat{S}^{l0}_{\mathbf{u}}$ and $\widehat{S}^{l1}_{\mathbf{u}}$ is easy to write and valid everywhere but at the discontinuity (when $\widehat{S}^{ls}_{\mathbf{u}} = \varepsilon$).

$$\widehat{S}^{l0}_{\mathbf{u}} = \frac{\widehat{S}^{ls}_{\mathbf{u}}}{\widehat{S}^{ls}_{\mathbf{u}} - \varepsilon}\widehat{S}^{l1}_{\mathbf{u}} \tag{8.15}$$

When the thresholds are different, one need to distinguish the case $\varepsilon_1 < \varepsilon_0$ and $\varepsilon_1 > \varepsilon_0$ and then the sub-cases $\widehat{S}^{ls}_{\mathbf{u}} < \min(\varepsilon_1, \varepsilon_0)$, $\widehat{S}^{ls}_{\mathbf{u}} \in]\varepsilon_1, \varepsilon_0[$ and $\widehat{S}^{ls}_{\mathbf{u}} > \max(\varepsilon_1, \varepsilon_0)$. The final result does not feed the comment. One can see that $\widehat{S}^{l0}_{\mathbf{u}} \to \widehat{S}^{l1}_{\mathbf{u}}$ either when $\varepsilon \to 0$ (both converge toward $\widehat{S}^{ls}_{\mathbf{u}}$ when the penalty decreases) either when $\widehat{S}^{ls}_{\mathbf{u}} \to +\infty$. It highlights that the use of L^1 or L^0 penalty is only relevant for small Sobol indices. For large Sobol indices, $\widehat{S}^{ls}_{\mathbf{u}}$ has the advantage to be unbiased.

Even with an expression of $\widehat{S}^{l0}_{\mathbf{u}}$ and $\widehat{S}^{l1}_{\mathbf{u}}$ as a function of $\widehat{S}^{ls}_{\mathbf{u}}$, for which the asymptotic behaviour is known, the asymptotic law of the penalized estimators are not straightforward. The Delta method does not apply because neither soft nor hard threshold functions are differentiable.

Lin et al. (2010, 2008) argue in favour of the L^0 penalty. They compare L^1 and L^0 penalties according to the predictive risk function $R(\beta, \widehat{\beta}) = \mathbb{E}\left[\|X\beta - X\widehat{\beta}\|_2^2\right]$ and show that the risk ratio of L^0 over L^1 is bounded while the risk ratio of L^1 over L^0 is not. The final estimate of L^0 is better, but the algorithm to get it are not efficient. Indeed, Natarajan (1995) proved that the L^0-penalized least squares is a NP-hard problem. Hence, even if the L^0 estimate is better, more efficient algorithms exist for the L^1 estimate.

8.3 Choice of penalty by cross-validation

8.3.1 General principle of cross-validation

Given a linear model $Y = X\beta + \epsilon$, one wants to estimate β and the uncertainty on the estimation. The principle of cross-validation is to split the sample X in two part: a part dedicated to the estimation of the coefficient in the regression, another part dedicated to the prediction of the model with the estimated sample. On the part dedicated to the prediction, one has both the reference value (given in the sample) and the predicted value. Hence, one can have a score of error on the model.

The sample (Y, X) where $Y \in \mathbb{R}^N$ and $X \in \mathbb{R}^{N \times d}$ is divided into one sample (Y_A, A) used for the estimation of the coefficient (the *training* sample), and a sample (Y_B, B) used for the prediction and error estimation (the *testing* sample). We denote N_A the size of the learning sample.

$$Y = \begin{pmatrix} y^1 \\ \vdots \\ y^{N_A} \\ y^{N_A+1} \\ \vdots \\ y^N \end{pmatrix} \begin{matrix} \left.\begin{matrix} \\ \\ \\ \end{matrix}\right\} Y_A \\ \left.\begin{matrix} \\ \\ \\ \end{matrix}\right\} Y_B \end{matrix}$$

$$X = \begin{pmatrix} X_1^1 & \dots & X_d^1 \\ \vdots & & \vdots \\ X^{N_A} & \dots & X_d^{N_A} \\ X^{N_A+1} & \dots & X_d^{N_A+1} \\ \vdots & & \vdots \\ X^N & \dots & X_d^N \end{pmatrix} \begin{matrix} \left.\begin{matrix} \\ \\ \\ \end{matrix}\right\} A \\ \left.\begin{matrix} \\ \\ \\ \end{matrix}\right\} B \end{matrix}$$

The training phase provides the estimated coefficients $\widehat{\beta}$ in the linear model $Y = \beta X + \epsilon$. The regression (with or without penalty) is performed on the sample (Y_A, A). For instance, for the ordinary least squares, we have the formula

$$\widehat{\beta} = (A^T A)^{-1} A^T Y_A$$

Using this estimated coefficient, the output is predicted with the predictors of the second sample. The comparison with the observed output provides an estimation of the uncertainty of prediction:

$$\epsilon \simeq Y_B - B\widehat{\beta}$$

In particular, one can check the bias, variance and mean squared error. In our case, we are interested in the uncertainty of estimation. The uncertainty of estimation has to be derived from the uncertainty of prediction.

8.3.2 Uncertainty of prediction and uncertainty of estimation

The uncertainty on prediction quantifies the error made by the model when it is applied on new data. The uncertainty on estimation quantifies the error made in the estimation by comparing to a new dataset. By splitting the sample into a training sample and a testing sample, one can access the uncertainty of prediction. But the uncertainty of estimation is not directly accessible and has to be derived from the uncertainty of prediction. If we consider a linear model $Y = X\beta + \epsilon$, with $Y \in \mathbb{R}$, $X \in \mathbb{R}^d$, $\beta \in \mathbb{R}^d$ and we assume we have an estimation $\widehat{\beta}$ of the coefficient which is independent of X.

The uncertainty of the prediction $\widehat{Y} = X\widehat{\beta}$ of the variable Y is described by its bias, variance, and mean-squared error (MSE).

$$\mathsf{Bi}_Y = \mathbb{E}\left[\widehat{Y} - Y\right] \tag{8.16}$$

$$\mathsf{Var}_Y = V\left(\widehat{Y}\right) = \mathbb{E}\left[(\widehat{Y} - \mathbb{E}\left[\widehat{Y}\right])^2\right] \tag{8.17}$$

$$\mathsf{MSE}_Y = \mathbb{E}\left[(\widehat{Y} - Y)^2\right] \tag{8.18}$$

These statistics describe the uncertainty of prediction. But for this application, we are more interested on the error of estimation: bias, variance and MSE for the estimated coefficients β.

$$\mathsf{Bi}_\beta = \mathbb{E}\left[\widehat{\beta}\right] - \beta \tag{8.19}$$

$$\mathsf{Var}_\beta = V\left(\widehat{\beta}\right) = \mathbb{E}\left[(\widehat{\beta} - \mathbb{E}\left[\widehat{\beta}\right])(\widehat{\beta} - \mathbb{E}\left[\widehat{\beta}\right])^T\right] \tag{8.20}$$

$$\mathsf{MSE}_\beta = \mathbb{E}\left[(\widehat{\beta} - \beta)^T(\widehat{\beta} - \beta)\right] \tag{8.21}$$

Note that they all are of different dimensions: $\mathsf{Bi}_\beta \in \mathbb{R}^d$, $\mathsf{Var}_\beta \in \mathbb{R}^{d\times d}$ and $\mathsf{MSE}_\beta \in \mathbb{R}$. Although, they are linked by the following relation:

$$\mathsf{MSE}_\beta = \mathsf{Bi}_\beta^T \mathsf{Bi}_\beta + \mathrm{tr}(\mathsf{Var}_\beta) \tag{8.22}$$

where $\mathrm{tr}(\cdot)$ is the trace operator.

The uncertainty of prediction and estimation are linked with the following relations when $\widehat{\beta}$ is independent from X:

$$\mathsf{Bi}_Y = \mathbb{E}\left[X\right] \mathsf{Bi}_\beta \tag{8.23}$$

$$\mathsf{Var}_Y = \mathbb{E}\left[X\mathsf{Var}_\beta X^T\right] + V\left(X\mathbb{E}\left[\widehat{\beta}\right]\right) \tag{8.24}$$

$$\mathsf{MSE}_Y = \mathsf{Bi}_\beta^T \mathbb{E}\left[X^T X\right] \mathsf{Bi}_\beta + \mathbb{E}\left[\mathrm{tr}(X\mathsf{Var}_\beta X^T)\right] + \sigma_0^2 \tag{8.25}$$

Proof is in the appendix B.3.4.

In the case of the Lasso method, the cross-validation is repeated for different values of penalty. As the estimator given by the ordinary least squares is unbiased, the bias of esti-

mation should decrease with the penalty. Conversely, a large penalty shrinks the coefficients and thus reduces the variance of the estimator but its bias grows. In the middle, we expect the mean squared error to reach a minimum.

$$\lim_{\lambda \to 0} \mathsf{Bi}_\beta(\lambda) = 0 \quad \text{and} \quad \lim_{\lambda \to +\infty} \mathsf{Var}_\beta(\lambda) = 0$$

With the testing sample, one can estimate the bias, variance and mean squared error of prediction (equations (8.16),(8.17),(8.18)). They can be linked to the same statistics for estimation (equations (8.19),(8.20),(8.21)) through the formulae (8.23), (8.24) and (8.25). The penalty is then chosen to minimise the error of prediction $\mathsf{MSE}_Y(\lambda)$. When this minimum is reached, the chosen penalty makes a good comprise between bias and variance of estimation.

8.3.3 Application to Sobol indices estimation

For our particular problem, the linear model is not of the form $Y = \mathbf{X}\beta + \epsilon$. Instead, we have d linear models of the form $Y = a_{\mathbf{u}} Y_{\mathbf{u}} + \epsilon_{\mathbf{u}}$. There is only one predictor which verifies $\mathbb{E}[Y_{\mathbf{u}}] = 0$ and $\mathbb{E}[Y_{\mathbf{u}}^2] = \sigma^2$, for any $\mathbf{u}$. The error $\epsilon_{\mathbf{u}}$ has no reason to be the same for each model: $\mathbb{E}[\epsilon_{\mathbf{u}}] = 0$ and $\mathbb{E}[\epsilon_{\mathbf{u}}^2] = \sigma_{0\mathbf{u}}^2$. Applying the formulae (8.23), (8.24) and (8.25) we have:

$$\mathsf{Bi}_Y^{\mathbf{u}} = \overbrace{\mathbb{E}[Y_{\mathbf{u}}]}^{=0} \mathsf{Bi}_a^{\mathbf{u}} = 0 \tag{8.26}$$

$$\mathsf{Var}_Y^{\mathbf{u}} = \sigma^2 (\mathsf{Var}_a^{\mathbf{u}} + \mathbb{E}[\widehat{a_{\mathbf{u}}}]^2) \tag{8.27}$$

$$\mathsf{MSE}_Y^{\mathbf{u}} = \sigma^2 (\mathsf{Bi}_a^{\mathbf{u}})^2 + \sigma^2 \mathsf{Var}_a^{\mathbf{u}} + \sigma_{0\mathbf{u}}^2 = \sigma^2 \mathsf{MSE}_a^{\mathbf{u}} + \sigma_{0\mathbf{u}}^2 (1 - \sigma^2) \tag{8.28}$$

In practice, the estimators of bias, variance and mean squared error of prediction are accessible through the formulae:

$$\widehat{\mathsf{Bi}_Y^{\mathbf{u}}} = \frac{1}{N} \sum_{i=1}^{N} (y_{\mathbf{u}}^i \widehat{a_{\mathbf{u}}} - y^i) \tag{8.29}$$

$$\widehat{\mathsf{Var}_Y^{\mathbf{u}}} = \frac{1}{N-1} \sum_{i=1}^{N} \left(y_{\mathbf{u}}^i \widehat{a_{\mathbf{u}}} - \frac{1}{N} \sum_{i=1}^{N} y_{\mathbf{u}}^i \widehat{a_{\mathbf{u}}} \right)^2 \tag{8.30}$$

$$\widehat{\mathsf{MSE}_Y^{\mathbf{u}}} = \frac{1}{N} \sum_{i=1}^{N} (y^i - y_{\mathbf{u}}^i \widehat{a_{\mathbf{u}}})^2 \tag{8.31}$$

On the two last series of equation, one can see that the estimator for the bias is useless. Indeed, despite the link (8.23) between bias of prediction and bias of estimation, despite the fact that $\mathsf{Bi}_a(\lambda)$ is expected to increase with λ, the estimator (8.29) cannot be used to retrieve that trend because of the relation (8.26).

For the variance and mean-squared error, we would rather have a score for all the coefficients, not one for each $\mathbf{u}$. Applying the definition of the MSE for any vector of parameters β (equation 8.21) to the case $\beta = \mathbf{a}$ and $\beta = (a_{\mathbf{u}} Y_{\mathbf{u}} + \epsilon_{\mathbf{u}}, \mathbf{u} \in I')$, the relevant global MSE is the sum of MSE for each $\mathbf{u}$.

$$\mathsf{MSE}_Y = \sum_{\mathbf{u} \in I'} \mathsf{MSE}_Y^{\mathbf{u}} \quad \text{and} \quad \mathsf{MSE}_a = \sum_{\mathbf{u} \in I'} \mathsf{MSE}_a^{\mathbf{u}}$$

$$\mathrm{tr}(\mathsf{Var}_Y) = \sum_{\mathbf{u} \in I'} \mathsf{Var}_Y^{\mathbf{u}} \quad \text{and} \quad \mathrm{tr}(\mathsf{Var}_a) = \sum_{\mathbf{u} \in I'} \mathsf{Var}_a^{\mathbf{u}}$$

Finally,

$$\mathrm{tr}(\mathsf{Var}_Y) = \sigma^2 \left(\mathrm{tr}(\mathsf{Var}_a) + \sum_{\mathbf{u} \in I'} \mathbb{E}\left[\widehat{a_{\mathbf{u}}}\right]^2 \right)$$

$$\mathsf{MSE}_Y = \sigma^2 \mathsf{MSE}_a + (1 - \sigma^2) \sum_{\mathbf{u} \in I'} \sigma_{0\mathbf{u}}^2$$

In the equation of variance, the terms $\mathbb{E}\left[\widehat{a_{\mathbf{u}}}\right]^2$ vary with penalty (they are linked to the bias which is not accessible). The variations of $\mathrm{tr}(\mathsf{Var}_Y)$ against λ are thus not equal to the variations of $\mathrm{tr}(\mathsf{Var}_a)$. In the equation of MSE, $\sigma^2 = V(Y)$ is a constant, $\sigma_{0\mathbf{u}}^2 = V(\epsilon_{\mathbf{u}})$ is the minimum variance of the least squares problem. It is also a constant (it depends only on $\mathbf{u}$). The variations of MSE_Y are the same as MSE_a. Hence, the error of estimation is minimum when the error of prediction is minimum.

In conclusion, the penalty will be chosen to minimize the error of prediction. In the particular case of centred design, the bias of prediction is longer linked to the bias of estimation. The variance of prediction rely on additional terms that are still to be estimated to complete the link between prediction and estimation. As a consequence, only mean-squared error plot will be used.

8.3.4 Results of numerical experiments

The three estimators presented in the last section will be experimented on the application case of turbulence reconstruction. The sample of inputs X and Z are generated with latin hypercubes. For both X and Z, 4000 values of each input are generated. The split between samples for cross-validation have been made randomly, with a proportion of 65% for the training sample (2400 values) and 35% for the test sample (1600 values). Once the sample has been split, the random state of the splitting is saved in case the experiment is repeated in the same conditions. The experiment have been carried out with the meta-model of the output r_V (the root-mean squared error on the wind) because it is easy to interpret. The algorithm used to minimize the cost functions (least squares and Lasso) is the conjugated gradient.

The figures (8.4) and (8.5) show the evolution of the estimated mean-squared error $\widehat{\mathsf{MSE}_Y}$ of the Lasso for different penalty values. On the left (figure 8.4) the Lasso estimate have

calculated from the Monte-Carlo estimate, on which the soft-threshold function has been applied, using the proposition 8.1. On the right (figure 8.5) the Lasso estimate have calculated by the minimization of the cost function defined by (8.7) (L^1 penalized least squares). One can see a clear minimum on both. Although, the slope is much more regular when the soft threshold is applied. Indeed, it avoids the weaknesses of the minimization: do not reach the exact minimum but something close enough, get stuck at a local minimum... Overall, the comparison of both figures corroborates the minimization is trustworthy. But in the objective to apply another minimum finder to such curve, the soft threshold one is recommended. Moreover, the soft threshold one is much faster to compute.

As a conclusion, to find the good penalty value by cross-validation, we recommend to do first an ordinary least squares regression on the training sample, then to get the Lasso estimate by soft thresholding for all the penalty values and eventually to compute the mean squared error on the testing sample. This recommendation holds only for problems which have a result similar to the proposition 8.1.

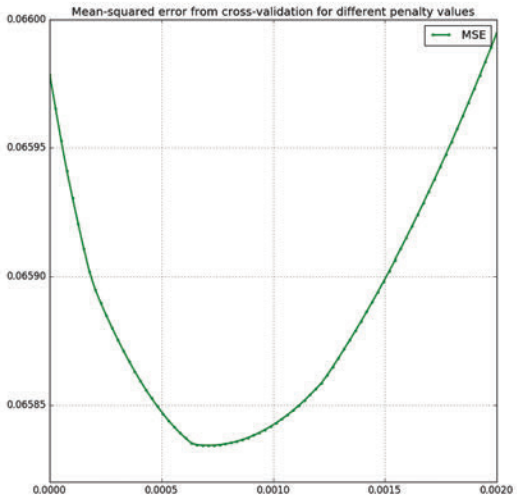

Figure 8.4 – Estimated mean squared error against the penalty in Lasso estimation. Obtained with soft thresholding of the Monte Carlo estimate.

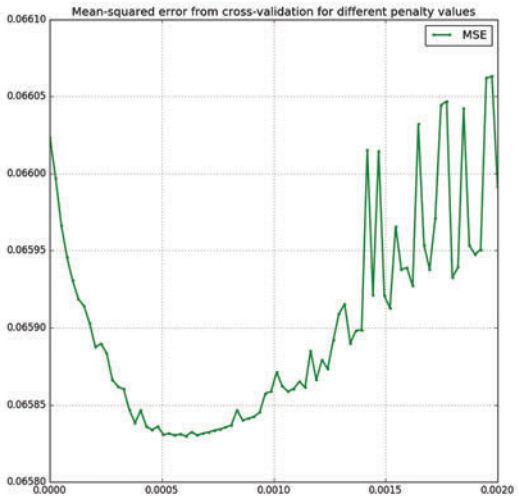

Figure 8.5 – Estimated mean squared error against the penalty in Lasso estimation. Obtained with the minimization of the cost function.

This methodology can be extended to the L^0 penalty. The best subset estimator resulting from L^0 penalized regression has been shown to be accessible through a hard thresholding of the least squares estimator (proposition 8.2). This was the only method of estimation tested here since only greedy algorithm can solve the L^0 penalized minimization. As a consequence, the parameter to check will not be the penalty λ_0 but the threshold $\varepsilon_0 = \sqrt{\frac{\lambda_0}{\sigma^2}}$. The Monte Carlo estimate is calculated on the training sample. For each threshold value, the mean squared error is estimated on the testing sample. It results the curve in figure 8.6.

One can see the step-like shape of the curve: the threshold does not have influence until it reaches the next coefficient value. As a consequence, the minimum is not unique. For this example, it is reached for a threshold around 0.1, which a large value. It let only two non-zero indices. It points out the method of selection is not perfect and might be too selective. In (Fruth et al., 2011) the value of 0.02 is used to threshold second order Sobol indices (figure 2 in the 2011 version on HAL). This value will be used here as well.

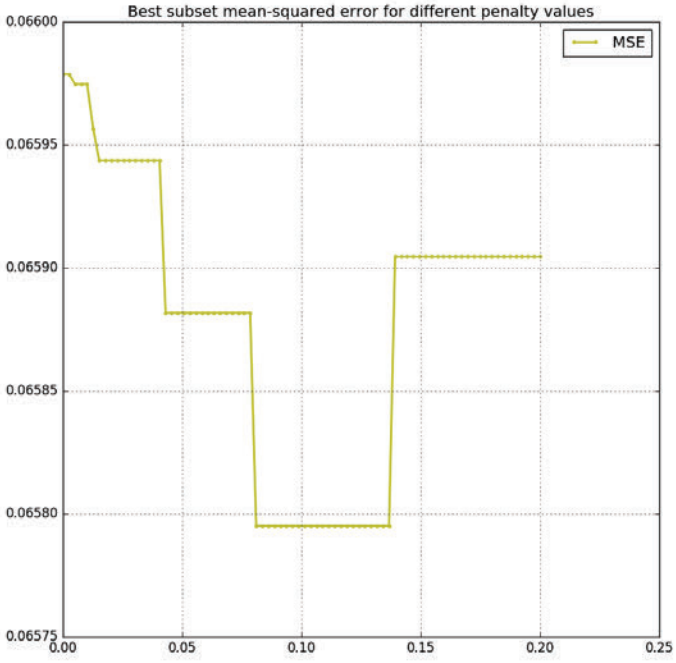

Figure 8.6 – Estimated mean squared error against the threshold in best subset estimation.

The figure 8.7 shows the evolution of the coefficients with the penalty. On the x-axis is the value of the penalty in logarithmic scale. On the y-axis is the value of the estimated coefficients. One can see that for a penalty almost null, the coefficients are all non-zeros. Actually they are equal to their ordinary least squares estimate. For a very large penalty, all coefficients are null. When the penalty decreases, they raise one after another. The introduction of a new coefficient can sometimes influence the curve of another coefficient. This is the sign of a correlation between them (as in (Hesterberg et al., 2008), figure 2). No such feature is visible in the figure. This is not surprising since the inputs of the sensitivity analysis have been simulated independently. Although it is good to be confirmed by this observation.

Four estimators have been tested: the straightforward Monte Carlo, the ordinary least squares, the Lasso and the best subset. They are displayed in figure (8.8). As expected, the least squares (blue) and the Monte Carlo (black dashed line) are two realisations of the same

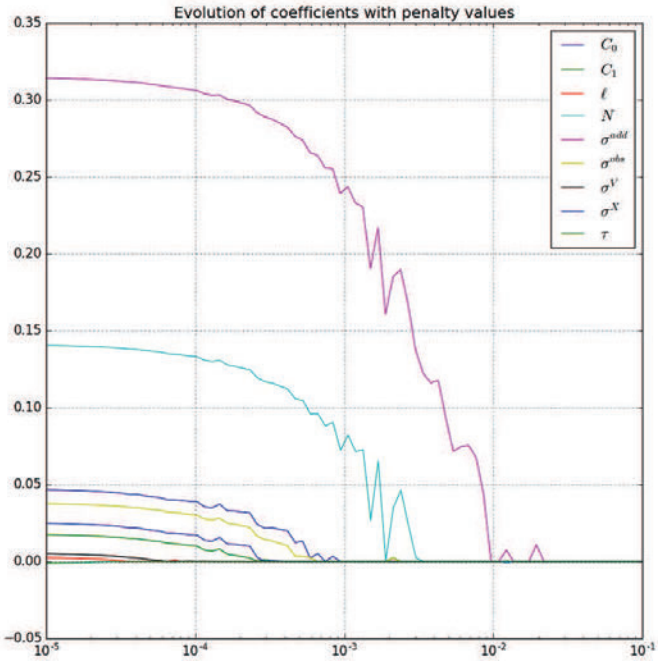

Figure 8.7 – Value of the coefficients estimated by Lasso regression against the penalty (in log-scale). The coefficients are all at 0 for large penalty and raise in order of importance up to their value as obtained with ordinary least square.

estimator. The Lasso (green) shrinks all the coefficients up to 0. It results that only the main indices are kept non-zero and the negative estimation of small indices are filtered. The best subset (yellow) also selects the major coefficients, but it does not shrink them. The hard threshold was set to the value $\varepsilon_0 = 0.02$.

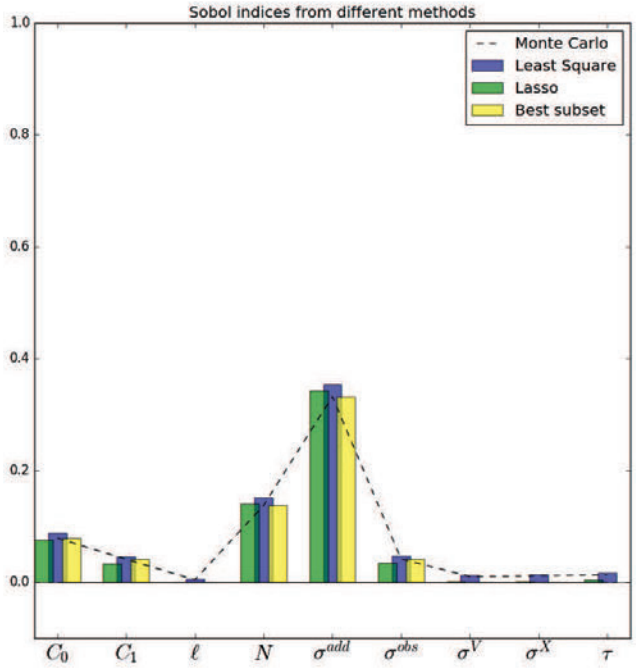

Figure 8.8 – Three estimators ensuing from regression (coloured bars) are compared to the Monte Carlo estimator (black dashed line). One can see that the ordinary least square (blue) gives the same estimation (more or less some randomness due to estimation). The best subset is exactly equal to the Monte Carlo, excepted for indices smaller than the threshold, which are 0. The Lasso estimator gives a shrunk estimation bounded to 0.

8.4 Conclusion

Sobol indices summarize the influence of a group of parameters with a real number in $[0, 1]$. But the number of groups grows exponentially with the number of parameters (if the code has p parameters, there are 2^p groups of parameters). In practice, only few of them are really influencing the code. Moreover, the interpretation of the Sobol indices will focus only on the main ones. That is to say, a good estimation of Sobol indices is not necessarily an unbiased estimation.

Penalized regressions offer biased estimators with lower variance such that the total error is lower. From the initial remark that Sobol indices can be seen as the estimated parameter in a linear model, three regression types have been tested. The ordinary least squares give the same estimate as with Monte Carlo. The L^1 penalized least squares give the Lasso estimate. The L^0 penalized least squares give the best subset estimate. The Lasso shrinks all coefficients and set the smallest ones to exactly zero. The best subset does not shrink the coefficients but set the smallest ones to exactly zero. They are linked to the least squares estimate with a soft threshold and a hard threshold, respectively.

To set the penalty objectively, a cross-validation has been carried out for each penalty value in a given set. The penalty which gives the lowest mean squared error is chosen to

perform the final estimation. The application of this methodology on a single example has shown good results, but more experimentations are needed to assess if it can be repeated and trusted.

General conclusion

The present thesis analyses the sensitivity of the reconstruction method to filter wind measurements. This is important to improve the ability of lidar to perform turbulence measurements (in wind farms or in airport, for example). The presentation was divided in two parts: a first part dedicated to the state of the art of the different fields used in the reconstruction method, a second part dedicated to the applications and the results. This conclusion summarizes the original contributions of this work.

Major contributions

Tuning strategy

The results of the sensitivity analysis presented at the chapter 6 underlined key inputs parameters and relevant output scores. The key parameters are the number of particles, N, the true observation noise, σ^{add} and the given observation noise, σ^{obs}. The relevant output are the wind spectrum slope, b, the wind RMSE, r_V and the execution time T_{exe}. Additional experiments of the chapter 7 show how the key inputs influence the relevant outputs. From this knowledge, we highlight a tuning strategy to set the most influential inputs. The tuning strategy is the following:

1. Set N to a low value, such that T_{exe} is really small.
2. For σ^{obs} ranging around the *a priori* accuracy of the instrument, calculate the wind spectrum slope b.
3. Set σ^{obs} to the value which gives b the closest to -5/3. σ^{obs} is then almost equal to σ^{add}.
4. Set N to the maximum affordable value. The error on wind retrieval is now minimum, estimated by $K\frac{\sigma^{obs}}{\sqrt{N}}$ with $K = 2.33$.

Thanks to the tuning strategy coming out of this work, the reconstruction method should be easier to deploy on new dataset. The benefit of the tuning strategy could be assessed on other dataset from BLLAST. Beyond, automatic application of the tuning strategy would help making the reconstruction more autonomous.

Reconstruction system details and behaviour

The reconstruction method was described in previous publications (Baehr, 2008, 2010; Baehr et al., 2011; Suzat et al., 2011; Rottner and Baehr, 2014; Rottner, 2015). Such publications

were highlighting the originality of the method in comparison to existing methods and giving theorems about convergence. Deeper details could not be published because of the patenting process, which came out to pending in December, 2016 (Baehr et al., 2016). Publications are now authorized and this thesis is probably the most complete. Another paper, Rottner and Baehr (2017), was submitted in June 2017, but cannot be as detailed as this document. The level of details given in the chapter 5 is an important result of this PhD.

In addition, the validation scores built for the sensitivity analysis have been studied and some theoretical results about their behaviour are demonstrated. The theorem 5.2 links the number of null potential to the number of particles. It is based on a result from Del Moral (2004), itself coming from Azuma-Hoeffding's inequality. The theorem 5.3 links the number of null potential to the observation noise (true and given). This is an orginal result in agreement with the numerical experiments of the chapter 7. However, the numerical experiment does not test the theory. Dedicated experiments shall be carried out before claiming the theoretical result is matched by the experiment.

Sobol indices estimation

The chapter 8 tests an innovative way of estimation of Sobol indices. The Sobol indices expressed as a solution of a least squares problem was already known (Janon et al., 2014). But it has never been combined with penalties, as it is done in optimization under constaints. The idea is that only the few highest Sobol indices are useful in pratice. To make small Sobol indices go to exactly zero, a penalty is added to the function to minimize in the least square problem. The tested penalties are L^1 (the sum of absolute value of Sobol indices) and L^0 (the number of non-zero Sobol indices). The L^1 penalty shrinks all coefficients and set the smallest ones to exactly zero. The L^0 penalty does not shrink the coefficients but set the smallest ones to exactly zero. To set the penalty objectively, a cross-validation has been carried out for each penalty value in a given set. The penalty which gives the lowest mean squared error is chosen to perform the final estimation. The application of this methodology on a single example has shown good results, but more experimentations are needed to assess if it can be repeated and trusted.

Improvements in the implementation

The need of many runs to perform a sensitivity analysis motived the recoding of the reconstruction code from Scilab to Fortran 90. Indeed, Scilab is a high level interpreted language, while Fortran is a low level compiled language. The coding with a low level language is much harder than high level. Software engineering took a large part of the time in this PhD. It was the opportunity to re-think the algorithms. The conditioning step of the reconstruction especially, was improved (economy of one loop) The algorithm was presented in the chapter 5. Overall, the computing time was reduced by a factor 150. The 1D code used here processes 2 hours of data in 70 seconds (for 1400 particles). The previous code was processing it in about 3 hours. This result must be tempered by the fact that the Scilab code performs 3D

reconstruction.

Prospects

Influence of the meta-model

It is a legitimate to wonder to what extend the presented results and conclusions are dependent from the choice of meta-model. Although a rigorous assessment (systematic cross-validation with different kernel types for example) was not possible within the allocated time, the whole sensitivity analysis was repeated with a Matérn 3/2 variogram instead of the Gaussian one. The results, in figures 8.9 to 8.12, are presented in the same way that figures 6.37 and 6.38: the tile has inputs in abscissa, outputs in ordinate and the Sobol indices of a given input for a given output is depicted in shade of color. First order simple Sobol indices (direct influence share) are in blue (figures 8.9 and 8.10). The interaction part (difference between total and simple first order indices) is in green (figures 8.11 and 8.12). The only visible difference is the line of the output N_{G0}: the interaction share is much smaller with the Matèrn variogram (as a consequence, direct effect is stronger). This difference is not clear to interpret and it does not contest the conclusions of this work. Therefore, this experiment is agreeing that the conclusions are not dependent from the choice of the meta-model.

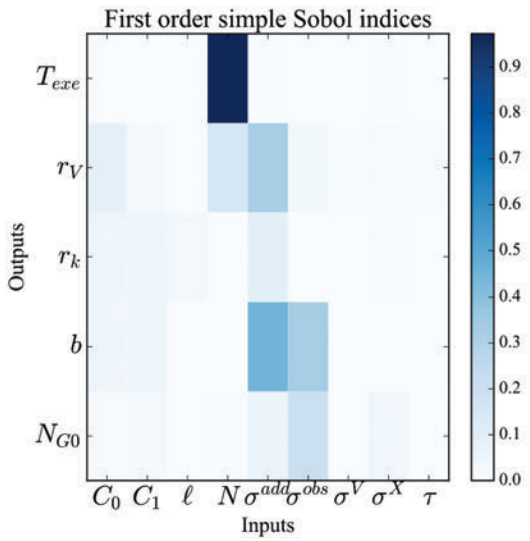

Figure 8.9 – First order Sobol indices with **Gaussian** variogram.

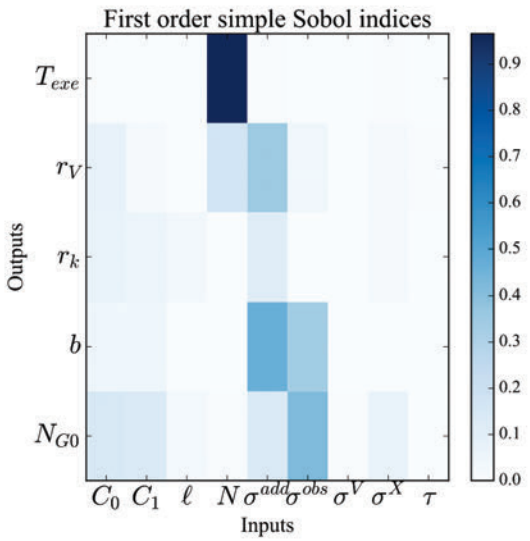

Figure 8.10 – First order Sobol indices with **Matérn 3/2** variogram.

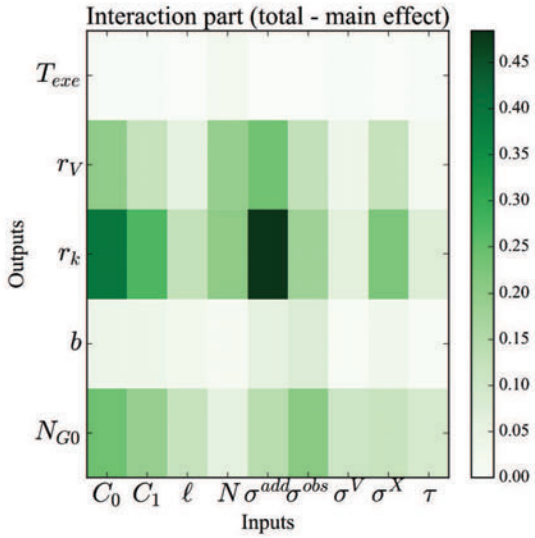

Figure 8.11 – Interaction part with **Gaussian** variogram.

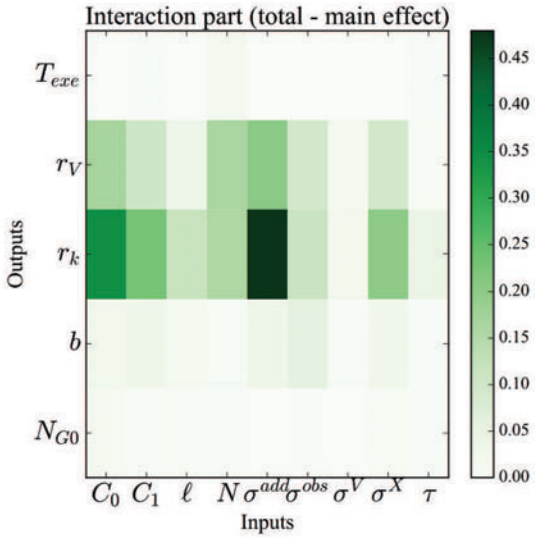

Figure 8.12 – Interaction part with **Matérn 3/2** variogram.

Estimation with penalised regression

The results presented in this thesis about the estimation of Sobol indices with penalised regression are only a demonstrative example. The method should be tested on a complete real case example, and compared to other well proven estimation methods. Mathematical properties (invariances, convergence...) of such estimators are still to be explored.

Sensitivity analysis feedback

The sensitivity analysis carried out here was the first ever done in the reconstruction. Strong of this first experiment, we can do recommendations for a second study.

The scores can be discussed. Although the initial idea of the score RMSE on TKE was worth to try, it appears to be not as informative as expected. The effects of the integration time, τ, are compensated in Sobol indices estimation. At the chapter 1, it was told that spatial and time variances cannot be compared for vertical velocity. The value of this score is not interpretable, nor are its trends. Instead, an average value of LSKTE would have been informative. The number of particles rejected at the selection is also a good indicator of malfunctions in the reconstruction. It could be a good score.

As a first attempt, the stochastic nature of the code was not taken into account (the argument is that N is always large enough to ensure convergence). In a second experiment, this aspect should be included. Likewise, instead of estimating a multidimensional Sobol index, Sobol indices have been estimated independently on each component. Although the difference of variance (due to units) was an argument to justify the average Sobol indices used

in the chapter 6, multidimensional Sobol index could be worth to be estimated the next time.

Reconstruction method

The present study was restricted to the 1-dimensional case, for two reasons: the recoding in Fortran is time-consuming and the 1D code runs faster. Given that the target of this thesis was to make the sensitivity analysis, the 1D code was enough. However, turbulence is very different in 3D (see chapter 1 and the comparison between TKE estimators) and lidar measurements are limited by the Cyclop's dilemma (while they are not in 1D). Thus, the extension to 3-dimensional case is a very interesting prospect, even if some major results (like the tuning strategy) might hold.

Known limitations of the reconstruction method have been recalled in the chapter 5. One of them is that it does not work in stable conditions. Further work on the Lagrangian model must be done in order to get a suitable model. Given the differences of nature between turbulent and stable cases, switching model techniques might be helpful to solve this issue.

The dataset used as a reference was taken in fair weather, well developed turbulence. A prospect would be to make the same study with another reference. It could tell if the present study is confirmed whatever the reference is. It is likely that the conclusion will be different if the reference is taken in sable atmosphere. Although the Lagrangian model is not expected to work in stable cases, the sensitivity analysis might points out what are the parameters to change in order to adapt the model to such cases.

Part III

Appendices

Appendix A

Theoretical background

A.1 Probability

This section intends to homogenize the knowledge common to most of readers, including those not practising probability on a daily basis. There exists already myriad of books on probability where more details (such as demonstrations) and more examples can be found. Some of them have been used to write this section, as Barbe and Ledoux (1998) (in French) and Gardiner (2009); Øksendal (2013) (in English) in addition to many roaming lectures.

A.1.1 Elements of measure theory

Let E be a non-empty space in which belong the object to measure. For example, if one wants to measure lengths, E will be the set of real numbers. The space E will be called the *state* space. The set of all parts of E is denoted by $\mathcal{P}(E)$. Parts of the state space are accessible for measure only if they are in a **σ-algebra**.

Definition A.1 (σ-algebra)**.**

With words *A σ-algebra is a subset of $\mathcal{P}(E)$ stable by complementarity and countable union.*

Formally *$\mathcal{E}$ is a σ-algebra if it satisfies the 3 following statements:*

- $E \in \mathcal{E}$
- $\forall A \in \mathcal{E},\ A^{\mathsf{c}} \in \mathcal{E}$
- $\forall n \in \mathbb{N},\ A_n \in \mathcal{E},\ \bigcup_{n\in\mathbb{N}} A_n \in \mathcal{E}$

In a set E, there are many σ-algebras. As an example, $\{\emptyset, E\}$ is a σ-algebra of E (it is called the *coarse* σ-algebra). $\mathcal{P}(E)$ is a σ-algebra of E (it is called the *discrete* σ-algebra). For any subset $A \subset E$, $\{\emptyset, A, A^{\mathsf{c}}, E\}$ is a σ-algebra of E (it is called the σ-algebra *generated by* A).

A very common σ-algebra is the one corresponding to lengths, surfaces or volumes. On $\mathbb{R}$, it is the σ-algebra generated by the intervals, denoted by $\mathcal{B}(\mathbb{R})$. On a more general space E, it is the σ-algebra generated by the open sets of E, denoted by $\mathcal{B}(E)$. Lengths, surfaces or volumes are then given by the **measure** of the elements in the σ-algebra.

Definition A.2 (Measure)**.**

With words *A measure μ is an application associating to any measurable element a positive real number, such that*

- *the measure of the empty set is zero.*
- *the measure of the union of disjoint sets is the sum of each set measure.*

Formally

$$\mu : \begin{array}{c} \mathcal{E} \longrightarrow [0, +\infty] \\ A \longmapsto \mu(A) \end{array}$$

and satisfies the 2 following statements:

- $\mu(\emptyset) = 0$
- $\forall n \in \mathbb{N}$, $A_n \in \mathcal{E}$ *such that* $\forall i \neq j$, $A_i \cap A_j = \emptyset$, $\quad \mu\left(\bigcup_{n\in\mathbb{N}} A_n\right) = \sum_{n\in\mathbb{N}} \mu(A_n)$

Intuitively, what in this definition makes it a measure? First, the fact that it is a mapping that associates to each measurable set a real number. The measure "summarizes" the set by a real number (for example its size). Second, the additivity: the size of disjoint sets is the addition of the size of all sets.

The measure defined on $\mathcal{B}(E)$ that correspond to lengths, surfaces and volumes is called the Borel measure λ. When this measure is extended to null subsets[1], it is called the Lebesgue measure and denoted Λ. [2]

Probability are measures on another space than the state space. Let space Ω be a space endowed with a σ-algebra $\mathcal{F}$. A measurable element of the probability space $A \in \mathcal{F}$ is a called an **event**. The space Ω is called the **universe**.

[1] a set N is null for the measure λ if $\exists A \in \mathcal{B}$, $N \subset A$ and $\lambda(A) = 0$

[2] Non measurable elements exist only if one accepts the axiom of choice. But this axiom is controversial because it yields to paradoxical results, such as Banach-Tarski theorem (well explained in this Youtube video). In summary any subset of $\mathbb{R}$, unless very exotic, is measurable.

Definition A.3 (Probability)**.**

With words *A probability is a measure with maximum value 1.*

Formally

$$\mathbb{P} : \begin{array}{c}(\Omega, \mathcal{F}) \longrightarrow [0,1] \\ A \in \mathcal{F} \longmapsto \mathbb{P}(A)\end{array}$$

with $\mathbb{P}(\Omega) = 1$.

Hence, the probability for an event to occur is the "size" of the event, as measured by $\mathbb{P}$.

A.1.2 Random variables

Measure theory is the starting point to study random variables. By default, random variables are real valued, for the sake of simplicity (and because the differences are most of the time an extension of the notations to complex or multi-dimensional case).

A.1.2.1 Definition

Definition A.4 (Random variable)**.**

With words *A random variable X is a measurable function from a probability space (hidden) to a state space (accessible by measurement).*

Formally

$$X : \begin{array}{c}(\Omega, \mathcal{F}, \mathbb{P}) \longrightarrow (E, \mathcal{E}) \\ \omega \longmapsto X(\omega)\end{array}$$

where X verifies

$$\forall A \in \mathcal{E},\ X^{-1}(A) \in \mathcal{F}.$$

with $\quad X^{-1}(A) = \{\omega \in \Omega : X(\omega) \in A\}$.

Given $\omega \in (\Omega, \mathcal{F}, \mathbb{P})$, the value $X(\omega)$ is called a ***realization*** *of X. The figure A.1 gives a visual sight of the notation.*

The probability space $(\Omega, \mathcal{F}, \mathbb{P})$ is considered as hidden. It is the source of randomness: nothing is known about Ω but the σ-algebra $\mathcal{F}$ and the probability $\mathbb{P}$ exist. In a coin toss, for example, Ω could be the $\mathbb{R}^3 \times \mathbb{R}^3$ space of the initial position and speed of coin... or it could be $\mathbb{R}^3 \times \mathbb{R}^3 \times \mathbb{R}^3$ space of the initial position and speed of coin and wind speed... or even more complex. Instead of trying to set what could be influencing the coin, we settle that it is

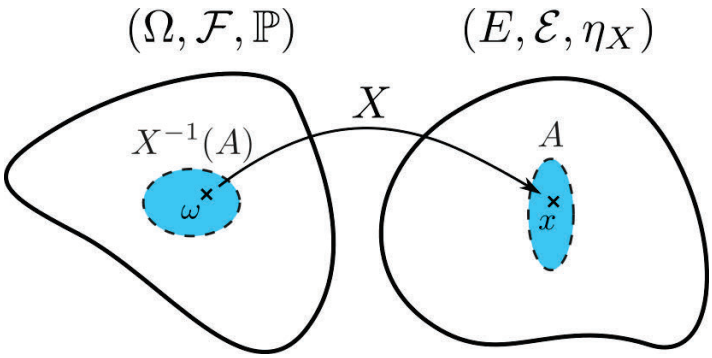

Figure A.1 – Diagram to introduce random variables: the random variable X is a measurable function from an unknown departure space Ω to a measurable arrival space E.

unknown, and the unknown part is the source of randomness. Informally, randomness is an unknown variable.

A.1.2.2 Probability law

Given a random variable X (definition A.4), the departure space $(\Omega, \mathcal{F}, \mathbb{P})$ is equipped with the measure $\mathbb{P}$. The arrival space $(E, \mathcal{E})$ is measurable. With this ingredients, one can define a measure on the arrival space: the probability law of X.

Definition A.5 (Law of a random variable)**.**

With words *The law η_X of the random variable X is the pushforward image of the probability $\mathbb{P}$ on the state space.*

Formally

$$\forall A \in \mathcal{E},\ \eta_X(A) = \mathbb{P}\left(X^{-1}(A)\right)$$

with $X^{-1}(A) = \{\omega \in \Omega,\ X(\omega) \in A\}$.

To ensure the pre-image $X^{-1}(A)$ is measurable by $\mathbb{P}$, the fact the X is a measurable function is essential. As $\mathbb{P}$ is a probability, η_X arrival values are in $[0, 1]$:

$$\eta_X : \begin{array}{ccc} \mathcal{E} & \longrightarrow & [0,1] \\ A & \longmapsto & \eta_X(A) = \mathbb{P}\left(X^{-1}(A)\right) \end{array}$$

As a consequence, η_X is also a probability on $(E, \mathcal{E})$:

$$\eta_X(E) = \mathbb{P}(\Omega) = 1 \tag{A.1}$$

A.1.2.3 Probability density function

Usually, in problems with Euclidian geometry, the state space $(E, \mathcal{E})$ is equipped with the Lebesgue measure Λ (the measure which correspond to length, areas and volumes, including negligible elements). It is very informative to know how the probability law η_X of the random variable X is different from the Lebesgue measure Λ. Both η_X and Λ are measures on $(E, \mathcal{E})$. Given a measurable element $A \in \mathcal{E}$, we want to compare $\eta_X(A) = \int_{x \in A} d\eta_X(x)$ and $\Lambda(A) = \int_{x \in A} d\Lambda(x)$. In particular, is there a weight function f_X (with which properties?) such that

$$\int_{x \in A} d\eta_X(x) = \int_{x \in A} f_X(x) d\Lambda(x)$$

The answer of this question is given by the theorem of Radon-Nikodym.

Theorem A.1 (Radon-Nikodym)**.**
Let ν and μ be two positive and σ-finite measures on the measurable space $(E, \mathcal{E})$ such that μ is absolutely continuous with respect to ν ($\forall A \in \mathcal{E}, \mu(A) = 0 \Rightarrow \nu(A) = 0$).
Then there exists a function h such that

$$h : E \to [0, +\infty[, \ / \ \forall A \in \mathcal{E}, \quad \mu(A) = \int_A h d\nu$$

.
The function h is called the Radon derivative of μ with respect to ν (or "density of μ w.r.t ν") and we denote

$$h = \frac{d\mu}{d\nu}$$

Notice that the function h is almost unique. The ambiguity relies on negligible sets for μ. The **probability density function** (or PDF) is the Radon derivative of the probability law, η_X, with respect to a measure of interest, ν.

Definition A.6 (Probability density function)**.**

With words *The probability density function of a random variable X is the weight function to compare the probability law with a measure of interest ν.*

Formally

$$f_X : \begin{array}{ccc} E & \to & [0, +\infty[\\ x & \mapsto & f_X(x) \end{array}$$

such that

$$\forall A \in \mathcal{E}, \quad \int_{x \in A} d\eta_X(x) = \int_{x \in A} f_X(x) d\nu(x)$$

To be fully exact, one should always precise the measure of interest ν to which the PDF refers. In our case, the measure of interest is the Lebesgue measure (corresponding to lengths,

surfaces and volumes): $\nu = \Lambda$. It follows that f_X is Lebesgue-integrable with integral 1.

$$\int_{x \in E} f_X(x) d\Lambda(x) = \eta_X(E) = 1 \tag{A.2}$$

The primitive of the probability function with 0 for limit when $x \to -\infty$, denoted by $F_X(x)$, is called the **cumulative distribution function** or CDF. For 1-dimentional real-valued random variable[3], it is defined by equation A.3.

$$F_X(x) = \int_{-\infty}^{x} f_X(y) dy = \eta_X(]-\infty, x]) = \mathbb{P}(X \leqslant x) \tag{A.3}$$

The last expression allows to define the CDF even when the random variable has no PDF. For example, the random variable with the Cantor function as cumulative density function has no probability density function. Indeed, the law of such a random variable is not absolutely continuous with respect to Lebesgue measure[4]. Hence the Radon-Nikodym theorem does not apply. It gives an example of a random variable that have a continuous CDF but no PDF.

A.1.2.4 Expected value

A random variable (function from unknown space) is fully described by its probability law (measure) or its probability density function (real positive valued function on the state space), when it exists. The expected value describes the central trend of the random variable by a scalar[5] denoted $\mathbb{E}[X]$. It requires additional regularity of the random variable, expressed with L^p spaces.

Definition A.7 ($\mathcal{L}^p$ space)**.**

With words *The $\mathcal{L}^p$ space (shortcut for $\mathcal{L}^p(E, F)$) is the ensemble of functions from E to F, with $(E, \mathcal{E}, \mu)$ a measured space, which are integrable at order p for the measure μ.*

Formally

$$\mathcal{L}^p(E, F) = \left\{ f \,:\, E \to F \;\middle/\; \int |f(t)|^p d\mu(t) < +\infty \right\}$$

The application $\|f\|_p = (\int |f(t)|^p d\mu(t))^{\frac{1}{p}}$ is a semi-norm for $\mathcal{L}^p$ because $\|f\|_p = 0 \not\Rightarrow f = 0$ (take $f = \mathbf{1}_{x=0}(x)$ for instance). Hence, the space $\mathcal{L}^p$ is modified in order to make $\|f\|_p$ a norm. The modification consists in merging all functions equal almost everywhere, according to μ.

[3] When $E \subset \mathbb{R}^n$, the cumulative distribution function is defined by integration on the cuboid $\otimes_{i=1}^{n}]-\infty, x_i]$.
[4] if K_3 is the Cantor set, $\eta_X([0,1] \setminus K_3) = 0$, while $\Lambda([0,1] \setminus K_3) = 1$
[5] a single element of the state space. If E is multi-dimensional, $\mathbb{E}[X]$ will be multi-dimensional as well.

Definition A.8 (L^p space)**.**

With words *The L^p space is the $\mathcal{L}^p$.*

Formally

$$L^p(E,F) = \{[f],\ f \in \mathcal{L}^p(E,F)\}$$

with $[f]$ any element of $\{g \in \mathcal{L}^p(E,F),\ \mu(\{x, f(x) \neq g(x)\}) = 0\}$.

Applied to random variables, the previous definition with $p = 1$ is an assumption to define the expected value. Let $X \in L^1(\Omega, E)$ in the following definition.

Definition A.9 (Expected value)**.**

With words *The expected value of a random variable X is the average value of X considering every element ω in the universe Ω with the measure $\mathbb{P}$.*

Formally

$$\mathbb{E}[X] = \int_{\omega\in\Omega} X(\omega) d\mathbb{P}(\omega) = \int_{x\in E} x\, d\eta_X(x)$$

The equality $\int_{\omega\in\Omega} X(\omega)d\mathbb{P}(\omega) = \int_{x\in E} x\, d\eta_X(x)$ come from the definition of η_X and the substitution $x = X(\omega)$.

When X has a probability density function, the integral can be written with the Lebesgue measure, which is easier to estimate.

$$\mathbb{E}[X] = \int_{x\in E} x\, d\eta_X(x) = \int_{x\in E} x f_X(x)\, d\Lambda(x) \tag{A.4}$$

However, the existence of $\mathbb{E}[X]$ is not guaranteed. For example, the Cauchy distribution has no expected value. Let Z be a random variable with the following PDF:

$$f_Z(z) = \frac{1}{\pi}\frac{1}{1+z^2} \tag{A.5}$$

Then $z f_Z(z) \underset{z\to\infty}{\sim} 1/(\pi z)$, thus the integral $\int z f_Z(z) dz$ does not converge. The Cauchy distribution has no expected value.

A.1.2.5 Momenta

The definition of momenta involves the expected value $\mathbb{E}[X]$. To do so, it is denoted for any test function φ such that $\int \varphi(x) f_X(x) dx$ converges[6],

$$\mathbb{E}[\varphi(X)] = \int_{x\in E} \varphi(x)\, d\eta_X(x) = \int_{x\in E} \varphi(x) f_X(x)\, d\Lambda(x) \tag{A.6}$$

[6]The equality A.6 also defines the distribution associated to X.

Momenta are the scalars obtained by choosing φ of the form $x \mapsto x^n$ with $n \in \mathbb{N}$. The integer n is called the order of the momentum. They are defined for L^n random variables.

Definition A.10 (Momenta)**.**

With words *The n-order momentum of a random variable X is the mathematical expectation of X^n.*

Formally

$$\mathbb{E}\left[X^n\right] = \int_{x \in E} x^n \, d\eta_X(x)$$

Centered momentum are often used :

$$\mathbb{E}\left[(X - \mathbb{E}\left[X\right])^n\right] = \int_{x \in E} (x - \mathbb{E}\left[X\right])^n \, d\eta_X(x) \tag{A.7}$$

In particular, the 2-order centred momentum is the variance of X :

$$V(X) = \mathbb{E}\left[(X - \mathbb{E}\left[X\right])^2\right] = \mathbb{E}\left[X^2\right] - \mathbb{E}\left[X\right]^2 \tag{A.8}$$

It is of particular interested because it is easy to interpret as the discrepancy of the random variable around the mean value. For a Gaussian random variable, mean and variance are the only parameters needed to know everything about the random variable.

A.1.2.6 Conditional probability

Briefly, we recall some useful results for conditional probability such as the law of total probability or Bayes' theorem. Let A and B be two events, with $\mathbb{P}(B) \neq 0$. The conditional probability of A given B is denoted $\mathbb{P}(A|B)$.

Definition A.11 (Conditional probability)**.**

With words *The conditional probability of A given B is the ratio between $\mathbb{P}(A \cap B)$ and $\mathbb{P}(B)$.*

Formally

$$\mathbb{P}(A|B) = \frac{\mathbb{P}(A \cap B)}{\mathbb{P}(B)}$$

The conditional probability is the probability that A and B occur, considering the event B happens for sure. The events A and B are independent if and only if $\mathbb{P}(A|B) = \mathbb{P}(A)$. Noticing that $\mathbb{P}(A|B)\,\mathbb{P}(B) = \mathbb{P}(A \cap B) = \mathbb{P}(B|A)\,\mathbb{P}(A)$ one gets Bayes' formula:

Theorem A.2 (Bayes)**.** *Let A and B be two event of $(\Omega, \mathcal{F}, \mathbb{P})$ with $\mathbb{P}(B) \neq 0$*

$$\mathbb{P}(A|B) = \frac{\mathbb{P}(B|A)\,\mathbb{P}(A)}{\mathbb{P}(B)}$$

Bayes' formula gave its name to Bayesian statistics and probability, in opposition to the historical frequentist approach. The adjective *Bayesian* has now become synonym of *using a prior knowledge*. The names of the terms in the theorem also are commonly used in a broader sense.

- $\mathbb{P}(A|B)$ is the *posterior*, usually the output of Bayes' theorem. It tells what happens after the event B has been taken into account.
- $\mathbb{P}(A)$ is the *prior*, the external knowledge one wants to exploit. It can be a theoretical insight, some expert advice or the information of a model... The choice of the prior influences widely the result. The prior knowledge has to be trustworthy to take benefit of Bayesian formulation.
- $\mathbb{P}(B|A)$ is the *likelihood*, the information usually coming from the observations. The ratio $\mathbb{P}(B|A)/\mathbb{P}(B)$ is the normalized likelihood.

Some probability laws are known only conditionally to some events. A useful tool to exploit such knowledge is the formula of total probability:

Theorem A.3 (Law of total probability)**.** *Let A be an event of $(\Omega, \mathcal{F}, \mathbb{P})$ and $(B_n)_{n\in\mathbb{N}}$ a partition of Ω and such that $\mathbb{P}(B_n) \neq 0$.*

$$\mathbb{P}(A) = \sum_{n\in\mathbb{N}} \mathbb{P}(A|B_n)\,\mathbb{P}(B_n)$$

A.2 Simulation of random variables

As presented in the previous section, random variables are "measurable functions from a probability space to a state space" (definition A.4). They induce several objects such as probability law (def. A.5), probability density function (def. A.6), cumulative distribution function (eq. A.3)... But in practice, one has to transpose these objects into numerical equivalents, so that actual manipulations on them become possible. This section intents to present how random variables are generated on a computer. It is important because the quality of the pseudo-random generator is critical for the filtering method. It also helps to understand the non-linear filtering algorithm.

A.2.1 Monte Carlo approximation

Monte Carlo approximation consists in using independent copies of the target random variable, X, to estimate valuable information about X (expected value or PDF shape for example). As in the previous section, the state space is denoted $(E, \mathcal{E}, \eta_X)$ and the probability space is denoted $(\Omega, \mathcal{F}, \mathbb{P})$. They are both measured space with respective measures η_X (probability law of random variable X) and $\mathbb{P}$. Let us consider N independent copies of X, denoted by $X^1, ..., X^N$. Throughout the manuscript, the key character "$\rightsquigarrow$" will mean "follows the law". As an example, $X \rightsquigarrow \mathcal{U}(0,1)$ means "X follows the law $\mathcal{U}(0,1)$" (uniform between 0 and 1). Thus, for any $i \in [\![1, N]\!]$, $X^i \rightsquigarrow \eta_X$ and all X^i are independent.

The expected value, $\mathbb{E}[X]$, (when it exists) is approached by an ensemble average with an almost sure convergence (strong law of large numbers). The ensemble average is an unbiased estimator of the expected value. For any test function φ, we also have almost sure convergence.

$$\mathbb{E}[\varphi(X)] = \lim_{N\to\infty} \frac{1}{N} \sum_{i=1}^{N} \varphi(X^i)$$

As the previous equality holds for any test function φ, the empirical distribution η_X^N (defined by $< \eta_X^N, \varphi >= \frac{1}{N}\sum_{i=1}^{N} \varphi(X^i)$) converges almost surely toward the target distribution η_X (defined by $< \eta_X, \varphi >= \mathbb{E}[\varphi(X)]$). The empirical distribution is expressed with Dirac distribution (δ_a is defined by $< \delta_a, \varphi >= \varphi(a)$).

$$\eta_X = \lim_{N\to\infty} \eta_X^N = \lim_{N\to\infty} \frac{1}{N} \sum_{i=1}^{N} \delta_{X^i} \tag{A.9}$$

The probability density function, $f_X(x)$, (when it exists) is approached by a histogram. The probability for X to be in a neighbourhood of a point x (let say $V_x = [x - \Delta x/2, x + \Delta x/2]$) is expressed in two ways: one involve the probability density function, the other involve the

Mathematical object (def)	**Numerical equivalent**	**Link**
Probability law (A.5)	Monte Carlo approximation	$\eta_X = \lim_{N\to\infty} \eta_X^N = \frac{1}{N}\sum_{i=1}^{N} \delta_{X^i}$
Probability density function (A.6)	Histogram	$\int_{x\in V_x} f_X(x')dx' = \lim_{N\to\infty} \frac{\lvert\{X^i \in V_x\}\rvert}{N}$
Expected value (A.9)	Ensemble average	$\mathbb{E}\left[\varphi(X)\right] = \lim_{N\to\infty} \frac{1}{N}\sum_{i=1}^{N} \varphi(X^i)$

Table A.1 – Correspondence between theoretical objects and their numerical equivalent with Monte Carlo method.

histogram.

$$\begin{aligned} \eta_X([x-\Delta x/2, x+\Delta x/2]) &= \int_{x-\Delta x/2}^{x+\Delta x/2} d\eta_X(x') \\ &= \int_{x-\Delta x/2}^{x+\Delta x/2} f_X(x')dx' \\ &= f_X(x)\Delta x + o(\Delta x) \end{aligned} \tag{A.10}$$

$$\begin{aligned} \eta_X^N([x-\Delta x/2, x+\Delta x/2]) &= \int_{x-\Delta x/2}^{x+\Delta x/2} \frac{1}{N}\sum_{i=1}^{N} \delta_{X^i}(dx') \\ &= \frac{1}{N}\sum_{i=1}^{N} \underbrace{\int_{x-\Delta x/2}^{x+\Delta x/2} \delta_{X^i}(dx')}_{=1 \text{ if } X^i\in V_x, 0 \text{ else}} \\ &= \frac{1}{N}\lvert\{i,\, X^i \in [x-\Delta x/2, x+\Delta x/2]\}\rvert \end{aligned} \tag{A.11}$$

The probability density function appears in A.10 (approximation $\Delta x \to 0$). The equation A.11 leads to the proportion of sample present in $[x-\Delta x/2, x+\Delta x/2]$. Hence, PDF are numerically visualized with histograms.

A.2.2 Pseudo-random generators

All valuable approximations in table A.1 rely on the assumption that any X^i is an independent copy of X. How to obtain such a sample numerically? The main problem is that computer are deterministic machine. Perfect randomness is thus not accessible, but it is possible to build pseudo-random generator of numbers.

Pseudo-random generators are recursive sequences chosen to vary rapidly, but still dwell inside [0,1]. Thus, pseudo-random generators provide approximation of uniform-distributed samples. The generator of Fortran 90 and Scilab languages are tested, because both have been used to implement the reconstruction algorithm. Pseudo-random generators are of the

form of the equation A.12 (Hull and Dobell, 1962).

$$\begin{cases} x_{n+1} & = & ax_n + c \text{ [mod } m] \\ x_0 & & \text{given} \end{cases} \tag{A.12}$$

The starting point x_0 is called the **random seed**. Two sequences of same length generated with the same seed will be equal, even though they look random. This a useful tool to make repeatable random experiments. The seed can also be modified manually to ensures more randomness.

A random generator is said good when it fulfils the best the next 4 qualities (by order of importance):

1. The generated sample follows is uniformly distributed (its discrepancy is low).
2. Individuals in the sample are independent.
3. The period is large.
4. The sample is quickly generated.

The associated tests are recap in the table A.2 and further details are given below.

Tested criterion	Law $= \mathcal{U}(0,1)$		Independence	Period	Speed
Test	Kolmogorov-Smirnov	χ^2	Autocorrelation	Theory	Timing

Table A.2 – Recap of criteria and tests used for the verification of the pseudo-random numbers generators

The first property is assessed with two statistical tests. The Kolmogorov-Smirnov test compares the empirical cumulative distribution function with the theoretical CDF of $\mathcal{U}(0,1)$. The statistic of the test is $t = \sup_x |F_X^N(x) - F_X(x)|$ where $F_X^N(x)$ is the empirical CDF and $F_X(x)$ is the theoretical CDF. The χ^2 test compares the empirical histogram with the theoretical one, given a number of classes. The statistic of the test is $t = \sum_{j=1}^{J} \frac{(N\hat{p_j} - Np_j)^2}{Np_j}$ where j is a class, N is the size of the sample, $\hat{p_j}$ is the empirical probability for an individual to be in the class j and p_j its theoretical equivalent. For both tests, the null hypothesis is "the sample follows a $\mathcal{U}(0,1)$". The conclusions of these tests are shown in table A.3 and A.4.

The second property is checked by having a look on the auto-correlation. In figure A.2 (resp. A.3) is shown the autocorrelation of the Scilab (resp. Fortran) sample. On both graphics, the blue dashed line draw the punctual 95% prediction interval for an autocorrelation of 0. As long as the autocorrelation remains in between the two blue dashed lines, it can be neglected. Except few overshoots, the auto-correlation is within the prediction bound of 0. Both generators can be assumed to provide independent realisations every time.

$$\chi^2 \textbf{ test : } t = \sum_{j=1}^{J} \frac{(N\hat{p_j} - Np_j)^2}{Np_j}$$

	Score t	p-value	**Conclusion**
Scilab	10.954	$0.279 > \alpha$	H_0 not rejected
Fortran	9.05	$0.4327 > \alpha$	H_0 not rejected

Table A.3 – Results of χ^2 test with $J = 10$ classes and a sample of 10^4 individuals. The first type error threshold is chosen to $\alpha = 0.05$. The null hypothesis "the sample follows a $\mathcal{U}(0, 1)$" is accepted for both Scilab and Fortran generators.

$$\textbf{Kolmogorov-Smirnov test : } t = \sup_x |F_N(x) - F(x)|$$

	Score t	p-value	**Conclusion**
Scilab	0.0093	$0.3473 > \alpha$	H_0 not rejected
Fortran	0.0084	$0.4829 > \alpha$	H_0 not rejected

Table A.4 – Results of Kolmogorov-Smirnov test with a sample of 10^4 individuals. The first type error threshold is chosen to $\alpha = 0.05$. The null hypothesis "the sample follows a $\mathcal{U}(0, 1)$" is accepted for both Scilab and Fortran generators.

The third criterion (the periodicity) is given by the parameters in the equation A.12. For Fortran, the value of $2^{32} - 1$ is given in Marsaglia et al. (2003) for 1-dimensional samples. For Scilab, the documentation of the `rand` function gives the value of 2^{31}. Both are of order of magnitude 10^9. If the program needs more random values than the period, the generated sequence of random value will start over within a run of code. Having a large period ensures the pseudo-random generators are "random" until the end. To avoid this shortcoming, the random seed is reset to a new value at different moments in the program.

The last criterion (speed) is tested by timing the generation of the 10^4 values.

The four criteria and their test are given in the table A.2. The table A.5 gives the conclusions of these tests : both are good enough pseudo-random generators, Fortran's one is better for both speed and period.

Langage	**Time to generate 10^4 values (s)**	**Period**	**Independence**	**Uniformity**
Fortran	$2.3 \cdot 10^{-4}$	$2^{32} - 1$	OK	OK
Scilab	$3 \cdot 10^{-2}$	2^{31}	OK	OK

Table A.5 – Conclusions of all tests carried out on both generators. Both are good for use, but Fortran's one is way faster.

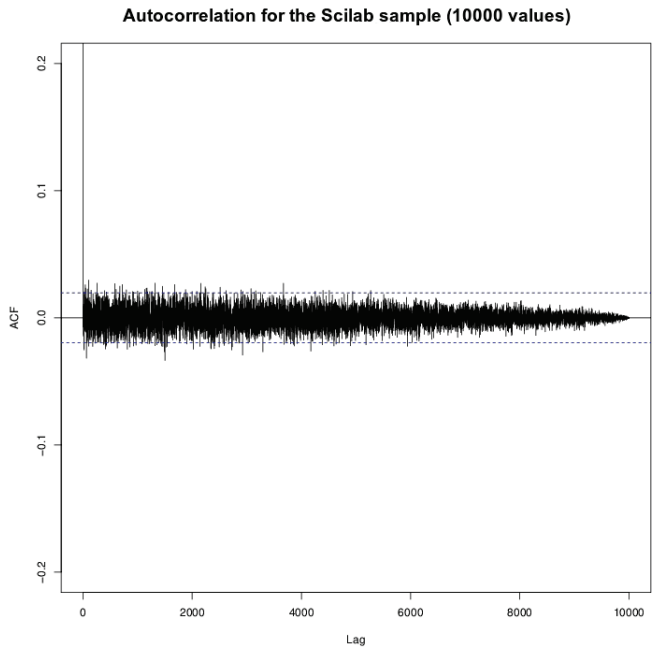

Figure A.2 – Autocorrelation of Scilab sample of 10000 values. Values inside the two dashed blue lines are in the punctual 95% prediction interval of a 0 correlation estimation.

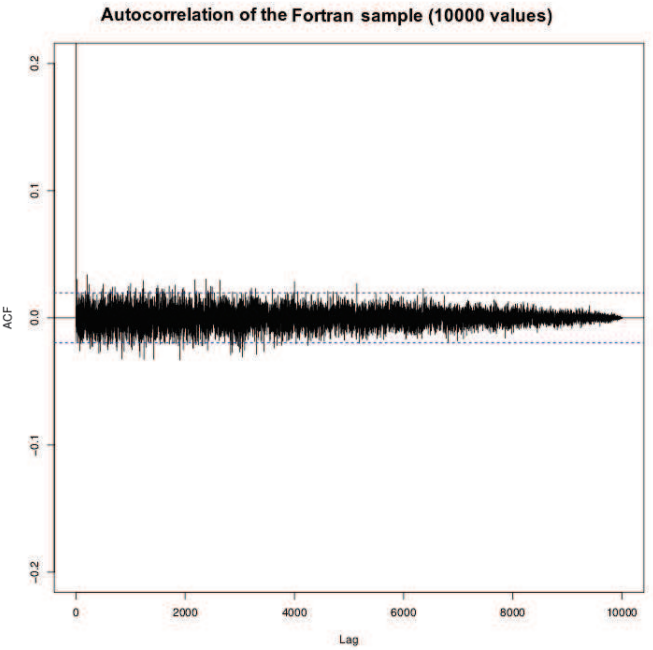

Figure A.3 – Autocorrelation of Fortran sample of 10000 values. Values inside the two dashed blue lines are in the punctual 95% prediction interval of a 0 correlation estimation.

A.2.3 Non-uniform sampling

As we have seen, pseudo-random generators provide good approximation of uniform-distributed samples. Others distributions are generated from uniform-distributed samples. Specific solutions exist to generate Gaussian-distributed sample (such as Box-Muller algorithm (Box et al., 1958)). We are interested in the simulation of *any* distribution. The distribution transform is used in the filtering method, to generate the posterior from the prior and the likelihood.

To describe the target distribution, the simplest way is to have a PDF (possibly unnormed). Let $G(x)$ a function on E that we call the **potential**. The potential associates to any x its weight in the target distribution. The interpretation of $G(x)$ is similar to $f_X(x)$. As a consequence, G have to be a real positive and integrable function.

$$G : \begin{array}{ccc} \mathbb{R} & \to & [0, +\infty[\\ x & \mapsto & G(x) \end{array} \qquad \text{with } \int_{-\infty}^{+\infty} G(y)dy < +\infty \tag{A.13}$$

Let $(u^i)_{i\in[\![1,N]\!]}$ be an uniform-distributed Monte Carlo sample. From this sample, we want to build a G-distributed sample $(x^i)_{i\in[\![1,N]\!]}$. As an example, we will take G the function drawn in blue on A.4 (sum of 2 Gaussian because bi-modal and simple). The potential G is an unnormed PDF. To get an actual PDF, one must use $G/\int G(y)dy$. Its associated normed

CDF is denoted w and is defined by equation A.14.

$$\forall x \in \mathbb{R}, \quad w(x) = \frac{\int_{-\infty}^{x} G(y)dy}{\int_{-\infty}^{+\infty} G(y)dy} \tag{A.14}$$

On figure A.4, an example of G is drawn in blue line and the corresponding w is drawn in red.

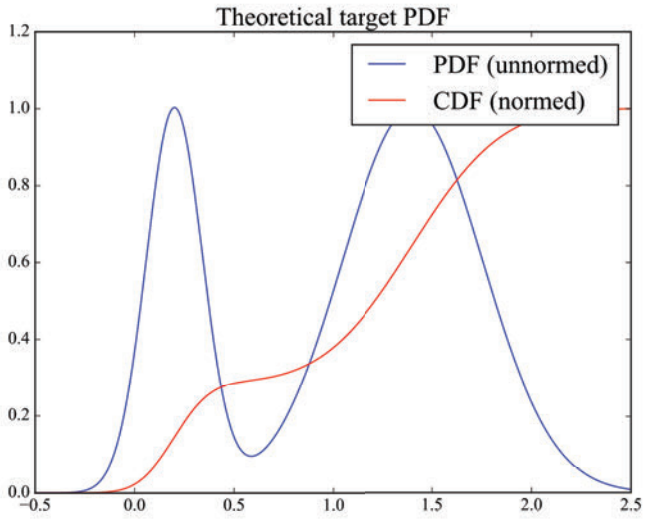

Figure A.4 – Example of unnormed PDF (or potential) G in blue (sum of 2 Gaussian) and its associated normed CDF w.

The cumulative density function goes from the range of variation of X to $[0, 1]$ and is steeper where G is high. An uniform-distributed sample is converted into a G-distributed sample by inverting the cumulative density function. Hence, one can build the G-distributed sample by applying the inverse of w to every $(u^i)_{i\in[\![1,N]\!]}$ (A.15).

$$\forall i \in [\![1, N]\!], \; x^i = \inf\{x, \, w(x) > u^i\} \tag{A.15}$$

In figure A.5, one can see an uniform-distributed sample $(u^i)_{i\in[\![1,N]\!]}$ on the y-axis, for which every element is inverted with the w function (same example as in figure A.4). Thus, on the x-axis is shown the resulting sample $(x^i)_{i\in[\![1,N]\!]}$ which is build according the relation A.15.

Theoretically, we have seen how to generate G-distributed random variable, for any real positive integrable function G. But in practice, computer do not use analogic functions but arrays of data. Hence, it is necessary to convert the previous reasoning in the discrete case in order to get an algorithm.

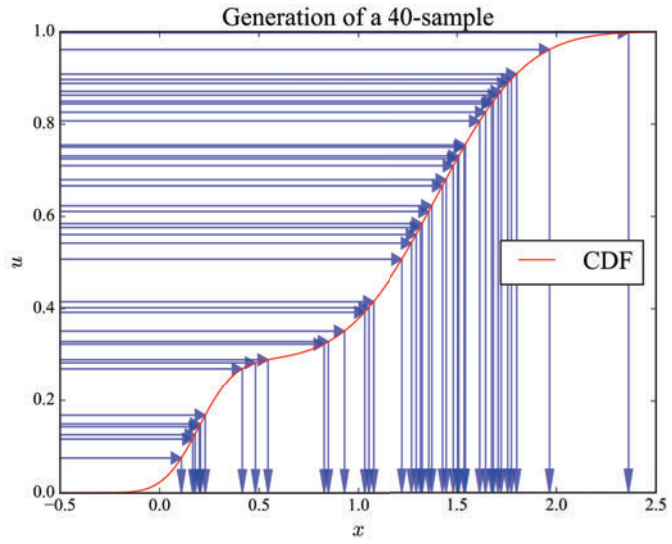

Figure A.5 – An uniform sample is changed into the target law sample using the inversion of CDF. On the y-axis, arrows are uniform-distributed, on the x-axis they are G-distributed.

Now $\mathbf{G}$ denotes an array of size M, ($\mathbf{G} = (G_1, ..., G_M) \in \mathbb{R}^M$) which gives the potential on a discrete set of points $\mathbf{x} = (x_1, ..., x_M) \in \mathbb{R}^M$[7]. For any $k \in [\![1, M]\!]$, $G_k = G(x_k)$. In this framework, $\mathbf{w} = (w_1, ..., w_M) \in \mathbb{R}^M$ is the discrete CDF, and its definition equation of w (A.14) is changed into (A.16):

$$\forall k \in [\![1, M]\!], \quad w_k = \frac{\sum_{m=1}^{k} G_m}{\sum_{m=1}^{M} G_m} \tag{A.16}$$

The inversion of w is modified as well, because the infimum has to belong to $\mathbf{x}$. Using the fact that $\mathbf{w}$ is a sorted array, the operation (A.15) is slightly modified into (A.17).

$$\forall i \in [\![1, N]\!], \; x^i = x_k \;\; \text{with } k = \min_{m \in [\![1,M]\!]} \{w_m > u^i\} \tag{A.17}$$

Gathering all the previous elements together, the algorithm A.1 is able to generate sample according to the potential G. This algorithm has been applied to the example given in figures A.4 and A.5 with $M = 1000$ (number of points in the discretization) and $N = 5000$ (size of the sample). The result is shown in figure A.6. One can see that the normed histogram (Monte Carlo equivalent of PDF) is closely comparable to the target PDF (normed potential G). It proves that the algorithm A.1 correctly simulate G-distributed random variable. This algorithm will be used many times to produce samples according to an empirical probability law, only described by arrays of number.

[7]Beware: x_k is a point on which $\mathbf{G}$ is known, x^i is a element of generated sample.

Algorithm A.1 Generate G-distributed samples : $X = \text{sampling}(\mathbf{G}, \mathbf{x})$

Input: $\mathbf{G} = (G_1, ..., G_M)$, $\mathbf{x} = (x_1, ..., x_M)$ # with $G_k = G(x_k)$
Output: $X = (x^1, ..., x^N) \rightsquigarrow G$
  $U = (u^1, ..., u^N) \rightsquigarrow \mathcal{U}(0, 1)$
  $\mathbf{w} = \text{cumsum}(\mathbf{G})/\text{sum}(\mathbf{G})$
  for $i \in [\![1, N]\!]$ **do**
    $k = \min_{m, \in [\![1,M]\!]}\{w_m > u^i\}$
    $x^i = x_k$
  end for
  return $X = (x^1, ..., x^N)$

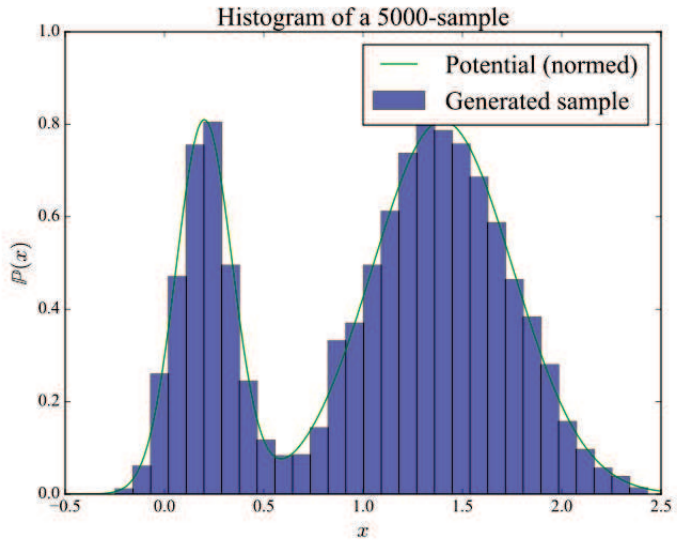

Figure A.6 – Example of generation of samples with the algorithm A.1. Histogram of the sample follows the shape of the potential G given.

A.3 Stochastic processes

The random variables used to describe physical phenomenon might be changing with time. Hence we introduce stochastic processes ("stochastic" has exactly the same sense as "random", but "stochastic" is the word in use). Introduction to stochastic processes can be found in Øksendal (2013) and Gardiner (2009).

Definition A.12 (Stochastic process)**.**

With words *A stochastic process is a family of random variable.*

Formally $(X_t)_{t\in[0,T]}$ *is a stochastic process means that*

$$\forall t \in [0,T],\ X_t : \begin{array}{c}(\Omega, \mathcal{F}, \mathbb{P}) \longrightarrow (E, \mathcal{E}) \\ \omega \longmapsto X_t(\omega)\end{array} \text{ is a random variable.}$$

with $T > 0$.
However, the trajectory of X_t *(the function* $t \mapsto X_t(\omega)$, $\forall \omega \in \Omega$*) is deterministic.*

A stochastic process is thus a function which depends on an random event: a "random function". Although, unlike a function, there is no representative curve for a stochastic process. Instead, one can draw its momentum or few trajectories. The average is a deterministic function ($t \mapsto \mathbb{E}[X_t]$). The variance is a deterministic function ($t \mapsto V(X_t) = \mathbb{E}\left[(X_t - \mathbb{E}[X_t])^2\right]$). Momenta provide only a partial information on the stochastic process. However, they help to get a mental image of a stochastic process. This is now illustrated on two famous examples: the Brownian motion, and the solution of Langevin equation.

A.3.1 The Brownian motion

In figure A.7 is shown an example of stochastic process with $\mathbb{E}[X_t] = 0$ and $\text{cov}(X_t, X_s) = \min(t, s)$. Some trajectories are drawn in red. The ensemble of trajectories expend around the mean following the increasing variance (dashed blue lines). From a single trajectory it is not obvious to see that expansion (figure A.8). This is why plotting several trajectories is a way to visualize the "random dimension": some features of the trajectory are explained by the global trend (the expansion), and other are just due to randomness (the side of expansion, local variations). For example, if one would have only the average value and a single realization (as in figure A.8) one would conclude that the realisation is in disagreement with the average, although it is simulated in the exact same way as in figure A.7.

We underline here a common problem in signal processing : how to infer about stochastic process from a single realisation? This point will be addressed in section A.4 (page 273).

The stochastic process shown figure A.7 is a really famous stochastic process: the Brownian motion. Its name comes from the biologist Robert Brown that was the first to observe it in the movement of particles inside a fluid in 1827. In 1905, Albert Einstein describes quantitatively this random movement of particles and links it with the diffusion equation (Einstein (1905), §4). The formal construction of Brownian motion as a stochastic process was done by Norbert Wiener in 1923. Hence the Brownian motion is also called a Wiener process. Its formal definition is the following:

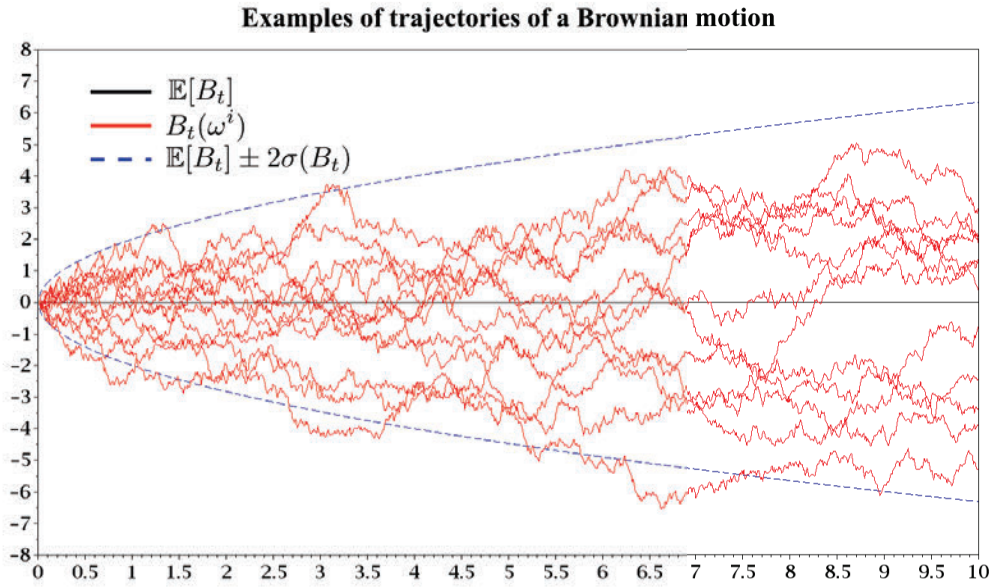

Figure A.7 – Example of stochastic process (Brownian motion): its average value (black) and its standard variation (dashed blue) give hints on the behaviour of realizations (red).

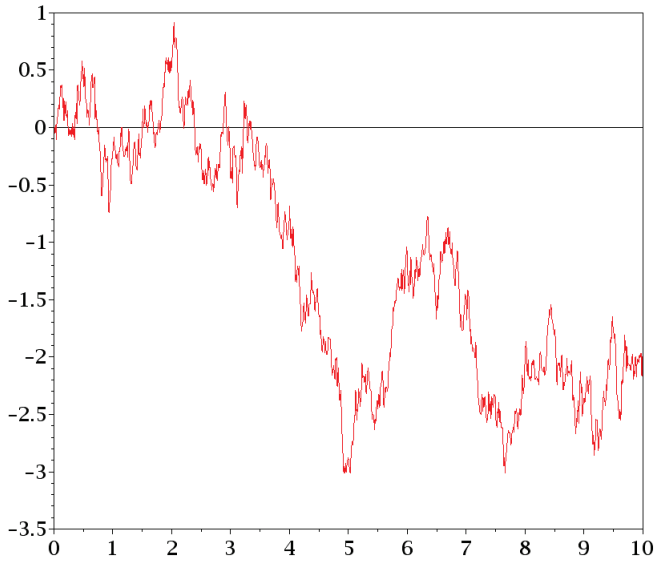

Figure A.8 – Same stochastic process (Brownian motion) with only its average value (black) and one realization (red).

Definition A.13 (Brownian motion)**.**

With words *We call a Brownian motion a Gaussian process $(B_t)_{t\in[0,T]}$ with mean zero and with covariance equal to the smallest time.*

Formally *Given $T > 0$,*

$$\forall t, s \in [0,T],\ \mathbb{E}[B_t] = \mathbb{E}[B_s] = 0,\ \mathrm{cov}(B_t, B_s) = \min(s,t)$$

where a *Gaussian process* is

Definition A.14 (Gaussian process)**.**

With words *A stochastic process $(X_t)_{t\in[0,T]}$ is Gaussian when every sample of it form a Gaussian vector (i.e. all linear combination of samples is Gaussian).*

Formally

$$\forall n \in \mathbb{N},\ \forall t_1, ..., t_n \in [0,T],\ \forall \theta \in \mathbb{R}^n,\ \sum_{i=1}^{n} \theta_i X_{t_i} \text{ is Gaussian}$$

In particular we have $B_t \rightsquigarrow \mathcal{N}(0, |t|)$ Hence its mean, variance and auto-covariance are given by

- $\mathbb{E}[B_t] = 0$
- $V(B_t) = |t|$
- $\mathrm{cov}(B_t, B_s) = \min(t, s)$

A.3.2 The Langevin equation

Another example is the Ornstein-Uhlenbeck process. It is the solution of the Langevin equation, which was historically made to describe the movement of a "large particle" dropped in a viscous fluid.

$$dV_t = -\frac{1}{\tau} V_t dt + \sigma dB_t \tag{A.18}$$

The equation A.18 is of different nature than usual partial differential equation: it is a stochastic differential equation (i.e. a differential equation on stochastic processes). Fundations of stochastic differential equations can be found in any course on stochastic calculus, and also in the book of Øksendal (Øksendal, 2013) and Gardiner (Gardiner, 2009). Stochastic differential equation relies on Ito integral (integral of a stochastic process along a stochastic process). The complete form of equation A.18 using Ito integral is

$$V_t - V_0 = \int_0^t -\frac{1}{\tau} V_s ds + \int_0^t \sigma dB_s \tag{A.19}$$

but the "differential" form is often preferred because it is shorter.

Using several theorem based on Ito integral, it is possible to solve the equation A.18 (see Gardiner (2009) p.103, Øksendal (2013) p. 71).

$$V_t = V_0 e^{-\frac{t}{\tau}} + \sigma \int_0^t e^{-\frac{t-s}{\tau}} dB_s \tag{A.20}$$

In particular, it gives an analytic expression of the mean, the variance and the auto-covariance of the solution process (Gardiner (2009) p. 104):

- $\mathbb{E}[V_t] = \mathbb{E}[V_0]\, e^{-\frac{t}{\tau}}$
- $V(V_t) = \sigma^2 \frac{\tau}{2} + \left(V(V_0) - \sigma^2 \frac{\tau}{2} \right) e^{-2\frac{t}{\tau}}$
- $\mathrm{cov}(V_t, V_s) = \left(V(V_0) - \sigma^2 \frac{\tau}{2} \right) e^{-\frac{t+s}{\tau}} + \sigma^2 \frac{\tau}{2} e^{\frac{t-s}{\tau}}$

Numerically, it is possible to simulate some trajectories (see figure A.9). One can see in

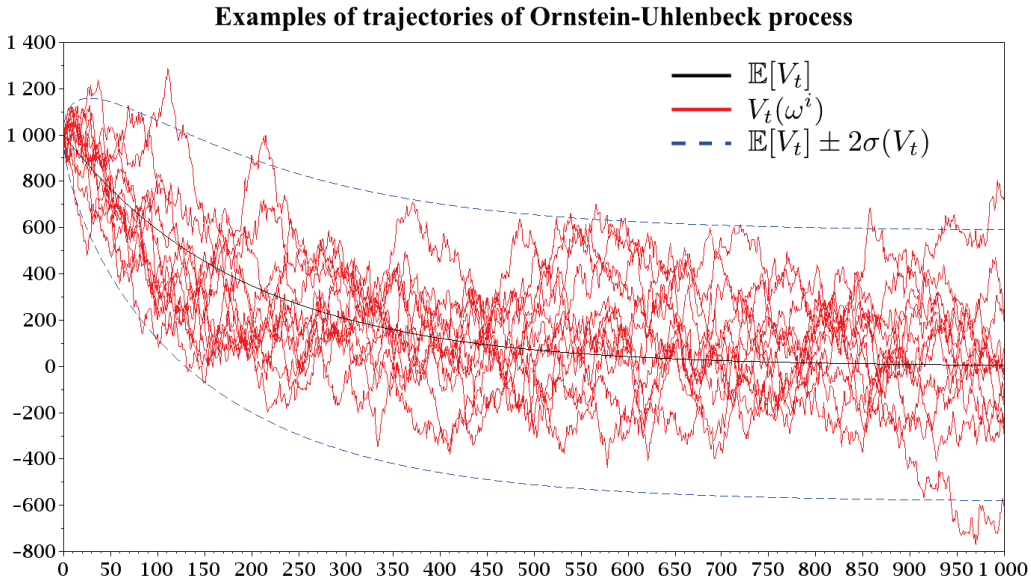

Figure A.9 – Same Ornstein-Uhlenbeck process (solution of Langevin equation): average (black) framed by standard variation (dashed blue) and few realizations.

figure A.9 that the behaviour of Ornstein-Uhlenbeck process is really different from the Brownian motion. While the average of Brownian motion is always equal to zero, the average of Ornstein-Uhlenbeck process is a converging exponential. While Brownian motion is infinitely expanding, the variance of Ornstein-Uhlenbeck process converges toward a constant value.

Physically, Langevin equation is a model for the movement of a "large particle" dropped in a viscous fluid. From figure A.9, we can tell that the particle will globally slow down in a first phase (until time-step 400) and get stabilized around a constant speed in a second phase.

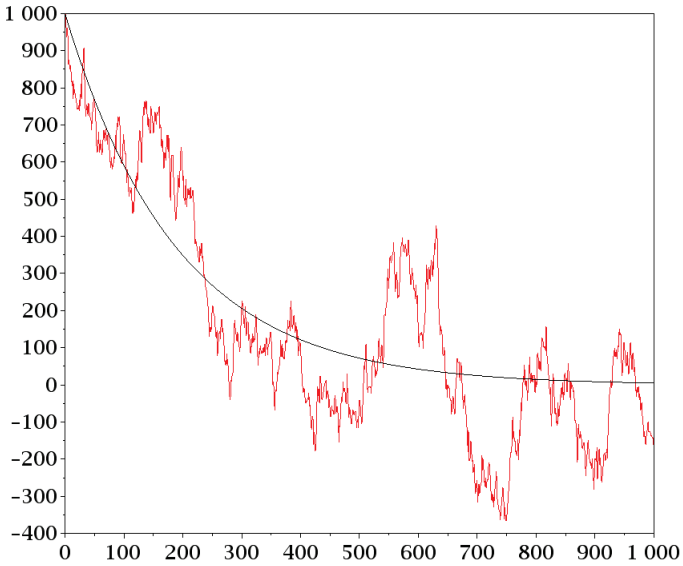

Figure A.10 – The Ornstein-Uhlenbeck process with only its average value (black) and one realization (red).

In this case, a single realization (as in figure A.10) will conserve the most important features of global process: first phase of decreasing, second phase around the average. The single realisation is more informative about the whole process.

A.4 Signal processing

Wind measurements are stochastic processes (because of random turbulence and random instrumental noise). What the instrument provides is a single realisation of the stochastic process "wind". This section aims to clarify how the realisation helps to know the stochastic process from which it is produced.

A.4.1 Stationarity and ergodicity

With time series of a single realization, we can compute statistics to describe the probability law of the signal. We consider only real-valued signals indexed by $t \in [0, T]$ with $T > 0$. The first assumption to do so is that the probability law of the signal does not change while we compute the statistics. This assumption is called **stationarity** :

Definition A.15 (Stationarity)**.**

With words *A signal is said stationary if the joint law of a time-sample does not change by translation in time*

Formally

$$\forall d \in \mathbb{N},\, \forall t_1, ..., t_d,\, \forall \tau,\, Law(X_{t_1}, ..., X_{t_d}) = Law(X_{t_1+\tau}, ..., X_{t_d+\tau})$$

This definition is stronger than just "the probability law of the signal does not change with time". Indeed, if a signal is stationary in the sense given by definition A.15, then $\forall t_1, t_2,\, Law(X_{t_1}) = Law(X_{t_2})$ (if we choose $\tau = t_2 - t_1$). So it is correct to say that if a signal is stationary, its probability law does not change with time. But the definition A.15 avoid also other problematic cases.

A weaker definition of stationarity is limited to the invariance of the p first moments (from Priestley (1981), def. 3.2.2).

Definition A.16 (Stationarity at order p)**.**

With words *A signal is said stationary at order p if the momenta up to p of the joint law of a time-sample does not change by translation in time.*

Formally

$$\forall d \in \mathbb{N},\, \forall t_1, ..., t_d,\, \forall \tau,\, \forall k \leqslant p,\, \mathbb{E}\left[(X_{t_1}^k, ..., X_{t_d}^k)\right] = \mathbb{E}\left[(X_{t_1+\tau}^k, ..., X_{t_d+\tau}^k)\right]$$

where $\mathbb{E}[\cdot]$ refers to the joint law.

In particular, the stationarity at order p ensures that the momenta only depends on the time

difference. For example, $\text{cov}(X_{t_1}, X_{t_2})$ depends only on $|t_1 - t_2|$.

$$V((X_{t_1}, X_{t_2})) = \begin{pmatrix} V(X_{t_1}) & \text{cov}(X_{t_1}, X_{t_2}) \\ \text{cov}(X_{t_1}, X_{t_2}) & V(X_{t_1}) \end{pmatrix} = V((X_0, X_{t_2 - t_1}))$$

if one takes $t_2 > t_1$ and $\tau = t_1$ in the definition.

As Gaussian processes are naturally very widespread, the process stationary at order 2 are common. Hence, it is sometimes said **weak-sense stationary**, which refers to process stationary at order 2. This definition is sufficient for most of applications.

Some applications (like kriging) do not require weak stationarity but only stationarity on the increments of the process. Such class of process are called **intrinsic**.

Definition A.17 (Intrinsic process)**.**

With words *A random signal X_t is intrinsic when its increments are centred with a variance depending only on the difference of time.*

Formally *X_t is intrinsic* $\iff$

- $\forall t, s,\ \mathbb{E}\left[X_{t+s} - X_t\right] = 0$
- $\exists \gamma : [0, +\infty[\to \mathbb{R},\ \forall t, s,\ V(X_{t+s} - X_t) = 2\gamma(s)$

Intrinsic processes are not necessarily stationary (not even at order one). For example, the Brownian motion is intrinsic but it is not stationary, as we will see later. Conversely, processes stationary at order 2 are intrinsic. Intrinsic process is the minimum property to introduce the tools that are commonly used in signal processing, such as:

- The mean :
$$\mu_X = \mathbb{E}\left[X_t\right]$$
- Autocovariance :
$$C_X(s) = \text{cov}(X_{t+s}, X_t)$$
- Autocorrelation :
$$\rho_X(s) = \frac{\text{cov}(X_{t+s}, X_t)}{\sqrt{V(X_t)\, V(X_{t+s})}}$$
- Variogram :
$$\gamma_X(s) = \frac{1}{2} V(X_{t+s} - X_t)$$

Autocovariance, autocorrelation and variogram are related in the case of stationary process at order 2. In this case, the mean μ_X and the variance σ_X^2 are constant.

$$V(X_{t+s} - X_t) = V(X_{t+s}) + V(X_t) - 2\text{cov}(X_{t+s}, X_t) = 2\sigma_X^2 - 2\text{cov}(X_{t+s}, X_t) \qquad \text{(A.21)}$$

Hence

$$\gamma_X(s) = \sigma_X^2 - C_X(s) \tag{A.22}$$

These probabilistic parameters are interesting because they give an intuitive interpretation of the process. Intuitively, the larger is s, the less X_{t+s} is linked to X_t. Hence, the form of C_X give an information about the "memory" of the process. A process with "long range memory" (i.e. with C_X decreasing slowly) does not need to be observed very often, because it is predictable. A process with "short range memory" (i.e. with C_X decreasing quickly) requires many observations to be described.

Stationarity is useful to define statistics invariant with time and thus common for a whole time series. But it is not enough to estimate these statistics from a single realization $x(t)$ of X_t. Such a realisation must be representative of the whole process: explore the same area of values, have the same variability. This property is called **ergodicity**. More precisely, under which condition is the time average is comparable to the expected value?

Let X_t be a stochastic process stationary at order 2. The time average is the stochastic process given by

$$M_\tau = \frac{1}{\tau}\int_0^\tau X_t dt \tag{A.23}$$

Since X_t is stationary at order 2, its average is constant and its auto-covariance depends only on the time gap ($\mathbb{E}[X_t] = \mu_X$ and $\mathbb{E}[X_{t_1}X_{t_2}] - \mu_X^2 = C_X(t_2 - t_1)$). Mean and variance of M_τ are expressed with these quantities.

$$\mathbb{E}[M_\tau] = \frac{1}{\tau}\int_0^\tau \mathbb{E}[X_t]\, dt = \mu_X \tag{A.24}$$

$$\begin{aligned}
V(M_\tau) &= \mathbb{E}\left[\left(\int_0^\tau X_t dt\right)^2\right] - \mu_X^2 \\
&= \frac{1}{\tau^2}\mathbb{E}\left[\int_{[0,\tau]^2} X_{t_1}X_{t_2} dt_1 dt_2\right] - \mu_X^2 \\
&= \frac{1}{\tau^2}\int_{[0,\tau]^2} C_X(t_2 - t_1) dt_1 dt_2 \\
&= \frac{1}{\tau^2}\int_{-\tau}^{\tau} dt \int_{-\tau}^{\tau} C_X(s) ds \qquad \text{with } s = t_2 - t_1, t = t_1 \\
&= \frac{2}{\tau}\int_0^\tau C_X(s) ds \qquad \text{because } C_X \text{ is even}
\end{aligned} \tag{A.25}$$

The time average M_τ (stochastic process) will be comparable to the expectation μ_X (scalar) if its variance tends to 0. This requires $\int_0^\tau C_X(s)ds = o\left(\frac{1}{\tau}\right)$. In particular, having $\int_0^{+\infty} C_X(s)ds < \infty$ is enough. Under this condition, the time average approximates correctly the expectation.

$$\text{For any } x(t) \rightsquigarrow X_t, \qquad \lim_{\tau\to\infty}\frac{1}{\tau}\int_0^\tau x(t)dt = \mu_X \tag{A.26}$$

For stochastic process less regular than stationary at order 2, it is still possible to define ergodicity but the criteria are readable. Let X_t be a non-stationary process, one can define the measure corresponding to the time average:

$$\nu_\tau : A \in \mathcal{E} \mapsto \frac{1}{\tau}\int_0^\tau \mathbb{P}\left(X_t \in A\right) dt \tag{A.27}$$

$\nu_\tau(A)$ is the ratio between the time X_t has spent in A versus the total time τ. If the random variable M_τ follows the law ν_τ, its expectation is given by $\mathbb{E}\left[M_\tau\right] = \int_E x\nu_\tau(dx) = \frac{1}{\tau}\int_0^\tau \int_E x\mathbb{P}\left(X_t \in dx\right) dt = \frac{1}{\tau}\int_0^\tau \mathbb{E}\left[X_t\right] dt$. Its variance is given by $V(M_\tau) = \frac{1}{\tau}\int_0^\tau V(X_t) + \frac{1}{\tau}\int_0^\tau \mathbb{E}\left[X_t\right]^2 - \frac{1}{\tau^2}\left(\int_0^\tau \mathbb{E}\left[X_t\right]\right)^2$. When it converges, the limit of ν_τ when $\tau \to +\infty$ is the equilibrium measure ν. A random variable following ν would be a "infinite time average". But the link between the expectation of the equilibrium measure and the expectation of X_t is subject to additional hypothesis. In consequence this manuscript will only focus on processes stationary at order 2, as ergodicity is not the core of the problem.

Definition A.18 (Ergodicity)**.**

With words *A random signal X_t is ergodic when its mathematical expectation can be approached by a time average. In particular, processes stationary at order 2 are ergodic their auto-covariance decreases faster than $1/\tau$.*

Formally

$$\lim_{\tau\to\infty} \mathbb{E}\left[\frac{1}{\tau}\int_0^\tau X_t dt\right] = \mu_X \text{ and } \lim_{\tau\to\infty} V\left(\frac{1}{\tau}\int_0^\tau X_t dt\right) = 0$$

If X_t is stationary at order 2, it is equivalent to

$$\int_0^\tau C_X(s) ds = o\left(\frac{1}{\tau}\right)$$

There is thus a distinction to make between theoretical quantities and reachable approximation of them. The link between them relies on these 2 strong assumptions : stationarity and ergodicity. Although there are strong, we usually assume they are verified because it is the only way to make signal processing. Theoretical and approached mean and auto-covariance are summarized in table A.6.

	Theoretical	**Approached**
Mean	$\mu_X = \mathbb{E}\left[X_t\right]$	$m_x(\tau) = \frac{1}{\tau}\int_0^\tau x(t)dt$
Auto-covariance	$C_X(s) + \mu_X^2 = \mathbb{E}\left[X_t X_{t+s}\right]$	$R_{xx}(\tau, s) = \frac{1}{\tau}\int_0^\tau x(t)x(t+s)dt$

Table A.6 – Theoretical and approached expression of mean and auto-covariance under stationarity and ergodicity assumption.

For stationary and ergodic processes, these statistics are the best approximation one can

have :

$$\mu_X = \lim_{\tau \to \infty} m_x(\tau) \tag{A.28}$$

$$C_X(s) + \mu_X^2 = \lim_{\tau \to \infty} R_{xx}(\tau, s) \tag{A.29}$$

Stationarity and ergodicity are the necessary hypothesis to infer properties of random process X_t from a single realization of it $x(t) = X_t(\omega)$. Since in most cases it is impossible to reproduce exactly the same experiment (especially in fluid dynamics), it is generally assumed that processes are stationary and ergodic, so it is possible to make signal processing on them.

The validity of these hypothesis depend strongly on the choice of the integration time τ. Indeed, a long integration time gives a better approximation of the expected value with time average (it ensures ergodicity). But a long integration time let the time for the signal probability law to change (it unvalidates stationnarity). On the other hand, a the signal probability law is more likely to stay the same within a short integration time (it ensures stationarity). But a short integration time deteriorates the approximation of mathematical expectation with time average (it unvalidates ergodicity).

A.4.2 Fourier transform

The Fourier transform is the basis of many interpretations in signal processing, as it makes the connection between the time-space and the frequency-space. At first, it is defined only for periodic functions, that we decompose in pure harmonics : it yields to Fourier series. The periodic function is described by a collection of coefficients that quantify the contribution of a frequency in the signal. Fourier transform is an extension of that to any integrable function. The integrable function is described by another function, that gives the continuous contribution of frequencies in the signal. The mean value is not important for spectral analysis, therefore the process X_t is supposed centred for this section.

Definition A.19 (Fourier transform)**.**

With words *The Fourier transform a function of time $x(t)$ is the decomposition of the signal onto a basis of purely oscillating functions. The result is a function of frequency $\hat{x}(\xi)$ giving the contribution of the frequency ξ in the original signal.*

Formally

$$\forall x \in L^1(\mathbb{R}, \mathbb{R}),\ \hat{x}(\xi) = \int_{-\infty}^{+\infty} x(t) e^{-i\xi \cdot t} dt$$

But most of the time, we use square-integrable function (function in L^2, not necessarily in L^1). The integral in the given definition of Fourier transform is not defined for L^2 functions. Fourier transform is extended to L^2 space by using the density of $L^1 \cap L^2$ in L^2 and the

continuity of the integral. On L^2, Fourier transform is a linear operator can conserve most of the properties of its L^1 equivalent.

Given a realisation $x(t)$ of the stochastic process X_t, the function $x : t \in [0, +\infty[\mapsto \mathbb{R}$ is assumed $L^1([0, +\infty[, \mathbb{R})$ and $L^2([0, +\infty[, \mathbb{R})$. The signal $x(t)$ is prolonged for $t < 0$ by 0.

A.4.3 Power spectral density

To visualize the frequency information brought by Fourier transform, we use the power spectral density. It represents the energetic contribution of frequencies.

Definition A.20 (Power spectral density)**.**

With words *Power spectral density is the Fourier transform of the autocorrelation.*

Formally

$$\Gamma_x(\xi) = \int_{s\in\mathbb{R}} \mathbb{E}\left[X_{s-t}X_t\right] e^{-i\xi\cdot s} ds$$

This definition is applied to ergodic and stationary processes to reach a computable expression. The auto-covariance is approximated as described in table A.6 :

$$\mathbb{E}\left[X_{s-t}X_t\right] = \lim_{\tau\to\infty} \frac{1}{\tau} \int_0^\tau x(t)x(s-t)dt \tag{A.30}$$

Wiener-Khinchin theorem gives another expression of the PSD, sometimes taken as definition (see Miller and Childers (2012), def. 10.1). Here is a sketch of the proof.

$$\begin{aligned}
\Gamma_x(\xi) &= \int_{s\in\mathbb{R}} \left(\lim_{\tau\to\infty} \frac{1}{\tau} \int_0^\tau x(t)x(s-t)dt \right) e^{-i\xi\cdot s} ds \\
&= \lim_{\tau\to\infty} \frac{1}{\tau} \int_{s\in\mathbb{R}} \int_0^\tau x(t)x(s-t)e^{-i\xi s} dt ds \\
&= \lim_{\tau\to\infty} \frac{1}{\tau} \int_0^\tau x(t) \underbrace{\left(\int_{s\in\mathbb{R}} x(s-t)e^{-i\xi s} ds \right)}_{=\hat{x}(\xi)e^{-i\xi t}} dt \\
&= \hat{x}(\xi) \lim_{\tau\to\infty} \frac{1}{\tau} \int_0^\tau x(t)e^{-i\xi t} dt \\
&\simeq \frac{|\hat{x}(\xi)|^2}{\tau_{max}}
\end{aligned}$$

Thus the power spectral density is estimated by the squared modulus of the Fourier transform divide by the sample length τ_{max}.

A.4.4 Examples

We will now illustrate these notions on the examples of stochastic processes seen before.

Brownian motion (definition A.13)

- $B_t \rightsquigarrow \mathcal{N}(0, |t|)$
- $\mathbb{E}[B_t] = 0$
- $V(B_t) = |t|$
- $\text{cov}(B_s, B_t) = \min(s, t)$

The Brownian motion is stationary at order 1 because its average is always 0. It is also intrinsic. But it is not stationary at order 2 because its variance depends on t (thus it is not stationary in strong sense, neither stationary in weak sense). As a consequence, the relation A.22 ($\gamma = \sigma^2 - C$) does not hold.

- The mean :
$$\mu_B = 0$$
- Autocovariance :
$$C_B(s) = \text{cov}(B_{t+s}, B_t) = \min(t + s, t) = t$$
- Autocorrelation :
$$\rho_B(s) = \frac{\text{cov}(B_{t+s}, B_t)}{\sqrt{V(B_{t+s})\, V(B_t)}} = \sqrt{\frac{t}{t+s}}$$
- Variogram :
$$\gamma_B(s) = |s|$$

The Brownian motion is not ergodic. A famous property of Brownian motion is that it is dilating to infinity (it reaches every point of $\mathbb{R}$ in finite time):

$$\text{Almost surely, } \limsup_{t \to +\infty} B_t = +\infty \text{ and } \liminf_{t \to +\infty} B_t = -\infty \tag{A.31}$$

Hence the function $\tau \mapsto \frac{1}{\tau} \int_{t_0}^{t_0+\tau} b(t)dt$ does not converge for almost every realization $b(t)$ of B_t. As the Brownian motion is not stationary at order 2, its auto-covariance depends on the time gap s and the starting time t. Thus, its spectrum cannot be defined the same way as definition A.20.

To conclude, the Brownian motion is not stationary nor ergodic. Since these properties are essential for a realization to be informative about the whole process, it explains why the single realization shown on figure A.8 is not informative about the Brownian motion. However it is intrinsic with a linear variogram.

Langevin equation (solution of equation A.18)

- $V_t = V_0 e^{-\frac{t}{\tau}} + \sigma \int_0^t e^{-\frac{t-s}{\tau}} dB_s$
- $\mathbb{E}[V_t] = \mathbb{E}[V_0] e^{-\frac{t}{\tau}}$
- $V(V_t) = \sigma^2 \frac{\tau}{2} + \left(V(V_0) - \sigma^2 \frac{\tau}{2} \right) e^{-2\frac{t}{\tau}}$
- $\text{cov}(V_{t+s}, V_t) = \left(V(V_0) - \sigma^2 \frac{\tau}{2} \right) e^{-\frac{2t+s}{\tau}} + \sigma^2 \frac{\tau}{2} e^{-\frac{s}{\tau}}$

The Ornstein-Ulhenbeck process (solution of Langevin equation) is not stationary, because both its mean and its variance depend on time. But, after few τ, both mean and variance reach a limit:

$$\mathbb{E}[V_\infty] = 0$$

$$V(V_\infty) = \sigma^2 \frac{\tau}{2}$$

This limit is called the *stationary solution* of Langevin equation. According to Gardiner (Gardiner (2009), p.74), the stationary solution is Gaussian

$$V_\infty \rightsquigarrow \mathcal{N}\left(0, \sigma^2 \frac{\tau}{2}\right)$$

Hence the stationary solution is order 2 stationary and intrinsic. Asymptotically when $t \to +\infty$, it gives the following expressions:

- The mean :
$$\mu_V = 0$$

- Autocovariance :
$$C_V(s) = \text{cov}(V_{t+s}, V_t) = \sigma^2 \frac{\tau}{2} e^{-\frac{s}{\tau}}$$

- Autocorrelation :
$$\rho_V(s) = \frac{\text{cov}(V_{t+s}, V_t)}{V(V_\infty)} = e^{-\frac{s}{\tau}}$$

- Variogram :
$$\gamma_V(s) = \sigma^2 \frac{\tau}{2} \left(1 - e^{-\frac{s}{\tau}}\right)$$

Exponential decrease of autocovariance is the example take by Gardiner for a sufficient condition for the process to be ergodic (Gardiner (2009), p. 58). Hence, the Ornstein-Ulhenbeck process is asymptotically ergodic.

Concerning its spectrum, the Fourier transform of its auto-covariance (which is an expo-

nential) is a Lorenzian function :

$$\begin{aligned}\Gamma_V(\xi) &= \int_{s\in\mathbb{R}} \sigma^2\frac{\tau}{2}e^{-\frac{s}{\tau}}e^{-i\xi\cdot s}ds \\ &= \sigma^2\frac{\tau}{2}\int_{s\in\mathbb{R}} e^{-\frac{s}{\tau}-i\xi\cdot s}ds \\ &= \frac{\sigma^2\frac{\tau}{2}}{1+4\pi^2\tau^2\xi^2}\end{aligned}$$

To conclude, the Ornstein-Ulhenbeck process is asymptotically stationary of order 2 and ergodic. Its spectrum decrease with a -2 slope in a log-log scale (usual for PSDs). Because of these properties the single realization shown on figure A.10 is informative about the whole process.

A.5 Conclusion

This appendix intended to refresh some basics and to set the notations and the definitions as they will be used in this document. The first section was giving the essential tools to understand what a random variable is. The second section focused the numerical generation of random variables. The third section introduced stochastic processes with two examples: the Brownian motion and the Ornstein-Ulhenbeck process. The fourth and last section made the link between the theoretical stochastic processes and the empirical time series of one realisation.

Random variables are everywhere in turbulence, in filtering and in sensitivity analysis. A random variable is a function from an unknown departure point (usually denoted ω). To represent this "unknown dimension", one makes samples of the same random variable. Such samples are generated on computer using pseudo-random numbers generators. Pseudo-random numbers generators of two programming languages have been tested. The algorithm to generate any random variable from a uniformly distributed sample has been explained. In particular, the algorithm A.1 for the generation of a sample distributed along a given potential is the key element of the filtering process.

Stochastic processes are families of random variables. As measurements are usually composed of time series, stochastic process are relevant to model them. Two examples are given: the Brownian motion and the Ornstein-Ulhenbeck process. The Brownian motion describes the diffusing movement of a particle inside a fluid. In average, the movement is null (there is no trend). But the variance steadily increases: the particle goes farer and farer but always comes back. The Ornstein-Ulhenbeck process is the solution of the Langevin equation. This equation is a simple model for a particle drop into a fluid. Conversely to the Brownian motion, there is a trend and the variance is bounded.

Signal processing can be used in many contexts. The small section with this name in this chapter intents to distinguish theoretical signals (stochastic process) from accessible signals

(a single realisation of the stochastic process). Quantities of importance for applications (average, variance, auto-covariance, variogram, spectrum) are introduced for both. It is shown are they can be compared under the assumptions of stationarity and ergodicity. They are illustrated on the two stochastic processes given in examples.

Appendix B

Proofs

B.1 Formulae on reconstruction outputs

B.1.1 Influence of N on N_{G0}

Theorem B.1 (Influence of N on N_{G0})**.** *If $N > 1$ is the number of particles and at any time there are particles in the probe volume, for any $n \in \mathbb{N}$, there exist $\alpha(n) > 0$ and $\beta(n) > 0$ such that*

$$\mathbb{P}\left(N_{G0} = n\right) \leqslant \alpha(n) e^{-N/\beta(n)} \tag{B.1}$$

Proof. A result of Del Moral (2004) (theorem 7.4.1, page 232) quoted by Baehr (2010) (theorem 2.2) on the degeneracy of the particle filter is useful to reckon the influence of N on N_{G0}. Here is the theorem written with the notation of this manuscript.

> If at any time there are particles in the probe volume , then $\forall N \geqslant 1$ and $\forall t \geqslant 0$, the time τ^N at which potential is null for all particles follows the inequality:
>
> $$\mathbb{P}\left(\tau^N \leqslant t\right) \leqslant a(t) e^{-N/b(t)} \tag{B.2}$$

When the potential vanishes, the system is re-initialized. Thus, the N_{G0} extinctions are independent and the time counter can be reset to zero. If the k-th extinction time is denoted τ_k^N and compared to the time t_k (reset to zero after each extinction), the number of null potential is written

$$\mathbb{P}\left(N_{G0} = n\right) = \prod_{k=1}^{n} \mathbb{P}\left(\tau_k^N \leqslant t_k\right) \leqslant \prod_{k=1}^{n} a(t_k) e^{-N/b(t_k)}$$

with the condition $\sum_{k=1}^{n} t_k \leqslant N_t$.

It tells there exist $\alpha(n) = \prod_{k=1}^{n} a(t_k)$ and $\beta(n) = \left(\sum_{k=1}^{n} 1/b(t_k)\right)^{-1}$ such that

$$\mathbb{P}\left(N_{G0} = n\right) \leqslant \alpha(n) e^{-N/\beta(n)} \tag{B.3}$$

Thus, the number of null potential decreases exponentially with N. □

B.1.2 Influence of σ^{obs} and σ^{add} on N_{G0}

Theorem B.2 (Influence of σ^{obs} and σ^{add} on N_{G0})**.** *If the following assumptions are satisfied*

- *The real wind $V^{\mathbf{r}}_{z,t}$ is stationary at order 2 and ergodic in space and time.*
- *The particles after conditioning $\tilde{V}_t$ are Gaussian with the same mean and variance as $V^{\mathbf{r}}_{z,t}$.*

Then, the average number of null potential N_{G0} is bounded from above by a function of σ^{obs} and σ^{add}.

$$\mathbb{E}\left[N_{G0}\right] \leqslant N_t N_z \frac{(\sigma^{add})^2 + 2k}{-\left((\sigma^{obs})^2 + 2k\right)\log\left(\iota^2 2\pi\left((\sigma^{obs})^2 + 2k\right)\right)} \tag{B.4}$$

with $\iota = 10^{-16}$, the zero machine threshold, and $k = \frac{1}{2}V\left(V^{\mathbf{r}}_{z,t}\right)$ (constant thanks to the stationarity assumption).

Proof. The number of null potential is defined as

$$N_{G0} = \left|\left\{(z,t)/\sum_{i=1}^{N} G_{obs}(z,t,i) = 0\right\}\right|$$

with $G_{obs}(z,t,i) = \exp\left(-\frac{\left(\tilde{V}_t^i - V^{\mathbf{o}}(z,t)\right)^2}{2(\sigma^{obs})^2}\right)$. The potential G_{obs} can be seen as a function of two random variables: $\tilde{V}_t^i$ (as a realisation of the random variable $\tilde{V}_t$) and $V^{\mathbf{o}}(z,t)$ (as a realisation of the random variable $V^{\mathbf{o}}_{z,t}$). Let us consider the random variable G:

$$G = \exp\left(-\frac{\left(\tilde{V}_t - V^{\mathbf{o}}_{z,t}\right)^2}{2(\sigma^{obs})^2}\right) \tag{B.5}$$

The sum on the N particles can be seen as the Monte Carlo approximation of the expectation along $\tilde{V}_t$. The observation is considered as a data, thus it is a conditional expectation:

$$\mathbb{E}\left[G|V^{\mathbf{o}}_{z,t}\right] \text{ estimated by } \sum_{i=1}^{N} G_{obs}(z,t,i)$$

If we consider the discrete random variable $T_{z,t}$ such that

$$T_{z,t} = \mathbf{1}_{\mathbb{E}\left[G|V^{\mathbf{o}}_{z,t}\right]=0} = \begin{cases} 1 \text{ if } \mathbb{E}\left[G|V^{\mathbf{o}}_{z,t}\right] = 0 \\ 0 \text{ else} \end{cases}$$

Then, $T_{z,t}$ follows a Bernoulli law with parameter $p_{z,t} = \mathbb{P}\left(\mathbb{E}\left[G|V^{\mathbf{o}}_{z,t}\right] = 0\right)$. And N_{G0} is thus the random variable equal to the sum of all $T_{z,t}$, for $z \in [\![1, N_z]\!]$ and $t \in [\![1, N_t]\!]$.

$$N_{G0} = \sum_{z,t} T_{z,t}$$

If the parameter $p_{z,t}$ were constant, N_{G0} would have follow a binomial law, but it is not

the case. Instead, we will find a bound for $p_{z,t}$ which depends on σ^{obs} and σ^{add} but not on z and t.

First, we express $\mathbb{E}\left[G|V^{\mathbf{o}}_{z,t}\right]$. To do so, we use the assumption that $\tilde{V}_t$ is Gaussian, of mean $\tilde{\mu}$ and variance $\tilde{\sigma}^2$.

$$\mathbb{E}\left[G|V^{\mathbf{o}}_{z,t}\right] = \frac{1}{\sqrt{2\pi}\tilde{\sigma}} \int \exp\left(-\frac{\left(x - V^{\mathbf{o}}_{z,t}\right)^2}{2(\sigma^{obs})^2}\right) \exp\left(-\frac{(x-\tilde{\mu})^2}{2\tilde{\sigma}^2}\right) dx$$

From Bromiley (2003), the product of these two Gaussian functions is expressed, and it yields to

$$\mathbb{E}\left[G|V^{\mathbf{o}}_{z,t}\right] = \frac{S(V^{\mathbf{o}}_{z,t})}{\sqrt{2\pi}\sigma} \int \exp\left(-\frac{(x-\mu)^2}{2\sigma^2}\right) dx = S(V^{\mathbf{o}}_{z,t})$$

with

$$\frac{1}{\sigma^2} = \frac{1}{(\sigma^{obs})^2} + \frac{1}{\tilde{\sigma}^2}\ , \quad \mu = \left(\frac{\tilde{\mu}}{\tilde{\sigma}^2} + \frac{V^{\mathbf{o}}_{z,t}}{(\sigma^{obs})^2}\right)\sigma^2 \quad \text{and} \quad S(V^{\mathbf{o}}_{z,t}) = \frac{1}{\sqrt{2\pi}\frac{\tilde{\sigma}\sigma^{obs}}{\sigma}} \exp\left(-\frac{\sigma^2}{2}\frac{(V^{\mathbf{o}}_{z,t} - \tilde{\mu})^2}{\tilde{\sigma}^2(\sigma^{obs})^2}\right)$$

Solving the equation $\mathbb{E}\left[G|V^{\mathbf{o}}_{z,t}\right] = 0$ yields to $S(V^{\mathbf{o}}_{z,t}) = 0$, which occurs when $|V^{\mathbf{o}}_{z,t} - \tilde{\mu}| = +\infty$. However, because of machine threshold, the equality $\mathbb{E}\left[G|V^{\mathbf{o}}_{z,t}\right] = 0$ is in reality equivalent to $\mathbb{E}\left[G|V^{\mathbf{o}}_{z,t}\right] < \iota$ (where $\iota = 10^{-16}$), which yields to the condition $|V^{\mathbf{o}}_{z,t} - \tilde{\mu}| > \beta(\sigma^{obs})$. Then, we know that theoretically $V^{\mathbf{o}}_{z,t} \rightsquigarrow \mathcal{N}\left(V^{\mathbf{r}}(z,t), (\sigma^{add})^2\right)$ and $\tilde{\mu} = \mathbb{E}\left[V^{\mathbf{r}}_{z,t}\right]$ by assumption. Hence, from Tchebychev inequality, we have

$$\mathbb{P}\left(|V^{\mathbf{o}}_{z,t} - \tilde{\mu}| > \beta(\sigma^{obs})\right) \leqslant \frac{1}{\beta(\sigma^{obs})^2}\left((\sigma^{add})^2 + (V^{\mathbf{r}}(z,t) - \mathbb{E}\left[V^{\mathbf{r}}_{z,t}\right])^2\right)$$

with $\beta(\sigma^{obs}) = \sqrt{-(\tilde{\sigma}^2 + (\sigma^{obs})^2)\log\left(\iota^2 2\pi(\tilde{\sigma}^2 + (\sigma^{obs})^2)\right)}$. In this upper bound, two terms will be rewritten with the wind variance: $\tilde{\sigma}^2 = 2k$ (by assumption) and $(V^{\mathbf{r}}(z,t) - \mathbb{E}\left[V^{\mathbf{r}}_{z,t}\right])^2$. Moreover, since the process $V^{\mathbf{r}}_{z,t}$ is assumed stationary at order 2, the wind variance is a constant and equal to $2k$, as stated in the assumptions. Since $V^{\mathbf{r}}(z,t)$ is a realization of the process $V^{\mathbf{r}}_{z,t}$, the term $(V^{\mathbf{r}}(z,t) - \mathbb{E}\left[V^{\mathbf{r}}_{z,t}\right])^2$ is a realization of the variance estimator when the average is known. The term $(V^{\mathbf{r}}(z,t) - \mathbb{E}\left[V^{\mathbf{r}}_{z,t}\right])^2$ itself is different for each time step t or vertical level z. But since the process $V^{\mathbf{r}}_{z,t}$ is assumed ergodic in time and space, the time and space average $\frac{1}{N_z N_t}\sum_{z,t}(V^{\mathbf{r}}(z,t) - \mathbb{E}\left[V^{\mathbf{r}}_{z,t}\right])^2$ converges toward $V\left(V^{\mathbf{r}}_{z,t}\right)$ when

$N_z N_t \to +\infty$. Hence, the expectation of N_{G0} can be bounded as follows:

$$\begin{aligned}
\mathbb{E}\left[N_{G0}\right] &= \sum_{z,t} \mathbb{E}\left[T_{z,t}\right] \\
&= \sum_{z,t} \mathbb{P}\left(\mathbb{E}\left[G|V^{\mathbf{o}}_{z,t}\right] = 0\right) \\
&\leqslant \sum_{z,t} \frac{(\sigma^{add})^2 + (V^{\mathbf{r}}(z,t) - \mathbb{E}\left[V^{\mathbf{r}}_{z,t}\right])^2}{\beta(\sigma^{obs})^2} \\
&= \frac{1}{\beta(\sigma^{obs})^2} \left(N_t N_z (\sigma^{add})^2 + \underbrace{\sum_{z,t} (V^{\mathbf{r}}(z,t) - \mathbb{E}\left[V^{\mathbf{r}}_{z,t}\right])^2}_{=N_t N_z 2k} \right) \\
&= N_t N_z \frac{(\sigma^{add})^2 + 2k}{-\left((\sigma^{obs})^2 + 2k\right) \log\left(\iota^2 2\pi \left((\sigma^{obs})^2 + 2k\right)\right)}
\end{aligned}$$

which gives the result.

□

B.2 Theorems in sensitivity analysis

B.2.1 ANOVA decomposition

Theorem B.3 (ANOVA decomposition)**.** *Let $f : [0,1]^p \to \mathbb{R}$ be an integrable function. Previous notations hold.*
Then, there exists a unique decomposition of f :

$$\begin{aligned}
f(x) &= \sum_{\mathbf{u} \in I} f_{\mathbf{u}}(x_{\mathbf{u}}) \\
&= f_{\emptyset} + \sum_{i=1}^{p} f_i(x_i) + \sum_{1 \leqslant i < j \leqslant p} f_{ij}(x_i, x_j) + \cdots + f_{1,\ldots,p}(x_1, \ldots, x_p)
\end{aligned} \tag{B.6}$$

such that

$$\forall \mathbf{u} \in I, \forall i \in \mathbf{u}, \int_0^1 f_{\mathbf{u}}(x_{\mathbf{u}}) dx_i = 0 \tag{B.7}$$

The proof of this theorem has been first made by Sobol in Sobol (1976), using Fourier-Haar decompositions. Then a simpler version is in Sobol (1993). This is a proof adapted to our notations.

Proof. (From Sobol (1993, 1976))
First we prove existence, then uniqueness of the family $(f_{\mathbf{u}})_{\mathbf{u} \in I}$ which satisfies properties (B.6) et (B.7).

Existence

Let consider the following functions :

$$g_{\mathbf{u}} : \begin{array}{ccc} [0,1]^{|\mathbf{u}|} & \to & \mathbb{R} \\ x_{\mathbf{u}} & \mapsto & g_{\mathbf{u}}(x_{\mathbf{u}}) = \displaystyle\int_{[0,1]^{|\bar{\mathbf{u}}|}} f(x) dx_{\bar{\mathbf{u}}} \end{array}$$

with the convention $g_{[\![1,p]\!]}(x_1, \ldots, x_p) = f(x)$.

The functions $f_{\mathbf{u}}$ will be built recursively thanks to the functions g. At first, with the hands, in order to satisfy the second part of theorem (B.7).

$$f_\emptyset = \int_{[0,1]^p} f(x) d\mathbf{x} = g_\emptyset$$

- $\forall i \in [\![1,p]\!]$, $f_i(x_i) = \displaystyle\int_{[0,1]^{p-1}} f(x) dx_1 \ldots dx_{i-1} dx_{i+1} \ldots dx_p - f_\emptyset = g_i(x_i) - f_\emptyset$
- $\forall i,j \in [\![1,p]\!]$, $f_{ij}(x_i, x_j) = g_{ij}(x_i, x_j) - f_i(x_i) - f_j(x_j)$
- $\forall i,j,k \in [\![1,p]\!]$, $f_{ijk}(x_i, x_j, x_k) = g_{ijk}(x_i, x_j, x_j) - f_{ij}(x_i, x_j) - f_{ik}(x_i, x_k) - f_{jk}(x_j, x_k)$
- $\ldots$

It will be proven that the functions of the decomposition are

$$f_{\mathbf{u}} : \begin{array}{ccc} [0,1]^{|\mathbf{u}|} & \to & \mathbb{R} \\ x_{\mathbf{u}} & \mapsto & f_{\mathbf{u}}(x_{\mathbf{u}}) = g_{\mathbf{u}}(x_{\mathbf{u}}) - \displaystyle\sum_{i \in \mathbf{u}} f_{\mathbf{u}\setminus i}(x_{\mathbf{u}\setminus i}) \end{array}$$

One can express the functions $(g_{\mathbf{u}})_{\mathbf{u}\in I}$ with the functions of the decomposition:

$$g_{\mathbf{u}}(x_{\mathbf{u}}) = \sum_{\mathbf{v} \subset \mathbf{u}} f_{\mathbf{v}}(x_{\mathbf{v}})$$

And because $g_{[\![1,p]\!]}(x_1, \ldots, x_p) = f(x)$, one gets directly the decomposition 4.1.

$$f(x) = \sum_{\mathbf{u} \in I} f_{\mathbf{u}}(x_{\mathbf{u}})$$

The property B.7 of the decomposition functions is still to be proven. Recursively on the cardinal of $\mathbf{u}$:

$\underline{|\mathbf{u}| = 1}$ Let $\mathbf{u} = i$. Then,

$$\begin{array}{rcl} \int_0^1 f_i(x_i) dx_i & = & \int_0^1 g_i(x_i) dx_i - f_\emptyset \\ & = & \int_0^1 \int_{[0,1]^{|\mathbf{v}|}} f(x) d\mathbf{x}_{\mathbf{v}} dx_i - f_\emptyset \text{ with } v = [\![1,p]\!] \setminus i \\ & = & \int_{[0,1]^p} f(x) d\mathbf{x} - f_\emptyset \\ & = & 0 \end{array}$$

$\star$ $\underline{|\mathbf{u}| = k-1 \Rightarrow |\mathbf{u}| = k}$ Let $\mathbf{u} \in I$ of cardinal k. The following property is assumed true for all $n \leqslant k$:

$$\forall \mathbf{v},\ |\mathbf{v}| = n,\ \forall i \in \mathbf{v},\ \int_0^1 f_{\mathbf{v}}(\mathbf{x}_{\mathbf{v}}) dx_i = 0$$

.

Then this property is also true for $\mathbf{u}$. Let $j \in \mathbf{u}$.

$$\begin{aligned}\int_0^1 f_{\mathbf{u}}(x_{\mathbf{u}})dx_j &= \underbrace{\int_0^1 g_{\mathbf{u}}(x_{\mathbf{u}})dx_j}_{f_{\mathbf{u}\setminus j}(x_{\mathbf{u}\setminus j})} - \sum_{i\in\mathbf{u}} \underbrace{\int_0^1 f_{\mathbf{u}\setminus i}(x_{\mathbf{u}\setminus i})dx_j}_{\begin{cases} 0 & \text{if } i \neq j \\ f_{\mathbf{u}\setminus j}(x_{\mathbf{u}\setminus j}) & \text{if } i = j \end{cases}} \\ &= f_{\mathbf{u}\setminus j}(x_{\mathbf{u}\setminus j}) - f_{\mathbf{u}\setminus j}(x_{\mathbf{u}\setminus j}) = 0\end{aligned}$$

because $|\mathbf{u} \setminus i| = k - 1$ hence the property is true by assumption. The change of $g_{\mathbf{u}}$ come from Fubini's theorem.

A family of functions $f_{\mathbf{u}}$, $\mathbf{u} \in I$ satisfying the theorem has been found. It proves the existence of such a family.

Uniqueness

To prove its uniqueness, let $\left(\tilde{f}_{\mathbf{u}}\right)_{\mathbf{u}\in I}$ and $(f_{\mathbf{u}})_{\mathbf{u}\in I}$ be two families of functions such that properties (B.6) and (B.7) are verified.

It will be proven that $\forall \mathbf{u} \in I$, $f_{\mathbf{u}} = \tilde{f}_{\mathbf{u}}$ recursively on the cardinal of $\mathbf{u}$.

$|\mathbf{u}| = 0$ By integration of (B.6) with respect to $(x_1, \ldots, x_p)$:

$$\int_{[0,1]^p} f(x)d\mathbf{x} = f_\emptyset = \tilde{f}_\emptyset$$

because $\forall \mathbf{u} \neq \emptyset$, $\exists i \in [\![1, p]\!]$, $i \in \mathbf{u}$ so $\int_{[0,1]^p} f_{\mathbf{u}}(x_{\mathbf{u}})d\mathbf{x} = \int_{[0,1]^p} \tilde{f}_{\mathbf{u}}(x_{\mathbf{u}})d\mathbf{x} = 0$ thanks to the property (B.7).

$\star$ $|\mathbf{u}| = k - 1 \Rightarrow |\mathbf{u}| = k$ Let $k \in [\![1, p]\!]$. It is assumed the elements of $\left(\tilde{f}_{\mathbf{u}}\right)_{\mathbf{u}\in I}$ and $(f_{\mathbf{u}})_{\mathbf{u}\in I}$ are equal for $|\mathbf{u}| < k$.

Let $\mathbf{v} \in I$, $|\mathbf{v}| = k$. One wants to prove that $\tilde{f}_{\mathbf{v}} = f_{\mathbf{v}}$. To achieve this, one makes the integration of (B.6) with respect to $x_{\bar{\mathbf{v}}}$:

$$\int_{[0,1]^{|\bar{\mathbf{v}}|}} f(x)d\mathbf{x} = f_\emptyset + \sum_{\mathbf{u}\in I} \int_{[0,1]^{|\bar{\mathbf{v}}|}} f_{\mathbf{u}}(x_{\mathbf{u}})d\mathbf{x}_{\bar{\mathbf{v}}} = \tilde{f}_\emptyset + \sum_{\mathbf{u}\in I} \int_{[0,1]^{|\bar{\mathbf{v}}|}} \tilde{f}_{\mathbf{u}}(x_{\mathbf{u}})d\mathbf{x}_{\bar{\mathbf{v}}}$$

In the sum, the terms $\mathbf{u} \in I$ of cardinal lower than k are equal on each side (hypothesis of recurrence). One takes them out of the sum. For f and $\tilde{f}$, the remaining integral is written as follows

$$\int_{[0,1]^{|\bar{\mathbf{v}}|}} f_{\mathbf{u}}(x_{\mathbf{u}})d\mathbf{x}_{\bar{\mathbf{v}}} = \begin{cases} f_{\mathbf{v}}(\mathbf{x}_{\mathbf{v}}) & \text{if } \mathbf{u} = \mathbf{v} \\ 0 & \text{if } \mathbf{u} \neq \mathbf{v} \end{cases}$$

The case $\mathbf{u} \neq \mathbf{v}$ is split in two sub-cases : $\exists i \in \mathbf{u}, i \notin \mathbf{v}$ or $\exists i \in \mathbf{u}, i \notin \mathbf{v}$.

If $\exists i \in \mathbf{u}, i \notin \mathbf{v}$, then $i \in \bar{\mathbf{v}}$ and the property (B.7) ensures nullity.

If $\exists i \in \mathbf{v}, i \notin \mathbf{u}$, then $|\mathbf{u}| \leqslant k$. Terms of cardinal lower than k have been removed thanks to the recurrence hypothesis. Only terms of equal cardinal are left. The two sub-cases lead thus to the same conclusion. We are back to the previous sub-case and the property (B.7) ensures nullity.

It has been shown that $\forall k \in [\![0,p]\!]$, $\forall \mathbf{u} \in I$, $|\mathbf{u}| = k$, $f_{\mathbf{u}} = \tilde{f}_{\mathbf{u}}$. One can conclude that

$$\forall \mathbf{u} \in I,\ f_{\mathbf{u}} = \tilde{f}_{\mathbf{u}}$$

Which ensures the uniqueness of the family $(f_{\mathbf{u}})_{\mathbf{u}\in I}$ and ends the proof. □

B.2.2 Orthogonality in ANOVA decomposition

Proposition B.1. *Let $f : [0,1]^p \to \mathbb{R}$ be integrable and $(f_{\mathbf{u}})_{\mathbf{u}\in I}$ the functions of its ANOVA decomposition. Then,*

$$\forall \mathbf{u}, \mathbf{v} \in I,\ \mathbf{u} \neq \mathbf{v},\ \int_{[0,1]^p} f_{\mathbf{u}}(x_{\mathbf{u}}) f_{\mathbf{v}}(x_{\mathbf{v}}) dx = 0 \tag{B.8}$$

Proof. (From Sobol (1993, 1976))
Soient $\mathbf{u}$ et $\mathbf{v}$ dans I tels que $\mathbf{u} \neq \mathbf{v}$. Précision le sens de $\mathbf{u} \neq \mathbf{v}$, négation de $\mathbf{u} = \mathbf{v}$.

$$\mathbf{u} = \mathbf{v} \quad \Leftrightarrow \quad \mathbf{u} \subset \mathbf{v} \ \wedge\ \mathbf{v} \subset \mathbf{u} \quad \Leftrightarrow \quad \forall i \in \mathbf{u}, i \in \mathbf{v} \ \wedge\ \forall j \in \mathbf{v}, j \in \mathbf{u}$$

Par négation, on a

$$\mathbf{u} \neq \mathbf{v} \quad \Leftrightarrow \quad \exists i \in \mathbf{u}, i \notin \mathbf{v} \ \vee\ \exists j \in \mathbf{v}, j \notin \mathbf{u}$$

Dans notre problème, $\mathbf{u}$ et $\mathbf{v}$ ont des rôles symétriques. On peut donc considérer $\exists i \in \mathbf{u}, i \notin \mathbf{v}$ ou bien $\exists j \in \mathbf{v}, j \notin \mathbf{u}$ indifféremment. Disons que l'on considère $\exists i \in \mathbf{u}, i \notin \mathbf{v}$. Alors, d'après le théorème de Fubini,

$$\int_{[0,1]^p} f_{\mathbf{u}}(x_{\mathbf{u}}) f_{\mathbf{v}}(x_{\mathbf{v}}) dx = \int_{[0,1]^{p-1}} \left(\int_0^1 f_{\mathbf{u}}(x_{\mathbf{u}}) f_{\mathbf{v}}(x_{\mathbf{v}}) dx_i \right) dx_{\bar{i}} = \int_{[0,1]^{p-1}} \left(f_{\mathbf{v}}(x_{\mathbf{v}}) \underbrace{\int_0^1 f_{\mathbf{u}}(x_{\mathbf{u}}) dx_i}_{=0} \right) dx_{\bar{i}} = 0$$

Le fait que $i \in \mathbf{u}, i \notin \mathbf{v}$ permet de sortir $f_{\mathbf{v}}(x_{\mathbf{v}})$ de l'intégrale et d'annuler $\int_0^1 f_{\mathbf{u}}(x_{\mathbf{u}}) dx_i$ grâce à la propriété (B.7). □

B.2.3 Orthogonality of Hoeffding spaces

Proposition B.2 (Orthogonality of Hoeffding spaces)**.**

$$\forall\, \mathbf{u}, \mathbf{v} \in I, \mathbf{u} \neq \mathbf{v}, \quad H^0_{\mathbf{u}} \perp H^0_{\mathbf{v}} \tag{B.9}$$

Proof. (From Chastaing (2013))
Comme pour la décomposition ANOVA, ce résultat se prouve en deux parties : d'abord un résultat du type (B.7), ensuite le résultat d'orthogonalité proprement dit (B.9).
Montrons d'abord

$$\forall \mathbf{u} \in I,\ \forall h_{\mathbf{u}} \in H^0_{\mathbf{u}},\ \forall i \in \mathbf{u},\ \int h_{\mathbf{u}}(x_{\mathbf{u}}) \eta_{X_i}(dx_i) = 0 \tag{B.10}$$

Soit $\mathbf{u} \in I$, $h_{\mathbf{u}} \in H^0_{\mathbf{u}}$ et $i \in \mathbf{u}$. Remarquons que $\{i, \bar{\mathbf{u}}\} = \overline{\{u \setminus i\}}$ que $\int \eta_{X_{\bar{\mathbf{u}}}}(dx_{\bar{\mathbf{u}}}) = 1$.
L'indépendance des composantes permet d'écrire

$$\begin{aligned}
\int h_{\mathbf{u}}(x_{\mathbf{u}})\eta_{X_i}(dx_i) &= \int \left(\int h_{\mathbf{u}}(x_{\mathbf{u}})\eta_{X_i}(dx_i) \right) \eta_{X_{\bar{\mathbf{u}}}}(dx_{\bar{\mathbf{u}}}) && \text{indépendance des composantes} \\
&= \int h_{\mathbf{u}}(x_{\mathbf{u}})\eta_{X_{\bar{\mathbf{v}}}}(dx_{\bar{\mathbf{v}}}) && \text{en prenant } \mathbf{v} = \mathbf{u} \setminus i \\
&= \mathbb{E}\left[h_{\mathbf{u}}(x_{\mathbf{u}})|X_{\mathbf{v}}\right] = 0 && \text{car } |\mathbf{v}| < |\mathbf{u}|
\end{aligned}$$

ce qui prouve le résultat intermédiaire.

Soit maintenant $\mathbf{u} \neq \mathbf{v} \in I$, $h_{\mathbf{u}} \in H^0_{\mathbf{u}}$ et $h_{\mathbf{v}} \in H^0_{\mathbf{v}}$. Comme $\mathbf{u} \neq \mathbf{v}$ on prend $i \in \mathbf{u}, i \notin \mathbf{v}$.

$$\int h_{\mathbf{u}}(x_{\mathbf{u}})h_{\mathbf{v}}(x_{\mathbf{v}})\eta_X(x) = \int h_{\mathbf{u}}(x_{\mathbf{v}}) \underbrace{\left(\int h_{\mathbf{u}}(x_{\mathbf{u}})\eta_{X_i}(dx_i) \right)}_{=0} \eta_{X_{\bar{i}}}(dx_{\bar{i}}) = 0$$

Le cas $i \in \mathbf{v}, i \notin \mathbf{u}$ est immédiat puisque $\mathbf{u}$ et $\mathbf{v}$ ont un rôle symétrique. □

B.2.4 Hoeffding's lemma

Lemme B.1 (Hoeffding projection)**.** *Considering*

- $X_1, ..., X_p$ *independent random variables.*
- $T \in L^2(\Omega, \mathbb{R})$ *(real random variable of finite variance* $\mathbb{E}\left[T^2\right] < +\infty$*).*

Then, for all $\mathbf{u} \in I$*, the orthogonal projection of* T *in* $H^0_{\mathbf{u}}$ *in written*

$$\pi_{H^0_{\mathbf{u}}}(T) = \sum_{\mathbf{v} \subset \mathbf{u}} (-1)^{|\mathbf{u}|-|\mathbf{v}|} \mathbb{E}\left[T|X_{\mathbf{v}}\right] \tag{B.11}$$

Proof. (From Chastaing (2013))
Soit $\mathbf{u} \in I$. Montrons d'abord que l'opérateur définit par l'équation (B.11) est le projecteur orthogonal de L^2 sur $H^0_{\mathbf{u}}$.
On désigne par $\pi_{H^0_{\mathbf{u}}}$ le projecteur orthogonal de L^2 sur $H^0_{\mathbf{u}}$. Son existence est garantie par le fait que $H^0_{\mathbf{u}}$ est une sous-espace vectoriel de L^2 ($H^0_{\mathbf{u}}$ est stable par combinaison linéaire puisque l'espérance est linéaire).
On désigne par $\phi_{\mathbf{u}}$ l'opérateur définit par l'équation (B.11) : $\phi_{\mathbf{u}}(T) = \sum_{\mathbf{v} \subset \mathbf{u}} (-1)^{|\mathbf{u}|-|\mathbf{v}|} \mathbb{E}\left[T|X_{\mathbf{v}}\right]$
On veut prouver que $\forall T \in L^2$, $\phi_{\mathbf{u}}(T) = \pi_{H^0_{\mathbf{u}}}(T)$.

Soit $T \in L^2$. Par définition de $\pi_{H^0_{\mathbf{u}}}$, $L^2 = \ker(\pi_{H^0_{\mathbf{u}}}) \overset{\perp}{\oplus} \mathrm{Im}(\pi_{H^0_{\mathbf{u}}}) = (H^0_{\mathbf{u}})^{\perp} \overset{\perp}{\oplus} H^0_{\mathbf{u}}$. Donc

$$\exists! \, (F', G') \in (H^0_{\mathbf{u}})^{\perp} \times H^0_{\mathbf{u}}, \; T = F' + G'$$

de plus $G' = \pi_{H^0_{\mathbf{u}}}(T)$ et $F' = T - \pi_{H^0_{\mathbf{u}}}(T)$.
Or,

$$T = \underbrace{T - \phi_{\mathbf{u}}(T)}_{F} + \underbrace{\phi_{\mathbf{u}}(T)}_{G}$$

donc il suffit de montrer que $G \in H^0_{\mathbf{u}}$ et $F \in (H^0_{\mathbf{u}})^\perp$ pour conclure par unicité de la décomposition orthogonale que $G = G'$ et $F = F'$. On aura alors prouvé que $\forall T \in L^2$, $\phi_{\mathbf{u}}(T) = G = G' = \pi_{H^0_{\mathbf{u}}}(T)$.

$\boxed{\phi_{\mathbf{u}}(T) \in H^0_{\mathbf{u}}}$

Soit $\mathbf{w} \in I$, $\mathbf{w} \subset \mathbf{u}$. Montrons que $\mathbb{E}\left[G|X_{\mathbf{w}}\right] = 0$.

$$\begin{aligned}
\mathbb{E}\left[\phi_{\mathbf{u}}(T)|X_{\mathbf{w}}\right] &= \sum_{\mathbf{v}\subset\mathbf{u}} (-1)^{|\mathbf{u}|-|\mathbf{v}|}\mathbb{E}\left[\mathbb{E}\left[T|X_{\mathbf{v}}\right]|X_{\mathbf{w}}\right] \\
&= \sum_{\mathbf{v}\subset\mathbf{u}} (-1)^{|\mathbf{u}|-|\mathbf{v}|}\mathbb{E}\left[\mathbb{E}\left[T|X_{\mathbf{v}}\right]|X_{\mathbf{v}\cap\mathbf{w}}\right] && \text{par indépendance des } X_i \\
&= \sum_{\mathbf{v}\subset\mathbf{u}} (-1)^{|\mathbf{u}|-|\mathbf{v}|}\mathbb{E}\left[T|X_{\mathbf{v}\cap\mathbf{w}}\right] && \text{car } \sigma(X_{\mathbf{v}\cap\mathbf{w}}) \subset \sigma(X_{\mathbf{v}})
\end{aligned}$$

Arrêtons-nous sur ce résultat en examinant quelques cas particuliers.
Pour $\mathbf{u} = \{i\}$,

$$\phi_i(T) = \mathbb{E}\left[T|X_i\right] - \mathbb{E}\left[T\right]$$

Pour $\mathbf{u} = \{i, j\}$,

$$\phi_{i,j}(T) = \mathbb{E}\left[T|X_i, X_j\right] - \mathbb{E}\left[T|X_i\right] - \mathbb{E}\left[T|X_j\right] + \mathbb{E}\left[T\right]$$

Pour $\mathbf{u} = \{i, j, k\}$,

$$\begin{aligned}
\phi_{i,j,k}(T) = \quad & \mathbb{E}\left[T|X_i, X_j, X_k\right] \\
& -\mathbb{E}\left[T|X_i, X_j\right] - \mathbb{E}\left[T|X_i, X_k\right] - \mathbb{E}\left[T|X_j, X_k\right] \\
& +\mathbb{E}\left[T|X_i\right] + \mathbb{E}\left[T|X_j\right] + \mathbb{E}\left[T|X_k\right] \\
& -\mathbb{E}\left[T\right]
\end{aligned}$$

Prenons par exemple $\mathbf{w} = \{i\}$ pour conditionner $\phi_{i,j,k}(T)$. On rappelle la convention $\mathbb{E}\left[T|\emptyset\right] = \mathbb{E}\left[T\right]$.

$$\begin{aligned}
\mathbb{E}\left[\phi_{i,j,k}(T)|X_i\right] &= \mathbb{E}\left[T|X_i\right] \\
&\quad -\mathbb{E}\left[T|X_i\right] - \mathbb{E}\left[T|X_i\right] - \mathbb{E}\left[T\right] \\
&\quad +\mathbb{E}\left[T|X_i\right] + \mathbb{E}\left[T\right] + \mathbb{E}\left[T\right] \\
&\quad -\mathbb{E}\left[T\right] \\
&= 2\mathbb{E}\left[T|X_i\right] - 2\mathbb{E}\left[T|X_i\right] + 2\mathbb{E}\left[T\right] - 2\mathbb{E}\left[T\right] \\
&= 0
\end{aligned}$$

De même si l'on prend $\mathbf{w} = \{i, j\}$ pour conditionner $\phi_{i,j,k}(T)$.

$$\begin{aligned}
\mathbb{E}\left[\phi_{i,j,k}(T)|X_i, X_j\right] = \quad & \mathbb{E}\left[T|X_i, X_j\right] \\
& -\mathbb{E}\left[T|X_i, X_j\right] - \mathbb{E}\left[T|X_i\right] - \mathbb{E}\left[T|X_j\right] \\
& +\mathbb{E}\left[T|X_i\right] + \mathbb{E}\left[T|X_j\right] + \mathbb{E}\left[T\right] \\
& -\mathbb{E}\left[T\right] \\
\mathbb{E}\left[\phi_{i,j,k}(T)|X_i, X_j\right] = \quad & \mathbb{E}\left[T|X_i, X_j\right] - \mathbb{E}\left[T|X_i, X_j\right] + \mathbb{E}\left[T|X_i\right] - \mathbb{E}\left[T|X_i, X_j\right] \\
& +\mathbb{E}\left[T|X_j\right] - \mathbb{E}\left[T|X_j\right] + \mathbb{E}\left[T\right] - \mathbb{E}\left[T\right] \\
\mathbb{E}\left[\phi_{i,j,k}(T)|X_i, X_j\right] = \quad & 0
\end{aligned}$$

On voit sur ces cas particuliers que la somme sur les $\mathbf{v} \subset \mathbf{u}$ se transforme en somme sur

$\mathbf{t} \subset \mathbf{w}$. On compte $\binom{|\mathbf{u}|-|\mathbf{w}|}{|\mathbf{t}|}$ termes identiques. On généralise ce résultat :

$$\begin{aligned}
\mathbb{E}\left[\phi_{\mathbf{u}}(T)|X_{\mathbf{w}}\right] &= \sum_{\mathbf{v}\subset\mathbf{u}} (-1)^{|\mathbf{u}|-|\mathbf{v}|}\mathbb{E}\left[T|X_{\mathbf{v}\cap\mathbf{w}}\right] \\
&= \sum_{\mathbf{t}\subset\mathbf{w}} \sum_{j=0}^{|\mathbf{u}|-|\mathbf{w}|} (-1)^{|\mathbf{u}|-|\mathbf{t}|-j}\binom{|\mathbf{u}|-|\mathbf{w}|}{j}\mathbb{E}\left[T|X_{\mathbf{t}}\right] \\
&= \sum_{\mathbf{t}\subset\mathbf{w}} (-1)^{|\mathbf{u}|-|\mathbf{t}|}\mathbb{E}\left[T|X_{\mathbf{t}}\right] \underbrace{\left(\sum_{j=0}^{|\mathbf{u}|-|\mathbf{w}|} (-1)^{j}\binom{|\mathbf{u}|-|\mathbf{w}|}{j}\right)}_{=0} \\
&= 0
\end{aligned}$$

On a montré que $\forall \mathbf{w} \in I$, $\mathbf{w} \subset \mathbf{u}$, $\mathbb{E}\left[\phi_{\mathbf{u}}(T)|X_{\mathbf{w}}\right] = 0$. Donc $\phi_{\mathbf{u}}(T) \in H_u^0$.

$\boxed{T - \phi_{\mathbf{u}}(T) \in (H_{\mathbf{u}}^0)^{\perp}}$

Soit $h_{\mathbf{u}} \in H_{\mathbf{u}}^0$. Montrons que $\mathbb{E}\left[(T - \phi_{\mathbf{u}}(T))h_{\mathbf{u}}(X_{\mathbf{u}})\right] = 0$.

$$\begin{aligned}
\mathbb{E}\left[(T - \phi_{\mathbf{u}}(T))h_{\mathbf{u}}(X_{\mathbf{u}})\right] &= \mathbb{E}\left[Th_{\mathbf{u}}(X_{\mathbf{u}})\right] - \mathbb{E}\left[\phi_{\mathbf{u}}(T))h_{\mathbf{u}}(X_{\mathbf{u}})\right] \\
&= \mathbb{E}\left[Th_{\mathbf{u}}(X_{\mathbf{u}})\right] - \underbrace{\mathbb{E}\left[\mathbb{E}\left[T|X_{\mathbf{u}}\right]h_{\mathbf{u}}(X_{\mathbf{u}})\right]}_{\alpha} - \sum_{\substack{\mathbf{v}\subset\mathbf{u}\\ \mathbf{v}\neq\mathbf{u}}} (-1)^{|\mathbf{u}|-|\mathbf{v}|}\underbrace{\mathbb{E}\left[\mathbb{E}\left[T|X_{\mathbf{v}}\right]h_{\mathbf{u}}(X_{\mathbf{u}})\right]}_{\beta}
\end{aligned}$$

Précisons les termes α et β :

$$\alpha = \mathbb{E}\left[\mathbb{E}\left[T|X_{\mathbf{u}}\right]h_{\mathbf{u}}(X_{\mathbf{u}})\right] = \mathbb{E}\left[\mathbb{E}\left[Th_{\mathbf{u}}(X_{\mathbf{u}})|X_{\mathbf{u}}\right]\right] = \mathbb{E}\left[Th_{\mathbf{u}}(X_{\mathbf{u}})\right]$$

car $X_{\mathbf{u}}$ est $X_{\mathbf{u}}$-mesurable, $h_{\mathbf{u}}$ est mesurable, donc $h_{\mathbf{u}}(X_{\mathbf{u}})$ est $X_{\mathbf{u}}$-mesurable.

$$\beta = \mathbb{E}\left[\mathbb{E}\left[T|X_{\mathbf{v}}\right]h_{\mathbf{u}}(X_{\mathbf{u}})\right] = \mathbb{E}\left[\mathbb{E}\left(\mathbb{E}\left[T|X_{\mathbf{v}}\right]h_{\mathbf{u}}(X_{\mathbf{u}})\middle|X_{\mathbf{v}}\right)\right] = \mathbb{E}\left[\mathbb{E}\left[T|X_{\mathbf{v}}\right]\underbrace{\mathbb{E}\left[h_{\mathbf{u}}(X_{\mathbf{u}})|X_{\mathbf{v}}\right]}_{=0}\right] = 0$$

Donc

$$\mathbb{E}\left[(T - \phi_{\mathbf{u}}(T))h_{\mathbf{u}}(X_{\mathbf{u}})\right] = \mathbb{E}\left[Th_{\mathbf{u}}(X_{\mathbf{u}})\right] - \mathbb{E}\left[Th_{\mathbf{u}}(X_{\mathbf{u}})\right] - 0 = 0$$

On vient de montrer que $(T - \phi_{\mathbf{u}}(T)) \perp h_{\mathbf{u}}(X_{\mathbf{u}})$, $\forall h_{\mathbf{u}}(X_{\mathbf{u}}) \in H_{\mathbf{u}}^0$. Donc $(T - \phi_{\mathbf{u}}(T)) \in (H_{\mathbf{u}}^0)^{\perp}$. Par unicité de la décomposition (propriété du projecteur orthogonal $\pi_{H_{\mathbf{u}}^0}$), on a bien

$$\forall T \in L^2,\ \pi_{H_{\mathbf{u}}^0}(T) = \sum_{\mathbf{v}\subset\mathbf{u}} (-1)^{|\mathbf{u}|-|\mathbf{v}|}\mathbb{E}\left[T|X_{\mathbf{v}}\right]$$

□

B.2.5 Hoeffding decomposition

Theorem B.4 (Hoeffding decomposition)**.** *Let $Y : (\Omega, \mathcal{F}, \mathbb{P}) \to (\mathbb{R}, \mathcal{B}(\mathbb{R}))$ et $X : (\Omega, \mathcal{F}, \mathbb{P}) \to (\mathbb{R}^p, \mathcal{B}(\mathbb{R}^p))$ such that $Y = f(X)$ with $f : (\mathbb{R}^p, \mathcal{B}(\mathbb{R}^p)) \to (\mathbb{R}, \mathcal{B}(\mathbb{R}))$, a measurable function. Previous notations hold.*
Under the following assumptions :

1. *Y has a finite variance (i.e. $\mathbb{E}\left[Y^2\right] < +\infty$).*
2. *The inputs X_i, $i \in [\![1, p]\!]$ are independent : $p_X(x) = \prod_{i=1}^p p_{X_i}(x_i)$.*

Then it exists an unique decomposition of Y with respect to $(X_i)_i$:

$$\begin{aligned} Y &= \sum_{\mathbf{u} \in I} f_{\mathbf{u}}(X_{\mathbf{u}}) \\ &= f_\emptyset + \sum_{i=1}^p f_i(X_i) + \sum_{1 \leqslant i < j \leqslant p} f_{ij}(X_i, X_j) + \cdots + f_{1,\ldots,p}(X_1, \ldots, X_p) \end{aligned} \tag{B.12}$$

such that

$$\forall \mathbf{u} \in I,\ f_{\mathbf{u}}(X_{\mathbf{u}}) = \sum_{\mathbf{v} \subset \mathbf{u}} (-1)^{|\mathbf{u}| - |\mathbf{v}|} \mathbb{E}\left[Y | X_{\mathbf{v}}\right] \tag{B.13}$$

Proof. (From Chastaing (2013))
Plaçons-nous dans le cadre de la projection de Hoeffding. Soit Y est de variance finie (i.e. $\mathbb{E}\left[Y^2\right] < +\infty$) telle que $Y = f(X)$. Par définition de L^2, $Y \in L^2(\Omega, \mathbb{R})$, et par définition des espaces de Hoeffding, $f \in H_{[\![1,p]\!]}$.

Montrons d'abord

$$\forall \mathbf{u} \in I,\ H_{\mathbf{u}} \subset \bigoplus_{\mathbf{v} \subset \mathbf{u}} H^0_{\mathbf{v}} \tag{B.14}$$

Soit $\mathbf{u} \in I$ et $h_{\mathbf{u}}(X_{\mathbf{u}}) \in H_{\mathbf{u}}$. D'après la proposition (B.2) (orthogonalité des espaces de Hoeffding), le projecteur orthogonal sur l'ensemble $\bigoplus_{\mathbf{v} \subset \mathbf{u}} H^0_{\mathbf{v}}$ s'écrit comme la somme des projecteurs orthogonaux sur chacun des ensembles $H^0_{\mathbf{v}}$.

$$\pi_{\bigoplus_{\mathbf{v} \subset \mathbf{u}} H^0_{\mathbf{v}}} = \sum_{\mathbf{v} \subset \mathbf{u}} \pi_{H^0_{\mathbf{v}}}$$

Ainsi,

$$\begin{aligned} h_{\mathbf{u}}(X_{\mathbf{u}}) - \pi_{\bigoplus_{\mathbf{v} \subset \mathbf{u}} H^0_{\mathbf{v}}}(h_{\mathbf{u}}(X_{\mathbf{u}})) &= h_{\mathbf{u}}(X_{\mathbf{u}}) - \sum_{\mathbf{v} \subset \mathbf{u}} \pi_{H^0_{\mathbf{v}}}(h_{\mathbf{u}}(X_{\mathbf{u}})) \\ &= h_{\mathbf{u}}(X_{\mathbf{u}}) - h_{\mathbf{u}}(X_{\mathbf{u}}) \qquad \text{car } \forall \mathbf{v} \subset \mathbf{u},\ \mathbf{v} \neq \mathbf{u},\ \pi_{H^0_{\mathbf{v}}}(h_{\mathbf{u}}(X_{\mathbf{u}})) = 0 \\ &= 0 \end{aligned}$$

On vient de montrer que $h_{\mathbf{u}}(X_{\mathbf{u}}) = \pi_{\bigoplus_{\mathbf{v} \subset \mathbf{u}} H^0_{\mathbf{v}}}(h_{\mathbf{u}}(X_{\mathbf{u}})) \in \bigoplus_{\mathbf{v} \subset \mathbf{u}} H^0_{\mathbf{v}}$ pour tout élément $h_{\mathbf{u}}(X_{\mathbf{u}})$ de $H_{\mathbf{u}}$. Donc $H_{\mathbf{u}} \subset \bigoplus_{\mathbf{v} \subset \mathbf{u}} H^0_{\mathbf{v}}$.

On applique ce résultat à $f \in H_{[\![1,p]\!]} \subset \bigoplus_{\mathbf{u}\in I} H^0_{\mathbf{u}}$.

$$f(X) = \sum_{\mathbf{u}\in I} \underbrace{\pi_{H^0_{\mathbf{u}}}(f(X))}_{f_{\mathbf{u}}(X_{\mathbf{u}})}$$

Et l'expression des $f_{\mathbf{u}}(X_{\mathbf{u}})$ découle du lemme de Hoeffding (B.1).

□

B.2.6 Variance decomposition

Corollary B.1. *Under the same assumptions than for the theorem* **??**,

$$V(Y) = \sum_{\mathbf{u}\in I} V(f_{\mathbf{u}}(X_{\mathbf{u}})) = \sum_{\mathbf{u}\in I} \left(V(\mathbb{E}\left[Y|X_{\mathbf{u}}\right]) + \sum_{\mathbf{v}\subset\mathbf{u}} (-1)^{|\mathbf{u}|-|\mathbf{v}|} V(\mathbb{E}\left[Y|X_{\mathbf{v}}\right]) \right) \tag{B.15}$$

Proof. (From Chastaing (2013))
Comme Y est de variance finie (hypothèse du théorème **??**), on peut prendre la variance dans l'équation 4.6.

$$\begin{aligned}
V(Y) &= V\left(\sum_{\mathbf{u}\in I} f_{\mathbf{u}}(X_{\mathbf{u}})\right) \\
&= \sum_{\mathbf{u}\in I} V(f_{\mathbf{u}}(X_{\mathbf{u}})) + \sum_{\substack{\mathbf{u},\mathbf{v}\in I \\ \mathbf{u}\cap\mathbf{v}\neq\mathbf{u},\mathbf{v}}} \underbrace{\operatorname{cov}(f_{\mathbf{u}}(X_{\mathbf{u}}), f_{\mathbf{v}}(X_{\mathbf{v}}))}_{=0 \text{ car } H^0_{\mathbf{u}} \perp H^0_{\mathbf{v}}} \\
&= \sum_{\mathbf{u}\in I} V\left(\sum_{\mathbf{v}\subset\mathbf{u}} (-1)^{|\mathbf{u}|-|\mathbf{v}|} \mathbb{E}\left[Y|X_{\mathbf{v}}\right]\right) \\
&= \sum_{\mathbf{u}\in I} \left(V(\mathbb{E}\left[Y|X_{\mathbf{u}}\right]) + \sum_{\substack{\mathbf{v}\subset\mathbf{u} \\ \mathbf{v}\neq\mathbf{u}}} (-1)^{|\mathbf{u}|-|\mathbf{v}|} V(\mathbb{E}\left[Y|X_{\mathbf{v}}\right]) + \sum_{\substack{\mathbf{v},\mathbf{w}\subset\mathbf{u} \\ \mathbf{v}\cap\mathbf{w}\neq \\ \mathbf{w},\mathbf{v}}} \underbrace{\operatorname{cov}(\mathbb{E}\left[Y|X_{\mathbf{w}}\right], \mathbb{E}\left[Y|X_{\mathbf{v}}\right])}_{=0 \text{ par indépendance}} \right) \\
&= \sum_{\mathbf{u}\in I} \left(V(\mathbb{E}\left[Y|X_{\mathbf{u}}\right]) + \sum_{\substack{\mathbf{v}\subset\mathbf{u} \\ \mathbf{v}\neq\mathbf{u}}} (-1)^{|\mathbf{u}|-|\mathbf{v}|} V(\mathbb{E}\left[Y|X_{\mathbf{v}}\right]) \right)
\end{aligned}$$

□

B.2.7 Simple, complete and total Sobol indices

Proposition B.3. *Let $\mathbf{u} \in I$. With the notation introduced above, simple, total and complete Sobol indices have the following expression :*

$$D_{\mathbf{u}} = V(\mathbb{E}[Y|X_{\mathbf{u}}]) + \sum_{\substack{\mathbf{v}\subset\mathbf{u}\\ \mathbf{v}\neq\mathbf{u}}} (-1)^{|\mathbf{u}|-|\mathbf{v}|} V(\mathbb{E}[Y|X_{\mathbf{v}}]) \tag{B.16}$$

$$D^C_{\mathbf{u}} = V(\mathbb{E}[Y|X_{\mathbf{u}}]) \tag{B.17}$$

$$D^T_{\mathbf{u}} = V(Y) - V(\mathbb{E}[Y|X_{\bar{\mathbf{u}}}]) \tag{B.18}$$

Proof. (Evoked in Owen (2013) and Homma and Saltelli (1996))

Expression 4.9 is the direct application of theorem 4.2.

- Expression 4.10 is obtained by writing the double sum and grouping the terms of same sign:

$$\begin{aligned}
D^C_{\mathbf{u}} &= \sum_{\substack{\mathbf{v}\in I\\ \mathbf{v}\subseteq\mathbf{u}}} D_{\mathbf{v}} = \sum_{\substack{\mathbf{v}\in I\\ \mathbf{v}\subseteq\mathbf{u}}} \sum_{\substack{\mathbf{w}\in I\\ \mathbf{w}\subseteq\mathbf{v}}} (-1)^{|\mathbf{v}|-|\mathbf{w}|} V(\mathbb{E}[Y|X_{\mathbf{w}}]) \\
&= V(\mathbb{E}[Y|X_{\mathbf{u}}]) + \sum_{\mathbf{t}\subset\mathbf{u}} \sum_{j=0}^{|\mathbf{u}|-|\mathbf{t}|} (-1)^{|\mathbf{u}|-|\mathbf{t}|-j} \binom{|\mathbf{u}|-|\mathbf{t}|}{j} V(\mathbb{E}[Y|X_{\mathbf{t}}]) \\
&= V(\mathbb{E}[Y|X_{\mathbf{u}}]) + \sum_{\mathbf{t}\subset\mathbf{u}} (-1)^{|\mathbf{u}|-|\mathbf{t}|} V(\mathbb{E}[Y|X_{\mathbf{t}}]) \underbrace{\sum_{j=0}^{|\mathbf{u}|-|\mathbf{t}|} (-1)^{j} \binom{|\mathbf{u}|-|\mathbf{t}|}{j}}_{=0} \\
&= V(\mathbb{E}[Y|X_{\mathbf{u}}])
\end{aligned}$$

- Expression 4.11 is a consequence of 4.10:

$$D^T_{\mathbf{u}} + D^C_{\bar{\mathbf{u}}} = \sum_{\substack{\mathbf{v}\in I\\ \mathbf{v}\cap\mathbf{u}\neq\emptyset}} D_{\mathbf{v}} + \sum_{\substack{\mathbf{v}\in I\\ \mathbf{v}\subseteq\bar{\mathbf{u}}}} D_{\mathbf{v}} = \sum_{\mathbf{v}\in I} D_{\mathbf{v}} = V(Y)$$

because $\{\mathbf{v}\in I, \mathbf{v}\cap\mathbf{u}\neq\emptyset\}\cup\{\mathbf{v}\in I, \mathbf{v}\subseteq\bar{\mathbf{u}}\} = I$ (see **?** and **?** equation 11). It follows that

$$D^T_{\mathbf{u}} = V(Y) - D^C_{\bar{\mathbf{u}}} = V(Y) - V(\mathbb{E}[Y|X_{\bar{\mathbf{u}}}])$$

□

B.3 Results related to penalized regression

B.3.1 Sobol indices estimation with regression

Lemme B.2. *For any set* $\mathbf{u}$ *of indices* ($\mathbf{u} \in I'$), *when*

$$(a_{\mathbf{u}}, b_{\mathbf{u}}) = \underset{(a,b)}{arg\min} \left\{ \mathbb{E}\left[(Y - aY_{\mathbf{u}} - b)^2 \right] + \mathbb{E}\left[(Y_{\mathbf{u}} - aY - b)^2 \right] \right\} \tag{B.19}$$

then

$$a_{\mathbf{u}} = S_{\mathbf{u}}$$

Proof. In the function to minimize, Y and $Y_{\mathbf{u}}$ have a symmetric role and follows the same law.

$$\begin{aligned} J(a,b) &= \mathbb{E}\left[(Y - aY_{\mathbf{u}} - b)^2 \right] + \mathbb{E}\left[(Y_{\mathbf{u}} - aY - b)^2 \right] \\ &= \mathbb{E}\left[Y^2\right] + a^2\mathbb{E}\left[Y_{\mathbf{u}}^2\right] + b^2 - 2a\mathbb{E}\left[Y_{\mathbf{u}}Y\right] - 2ab\mathbb{E}\left[Y_{\mathbf{u}}\right] - 2b\mathbb{E}\left[Y\right] \\ &\quad + \mathbb{E}\left[Y_{\mathbf{u}}^2\right] + a^2\mathbb{E}\left[Y^2\right] + b^2 - 2a\mathbb{E}\left[Y_{\mathbf{u}}Y\right] - 2ab\mathbb{E}\left[Y\right] - 2b\mathbb{E}\left[Y_{\mathbf{u}}\right] \\ &= 2\left(\mathbb{E}\left[Y^2\right] + a^2\mathbb{E}\left[Y^2\right] + b^2 - 2a\mathbb{E}\left[Y_{\mathbf{u}}Y\right] - 2ab\mathbb{E}\left[Y\right] - 2b\mathbb{E}\left[Y\right]\right) \end{aligned}$$

which is parabolic, thus has only one minimum, reached at the point denoted $(a_{\mathbf{u}}, b_{\mathbf{u}})$. We solve $\nabla J(a_{\mathbf{u}}, b_{\mathbf{u}}) = 0$.

$$\nabla J(a,b) = \begin{pmatrix} 4a\mathbb{E}\left[Y^2\right] + 4b\mathbb{E}\left[Y\right] - 4\mathbb{E}\left[Y_{\mathbf{u}}Y\right] \\ 4b + 4a\mathbb{E}\left[Y\right] - 4\mathbb{E}\left[Y\right] \end{pmatrix}$$

Setting the second component to zero of the gradient yields to equation :

$$b_{\mathbf{u}} = \mathbb{E}\left[Y\right](1 - a_{\mathbf{u}}) \tag{B.20}$$

Setting the first component to zero and using the last equation yield to

$$a_{\mathbf{u}} = \frac{\mathbb{E}\left[Y_{\mathbf{u}}Y\right] - \mathbb{E}\left[Y\right]^2}{\mathbb{E}\left[Y^2\right] - \mathbb{E}\left[Y\right]^2} = \frac{\mathrm{cov}(Y, Y_{\mathbf{u}})}{V(Y)} = S_{\mathbf{u}}$$

□

B.3.2 Solution of Lasso regression

Proposition B.4. *For any* $\mathbf{u} \in I'$, *the Lasso and least squares estimators are related according to the following formula:*

$$\widehat{S}_{\mathbf{u}}^{l1} = \max\left(\widehat{S}_{\mathbf{u}}^{ls} - \varepsilon_1, 0\right)$$

with $\varepsilon_1 = \frac{\lambda_1}{2\sigma^2}$.

Proof. The cost function to minimize is denoted

$$J: \begin{array}{ccc} \mathbb{R} & \to & \mathbb{R} \\ a & \mapsto & J(a) = \|Y - aY_{\mathbf{u}}\|_2^2 + \lambda_1 |a| \end{array}$$

For the sake of readability, notations including $\mathbf{u}$ are shortened as follow: $\sigma^2 = Y^T Y = Y_{\mathbf{u}}^T Y_{\mathbf{u}}$, $\widehat{a}^{ls} = \widehat{S}_{\mathbf{u}}^{ls} = (Y_{\mathbf{u}}^T Y_{\mathbf{u}})^{-1} Y_{\mathbf{u}}^T Y$. This cost function is developed.

$$J(a) = \sigma^2 \left(1 + a^2 - 2a\widehat{a}^{ls} + \frac{\lambda_1}{\sigma^2}|a|\right)$$

The function J is differentiable everywhere but in $a = 0$. For any $a \neq 0$,

$$\frac{\partial J}{\partial a}(a) = 2\sigma^2 \left(a - \widehat{a}^{ls} + \frac{\lambda_1}{2\sigma^2}\text{sign}(a)\right)$$

The term $\varepsilon_1 = \frac{\lambda_1}{2\sigma^2}$ appears, this notation holds for the rest of the proof. The derivative is discontinuous when $a = 0$. It jumps from $-\widehat{a}^{ls} - \varepsilon_1$ to $-\widehat{a}^{ls} + \varepsilon_1$. When we solve $\frac{\partial J}{\partial a}(\widehat{a}) = 0$ we must distinguish the case of $0 \in [-\widehat{a}^{ls} - \varepsilon_1, -\widehat{a}^{ls} + \varepsilon_1]$ (that is to say $|\widehat{a}^{ls}| \leqslant \varepsilon_1$). Three cases are to consider:

- $|\widehat{a}^{ls}| \leqslant \varepsilon_1$
- $\widehat{a}^{ls} > \varepsilon_1$
- $\widehat{a}^{ls} < -\varepsilon_1$

When $|\widehat{a}^{ls}| \leqslant \varepsilon_1$, there is no solution for the equation $\frac{\partial J}{\partial a}(\widehat{a}) = 0$. Nevertheless, when $|\widehat{a}^{ls}| \leqslant \varepsilon_1$, the value 0 is within the discontinuity at $a = 0$.

$$\lim_{a \to 0^+} \frac{\partial J}{\partial a}(a) = 2\sigma^2 \left(\varepsilon_1 - \widehat{a}^{ls}\right) \geqslant 0 \text{ and } \lim_{a \to 0^-} \frac{\partial J}{\partial a}(a) = -2\sigma^2 \left(\varepsilon_1 + \widehat{a}^{ls}\right) \leqslant 0$$

Hence, when $|\widehat{a}^{ls}| \leqslant \varepsilon_1$, $J(a)$ reaches its minimum at $\widehat{a} = 0$.

When $\widehat{a}^{ls} > \varepsilon_1$, setting the derivative to zero gives

$$\widehat{a} = \widehat{a}^{ls} - \varepsilon_1$$

When $\widehat{a}^{ls} < -\varepsilon$, setting the derivative to zero gives

$$\widehat{a} = \widehat{a}^{ls} + \varepsilon_1$$

Finally, all cases are gathered into the single following expression:

$$\widehat{a} = \text{sign}(\widehat{a}^{ls}) \max\left(|\widehat{a}^{ls}| - \varepsilon_1, 0\right)$$

In the case of Sobol indices, it is reasonable to dismiss the case $\widehat{a}^{ls} < -\varepsilon_1$ (it can happen either if the least square estimation is really bad or the penalty is very small). Going back to the problem 8.13, the Lasso estimator is given by $\widehat{S}_{\mathbf{u}}^{l1} = \widehat{a}$.

□

B.3.3 Solution of best subset regression

Proposition B.5. *For any $\mathbf{u} \in I'$, the best subset and least squares estimators are related according to the following formula:*

$$\widehat{S}^{l0}_{\mathbf{u}} = \widehat{S}^{ls}_{\mathbf{u}} \mathbf{1}_{\widehat{S}^{ls}_{\mathbf{u}} > \varepsilon_0}$$

with $\varepsilon_0 = \sqrt{\frac{\lambda_0}{\sigma^2}}$.

Proof. We assume exactly k upon d coefficients of the vector $\mathbf{a}$ are non-zero and we index $\mathbf{a}$ such that they are first.

$$\mathbf{a} = (a_{\mathbf{u}})_{\mathbf{u} \in I'} = (a_1, ..., a_k, 0, ..., 0)$$

The cost function to minimize depends on the number of non-zero:

$$J(k) = \sum_{i=1}^{k} \|Y - a_i Y_i\|_2^2 + (2^p - k)\|Y\|_2^2 + k\lambda_0$$

It is worth to set the next coefficient a_{k+1} to a non-zero value only if it shrinks the cost function:

$$\begin{aligned} a_{k+1} \neq 0 &\Leftrightarrow J(k+1) < J(k) \\ &\Leftrightarrow \|Y\|_2^2 - \|Y - a_{k+1} Y_{k+1}\|_2^2 - \lambda_0 > 0 \end{aligned}$$

and the next coefficient will take the value which maximizes the improvement. For any $\mathbf{u} \in I'$, the best subset estimation is the solution to

$$\max_a \left\{ \|Y\|_2^2 - \|Y - aY_{\mathbf{u}}\|_2^2 - \lambda_0 \right\}$$

This gain function to maximize is denoted $G(a)$.

$$\begin{aligned} G(a) &= \|Y\|_2^2 - \|Y - aY_{\mathbf{u}}\|_2^2 - \lambda_0 \\ &= \sigma^2 - (Y^T Y + a^2 Y_{\mathbf{u}}^T Y_{\mathbf{u}} - 2aY^T Y_{\mathbf{u}}) - \lambda_0 \\ &= 2\sigma^2 (a\widehat{a}^{ls} - \tfrac{a^2}{2} - \tfrac{\lambda_0}{2\sigma^2}) \end{aligned}$$

Solving $G'(\hat{a}) = 0$ gives $\hat{a} = \widehat{a}^{ls}$. Hence, when it is worth to add a non-zero coefficient, this coefficient is equal to the least square estimator. It is worth to add a non-zero coefficient if $G(\hat{a}) > 0$, that is to say when

$$(\widehat{a}^{ls})^2 - \frac{(\widehat{a}^{ls})^2}{2} - \frac{\lambda_0}{2\sigma^2} > 0 \quad \text{or when} \quad |\widehat{a}^{ls}| > \sqrt{\frac{\lambda_0}{\sigma^2}}$$

Combining these condition gives the result:

$$\hat{a} = \widehat{a}^{ls} \mathbf{1}_{|\widehat{a}^{ls}| > \varepsilon_0}$$

with $\varepsilon_0 = \sqrt{\lambda_0}/\sigma$.

□

B.3.4 Bias, variance and error of prediction and estimation

Formulae to link error of prediction $(Y - \hat{Y})$ and the error of estimation $(\beta - \hat{\beta})$ when the the errors are estimated by cross-validation with a testing sample independent from the training sample. Mentioned at section 8.23, page 235.

$$\mathsf{Bi}_Y = \mathbb{E}\left[X\right]\mathsf{Bi}_\beta \tag{B.21}$$

$$\mathsf{Var}_Y = \mathbb{E}\left[X\mathsf{Var}_\beta X^T\right] + V\Big(X\mathbb{E}\left[\widehat{\beta}\right]\Big) \tag{B.22}$$

$$\mathsf{MSE}_Y = \mathsf{Bi}_\beta^T\mathbb{E}\left[X^TX\right]\mathsf{Bi}_\beta + \mathbb{E}\left[\mathrm{tr}(X\mathsf{Var}_\beta X^T)\right] + \sigma_0^2 \tag{B.23}$$

Proof. of equations (B.21), (B.22) and (B.23).

Equation of the bias (B.21)**.**

$$\mathsf{Bi}_Y = \mathbb{E}\left[\widehat{Y} - Y\right] = \mathbb{E}\left[X(\widehat{\beta} - \beta) - \epsilon\right] = \mathbb{E}\left[X\right]\mathsf{Bi}_\beta$$

because $\widehat{\beta}$ is independent from X.

Equation of the variance (B.22)**.**
From the total variance formula, we have

$$\mathsf{Var}_Y = \mathbb{E}\left[V\Big(X\widehat{\beta}|X\Big)\right] + V\Big(\mathbb{E}\left[X\widehat{\beta}|X\right]\Big) = \mathbb{E}\left[X\underbrace{V\Big(\widehat{\beta}|X\Big)}_{=\mathsf{Var}_\beta}\right] + V\left(X\underbrace{\mathbb{E}\left[\widehat{\beta}|X\right]}_{=\mathbb{E}\left[\widehat{\beta}\right]}\right)$$

because $\widehat{\beta}$ is independent from X, the conditioning to X does not matter.

Equation of the MSE (B.23)**.**

From the law of total expectation, we have $\mathsf{MSE}_Y = \mathbb{E}\left[\mathbb{E}\left[(\widehat{Y} - Y)^T(\widehat{Y} - Y)|X\right]\right]$.

$$\begin{aligned}
\mathbb{E}\left[(\widehat{Y} - Y)^T(\widehat{Y} - Y)|X\right] &= \mathbb{E}\left[(\widehat{Y} - X\mathbb{E}\left[\widehat{\beta}\right] + X\mathbb{E}\left[\widehat{\beta}\right] - Y)^T(\widehat{Y} - X\mathbb{E}\left[\widehat{\beta}\right] + X\mathbb{E}\left[\widehat{\beta}\right] - Y)|X\right] \\
&= \underbrace{\mathbb{E}\left[(Y - X\mathbb{E}\left[\widehat{\beta}\right])^T(Y - X\mathbb{E}\left[\widehat{\beta}\right])|X\right]}_{\mathbf{I}} \\
&\quad \underbrace{+\mathbb{E}\left[(\widehat{Y} - X\mathbb{E}\left[\widehat{\beta}\right])^T(\widehat{Y} - X\mathbb{E}\left[\widehat{\beta}\right])|X\right]}_{\mathbf{II}} \\
&\quad \underbrace{+2\mathbb{E}\left[(Y - X\mathbb{E}\left[\widehat{\beta}\right])^T(\widehat{Y} - X\mathbb{E}\left[\widehat{\beta}\right])|X\right]}_{\mathbf{III}}
\end{aligned}$$

Because $\widehat{\beta}$ is the estimator built on the sub-sample (Y_A, A), we can assume that $\widehat{\beta}$ is independent of X. In particular, $\mathbb{E}\left[\widehat{\beta}\right] = \mathbb{E}\left[\widehat{\beta}|X\right]$, which is helpful to explicit the terms **I**, **II** and **III**.

The term **I** is linked to the bias on β:

$$\mathbf{I} = \mathbb{E}\left[(X\beta + \epsilon - X\mathbb{E}\left[\widehat{\beta}\right])^T(X\beta + \epsilon - X\mathbb{E}\left[\widehat{\beta}\right])|X\right] = \mathbb{E}\left[\mathsf{Bi}_\beta^T X^T X \mathsf{Bi}_\beta|X\right] + \mathbb{E}\left[\epsilon^2\right] = \mathsf{Bi}_\beta^T X^T X \mathsf{Bi}_\beta + \mathbb{E}\left[\epsilon^2\right]$$

with $\mathbb{E}\left[\epsilon^2\right] = \sigma_0^2$.
The term **II** is linked to the variance on β:

$$\mathbf{II} = \mathbb{E}\left[(X\widehat{\beta} - X\mathbb{E}\left[\widehat{\beta}\right])^T(X\widehat{\beta} - X\mathbb{E}\left[\widehat{\beta}\right])|X\right] = \mathrm{tr}(V\Big(X\widehat{\beta}|X\Big)) = \mathrm{tr}(X\mathsf{Var}_\beta X^T)$$

The term **III** is null:

$$\mathbf{III} = \mathbb{E}\left[(X\beta + \epsilon - X\mathbb{E}\left[\widehat{\beta}\right])^T(X\widehat{\beta} - X\mathbb{E}\left[\widehat{\beta}\right])|X\right] = (\beta - \mathbb{E}\left[\widehat{\beta}\right])^T X^T X \underbrace{\mathbb{E}\left[(\widehat{\beta} - \mathbb{E}\left[\widehat{\beta}\right])|X\right]}_{=0} = 0$$

Finally,

$$\mathbb{E}\left[(\widehat{Y} - Y)^T(\widehat{Y} - Y)|X\right] = \mathsf{Bi}_\beta^T X^T X \mathsf{Bi}_\beta + \mathrm{tr}(X\mathsf{Var}_\beta X^T) + \sigma_0^2$$

Taking the expectation gives the result.

□

Appendix C

Complete results of 2-by-2 experiments

C.1 Recap of framework

The system described by figure C.1 has been designed to assess the reconstruction system. Its inputs are parameters of the reconstruction or surroundings for which we want to know the influence (summarized table C.1). Its output are indicators of some qualities of the reconstruction method (summarized table C.2). A "2-by-2 experiment" is the run of the system when only 2 inputs are varying and all outputs are computed. The 2 inputs vary on a regular grid with 30 points for each (thus, 900 runs for each experiment).

To browse among the figures, use hyperlinks in

- the table of contents.
- the table C.3.
- the list of figures page 384.

Notation	Description	Place in the system
C_0	Kolmogorov "constant"	Reconstruction (Lagrangian model)
C_1	Fluctuation coefficient	Reconstruction (Lagrangian model)
ℓ	Spatial interaction length	Reconstruction (Lagrangian model)
N	Number of particles	Reconstruction (filtering)
σ^{add}	True observation noise	Simulation of observation
σ^{obs}	Guess of observation noise	Reconstruction (filtering)
σ^X	Discretization error in the Lagrangian model	Reconstruction (Lagrangian model)
σ^V	Default standard deviation of wind speed	Reconstruction (Lagrangian model)
τ	Integration time	Output computation

Table C.1 – Summary of input parameters for the sensitivity analysis

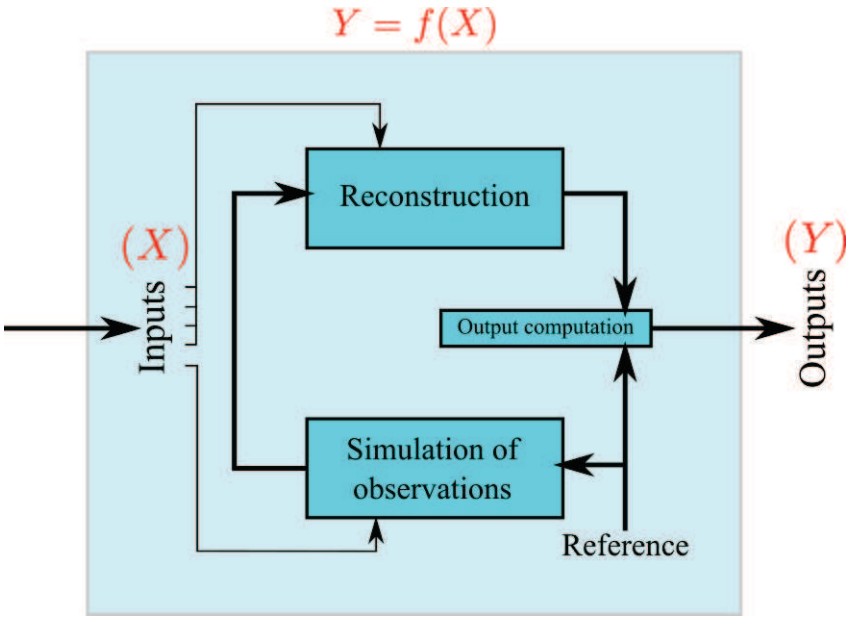

Figure C.1 – Diagram of the system on which is done the sensitivity analysis.

Notation	Description	Definition equation	Results
N_{G0}	Number of null potential	$N_{G0} = \lvert\{G = 0\}\rvert$	p.345
b	Slope of the wind PSD	$\Gamma(\kappa) = A\kappa^b$	p.349
r_k	Root-mean-squared error on the TKE	$\lVert\overline{k^{LS}(z,t)}^{\tau} - k^T(z,t')\rVert_2$	p.353
r_V	Root-mean-squared error on the wind	$r_V = \lVert\hat{V}_{z,t} - V_{z,t}^{ref}\rVert_2$	p.357
T_{exe}	Time of execution	$T_{exe} = t_{end} - t_{start}$	p.361

Table C.2 – Summary of output parameters for the sensitivity analysis

	C_0	C_1	ℓ	N	σ^{add}	σ^{obs}	σ^V	σ^X	τ
C_0		p.303	p.306					p.309	
C_1	p.303								
ℓ	p.306			p.312	p.315	p.318			
N			p.312		p.321	p.324			p.327
σ^{add}			p.315	p.321		p.330			p.333
σ^{obs}			p.318	p.324	p.330			p.336	p.339
σ^V								p.342	
σ^X	p.309					p.336	p.342		
τ				p.327	p.333	p.339			

Table C.3 – Couples of inputs experimented: results are on the indicated page (hyperlink). This table is a copy of 7.1.

C.2 Results by experiment (couple of inputs)

An experiment consists in the computation of all 5 outputs when only two inputs vary on a regular grid. Table C.3 gives all the experiments carried out. There are 13 experiments in total.

C.2.1 C_0 and C_1

In this experiment, only C_0 and C_1 vary. To check another experiment, go to table C.3 (hyperlinks in the table). To have more explanation about these inputs, go to table C.1.

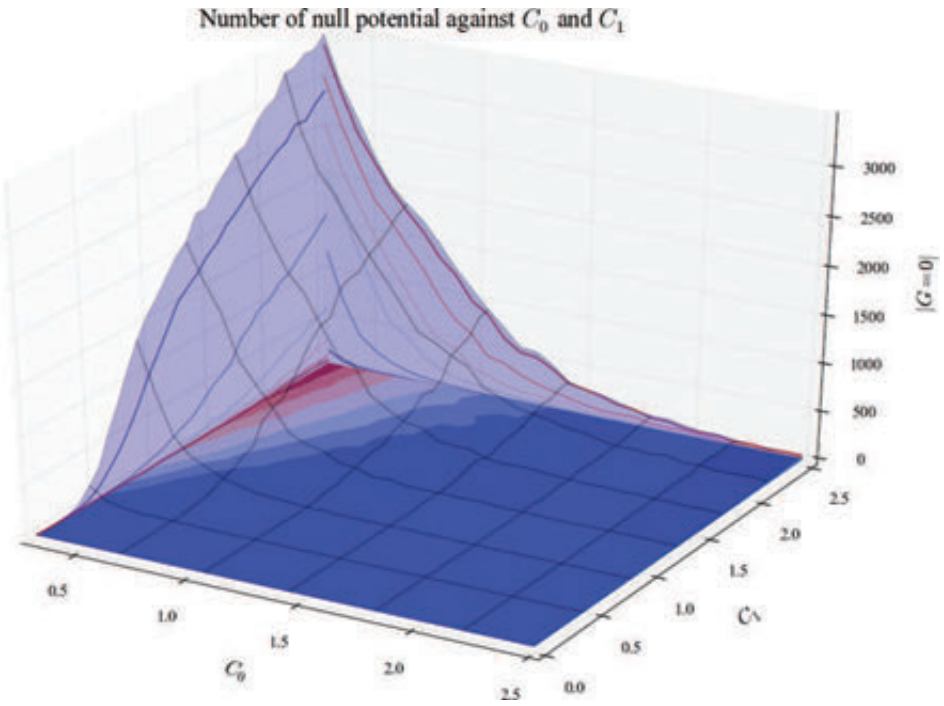

Figure C.2 – Number of null potential when C_0 and C_1 vary.

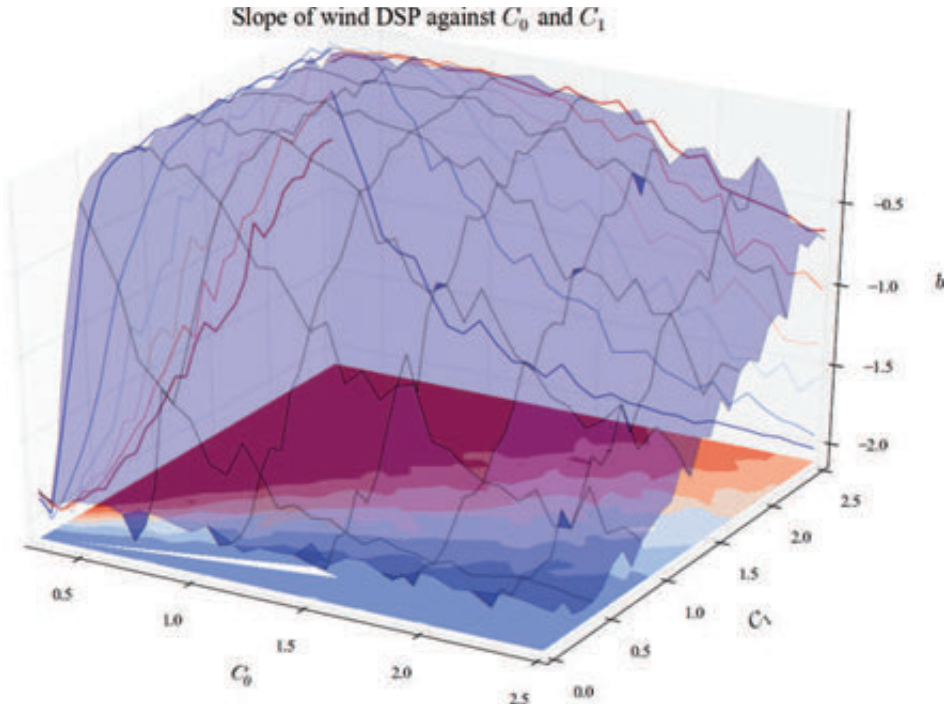

Figure C.3 – PSD slope when C_0 and C_1 vary.

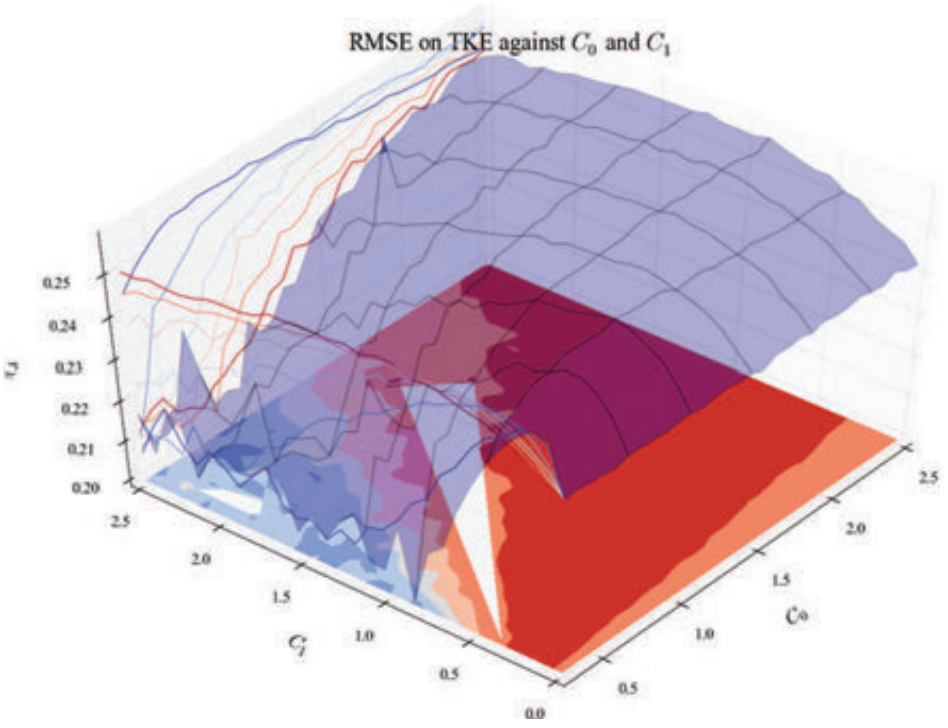

Figure C.4 – RMSE on TKE when C_0 and C_1 vary.

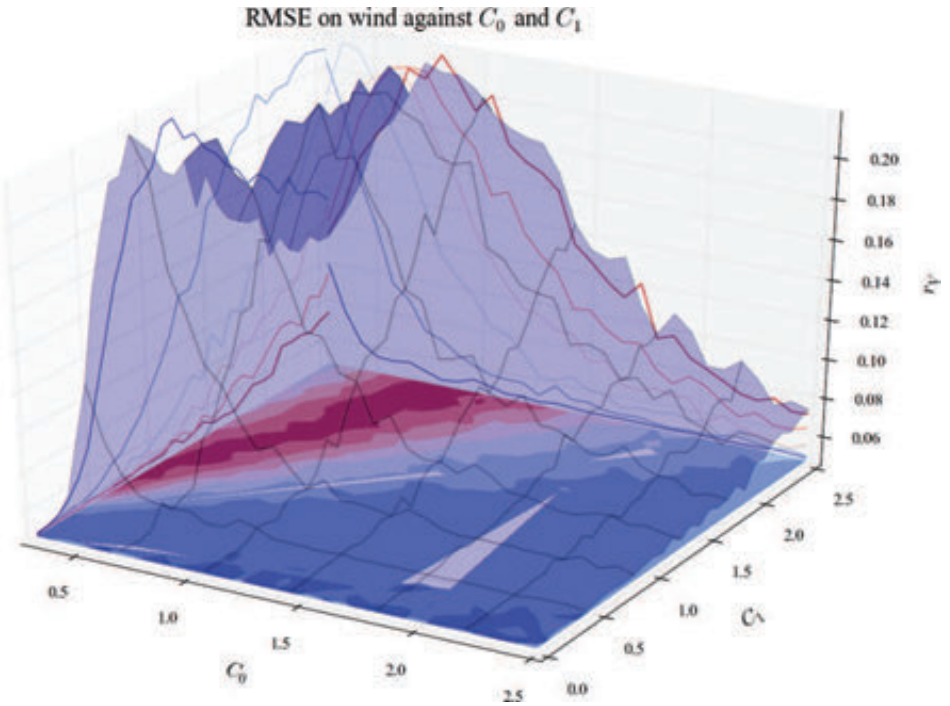

Figure C.5 – RMSE on wind when C_0 and C_1 vary.

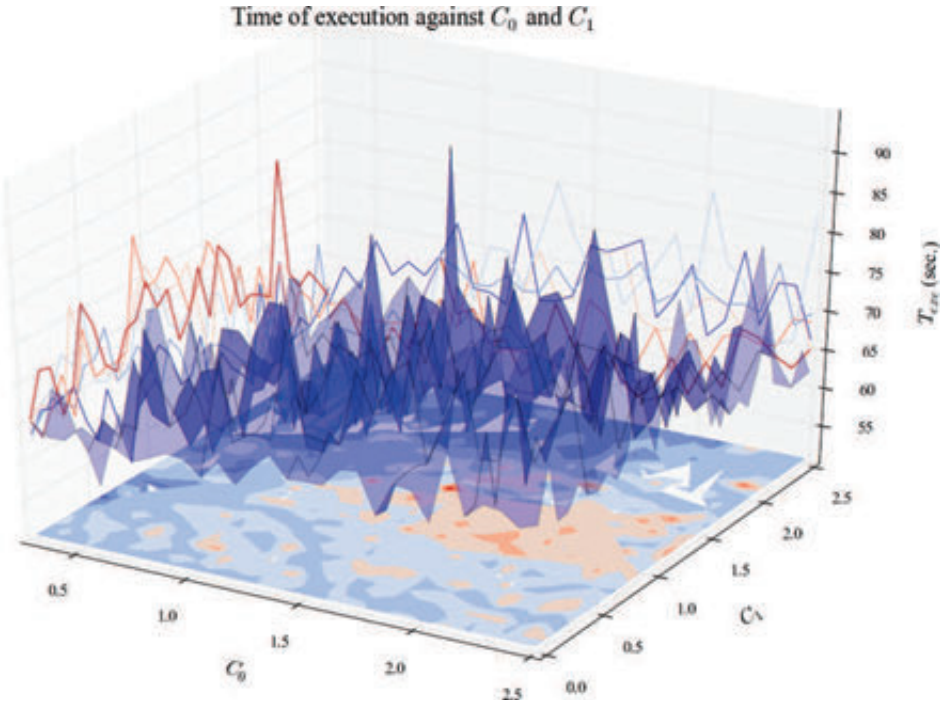

Figure C.6 – Execution time when C_0 and C_1 vary.

C.2.2 C_0 and ℓ

In this experiment, only C_0 and ℓ vary. To check another experiment, go to table C.3 (hyperlinks in the table). To have more explanation about these inputs, go to table C.1.

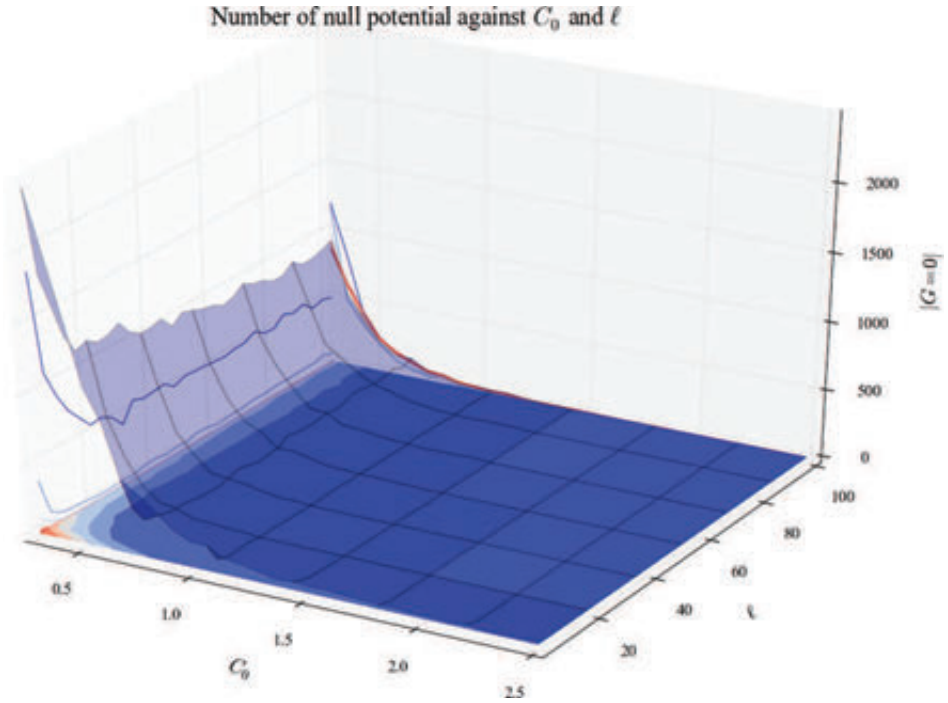

Figure C.7 – Number of null potential when C_0 and ℓ vary.

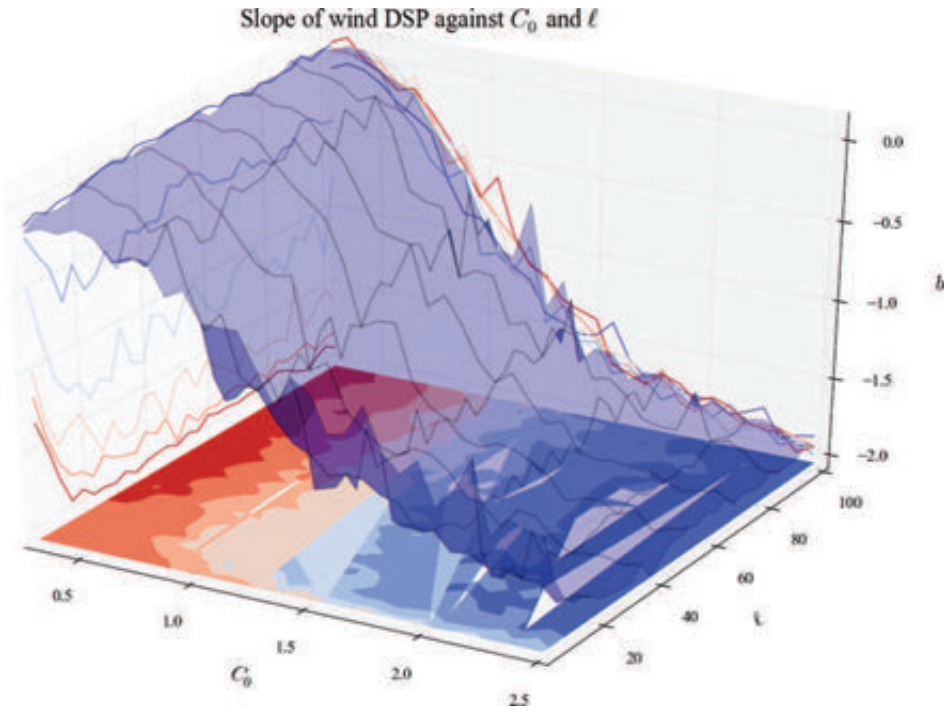

Figure C.8 – PSD slope when C_0 and ℓ vary.

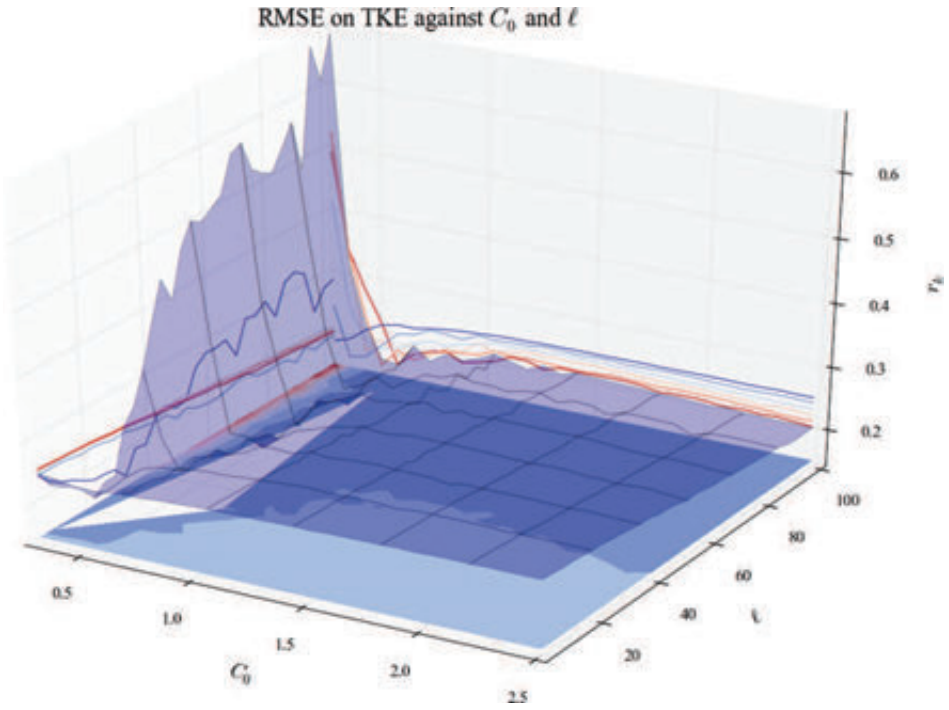

Figure C.9 – RMSE on TKE when C_0 and ℓ vary.

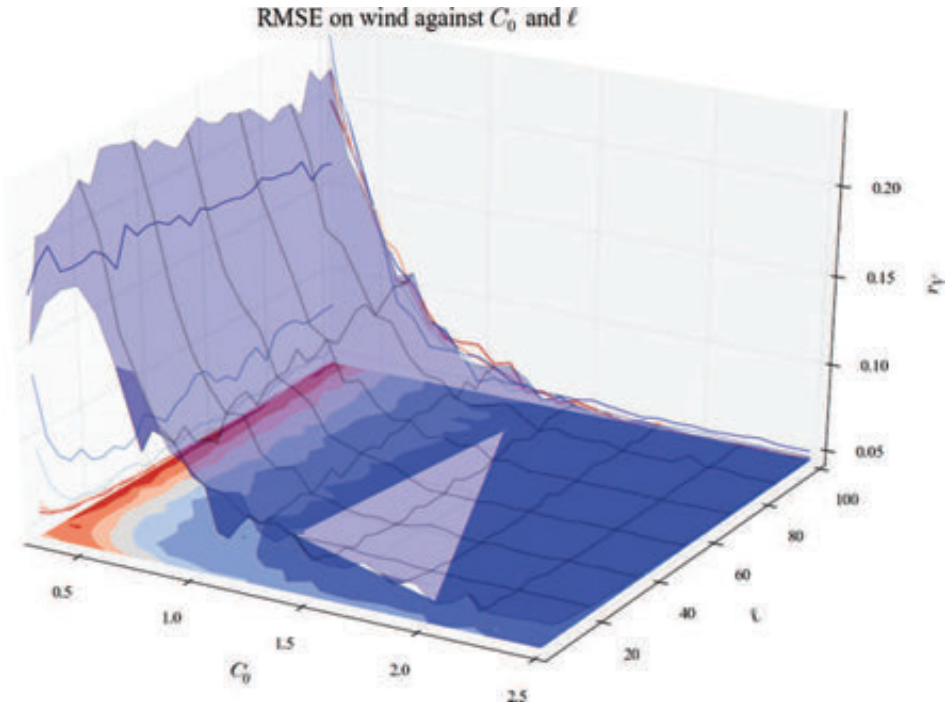

Figure C.10 – RMSE on wind when C_0 and ℓ vary.

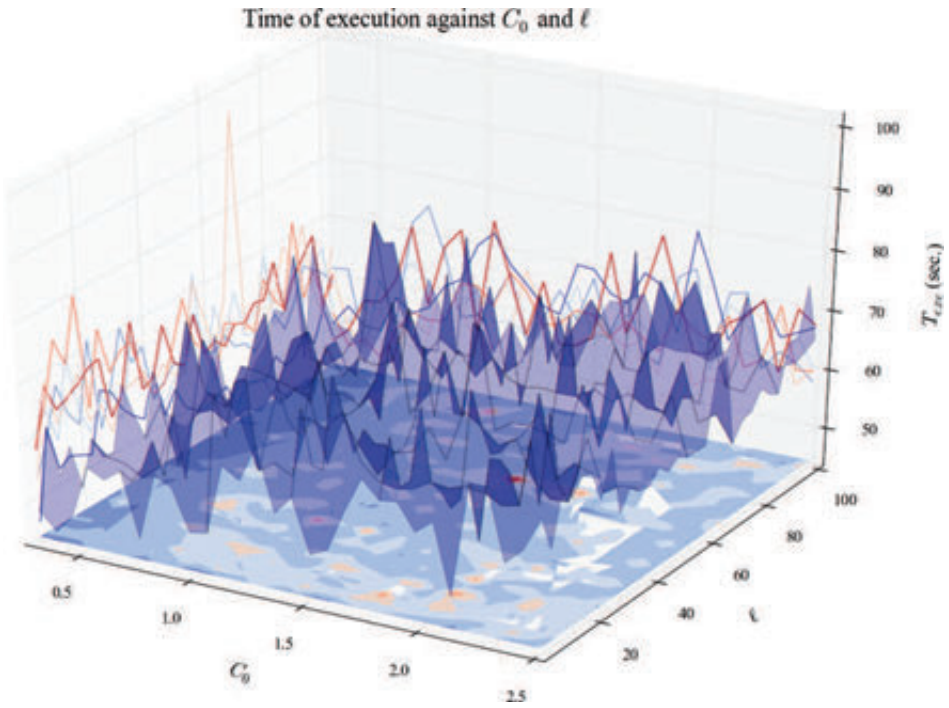

Figure C.11 – Execution time when C_0 and ℓ vary.

C.2.3 C_0 and σ^X

In this experiment, only C_0 and σ^X vary. To check another experiment, go to table C.3 (hyperlinks in the table). To have more explanation about these inputs, go to table C.1.

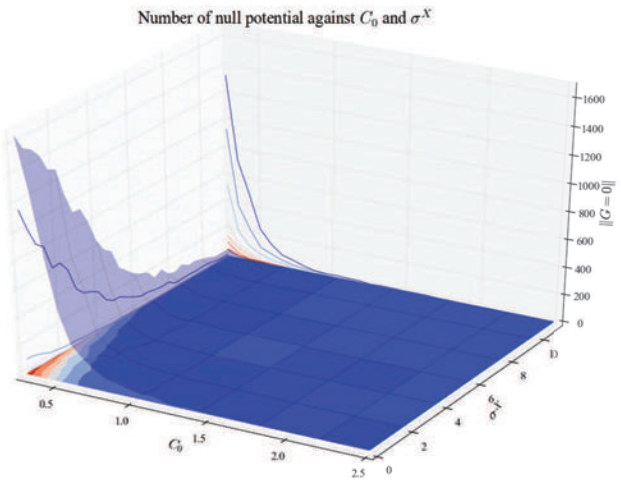

Figure C.12 – Number of null potential when C_0 and σ^X vary.

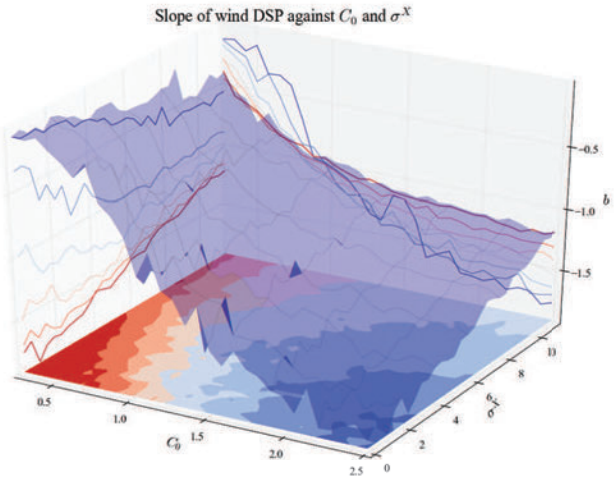

Figure C.13 – PSD slope when C_0 and σ^X vary.

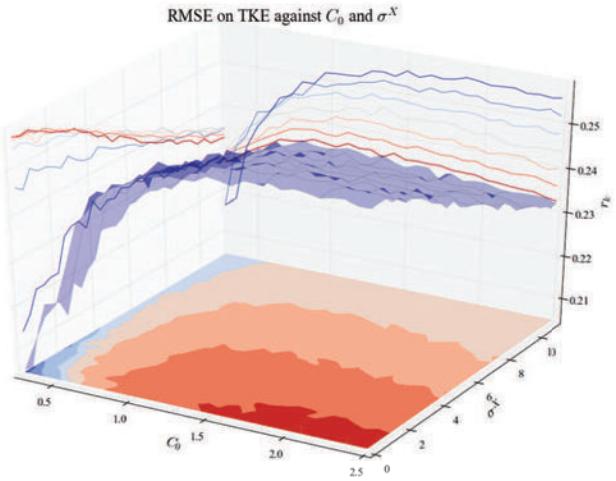

Figure C.14 – RMSE on TKE when C_0 and σ^X vary.

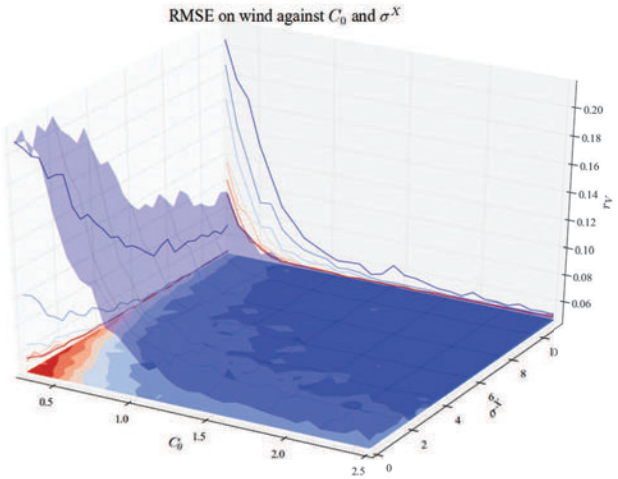

Figure C.15 – RMSE on wind when C_0 and σ^X vary.

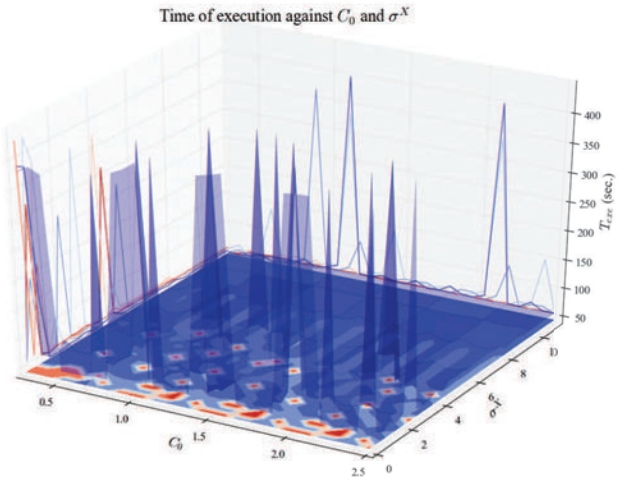

Figure C.16 – Execution time when C_0 and σ^X vary.

C.2.4 ℓ and N

In this experiment, only ℓ and N vary. To check another experiment, go to table C.3 (hyperlinks in the table). To have more explanation about these inputs, go to table C.1.

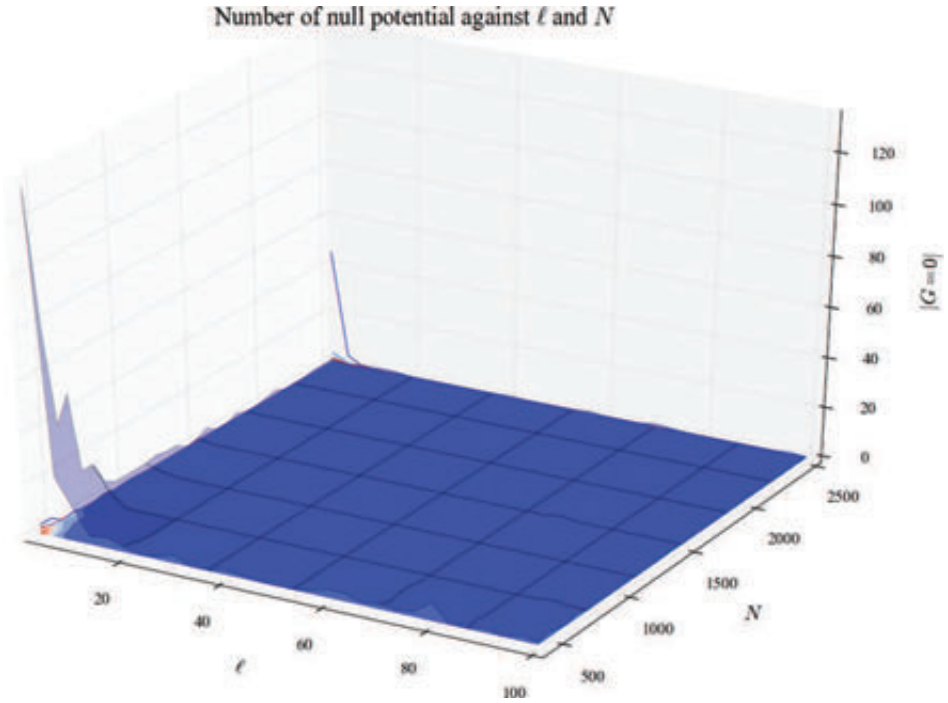

Figure C.17 – Number of null potential when ℓ and N vary.

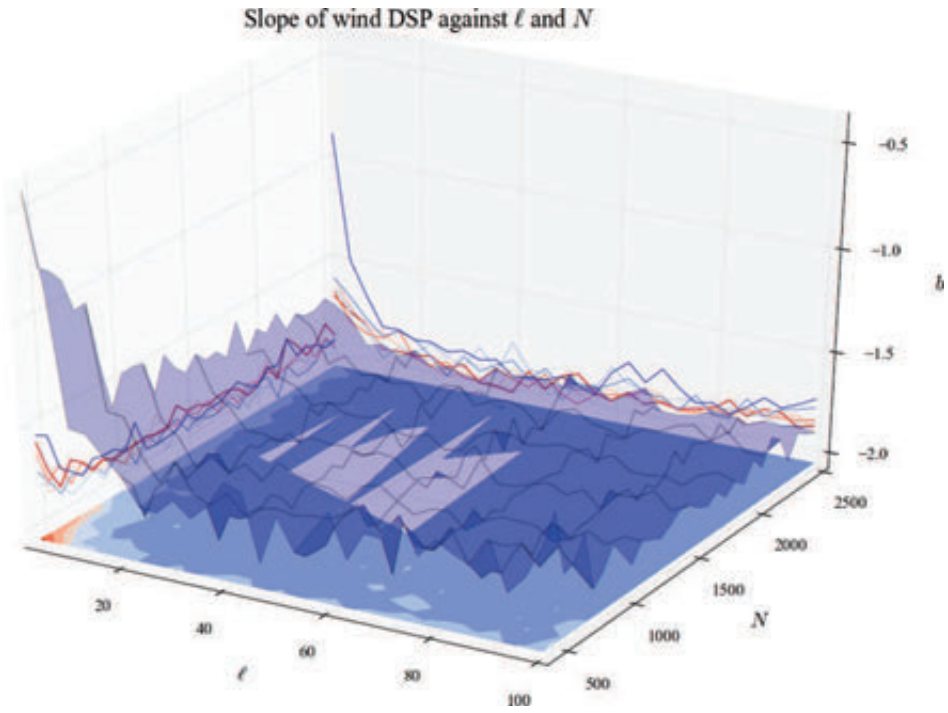

Figure C.18 – PSD slope when ℓ and N vary.

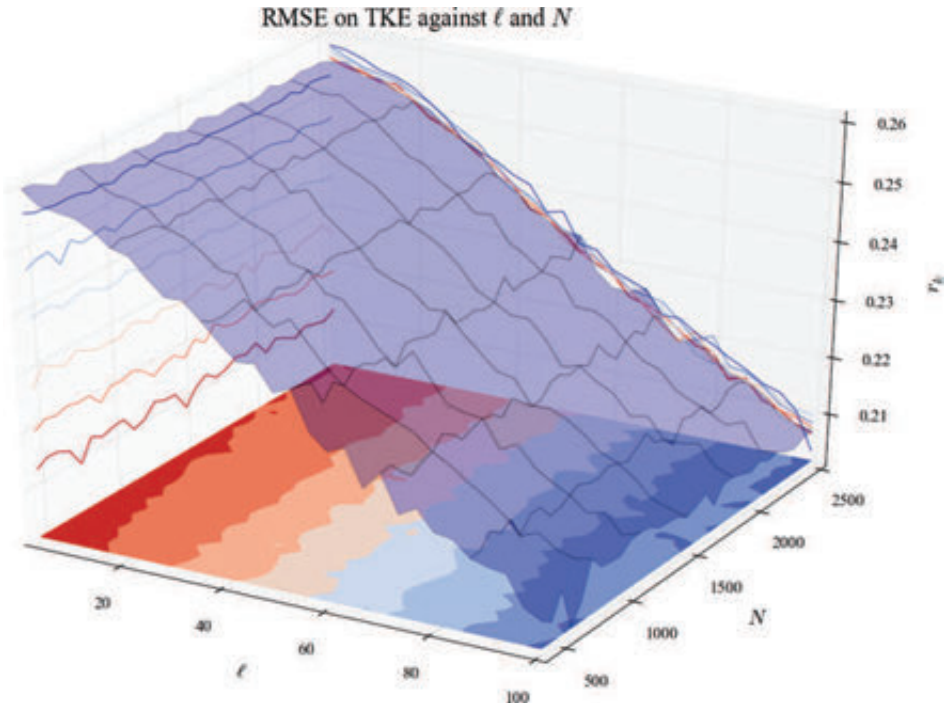

Figure C.19 – RMSE on TKE when ℓ and N vary.

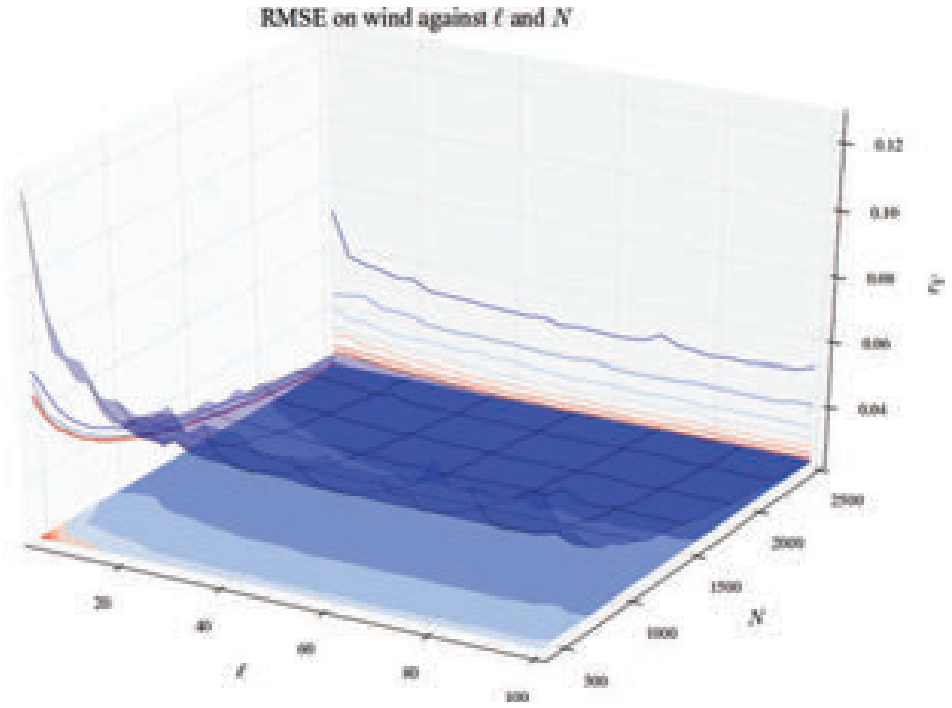

Figure C.20 – RMSE on wind when ℓ and N vary.

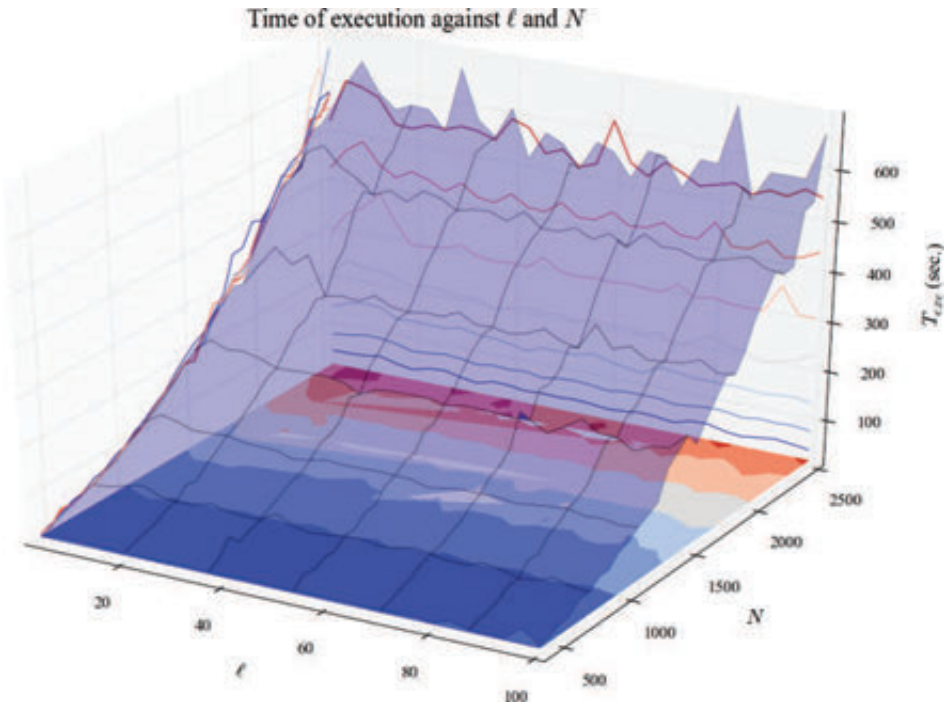

Figure C.21 – Execution time when ℓ and N vary.

C.2.5 ℓ and σ^{add}

In this experiment, only ℓ and σ^{add} vary. To check another experiment, go to table C.3 (hyperlinks in the table). To have more explanation about these inputs, go to table C.1.

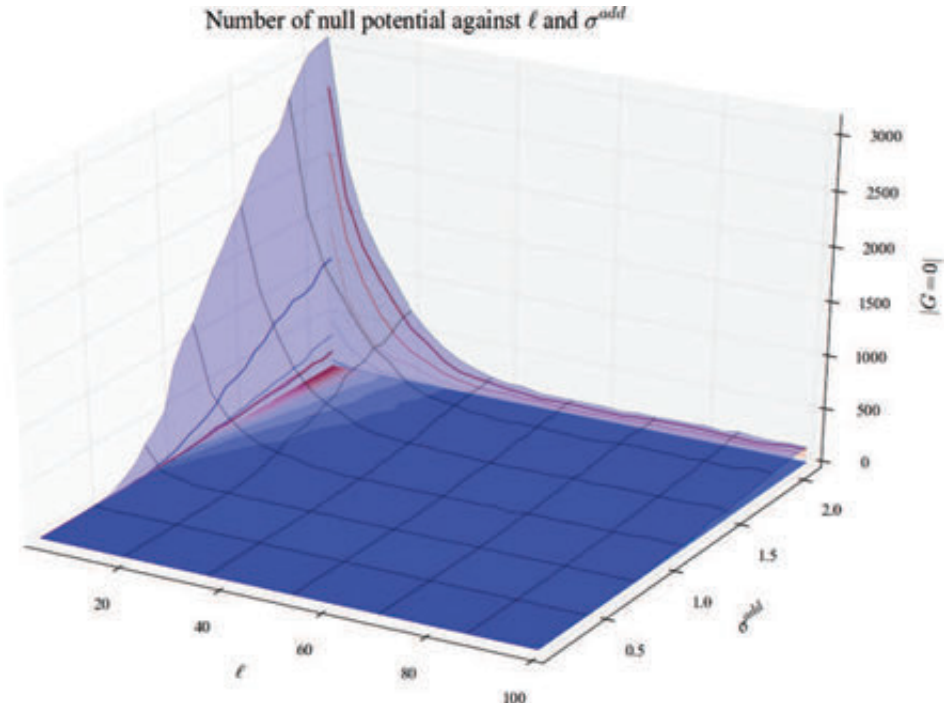

Figure C.22 – Number of null potential when ℓ and σ^{add} vary.

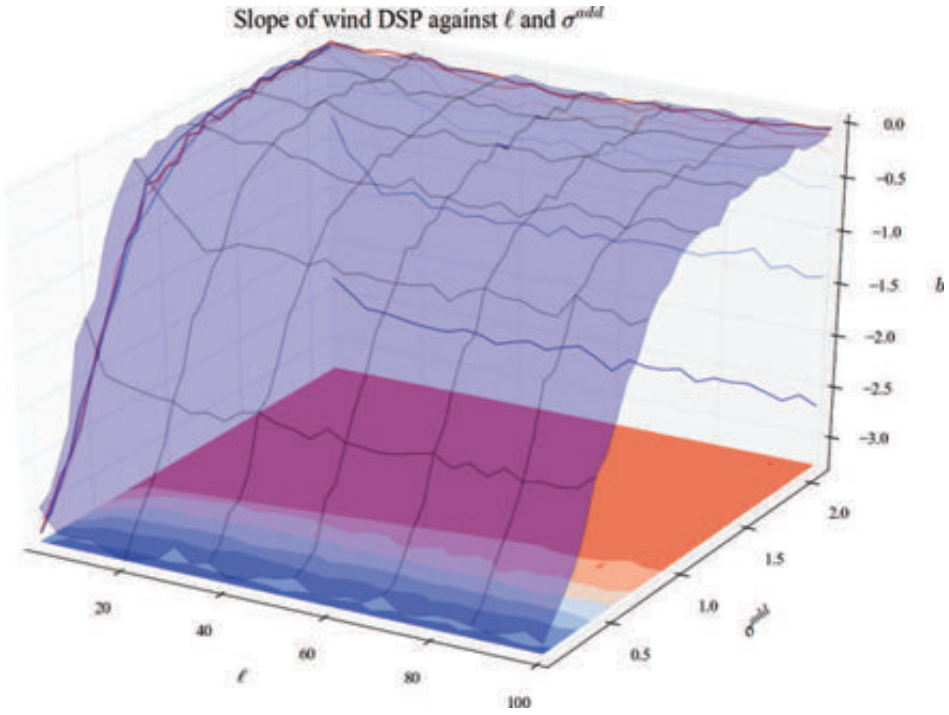

Figure C.23 – PSD slope when ℓ and σ^{add} vary.

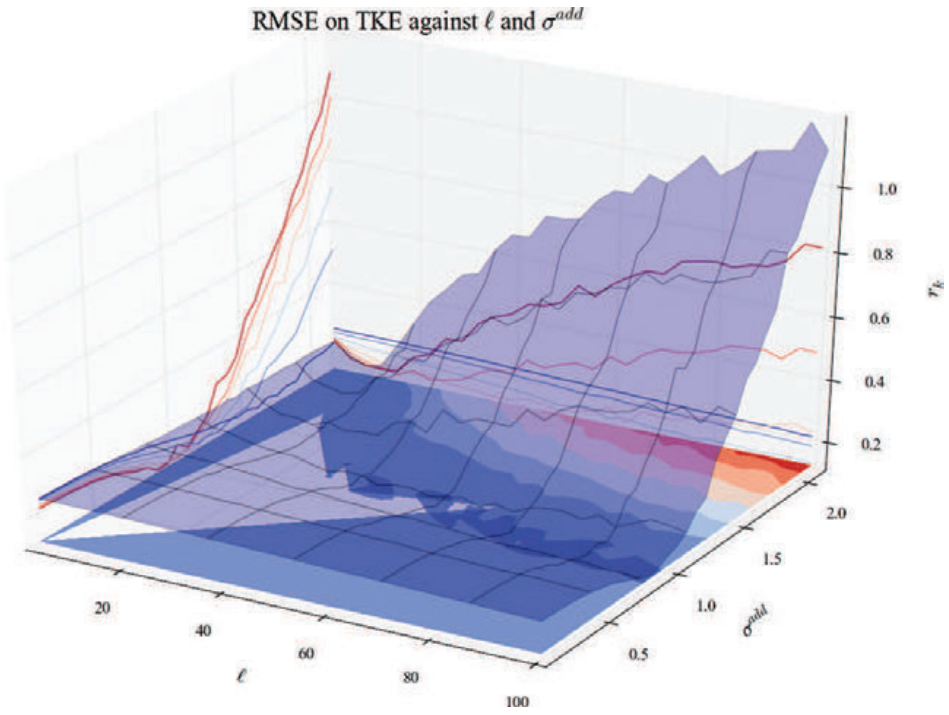

Figure C.24 – RMSE on TKE when ℓ and σ^{add} vary.

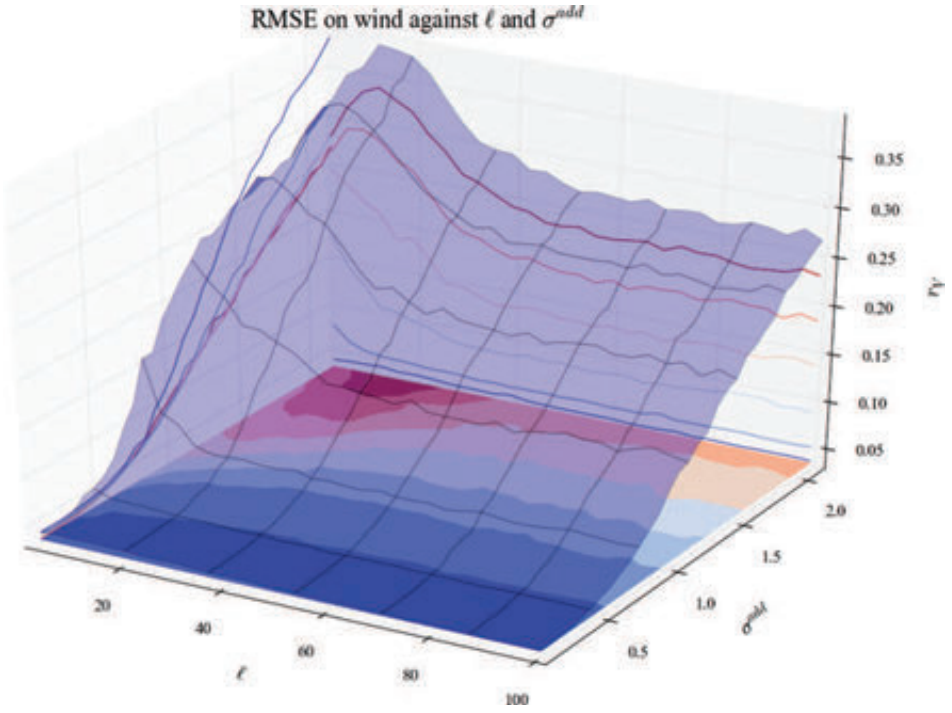

Figure C.25 – RMSE on wind when ℓ and σ^{add} vary.

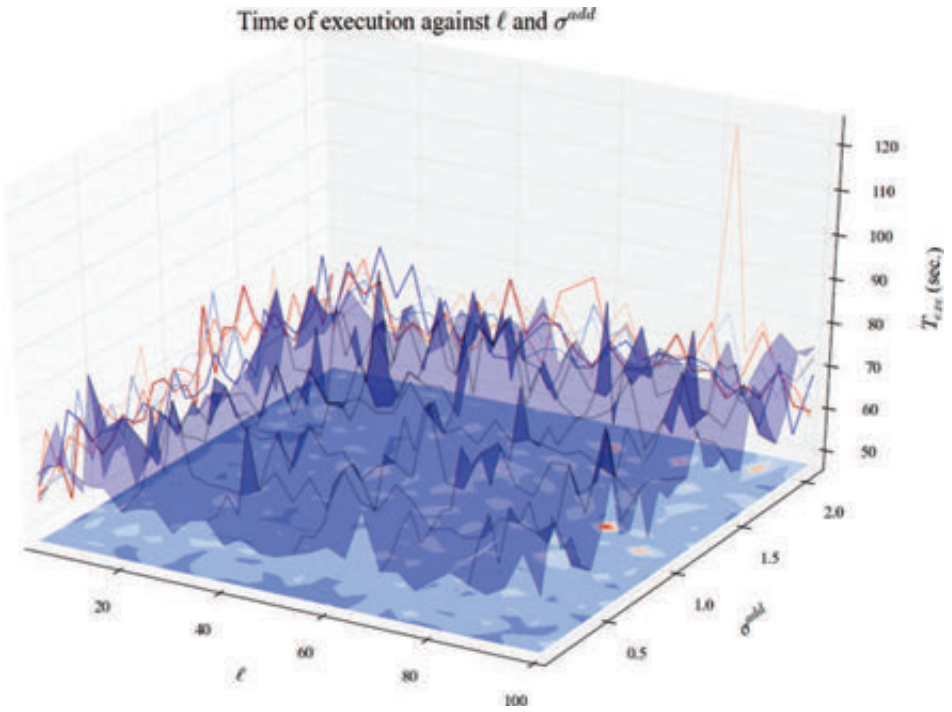

Figure C.26 – Execution time when ℓ and σ^{add} vary.

C.2.6 ℓ and σ^{obs}

In this experiment, only ℓ and σ^{obs} vary. To check another experiment, go to table C.3 (hyperlinks in the table). To have more explanation about these inputs, go to table C.1.

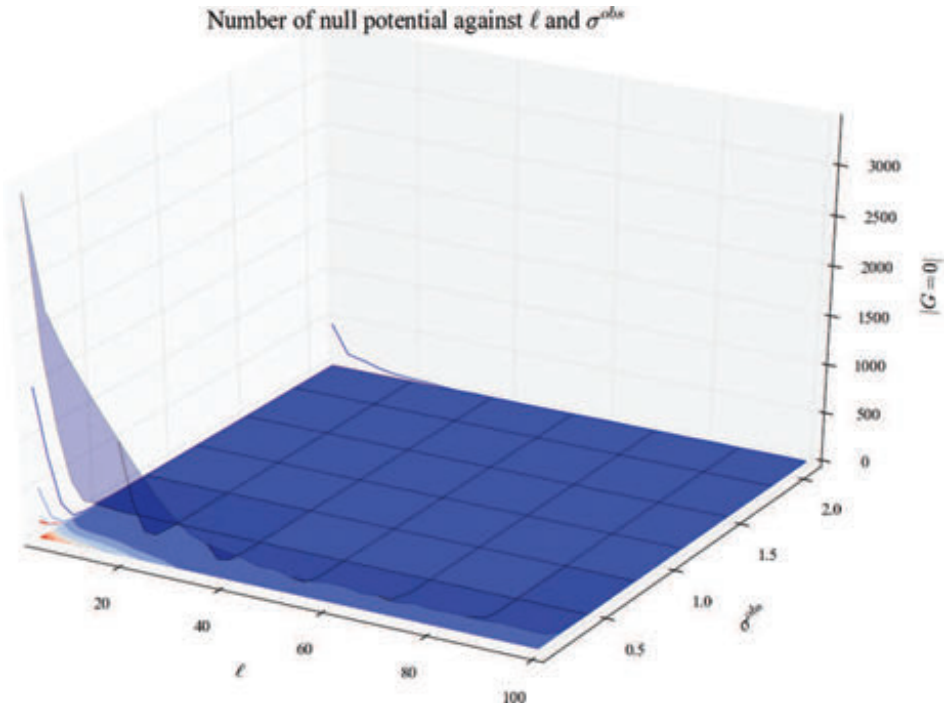

Figure C.27 – Number of null potential when ℓ and σ^{obs} vary.

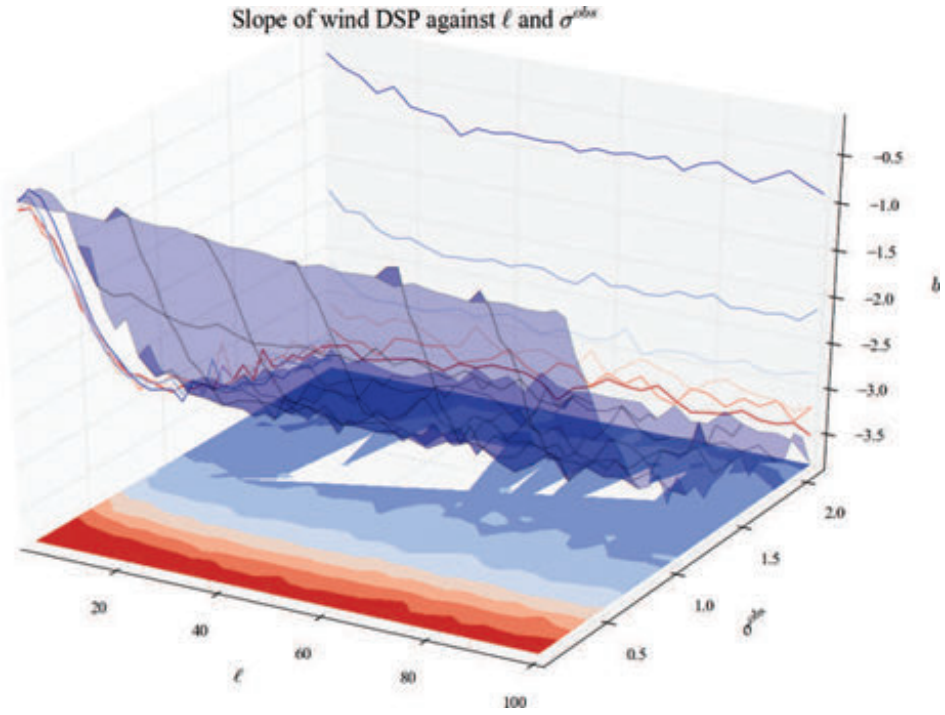

Figure C.28 – PSD slope when ℓ and σ^{obs} vary.

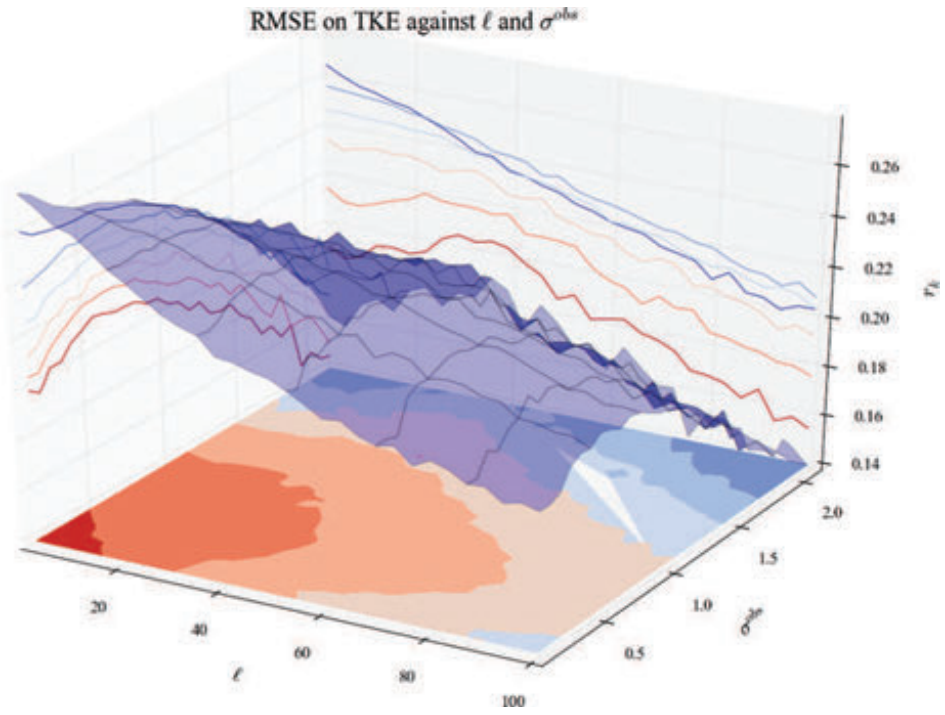

Figure C.29 – RMSE on TKE when ℓ and σ^{obs} vary.

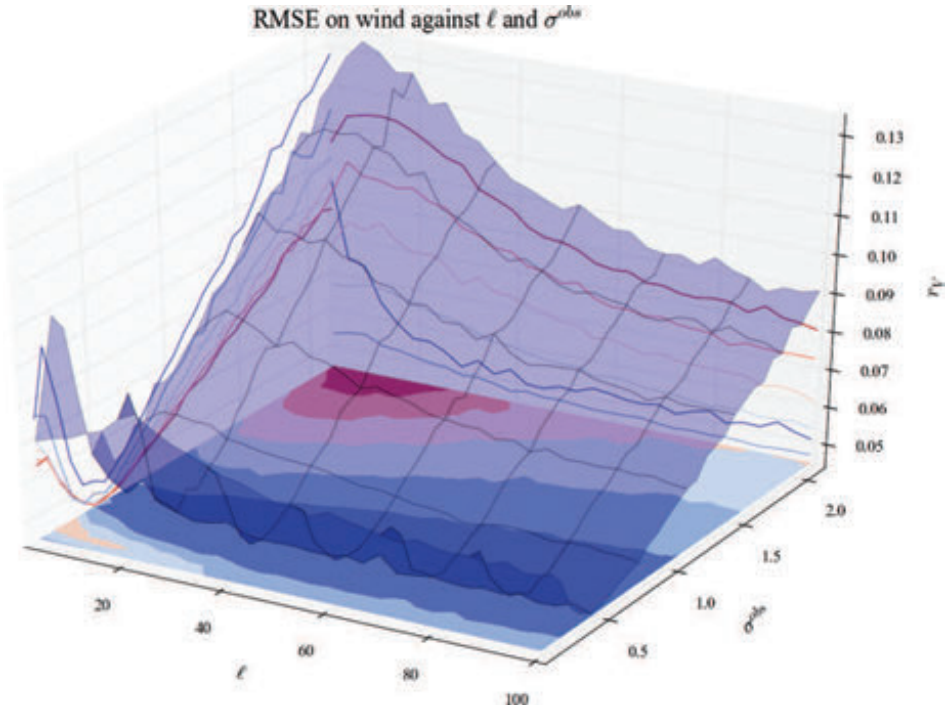

Figure C.30 – RMSE on wind when ℓ and σ^{obs} vary.

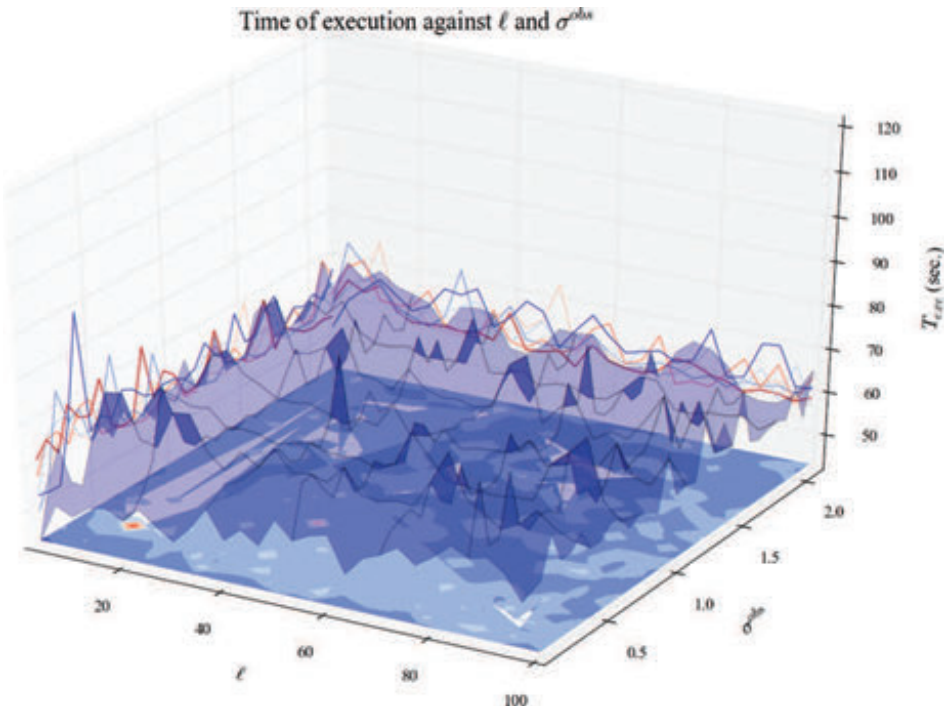

Figure C.31 – Execution time when ℓ and σ^{obs} vary.

C.2.7 N and σ^{add}

In this experiment, only N and σ^{add} vary. To check another experiment, go to table C.3 (hyperlinks in the table). To have more explanation about these inputs, go to table C.1.

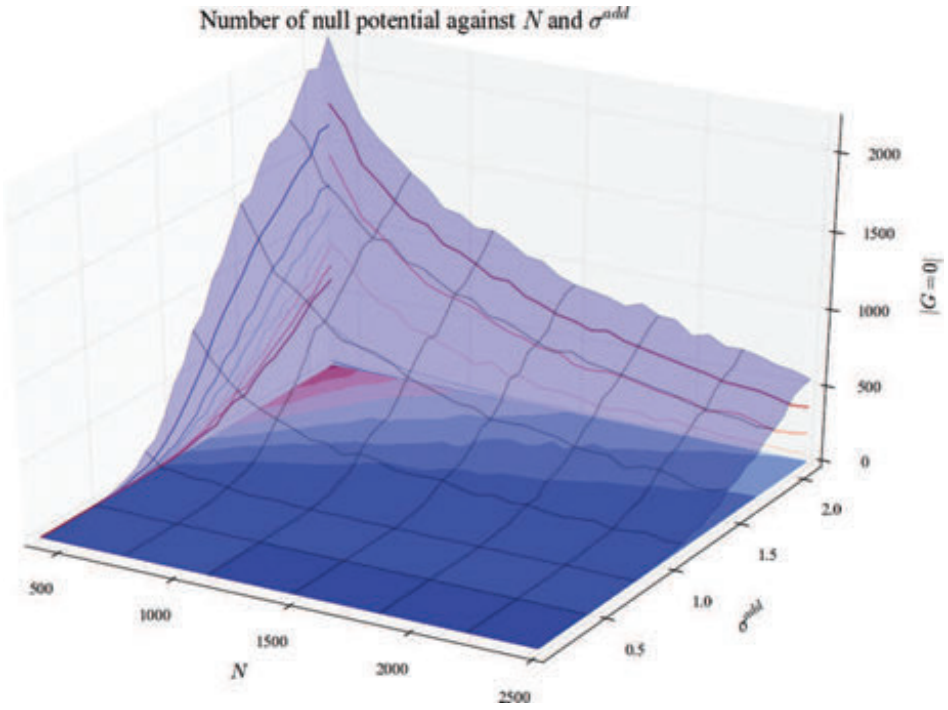

Figure C.32 – Number of null potential when N and σ^{add} vary.

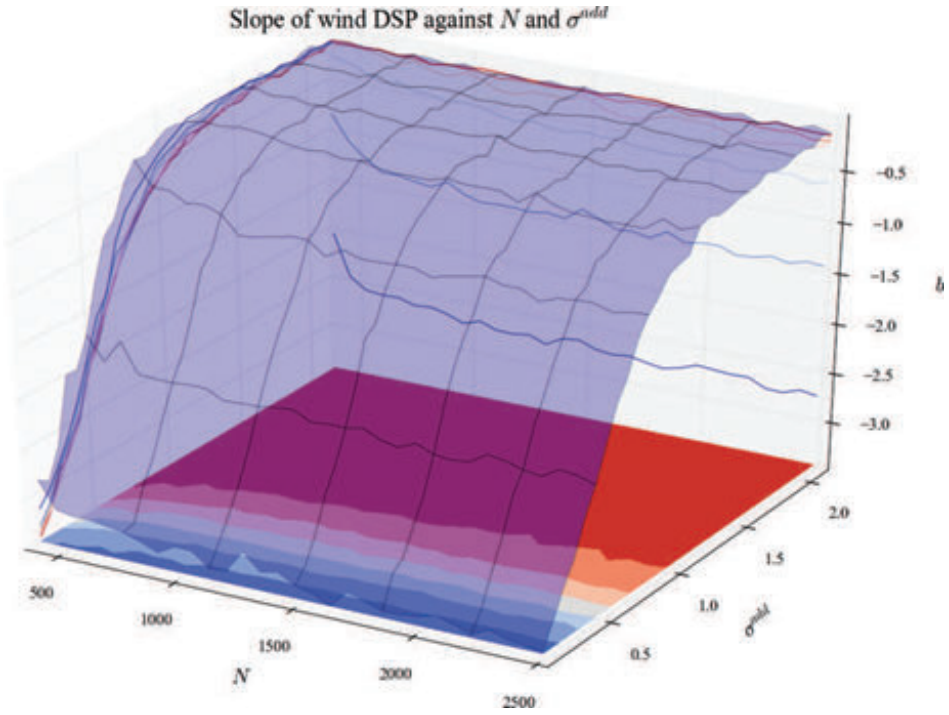

Figure C.33 – PSD slope when N and σ^{add} vary.

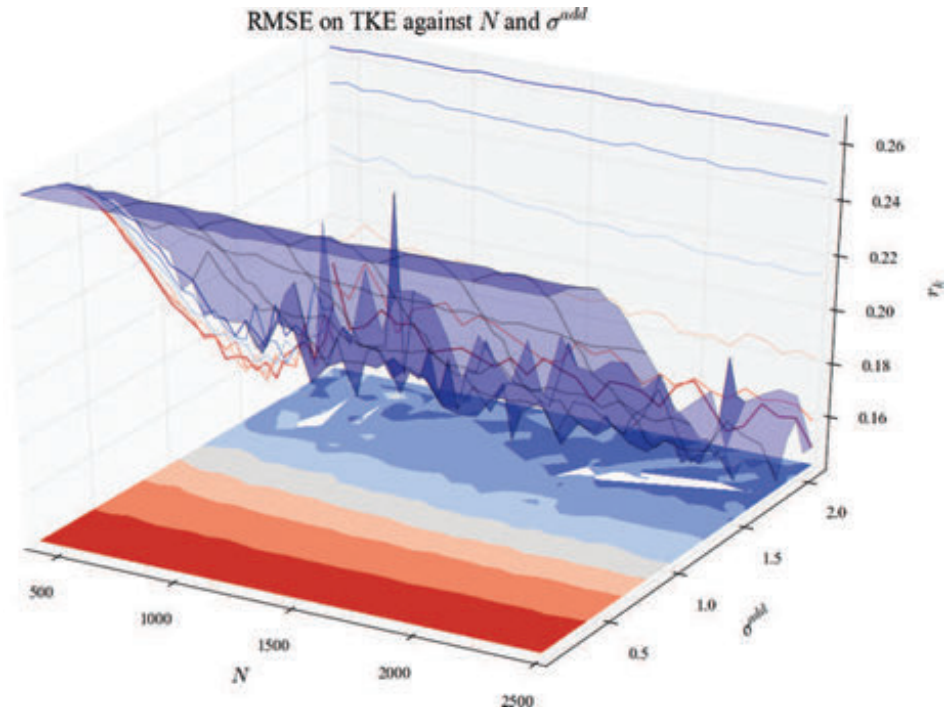

Figure C.34 – RMSE on TKE when N and σ^{add} vary.

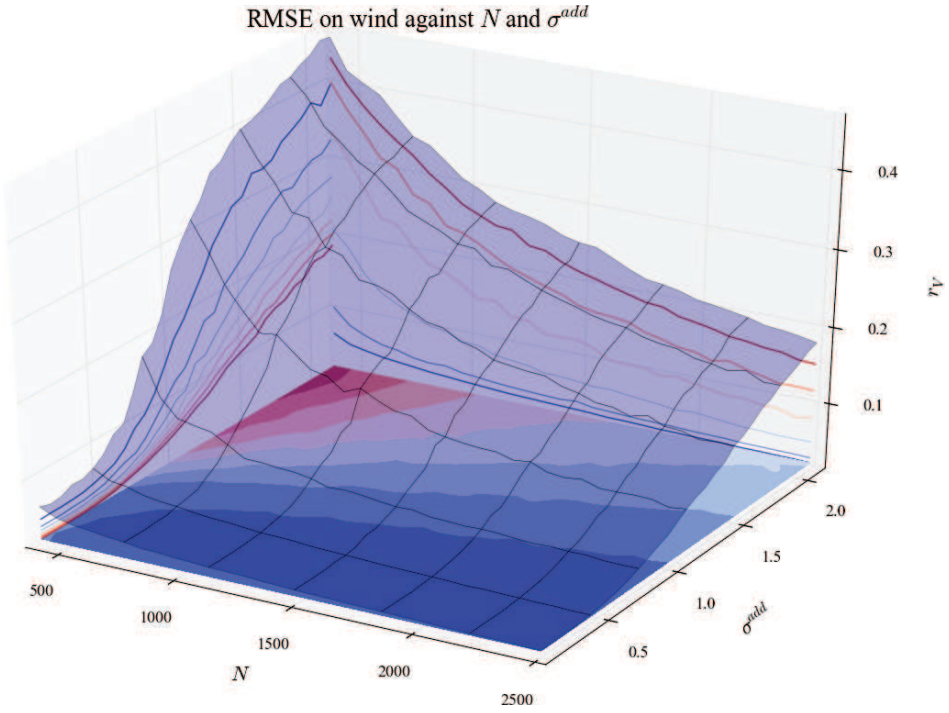

Figure C.35 – RMSE on wind when N and σ^{add} vary.

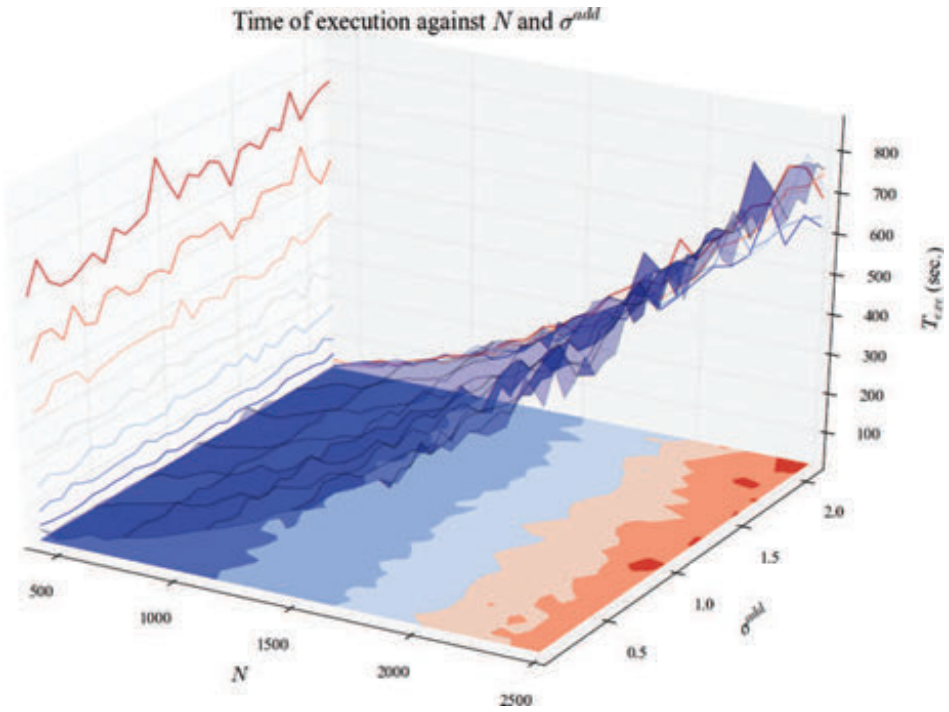

Figure C.36 – Execution time when N and σ^{add} vary.

C.2.8 N and σ^{obs}

In this experiment, only N and σ^{obs} vary. To check another experiment, go to table C.3 (hyperlinks in the table). To have more explanation about these inputs, go to table C.1.

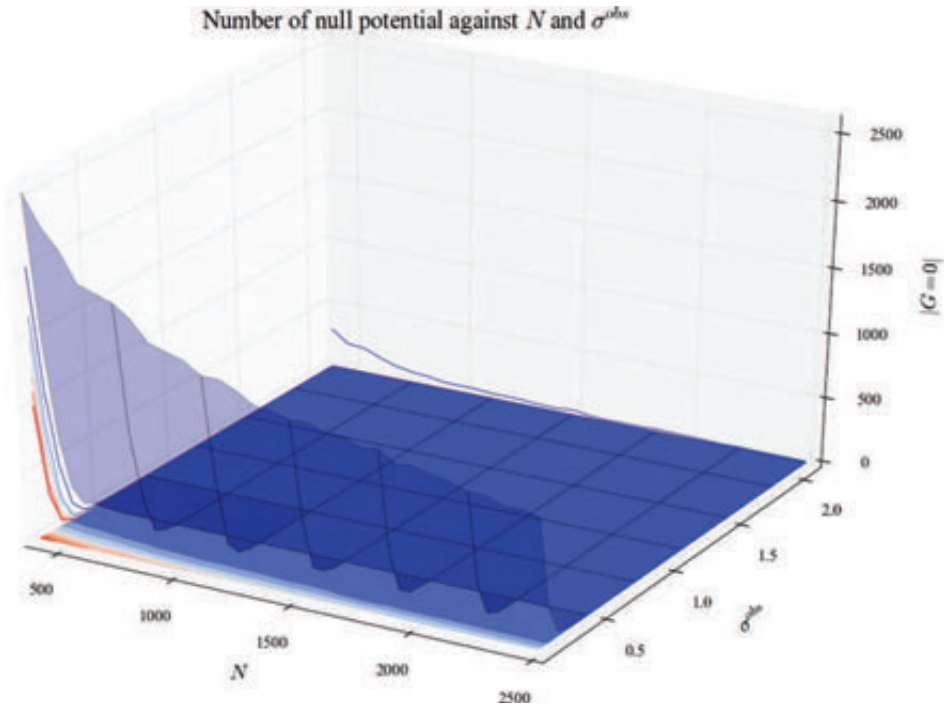

Figure C.37 – Number of null potential when N and σ^{obs} vary.

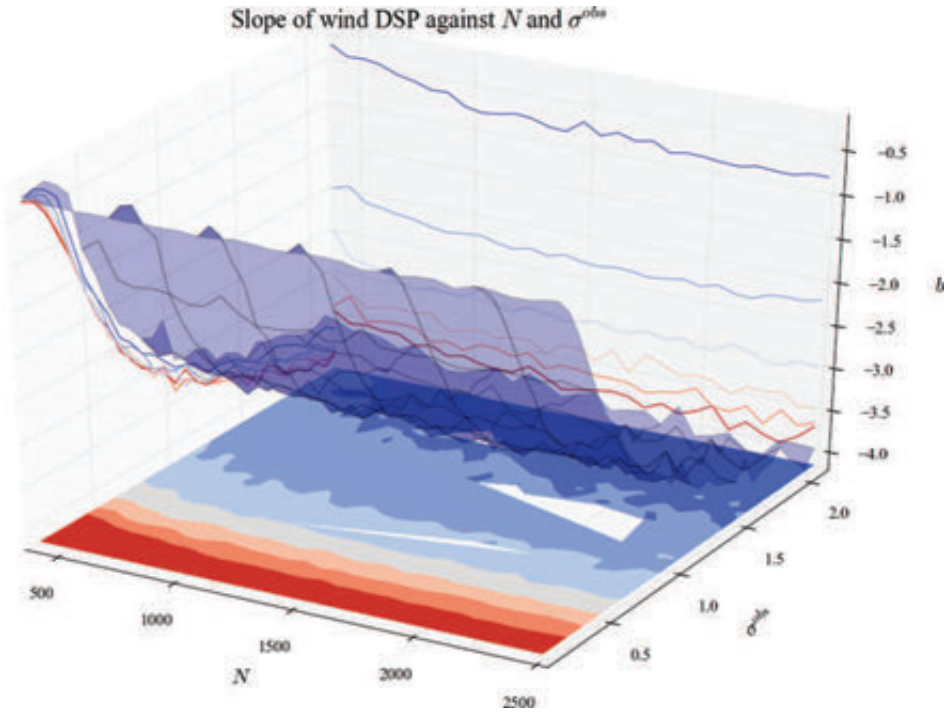

Figure C.38 – PSD slope when N and σ^{obs} vary.

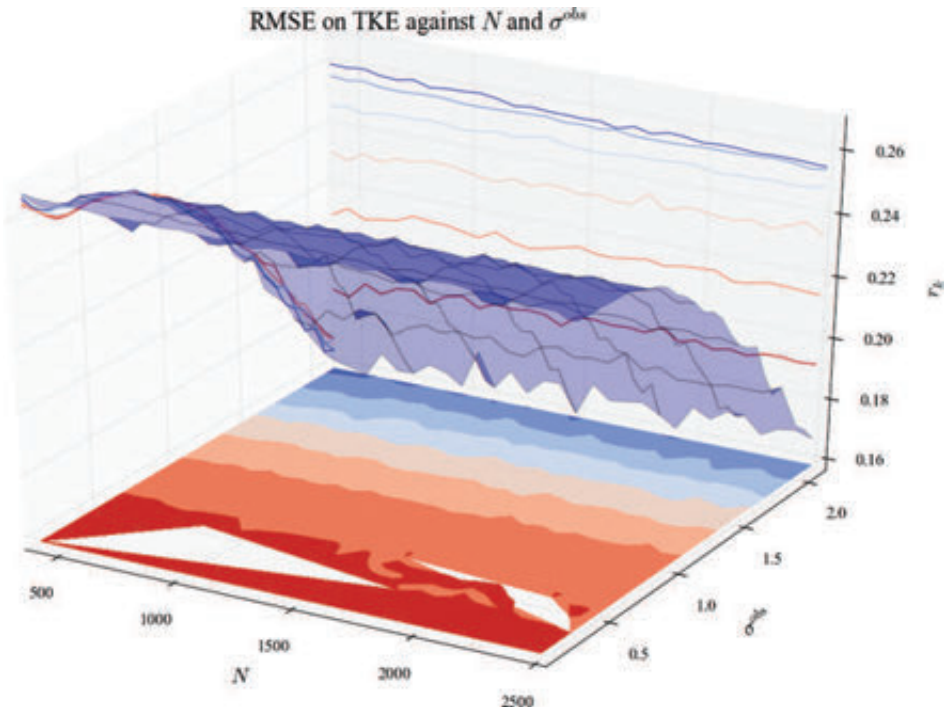

Figure C.39 – RMSE on TKE when N and σ^{obs} vary.

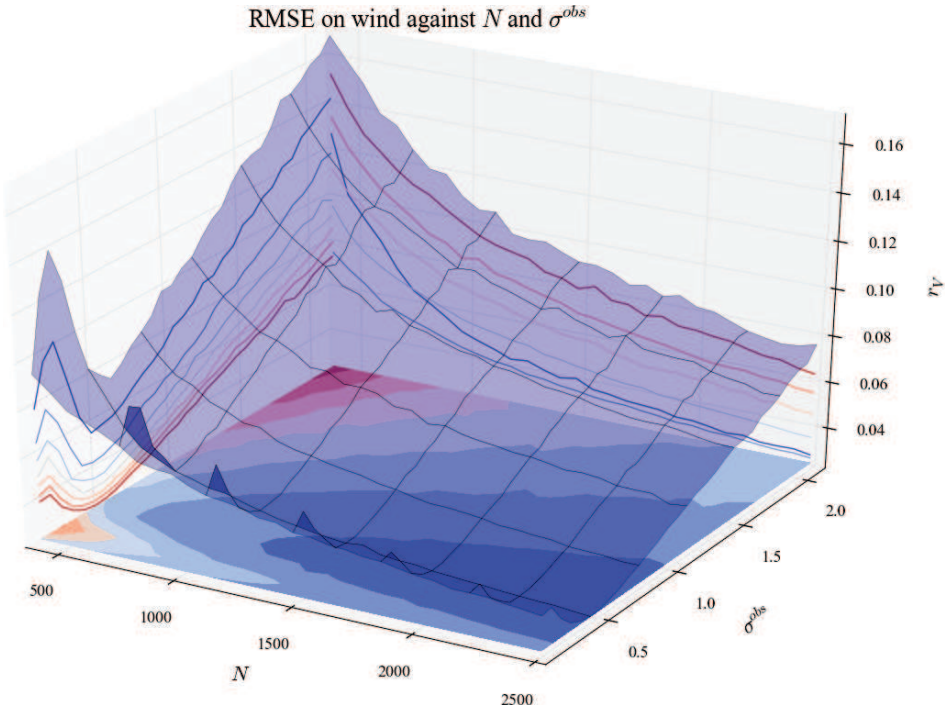

Figure C.40 – RMSE on wind when N and σ^{obs} vary.

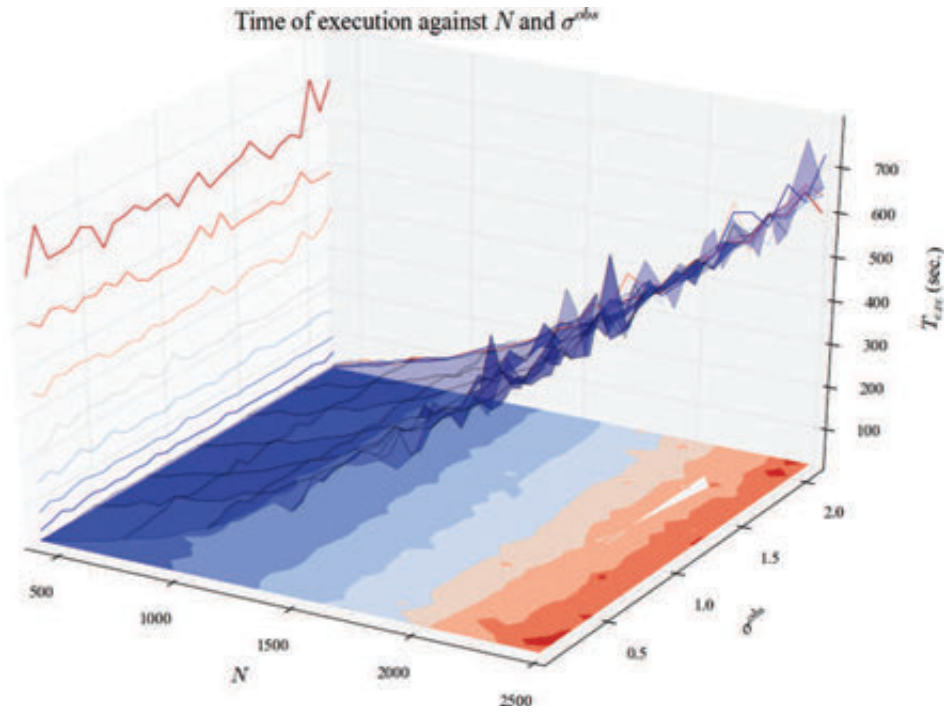

Figure C.41 – Execution time when N and σ^{obs} vary.

C.2.9 N and τ

In this experiment, only N and τ vary. To check another experiment, go to table C.3 (hyperlinks in the table). To have more explanation about these inputs, go to table C.1.

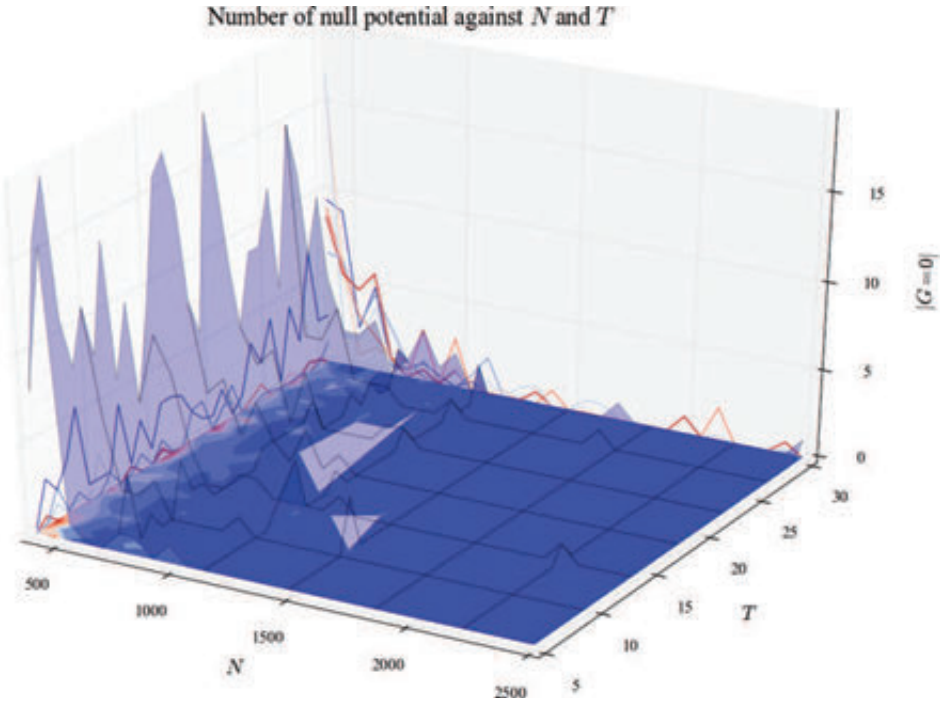

Figure C.42 – Number of null potential when N and τ vary.

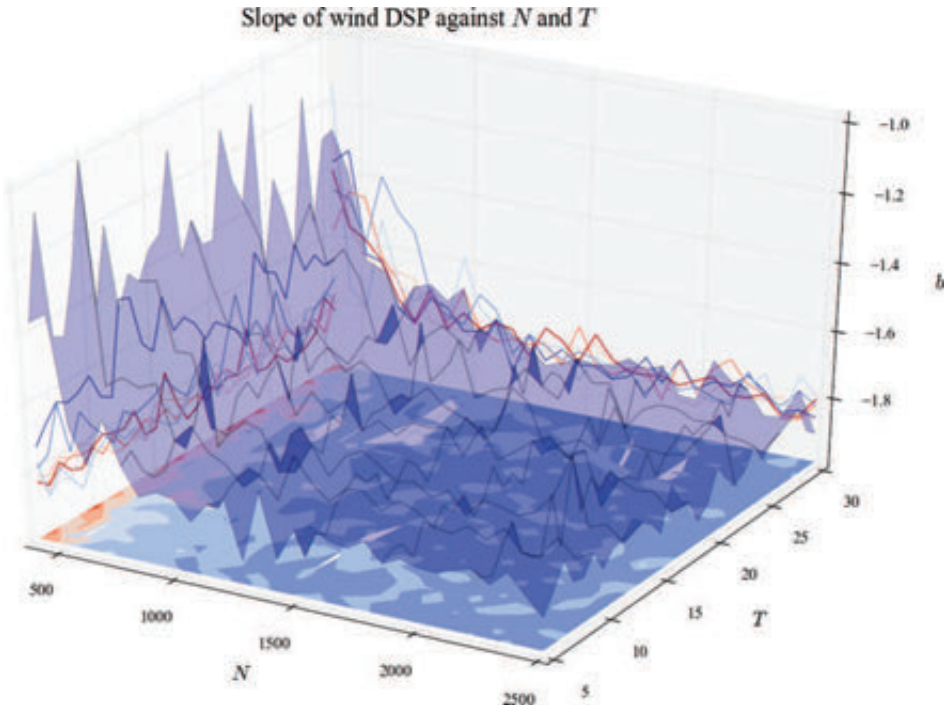

Figure C.43 – PSD slope when N and τ vary.

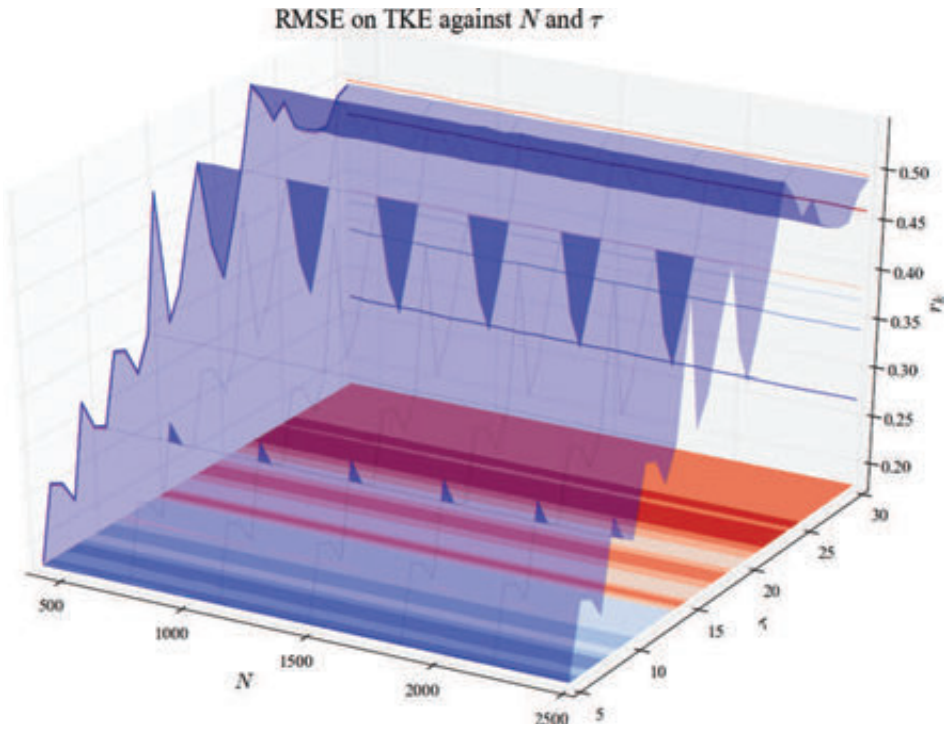

Figure C.44 – RMSE on TKE when N and τ vary.

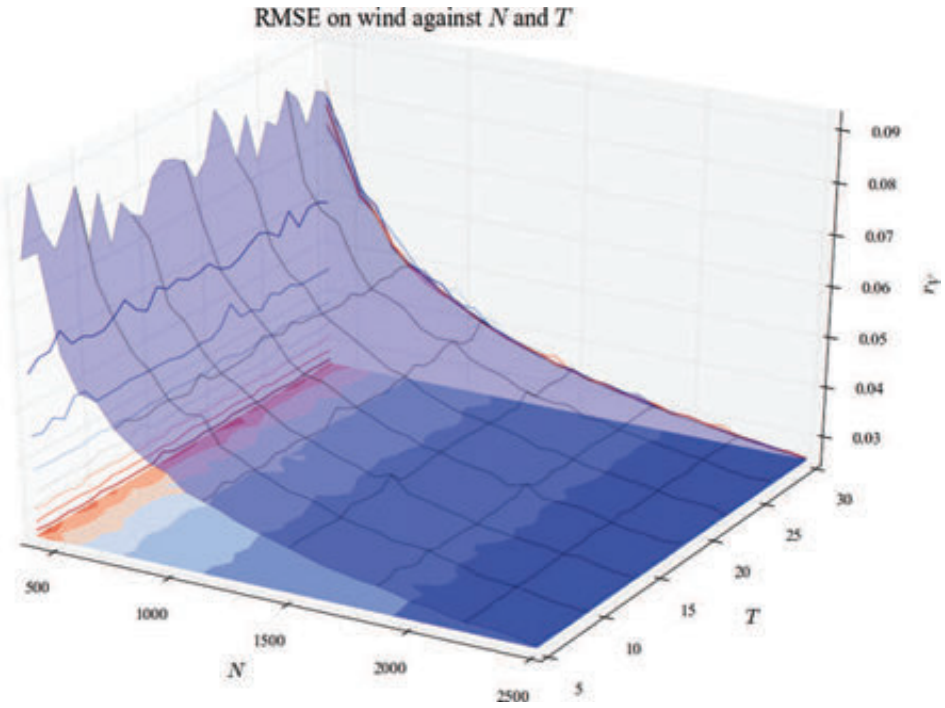

Figure C.45 – RMSE on wind when N and τ vary.

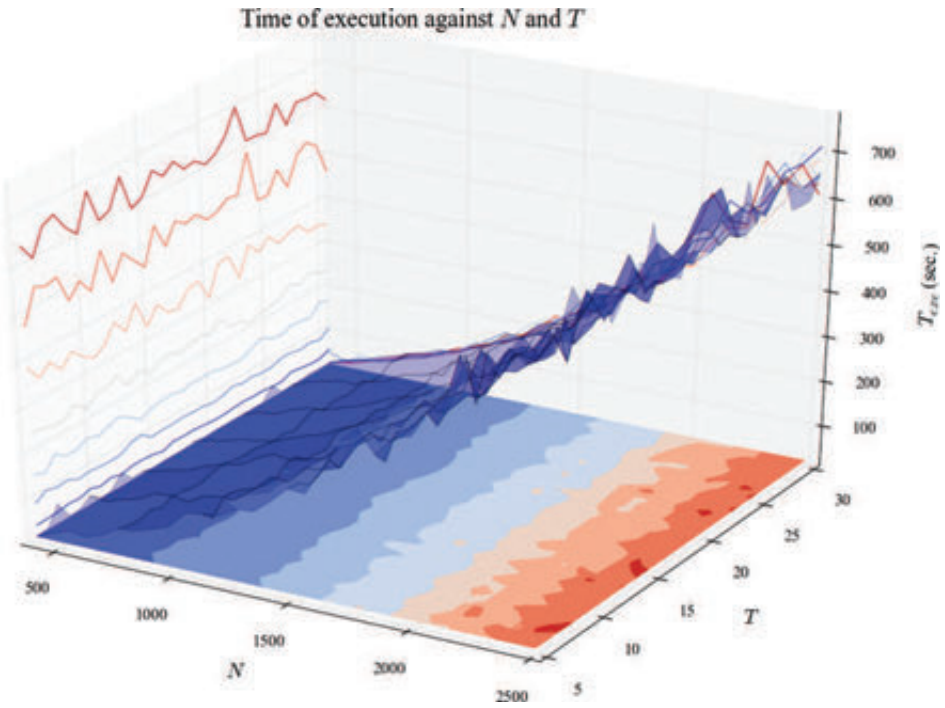

Figure C.46 – Execution time when N and τ vary.

C.2.10 σ^{add} and σ^{obs}

In this experiment, only σ^{add} and σ^{obs} vary. To check another experiment, go to table C.3 (hyperlinks in the table). To have more explanation about these inputs, go to table C.1.

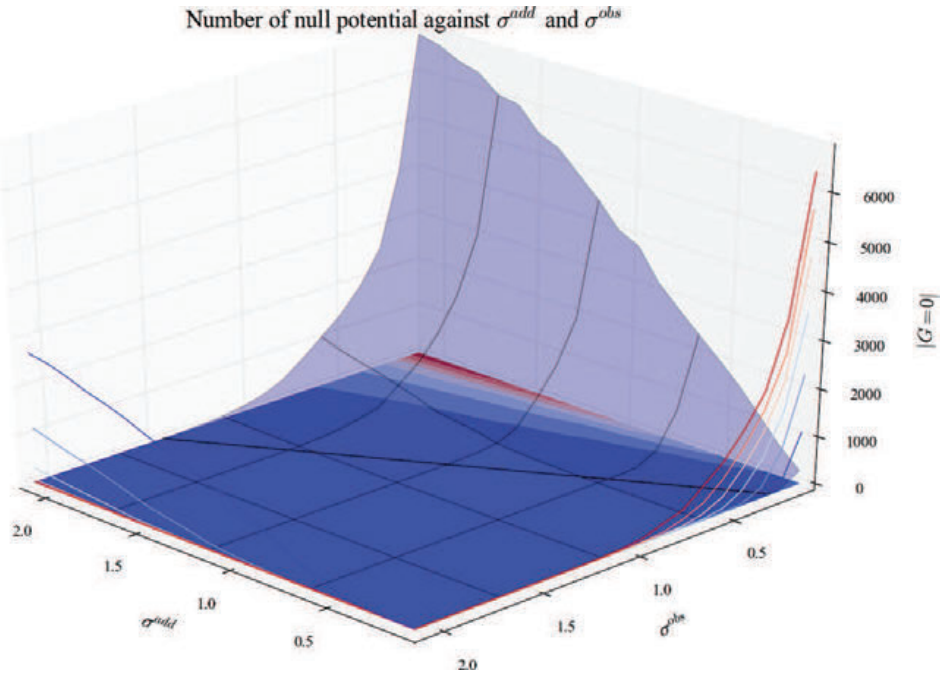

Figure C.47 – Number of null potential when σ^{add} and σ^{obs} vary.

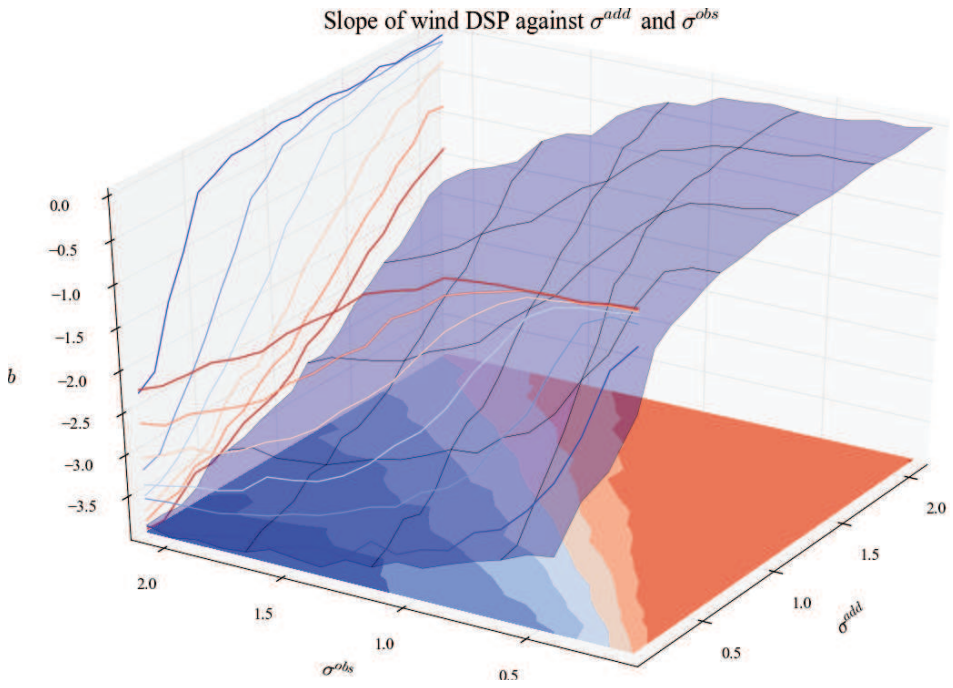

Figure C.48 – PSD slope when σ^{add} and σ^{obs} vary.

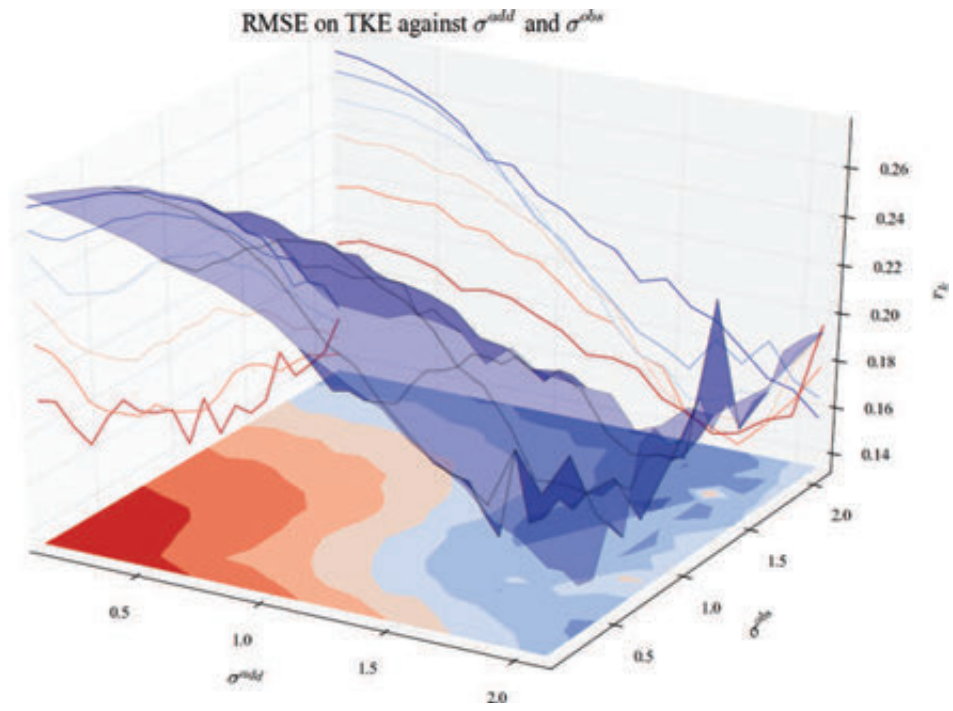

Figure C.49 – RMSE on TKE when σ^{add} and σ^{obs} vary.

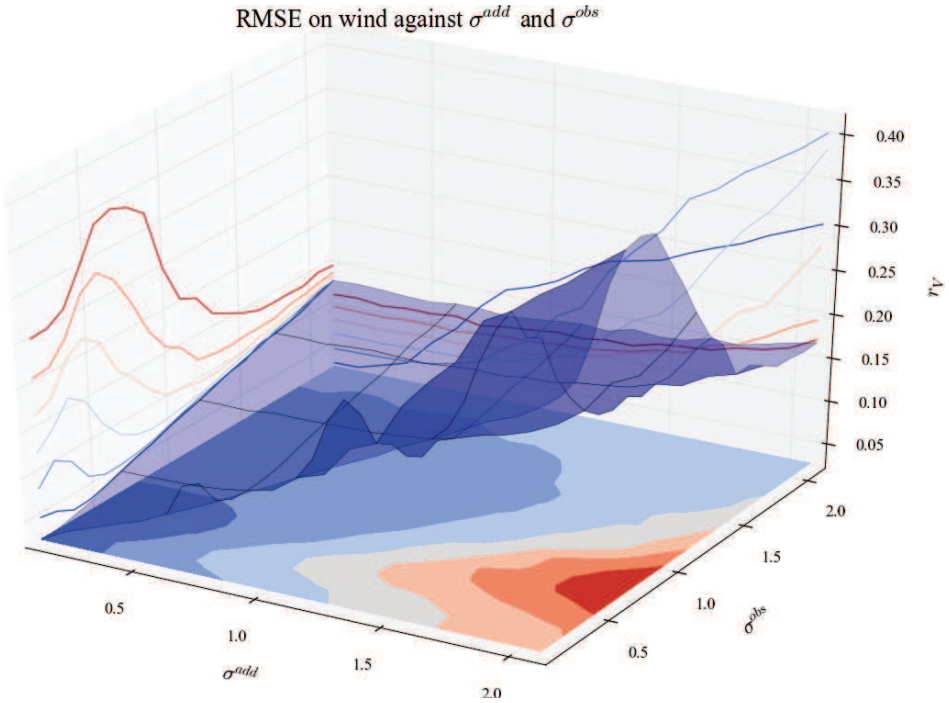

Figure C.50 – RMSE on wind when σ^{add} and σ^{obs} vary.

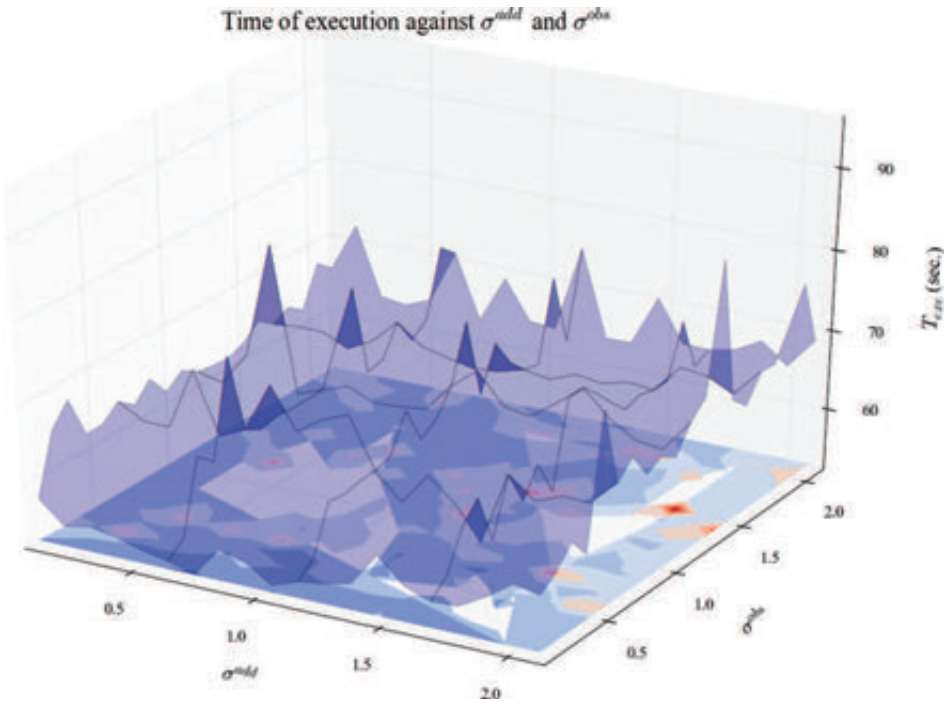

Figure C.51 – Execution time when σ^{add} and σ^{obs} vary.

C.2.11 σ^{add} and τ

In this experiment, only σ^{add} and τ vary. To check another experiment, go to table C.3 (hyperlinks in the table). To have more explanation about these inputs, go to table C.1.

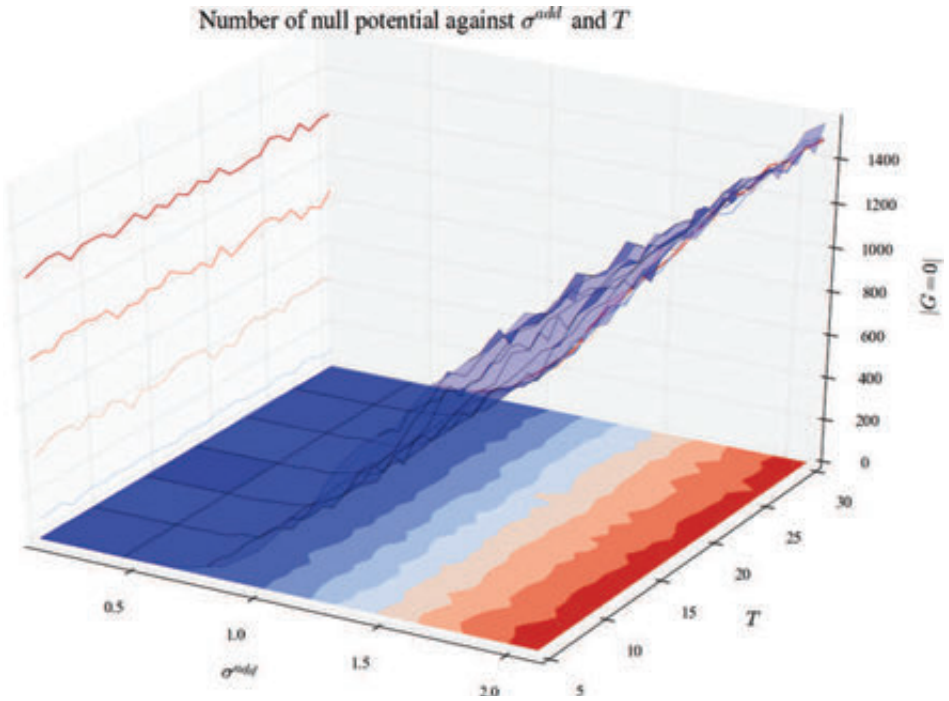

Figure C.52 – Number of null potential when σ^{add} and τ vary.

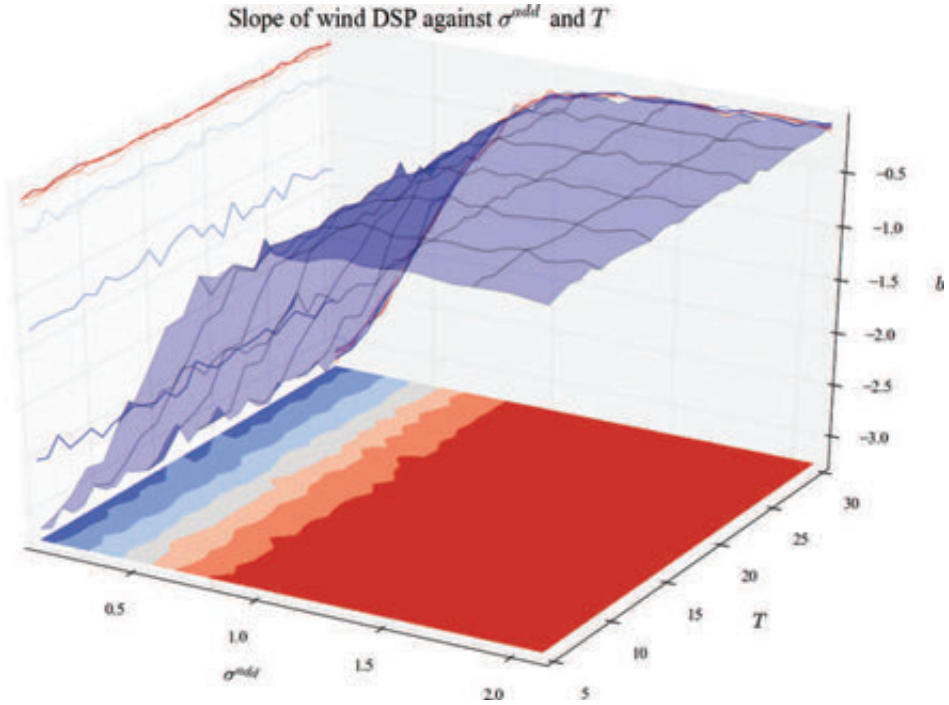

Figure C.53 – PSD slope when σ^{add} and τ vary.

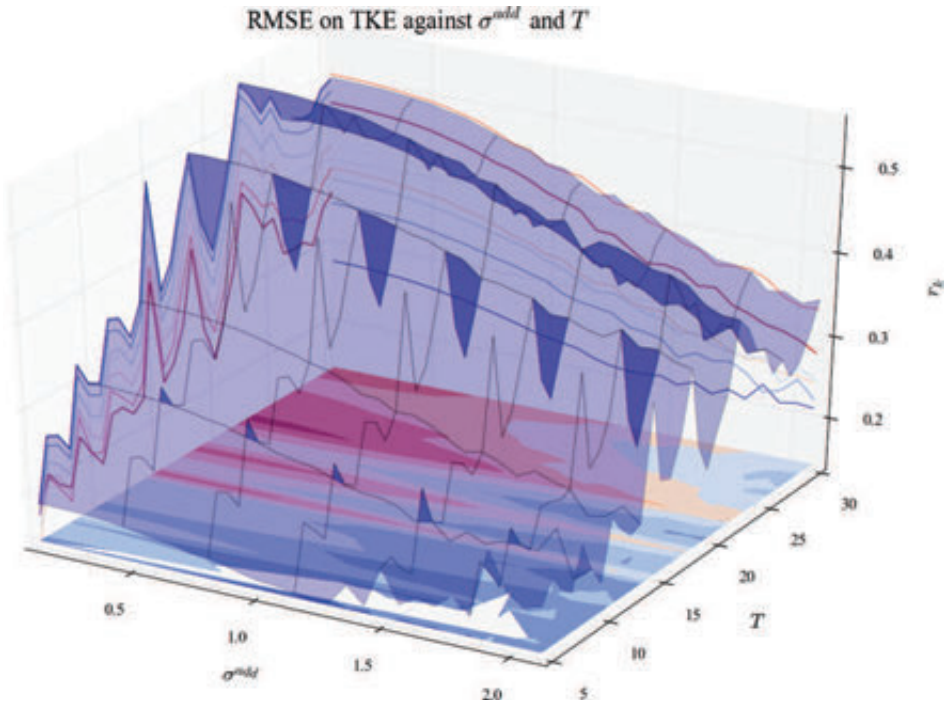

Figure C.54 – RMSE on TKE when σ^{add} and τ vary.

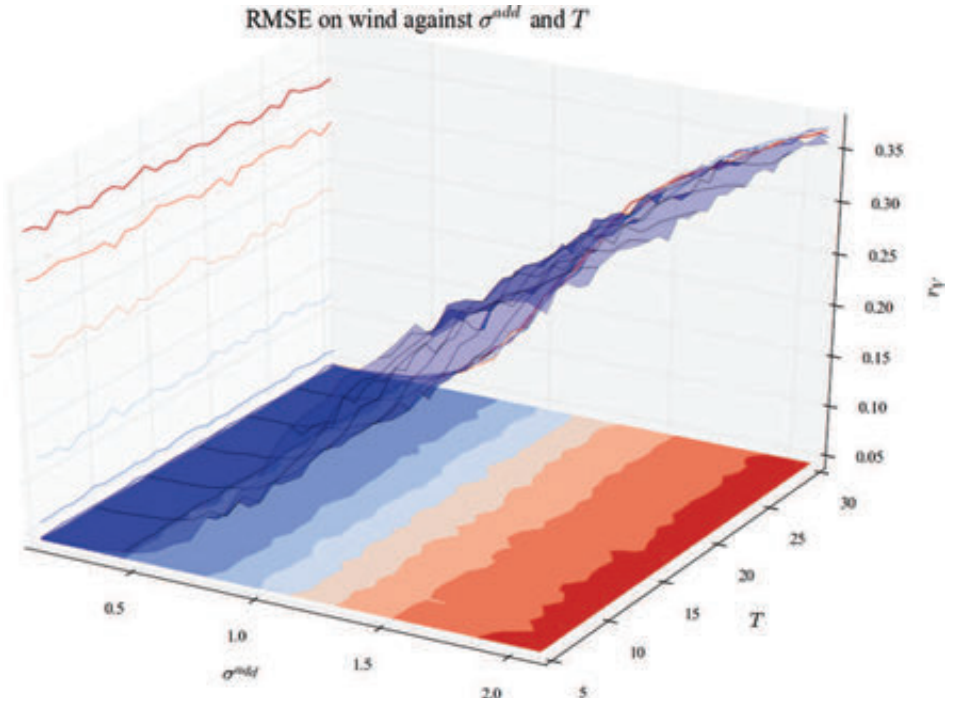

Figure C.55 – RMSE on wind when σ^{add} and τ vary.

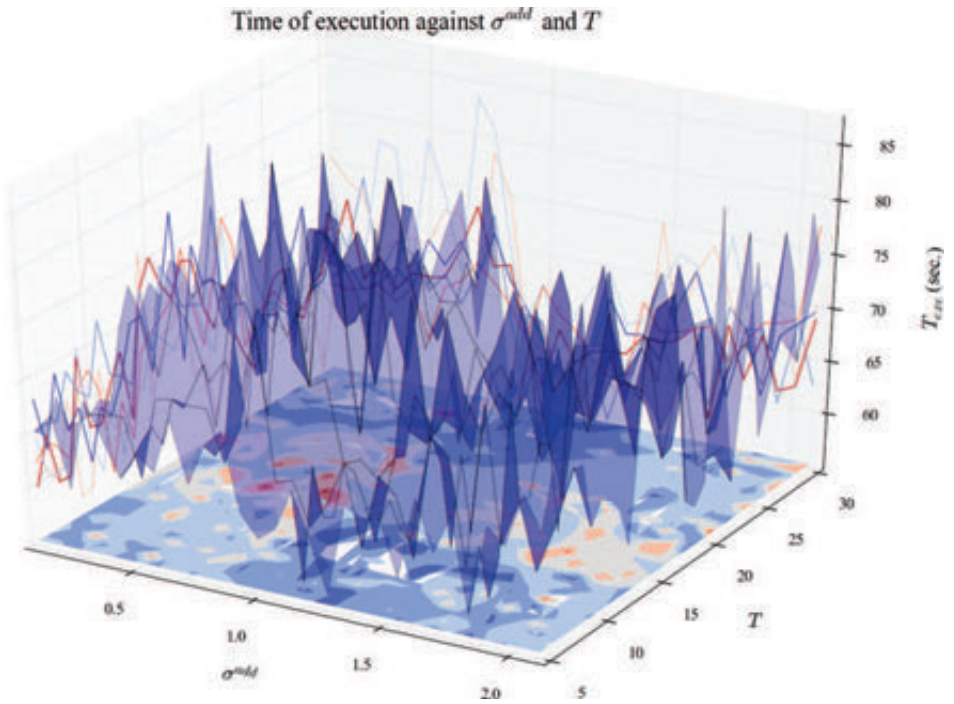

Figure C.56 – Execution time when σ^{add} and τ vary.

C.2.12 σ^{obs} and σ^X

In this experiment, only σ^{obs} and σ^X vary. To check another experiment, go to table C.3 (hyperlinks in the table). To have more explanation about these inputs, go to table C.1.

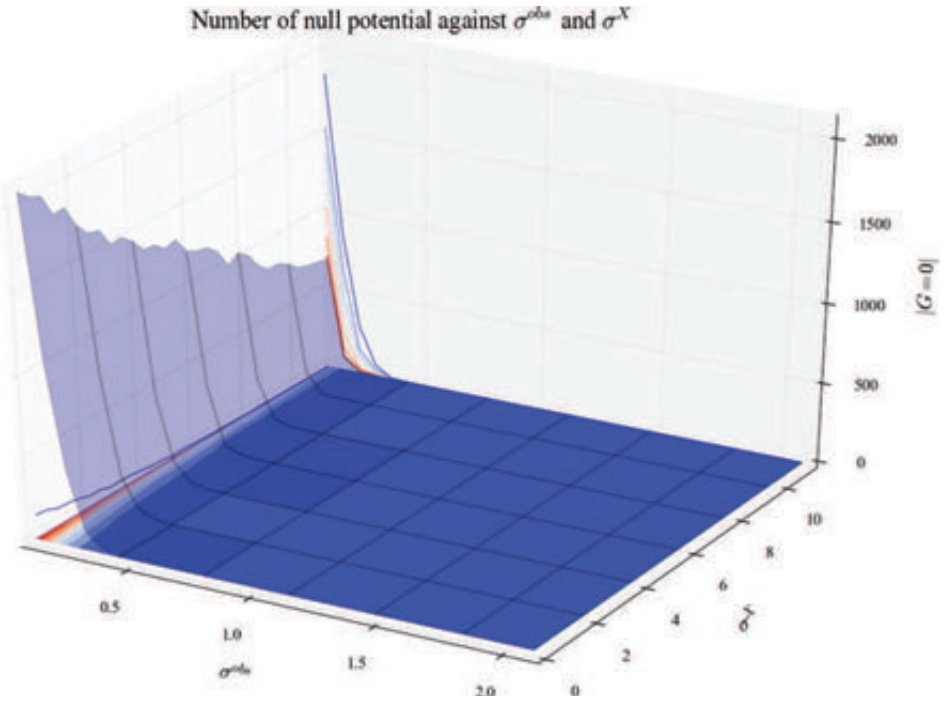

Figure C.57 – Number of null potential when σ^{obs} and σ^X vary.

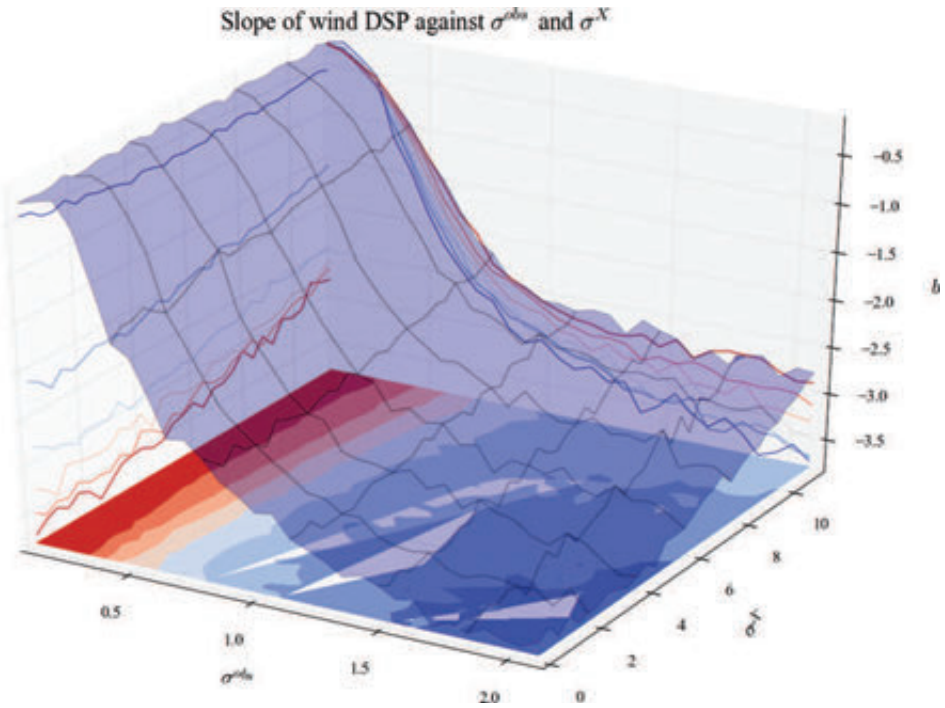

Figure C.58 – PSD slope when σ^{obs} and σ^X vary.

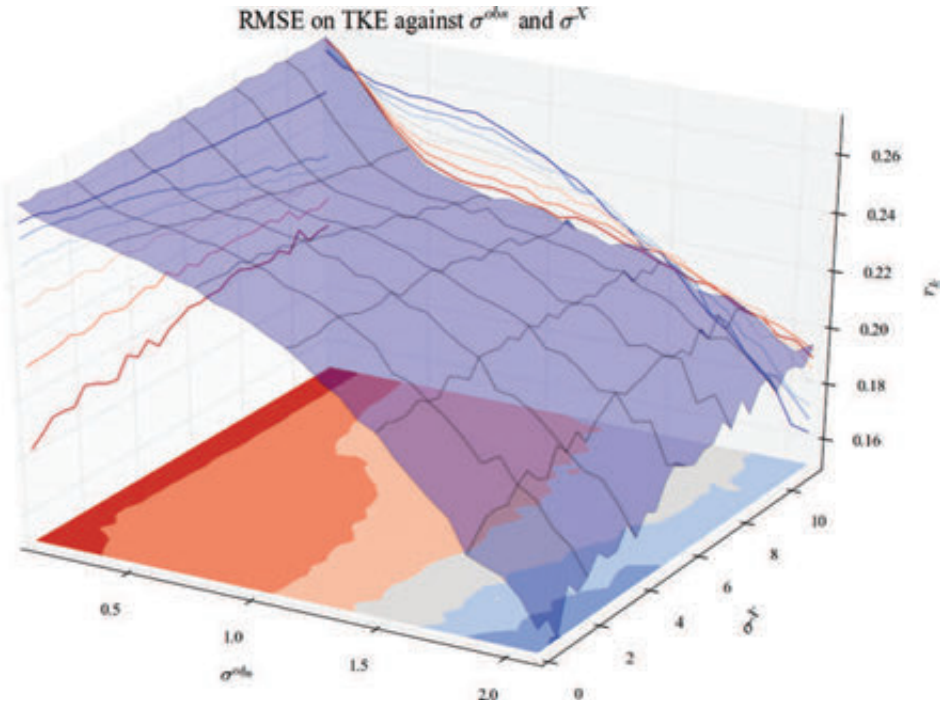

Figure C.59 – RMSE on TKE when σ^{obs} and σ^X vary.

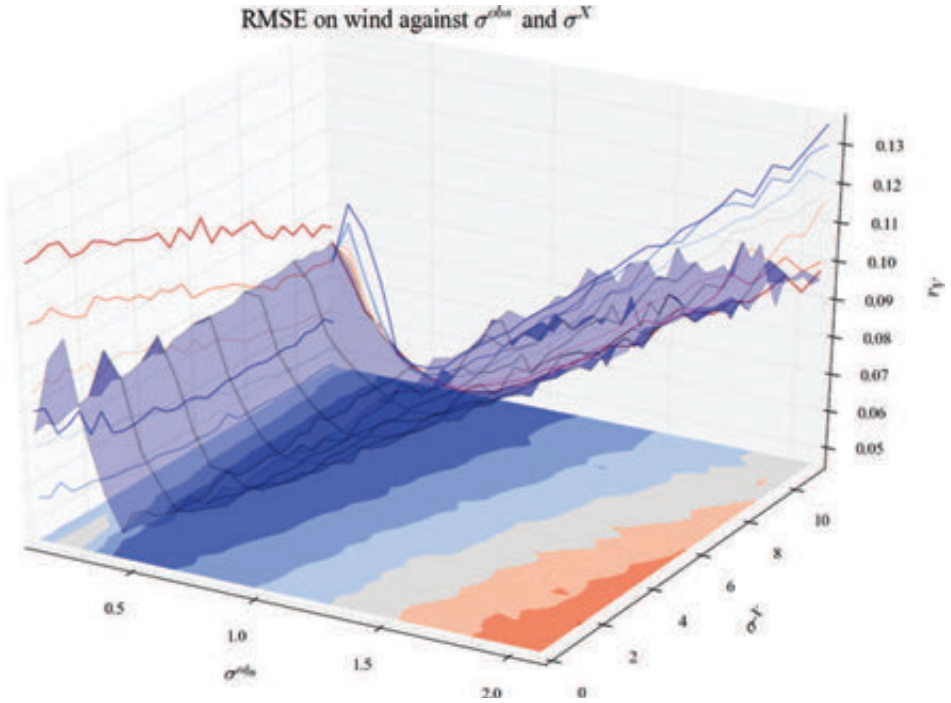

Figure C.60 – RMSE on wind when σ^{obs} and σ^X vary.

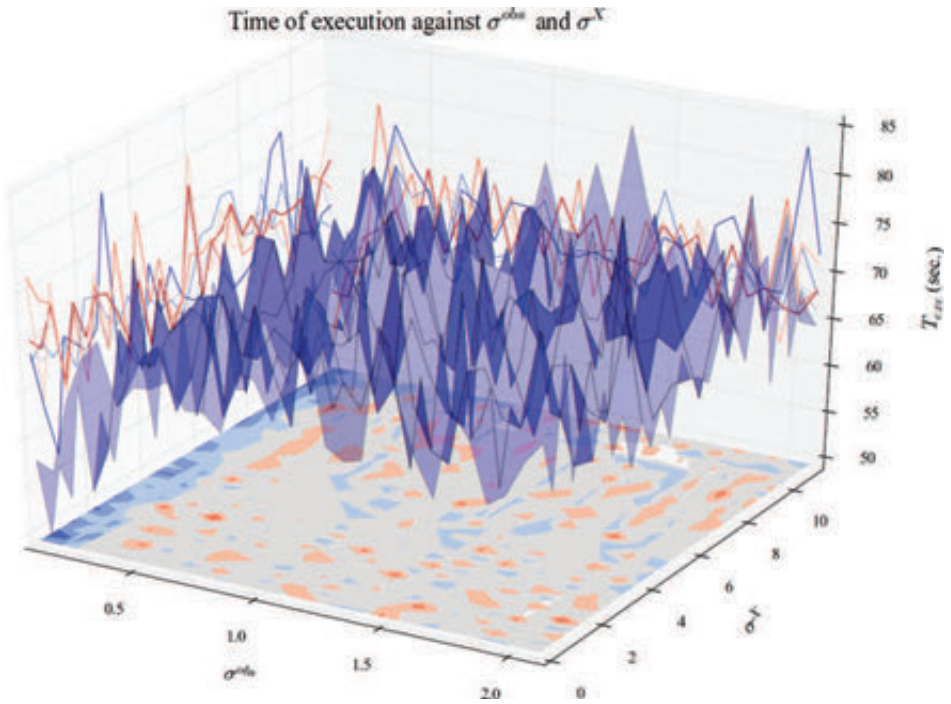

Figure C.61 – Execution time when σ^{obs} and σ^X vary.

C.2.13 σ^{obs} and τ

In this experiment, only σ^{obs} and τ vary. To check another experiment, go to table C.3 (hyperlinks in the table). To have more explanation about these inputs, go to table C.1.

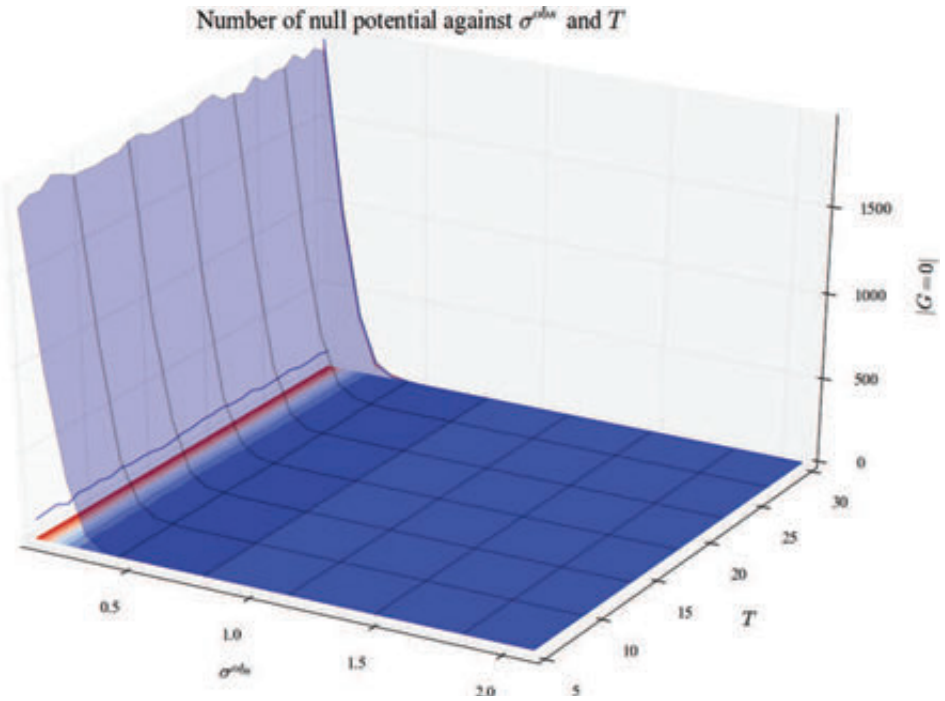

Figure C.62 – Number of null potential when σ^{obs} and τ vary.

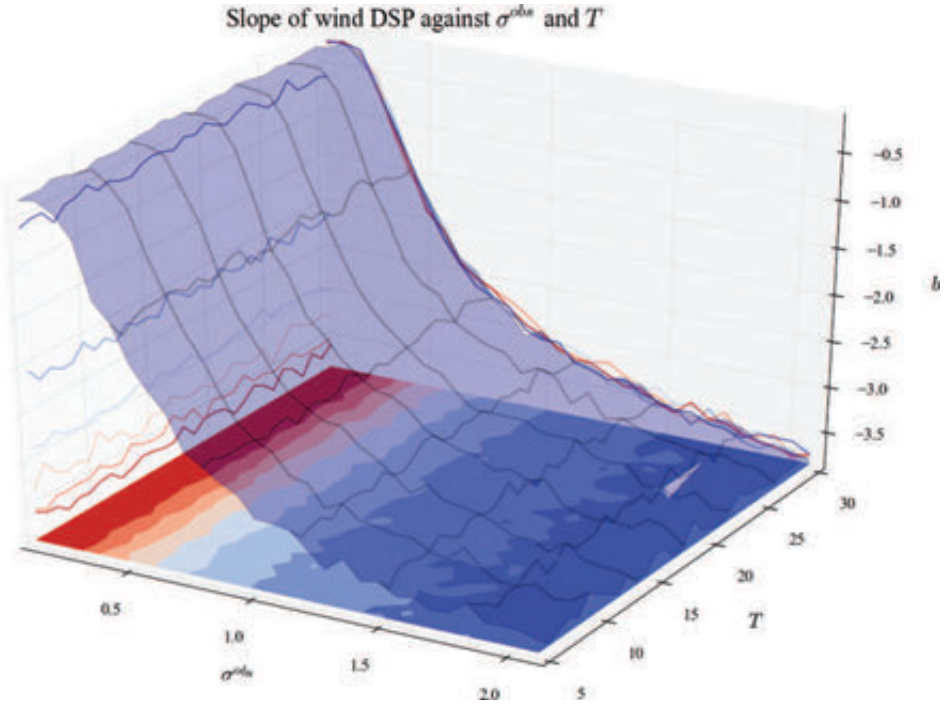

Figure C.63 – PSD slope when σ^{obs} and τ vary.

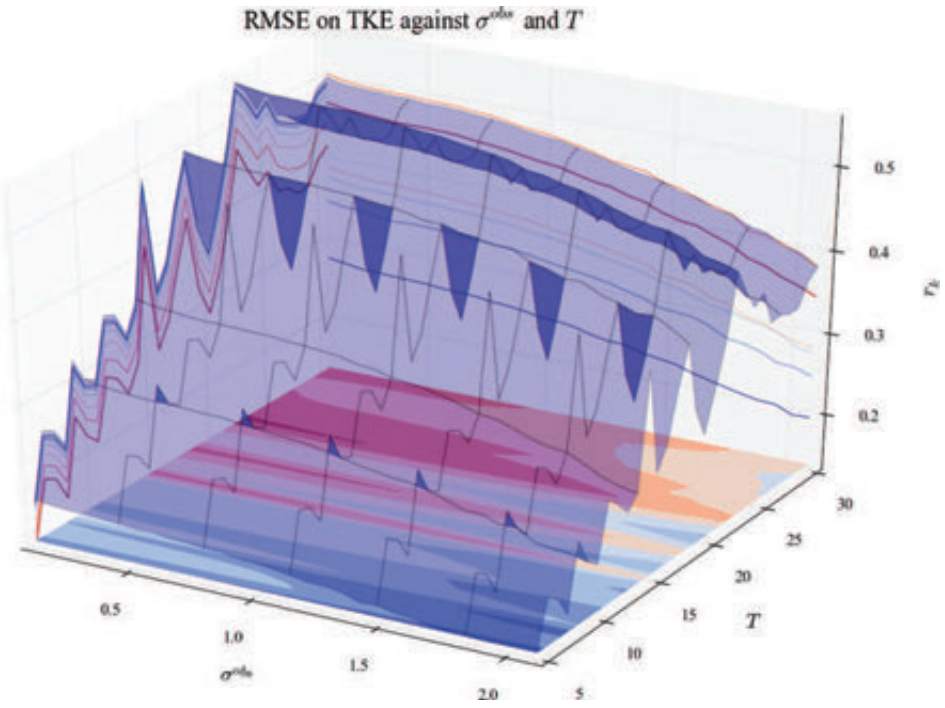

Figure C.64 – RMSE on TKE when σ^{obs} and τ vary.

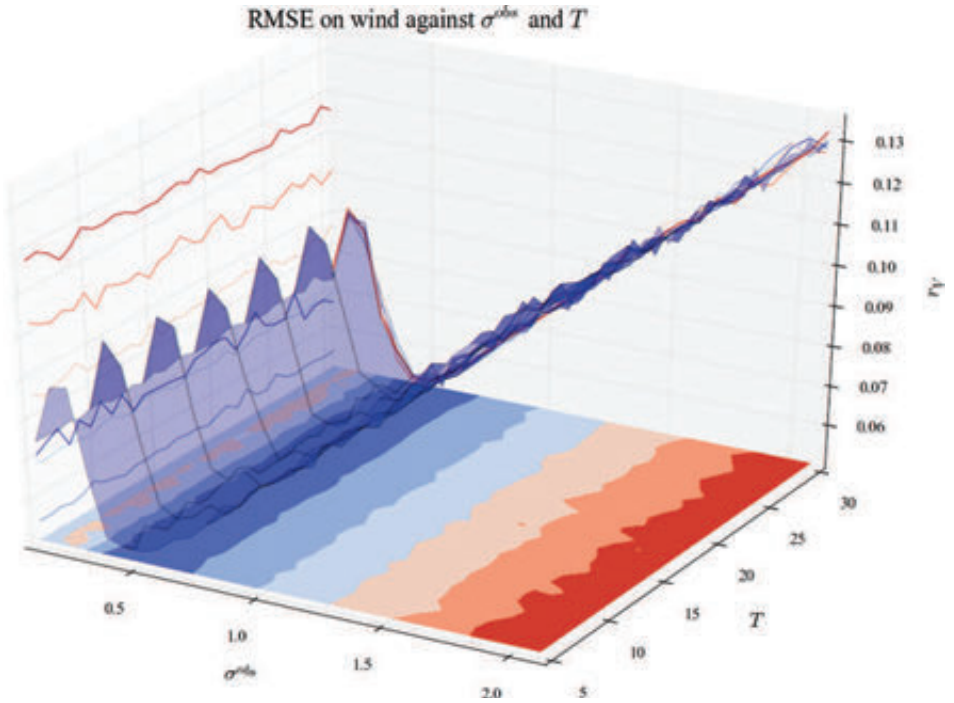

Figure C.65 – RMSE on wind when σ^{obs} and τ vary.

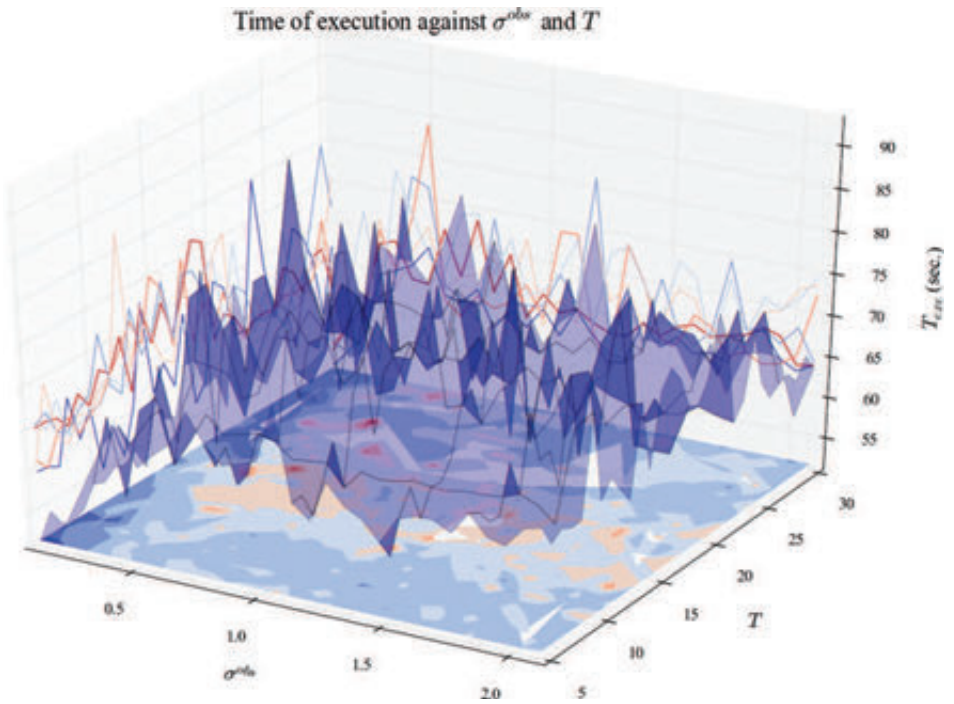

Figure C.66 – Execution time when σ^{obs} and τ vary.

C.2.14 σ^V and σ^X

In this experiment, only σ^V and σ^X vary. To check another experiment, go to table C.3 (hyperlinks in the table). To have more explanation about these inputs, go to table C.1.

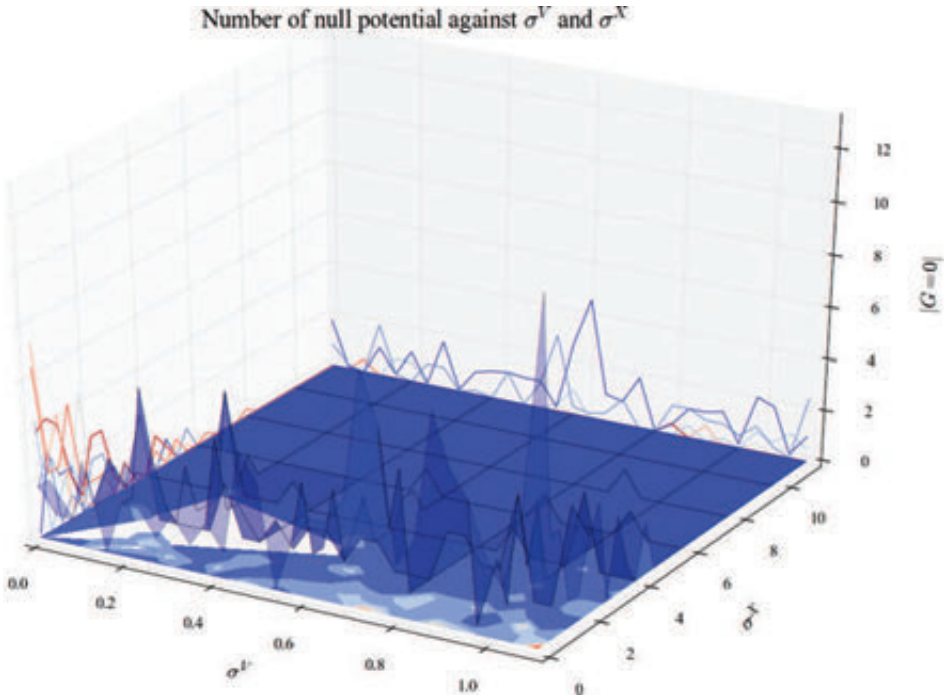

Figure C.67 – Number of null potential when σ^V and σ^X vary.

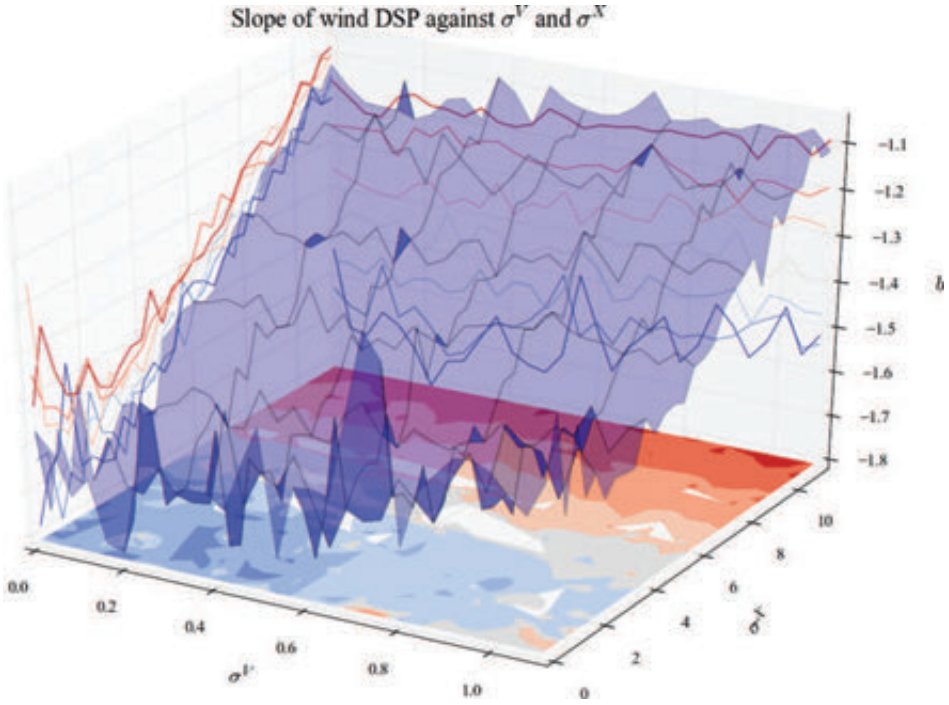

Figure C.68 – PSD slope when σ^V and σ^X vary.

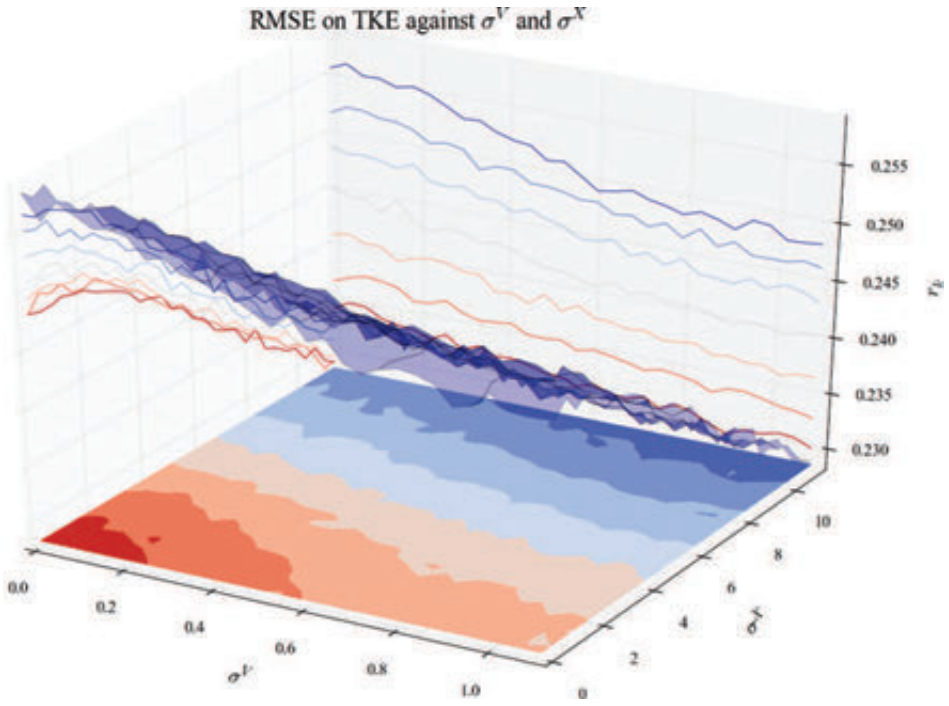

Figure C.69 – RMSE on TKE when σ^V and σ^X vary.

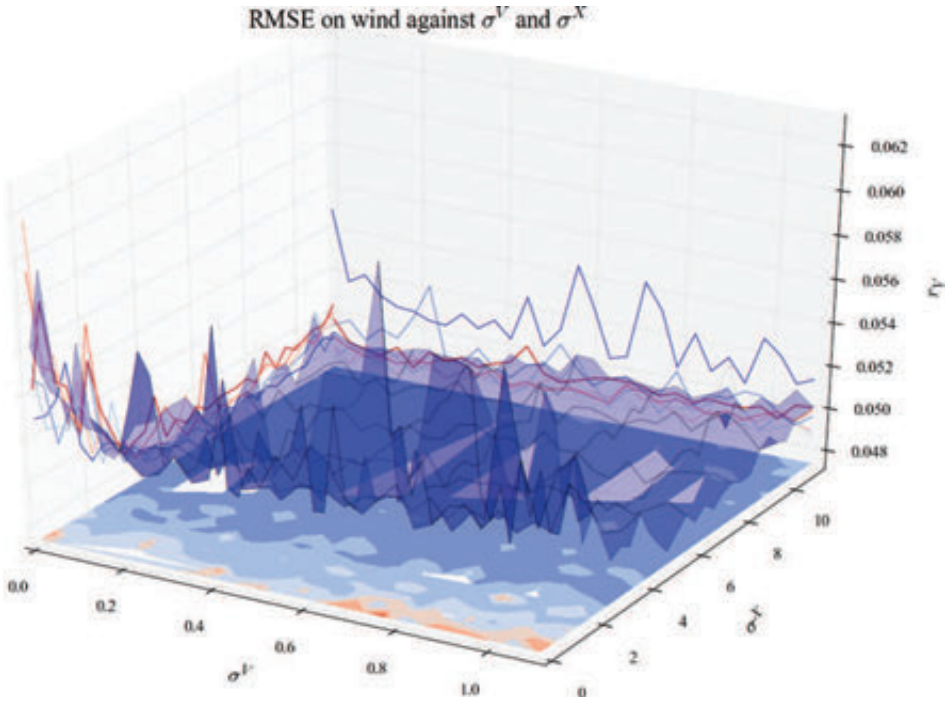

Figure C.70 – RMSE on wind when σ^V and σ^X vary.

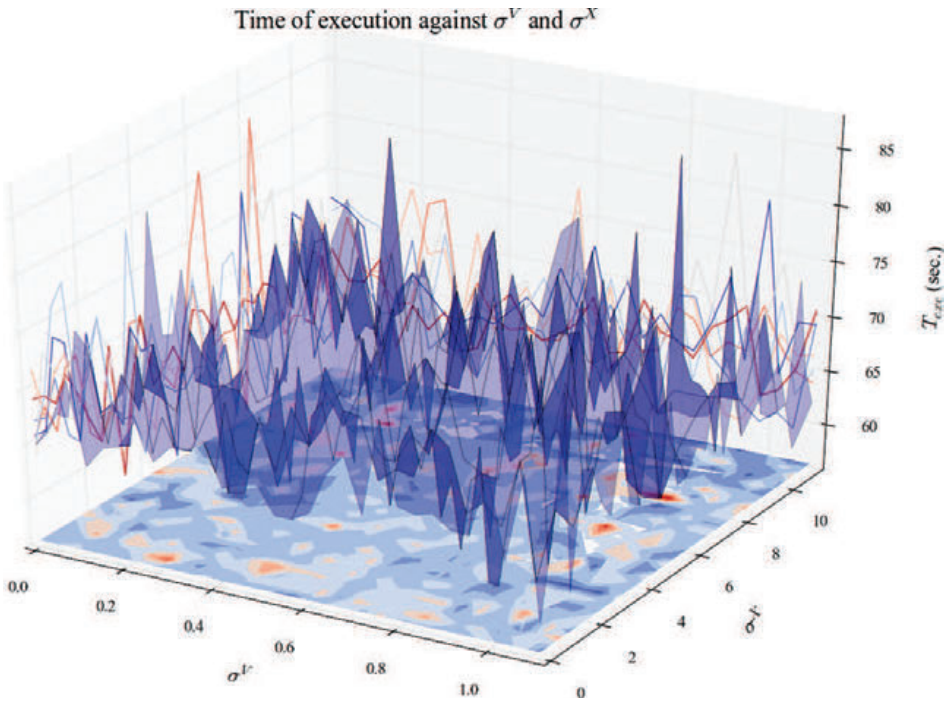

Figure C.71 – Execution time when σ^V and σ^X vary.

C.3 Results by output

C.3.1 Number of null potential

In this subsection are shown only the influence on the number of null potential N_{G0}. First are shown the Sobol indices for this output the most informative experiment and then the rest of experiments. To browse by experiment, use the hyperlinks in table C.3 (all outputs are computed for each experiment). To check another output, go back to table C.2. There is also a list of figures page 384.

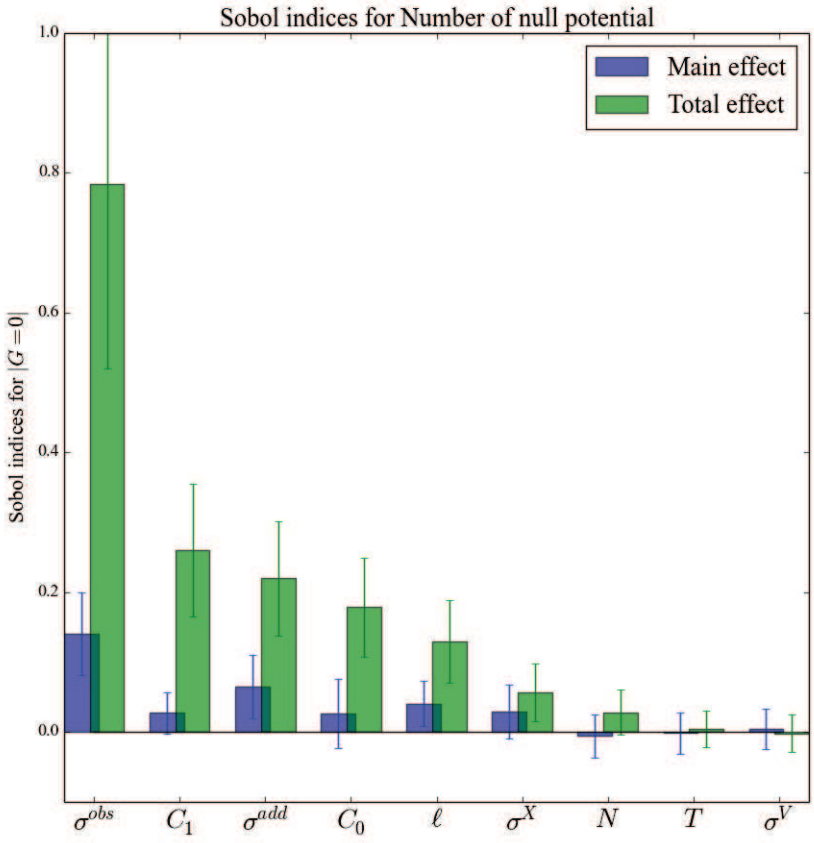

Figure C.72 – Sobol indices (score of influence) for number of null potential. Main effect in blue (effect of input alone), total effect in green (effect of input with all its interactions).

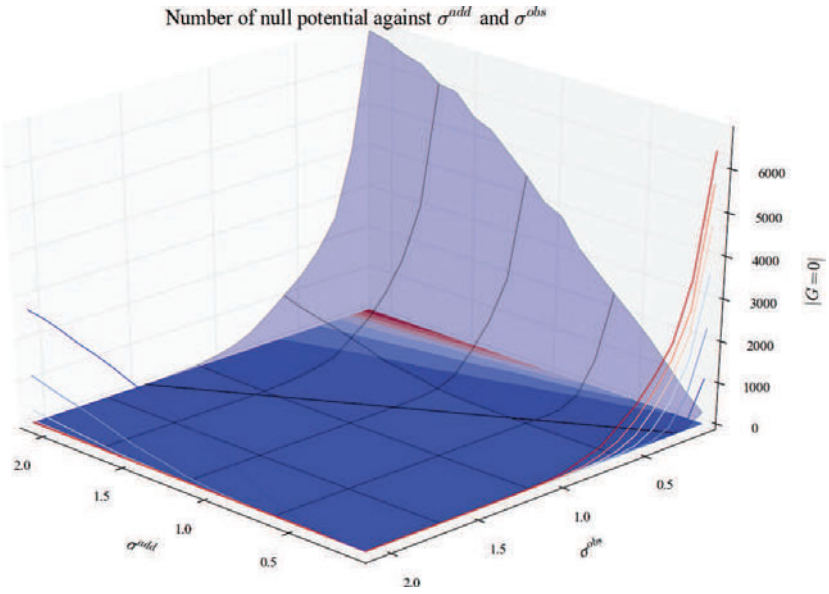

Figure C.73 – Number of null potential when σ^{add} and σ^{obs} vary.

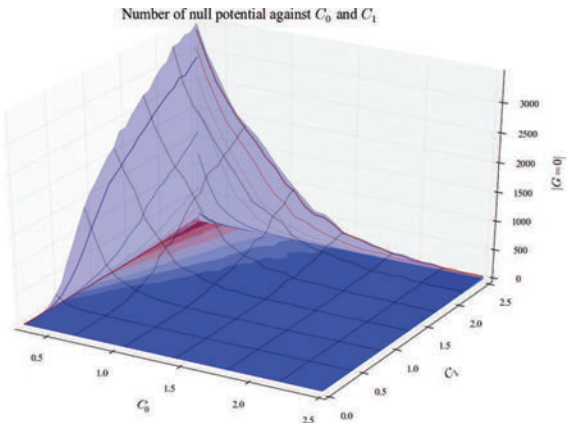

Figure C.74 – Number of null potential when C_0 and C_1 vary.

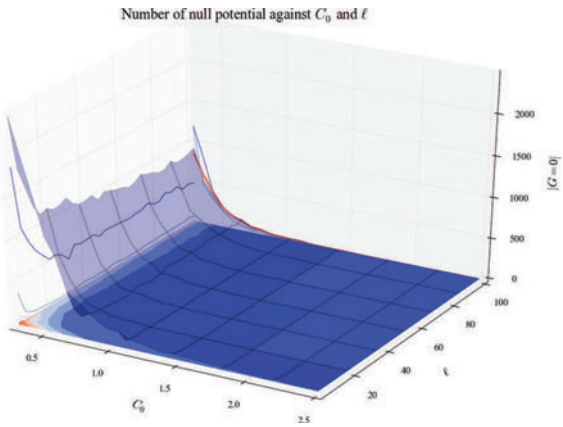

Figure C.75 – Number of null potential when C_0 and ℓ vary.

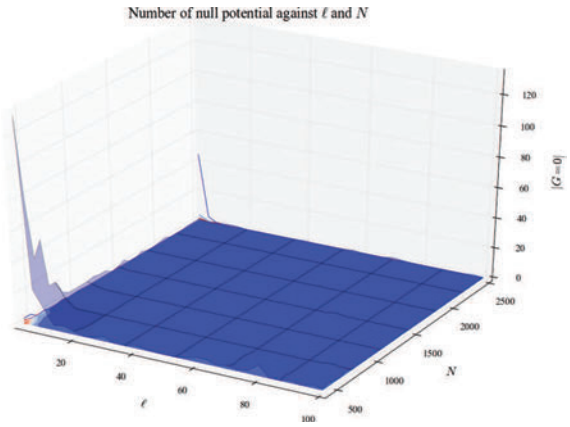

Figure C.76 – Number of null potential when ℓ and N vary.

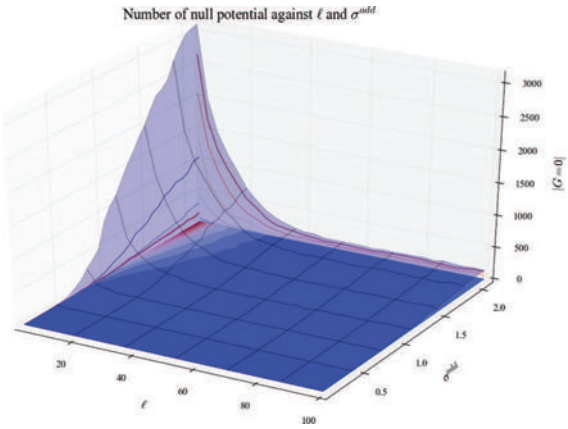

Figure C.77 – Number of null potential when ℓ and σ^{add} vary.

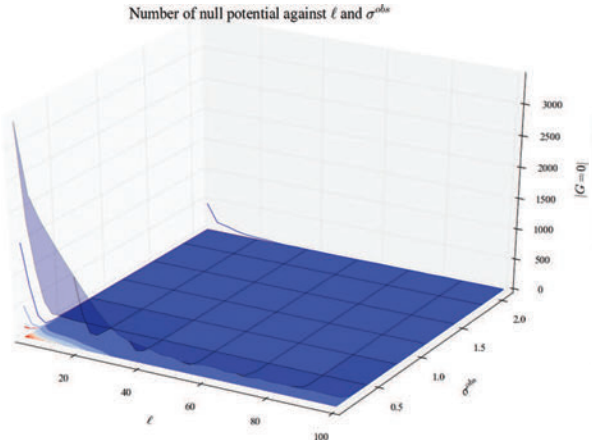

Figure C.78 – Number of null potential when ℓ and σ^{obs} vary.

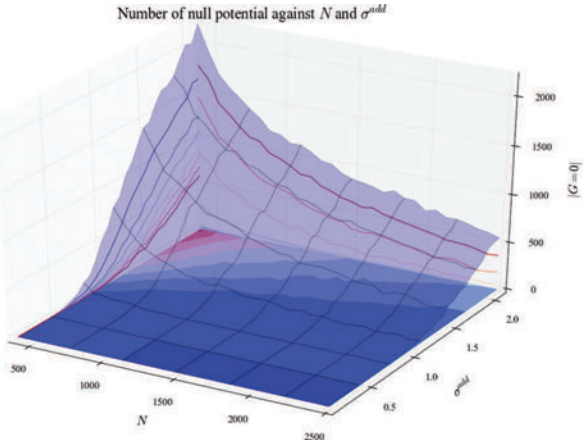

Figure C.79 – Number of null potential when N and σ^{add} vary.

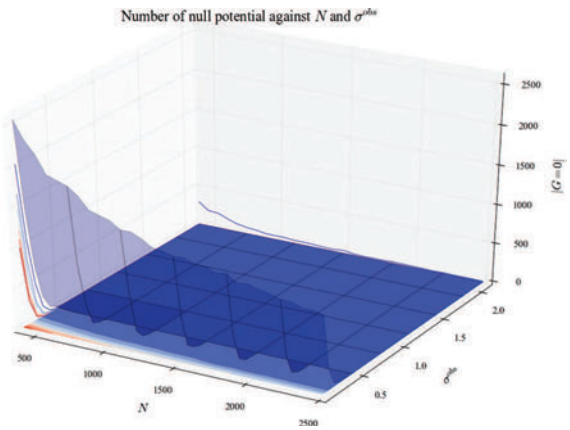

Figure C.80 – Number of null potential when N and σ^{obs} vary.

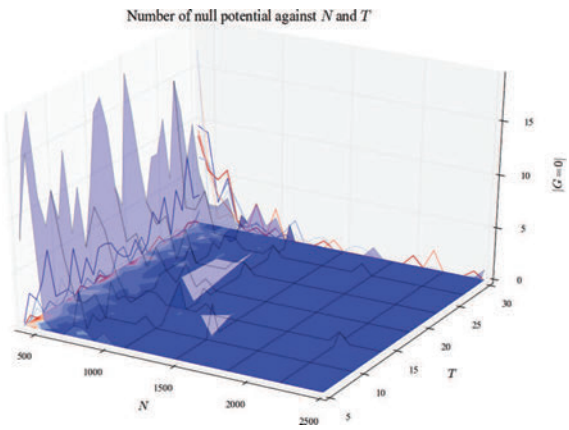

Figure C.81 – Number of null potential when N and τ vary.

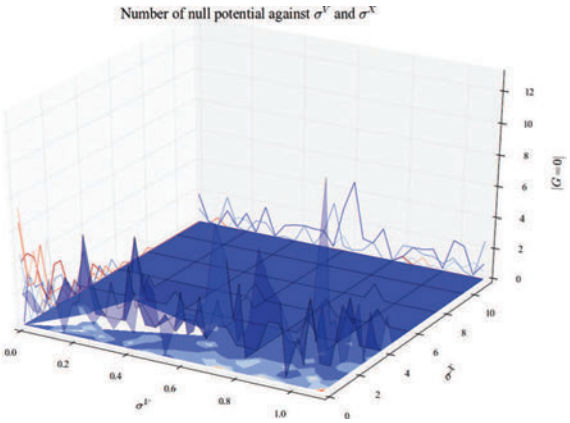

Figure C.82 – Number of null potential when σ^V and σ^X vary.

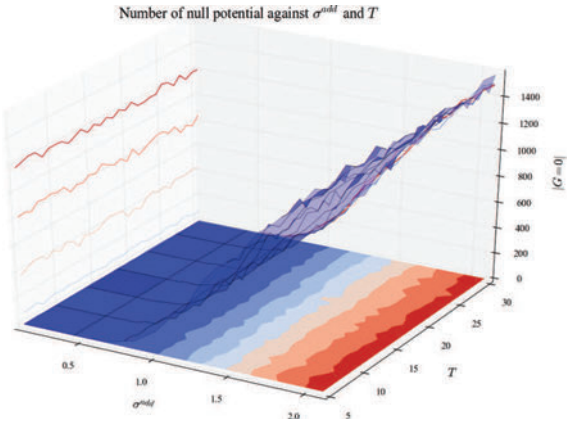

Figure C.83 – Number of null potential when σ^{add} and τ vary.

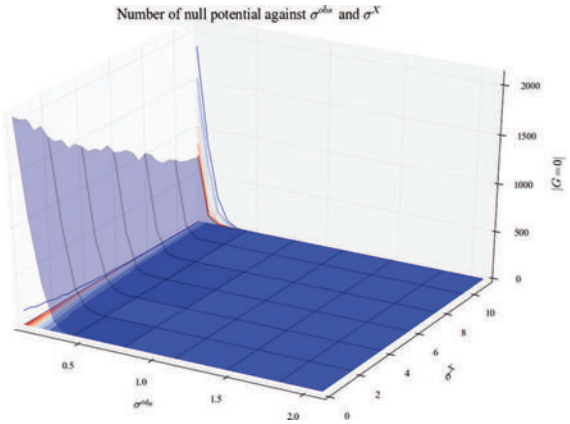

Figure C.84 – Number of null potential when σ^{obs} and σ^X vary.

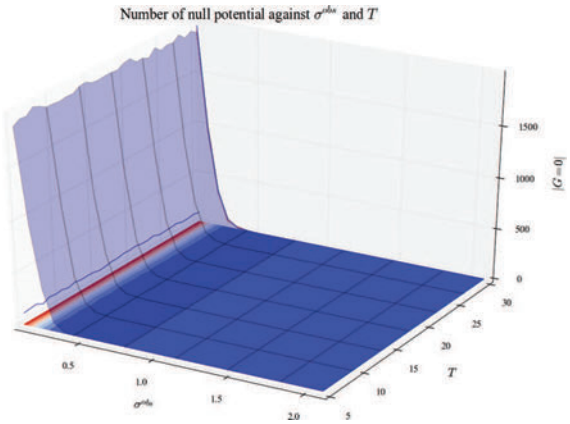

Figure C.85 – Number of null potential when σ^{obs} and τ vary.

C.3.2 Slope of PSD of wind

In this subsection are shown only the influence on the slope of the estimated wind power density spectrum b. First are shown the Sobol indices for this output the most informative experiment and then the rest of experiments. To browse by experiment, use the hyperlinks in table C.3 (all outputs are computed for each experiment). To check another output, go back to table C.2. There is also a list of figures page 384.

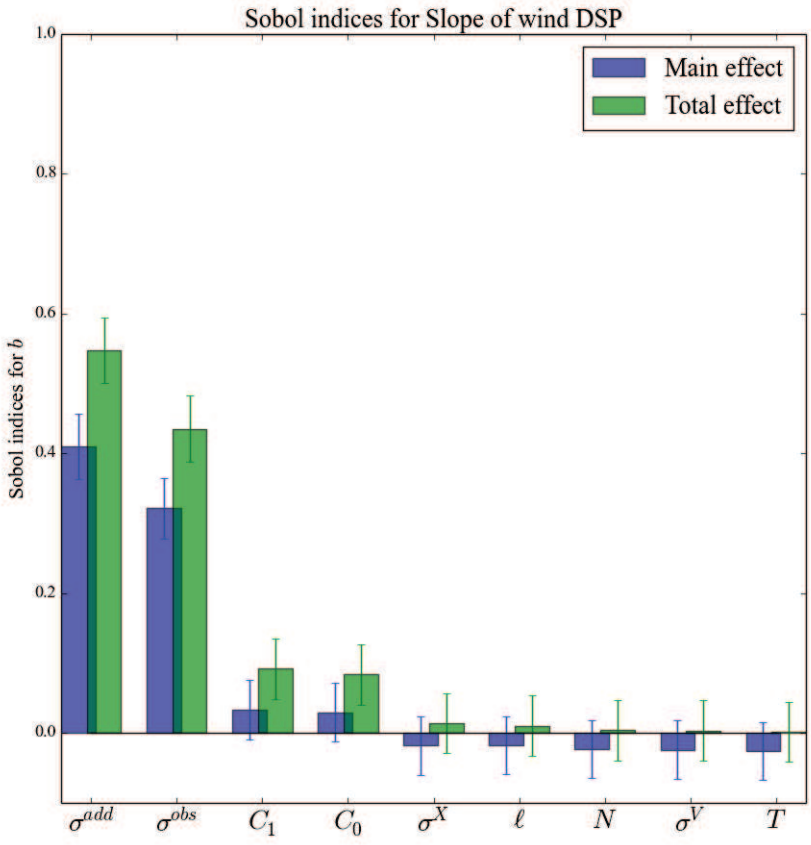

Figure C.86 – Sobol indices (score of influence) for PSD slope. Main effect in blue (effect of input alone), total effect in green (effect of input with all its interactions).

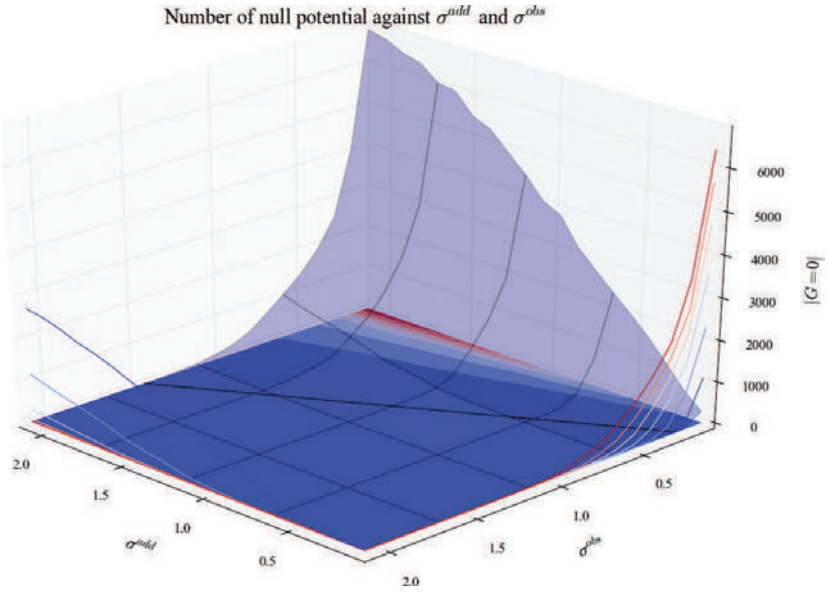

Figure C.87 – Slope of PSD when σ^{add} and σ^{obs} vary.

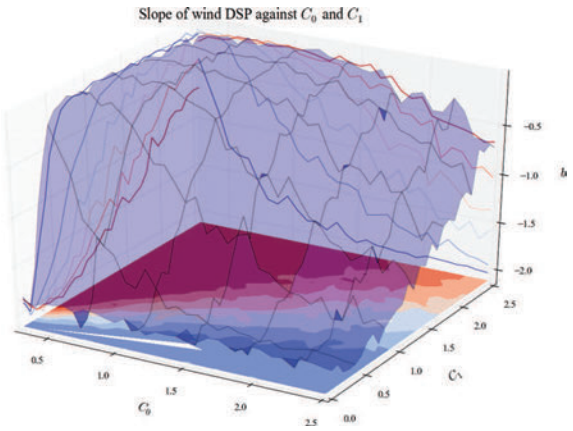

Figure C.88 – Slope of PSD when C_0 and C_1 vary.

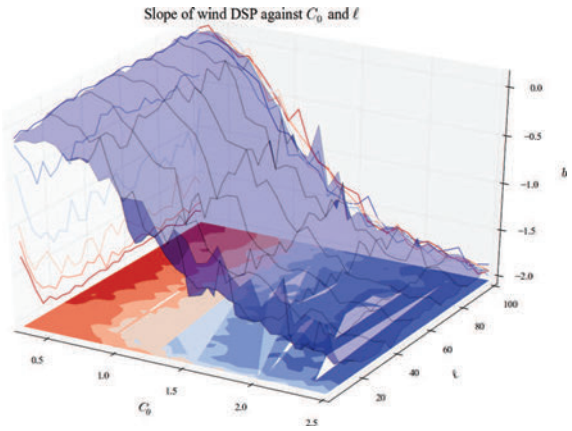

Figure C.89 – Slope of PSD when C_0 and ℓ vary.

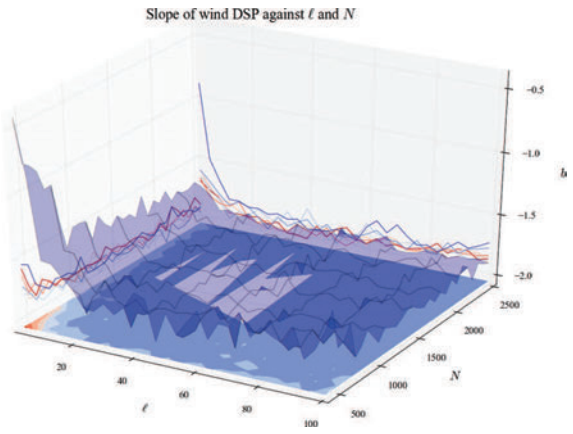

Figure C.90 – Slope of PSD when ℓ and N vary.

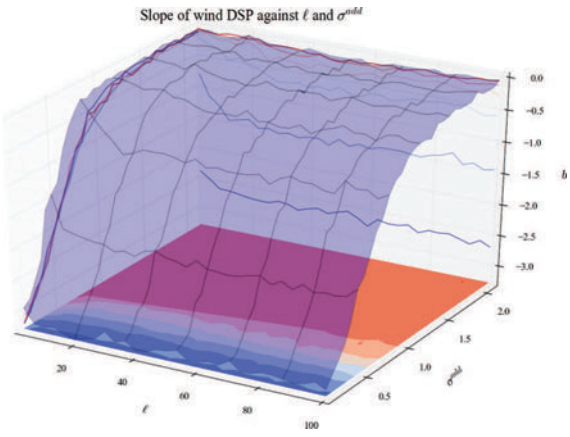

Figure C.91 – Slope of PSD when ℓ and σ^{add} vary.

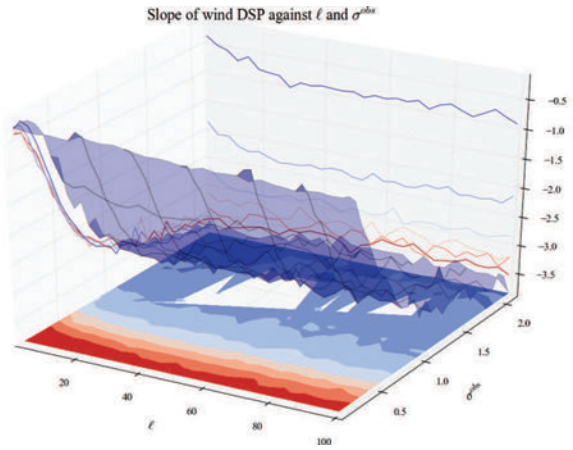

Figure C.92 – Slope of PSD when ℓ and σ^{obs} vary.

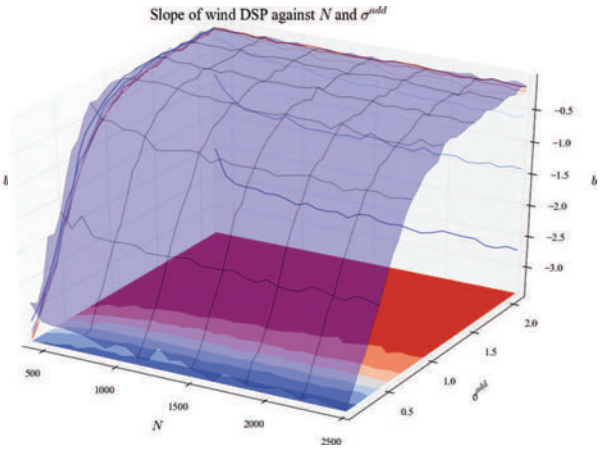

Figure C.93 – Slope of PSD when N and σ^{add} vary.

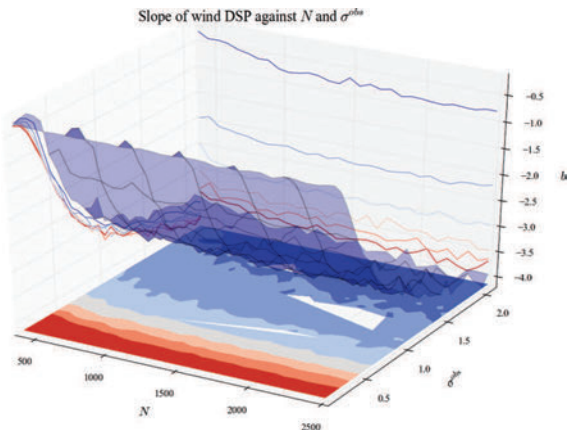

Figure C.94 – Slope of PSD when N and σ^{obs} vary.

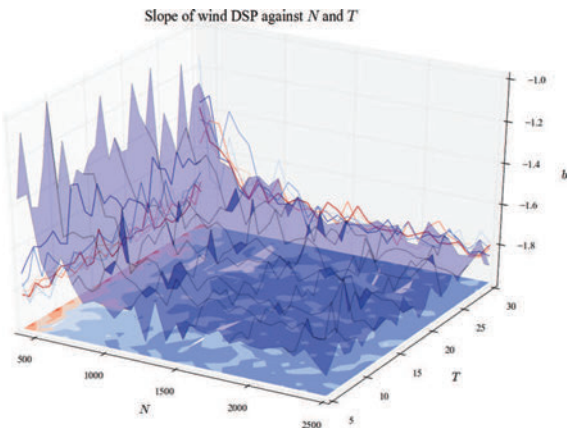

Figure C.95 – Slope of PSD when N and τ vary.

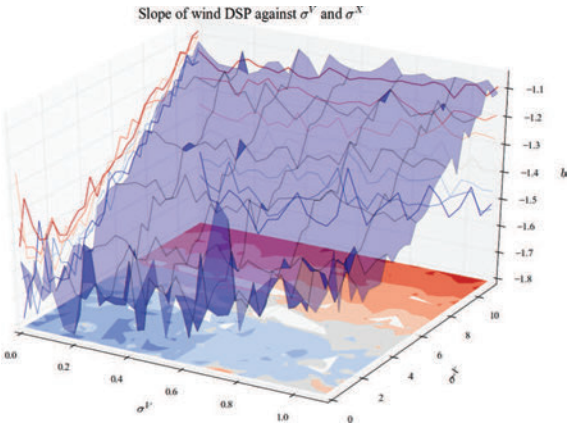

Figure C.96 – Slope of PSD when σ^V and σ^X vary.

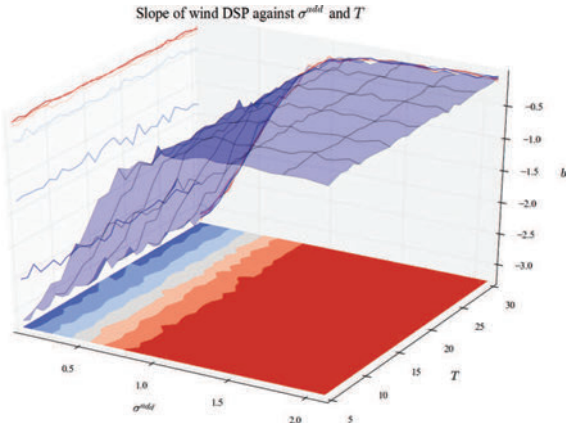

Figure C.97 – Slope of PSD when σ^{add} and τ vary.

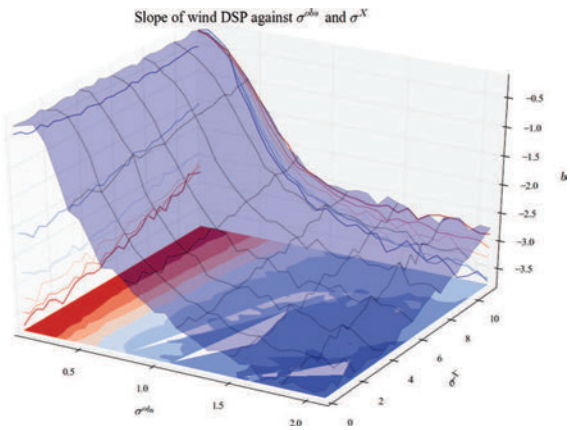

Figure C.98 – Slope of PSD when σ^{obs} and σ^X vary.

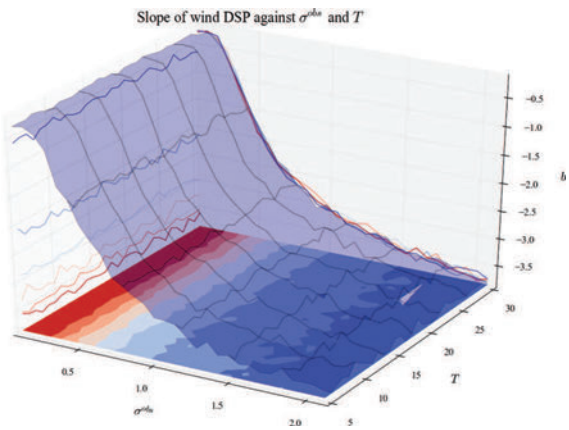

Figure C.99 – Slope of PSD when σ^{obs} and τ vary.

C.3.3 RMSE on TKE

In this subsection are shown only the influence on the root-mean-squared error on turbulent kinetic energy r_k. First are shown the Sobol indices for this output the most informative experiment and then the rest of experiments. To browse by experiment, use the hyperlinks in table C.3 (all outputs are computed for each experiment). To check another output, go back to table C.2. There is also a list of figures page 384.

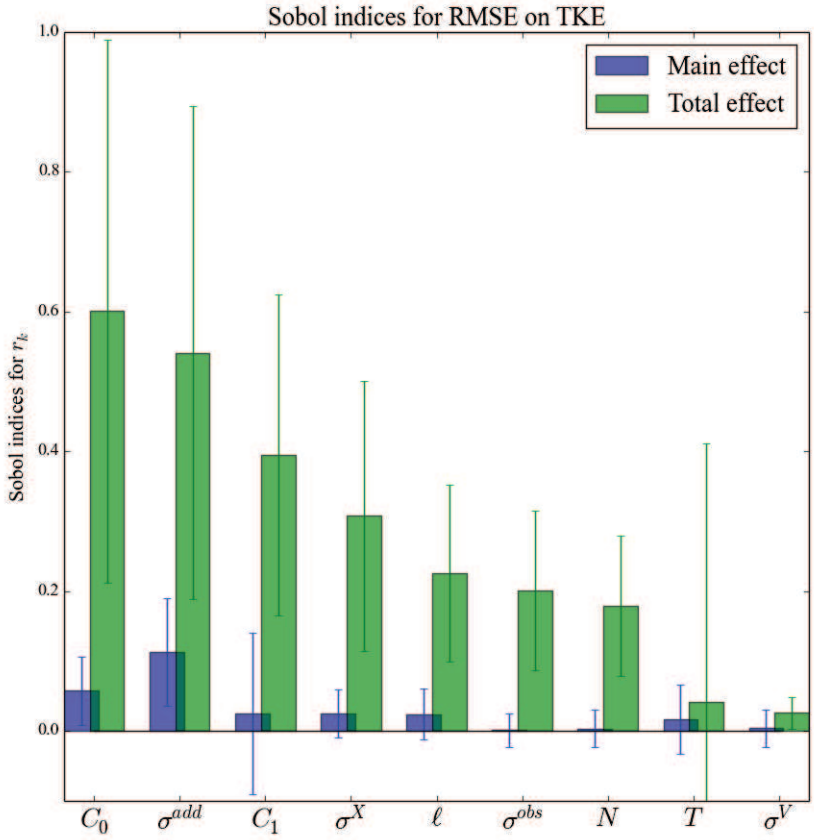

Figure C.100 – Sobol indices (score of influence) for TKE RMSE. Main effect in blue (effect of input alone), total effect in green (effect of input with all its interactions).

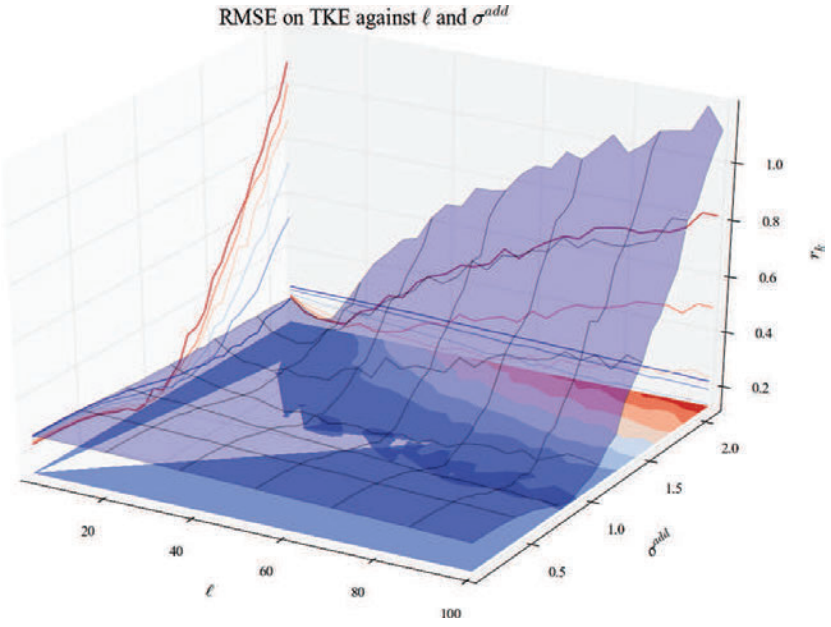

Figure C.101 – TKE RMSE when ℓ and σ^{add} vary.

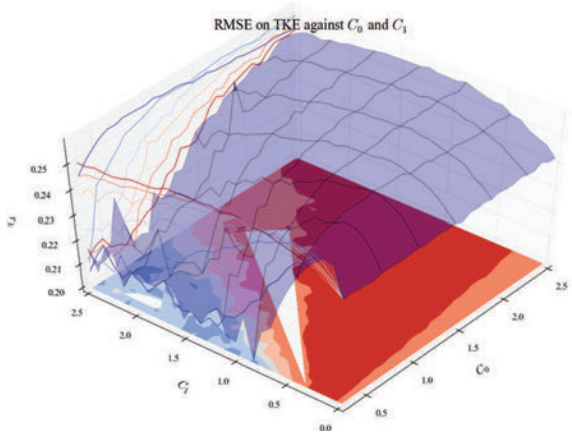

Figure C.102 – TKE RMSE when C_0 and C_1 vary.

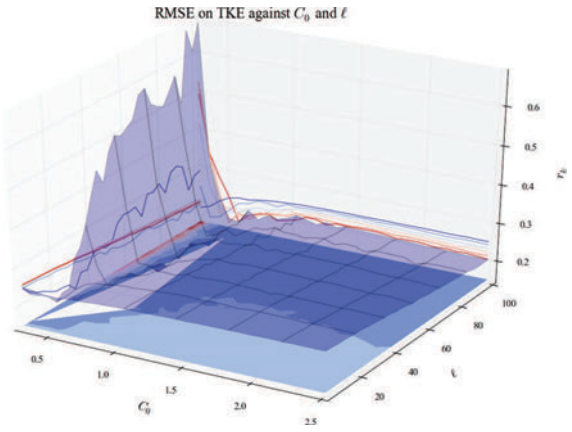

Figure C.103 – TKE RMSE when C_0 and ℓ vary.

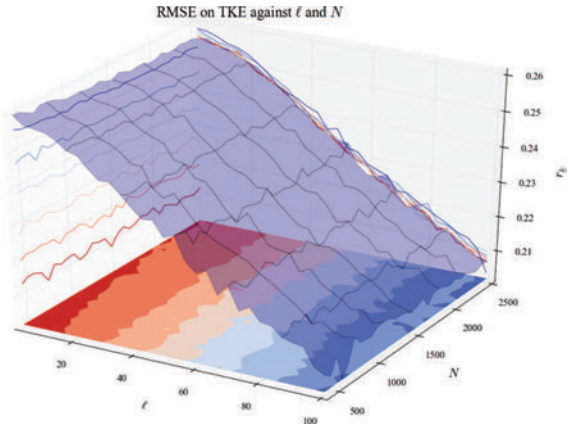

Figure C.104 – TKE RMSE when ℓ and N vary.

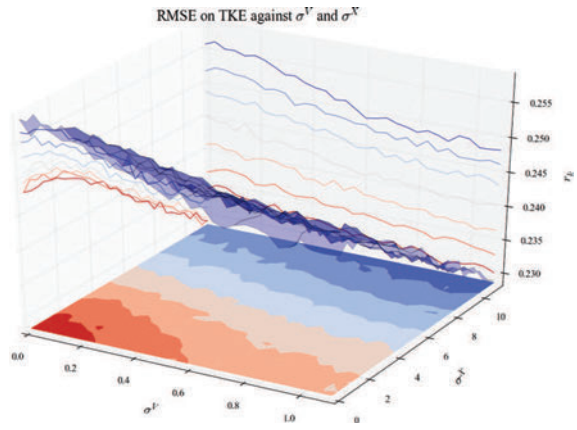

Figure C.105 – TKE RMSE when σ^V and σ^X vary.

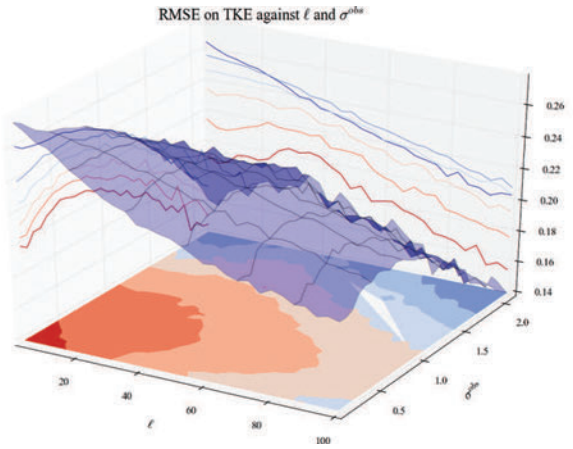

Figure C.106 – TKE RMSE when ℓ and σ^{obs} vary.

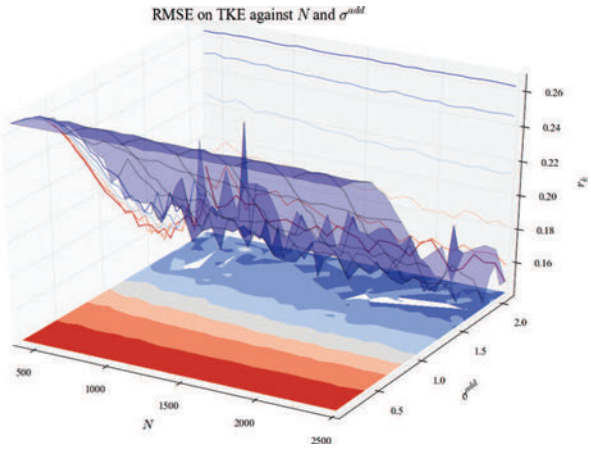

Figure C.107 – TKE RMSE when N and σ^{add} vary.

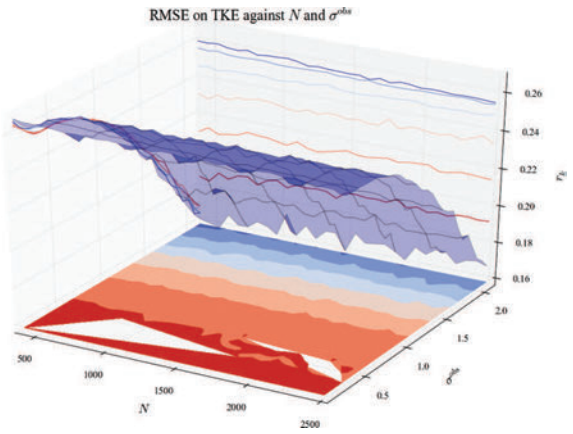

Figure C.108 – TKE RMSE when N and σ^{obs} vary.

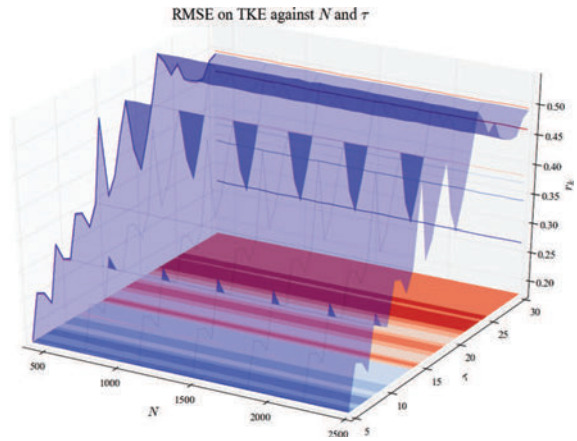

Figure C.109 – TKE RMSE when N and τ vary.

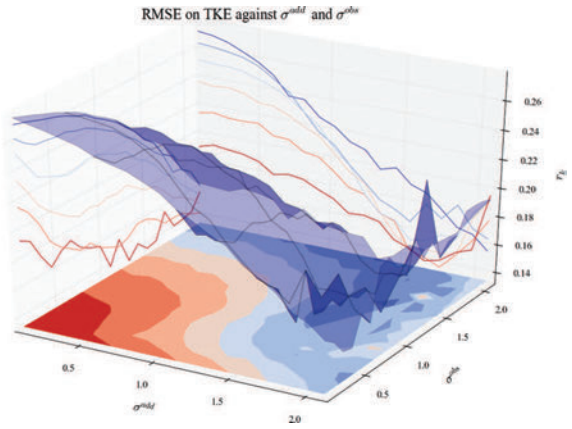

Figure C.110 – TKE RMSE when σ^{add} and σ^{obs} vary.

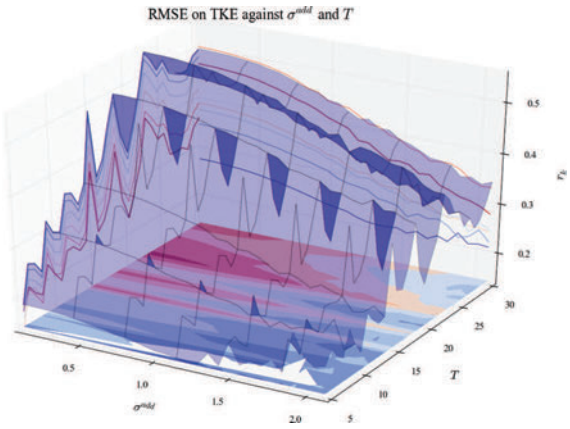

Figure C.111 – TKE RMSE when σ^{add} and τ vary.

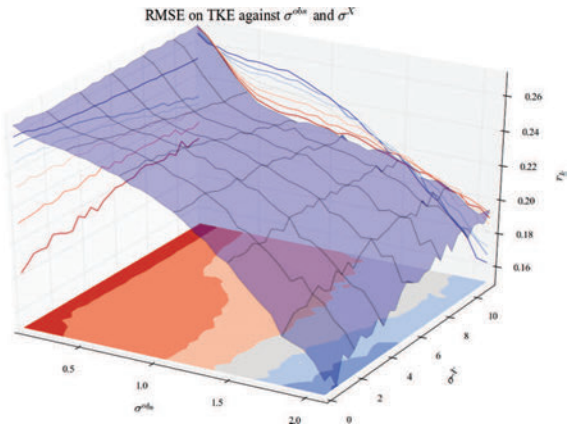

Figure C.112 – TKE RMSE when σ^{obs} and σ^{X} vary.

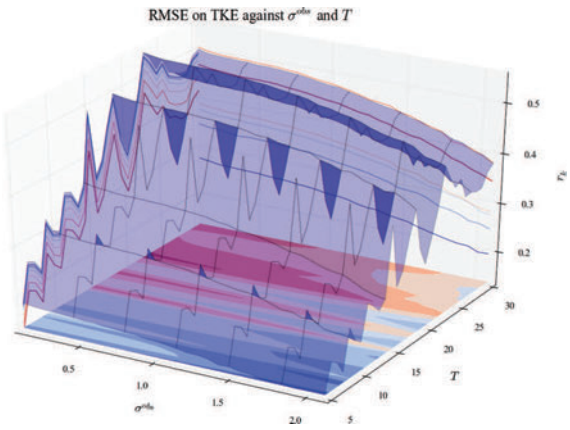

Figure C.113 – TKE RMSE when σ^{obs} and τ vary.

C.3.4 RMSE on wind

In this subsection are shown only the influence on the root-mean-squared error on vertical wind r_V. First are shown the Sobol indices for this output the most informative experiment and then the rest of experiments. To browse by experiment, use the hyperlinks in table C.3 (all outputs are computed for each experiment). To check another output, go back to table C.2. There is also a list of figures page 384.

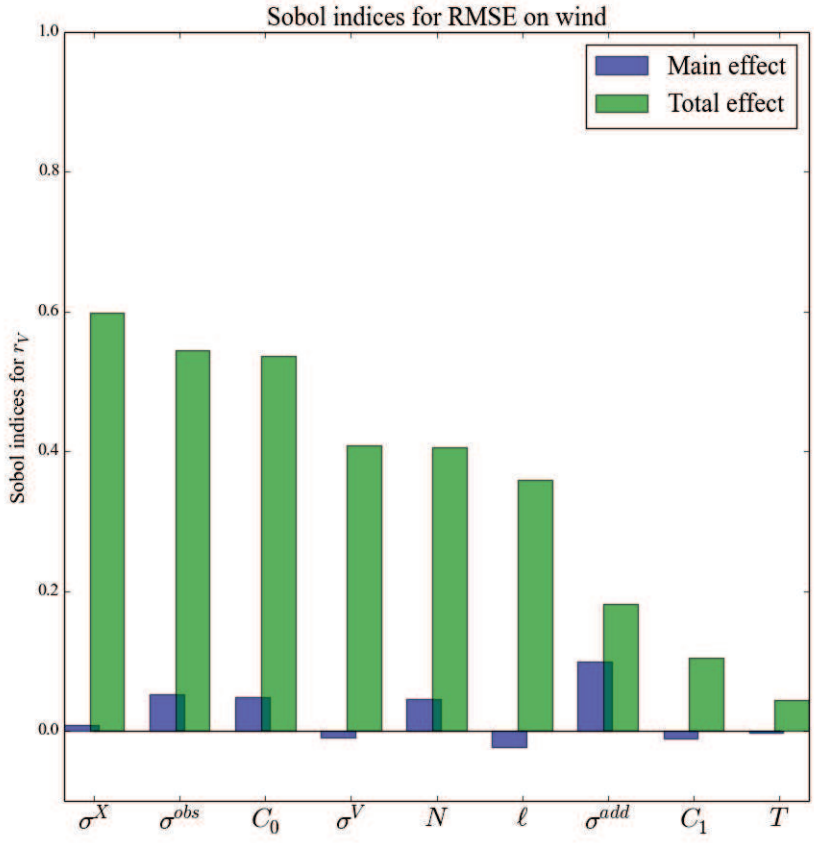

Figure C.114 – Sobol indices (score of influence) for wind RMSE. Main effect in blue (effect of input alone), total effect in green (effect of input with all its interactions).

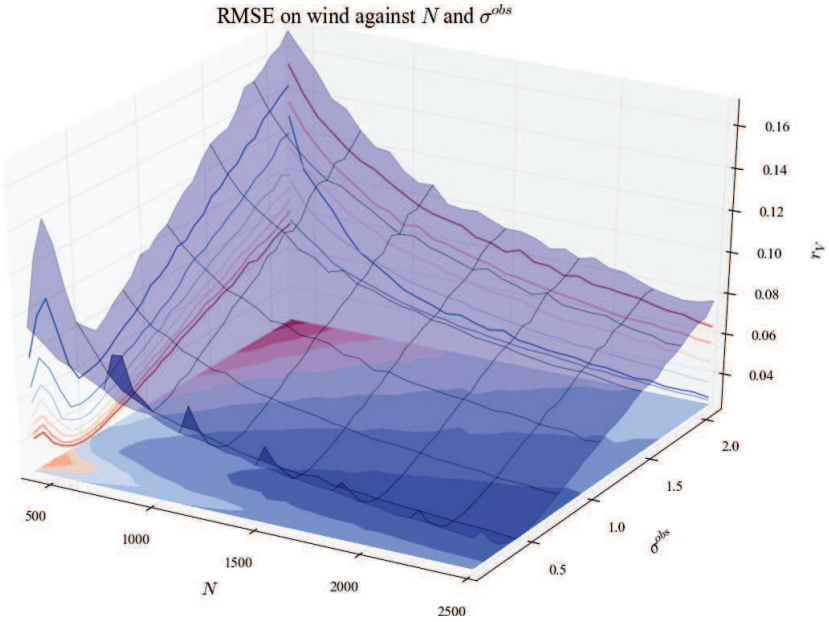

Figure C.115 – Wind RMSE when N and σ^{obs} vary.

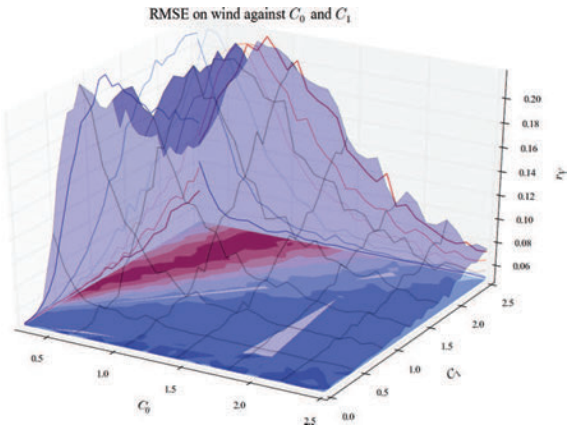

Figure C.116 – Wind RMSE when C_0 and C_1 vary.

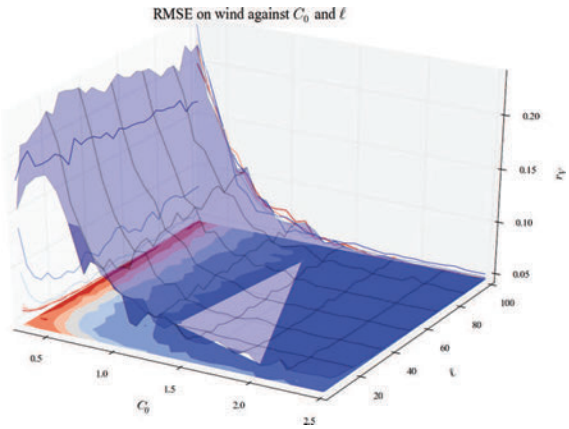

Figure C.117 – Wind RMSE when C_0 and ℓ vary.

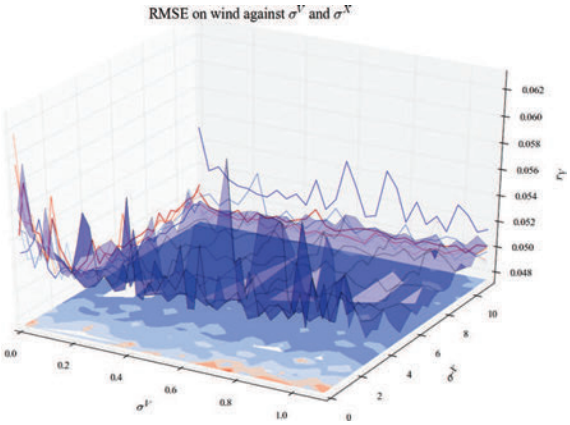

Figure C.118 – Wind RMSE when σ^V and σ^X vary.

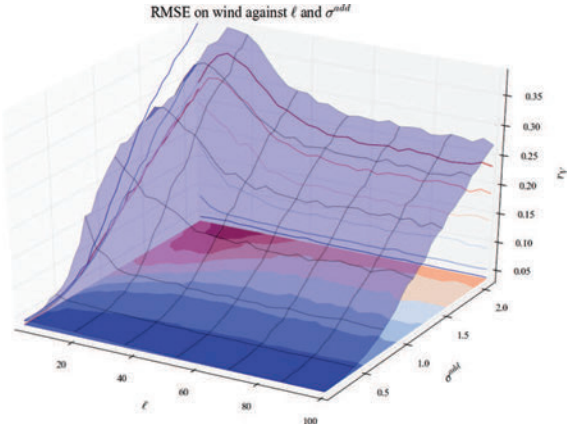

Figure C.119 – Wind RMSE when ℓ and σ^{add} vary.

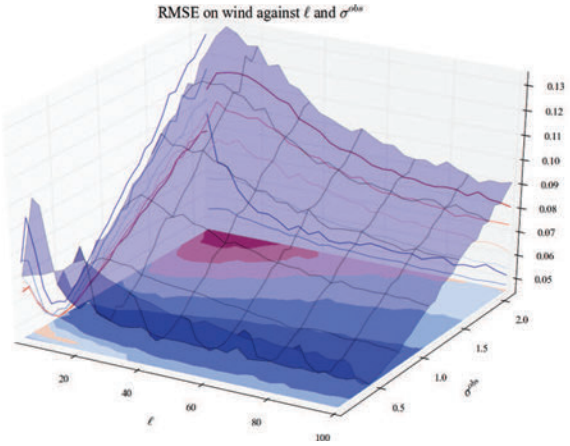

Figure C.120 – Wind RMSE when ℓ and σ^{obs} vary.

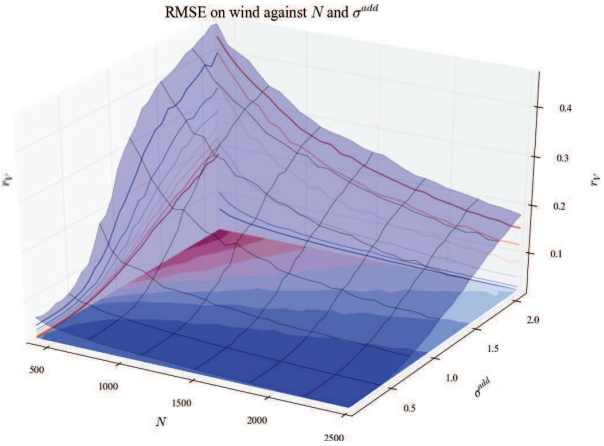

Figure C.121 – Wind RMSE when N and σ^{add} vary.

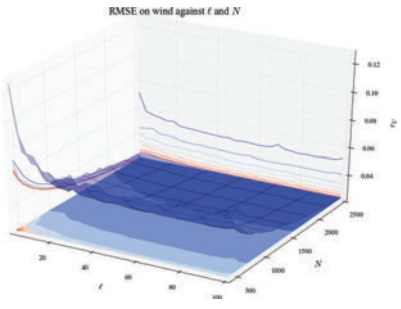

Figure C.122 – Wind RMSE when ℓ and N vary.

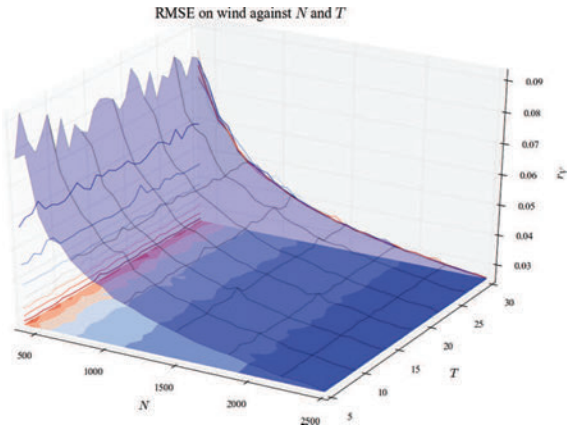

Figure C.123 – Wind RMSE when N and τ vary.

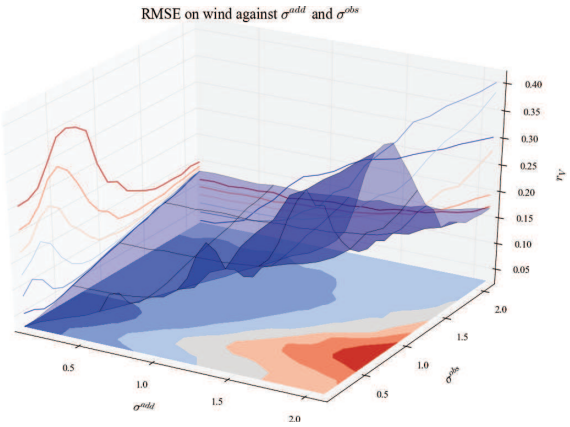

Figure C.124 – Wind RMSE when σ^{add} and σ^{obs} vary.

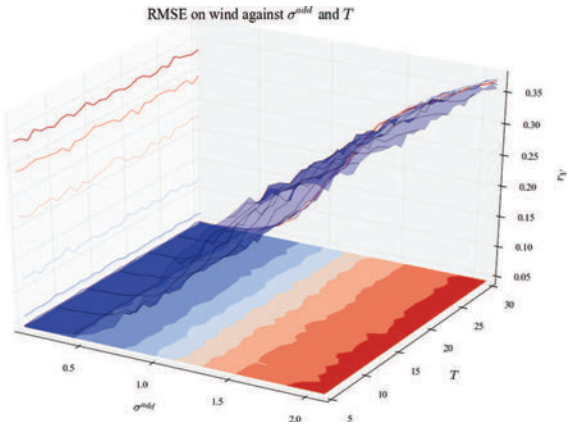

Figure C.125 – Wind RMSE when σ^{add} and τ vary.

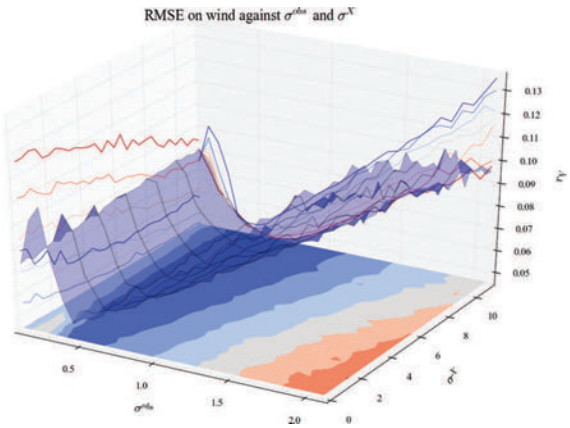

Figure C.126 – Wind RMSE when σ^{obs} and σ^{X} vary.

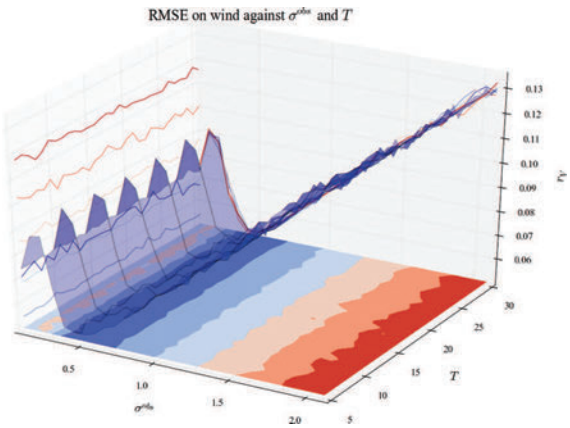

Figure C.127 – Wind RMSE when σ^{obs} and τ vary.

C.3.5 Execution time

In this subsection are shown only the influence on the execution time T_{exe}. First are shown the Sobol indices for this output the most informative experiment and then the rest of experiments. To browse by experiment, use the hyperlinks in table C.3 (all outputs are computed for each experiment). To check another output, go back to table C.2. There is also a list of figures page 384.

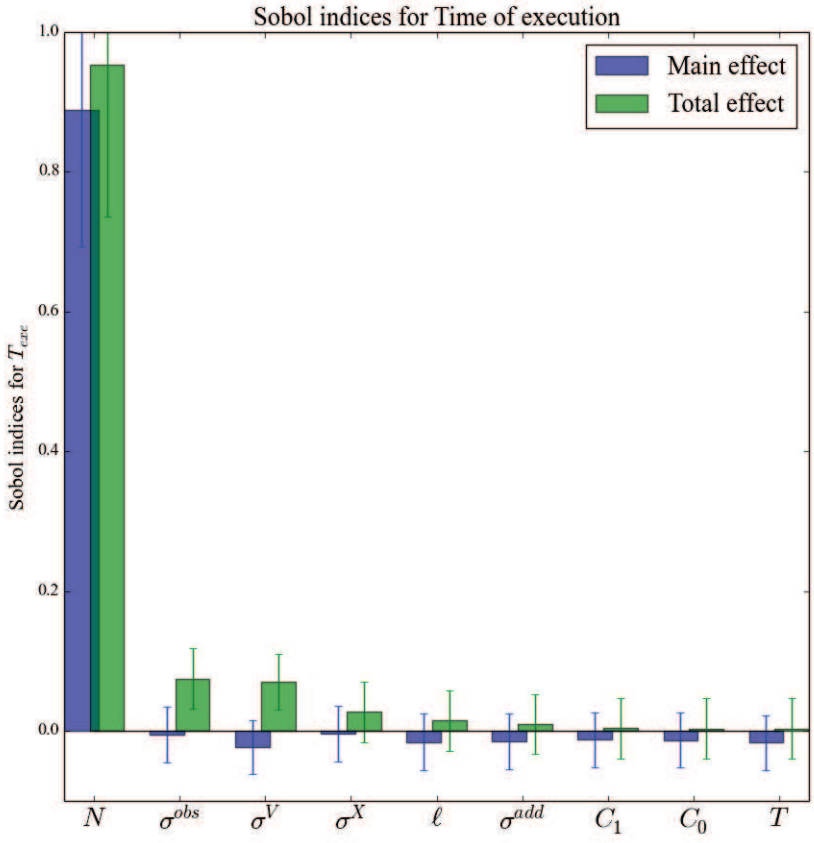

Figure C.128 – Sobol indices (score of influence) for execution time. Main effect in blue (effect of input alone), total effect in green (effect of input with all its interactions).

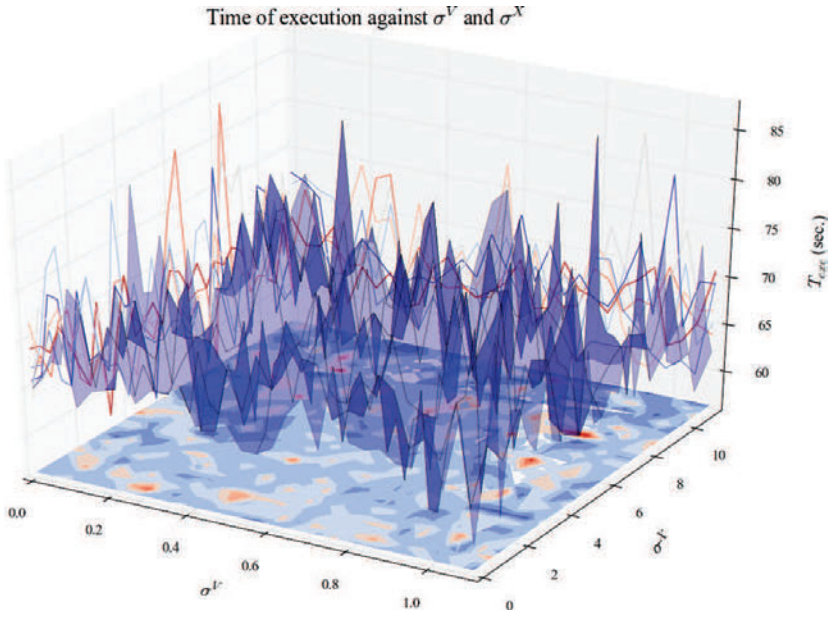

Figure C.129 – Execution time when σ^V and σ^X vary.

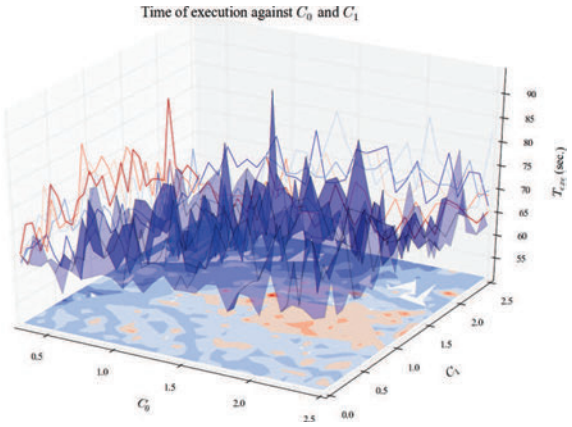

Figure C.130 – Execution time when C_0 and C_1 vary.

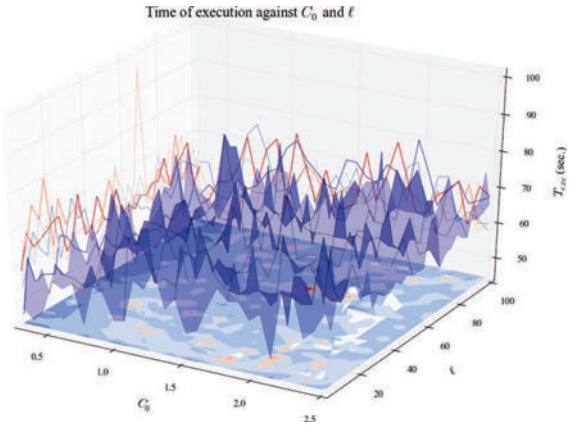

Figure C.131 – Execution time when C_0 and ℓ vary.

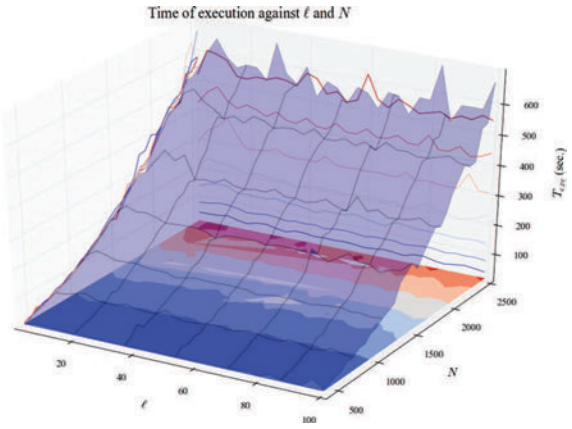

Figure C.132 – Execution time when ℓ and N vary.

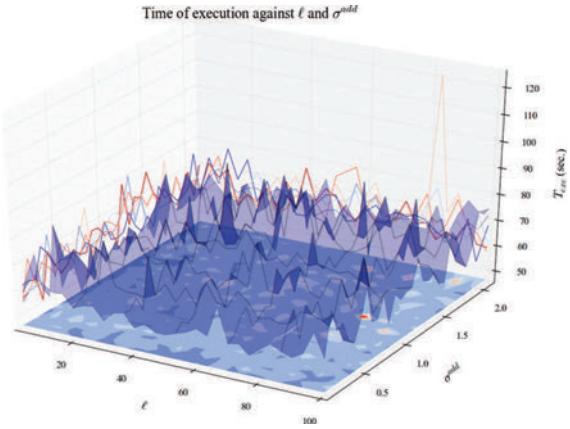

Figure C.133 – Execution time when ℓ and σ^{add} vary.

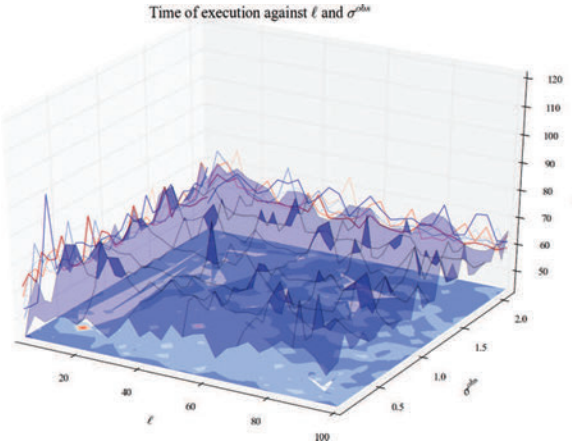

Figure C.134 – Execution time when ℓ and σ^{obs} vary.

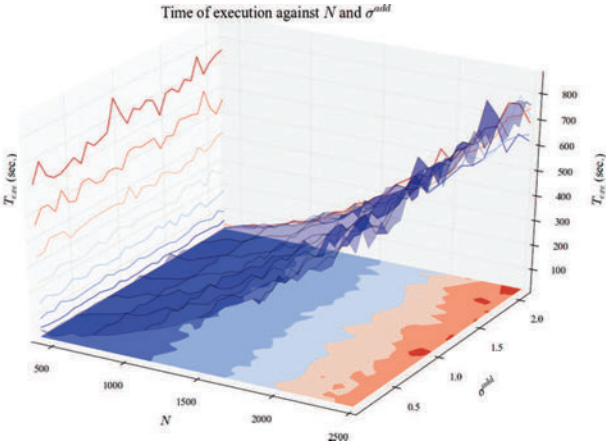

Figure C.135 – Execution time when N and σ^{add} vary.

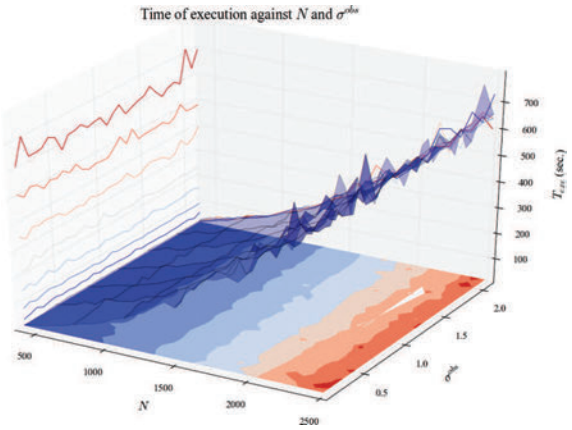

Figure C.136 – Execution time when N and σ^{obs} vary.

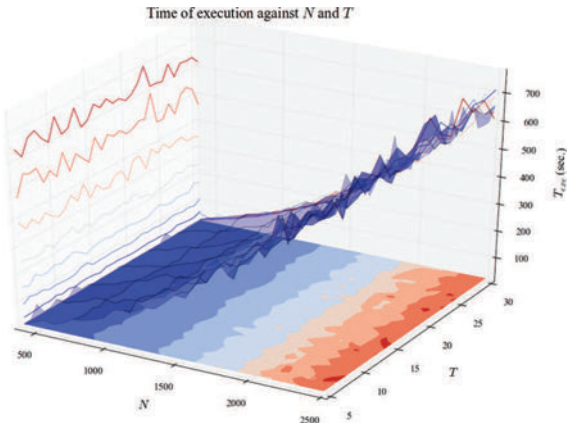

Figure C.137 – Execution time when N and τ vary.

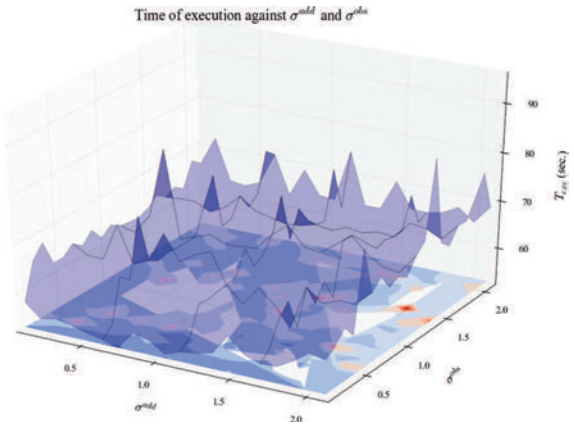

Figure C.138 – Execution time when σ^{add} and σ^{obs} vary.

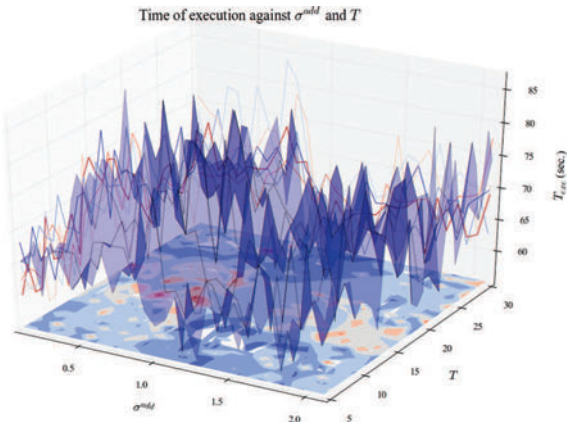

Figure C.139 – Execution time when σ^{add} and τ vary.

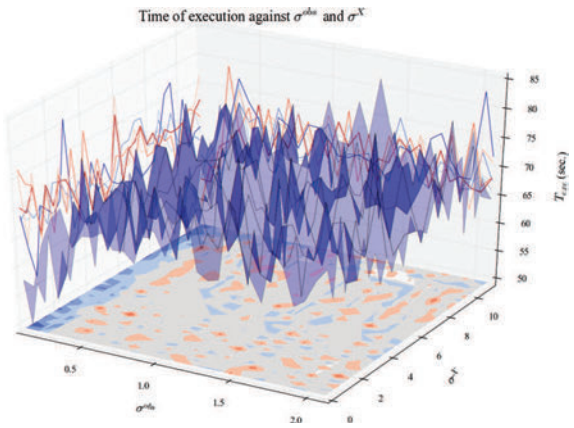

Figure C.140 – Execution time when σ^{obs} and σ^{X} vary.

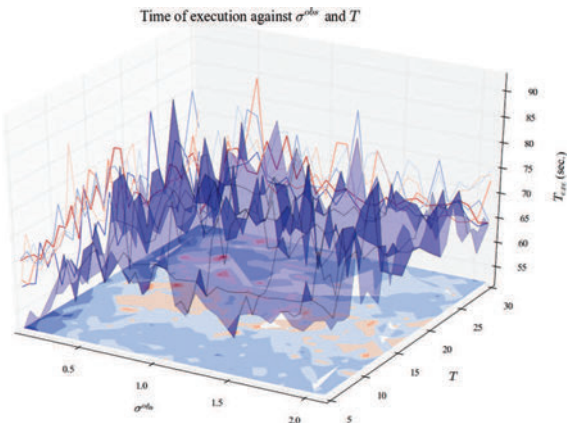

Figure C.141 – Execution time when σ^{obs} and τ vary.

Bibliography

(2010). Weather-related aviation accident study.

Akaike, H. (1998). Information theory and an extension of the maximum likelihood principle. In *Selected Papers of Hirotugu Akaike*, pages 199–213. Springer.

Arulampalam, M. S., Maskell, S., Gordon, N., and Clapp, T. (2002). A tutorial on particle filters for online nonlinear/non-gaussian bayesian tracking. *IEEE Transactions on signal processing*, 50(2):174–188.

Baehr, C. (2008). *Modélisation probabiliste des écoulements atmosphériques turbulents afin d'en filtrer la mesure par approche particulaire.* PhD thesis, Université Paul Sabatier-Toulouse III.

Baehr, C. (2010). Nonlinear filtering for observations on a random vector field along a random path. Application to atmospheric turbulent velocities. *ESAIM. Mathematical Modelling and Numerical Analysis*, 44(5):921.

Baehr, C., Beigbeder, C., Couvreux, F., Dabas, A., and Piguet, B. (2011). Retrieval of the turbulent and backscattering properties using a non-linear filtering technique applied to doppler lidar observations.

Baehr, C., Pannekoucke, O., et al. (2010). Some issues and results on the enkf and particle filters for meteorological models. *Chaotic Systems: Theory and Applications*, pages 27–24.

Baehr, C., Rottner, L., Suzat, F., and Rieutord, T. (2016). Procédé de construction d'une représentation tridimensionnelle d'une atmosphère, dispositif et programme correspondant.

Banta, R. M., Pichugina, Y. L., Kelley, N. D., Hardesty, R. M., and Brewer, W. A. (2013). Wind energy meteorology: insight into wind properties in the turbine-rotor layer of the atmosphere from high-resolution doppler lidar. *Bulletin of the American Meteorological Society*, 94(6):883–902.

Barbe, P. and Ledoux, M. (1998). *Probabilité (L3M1).* EDP Sciences.

Bengtsson, T., Bickel, P., Li, B., et al. (2008). Curse-of-dimensionality revisited: Collapse of the particle filter in very large scale systems. In *Probability and statistics: Essays in honor of David A. Freedman*, pages 316–334. Institute of Mathematical Statistics.

Bennett, M., Christie, S., Graham, A., and Raper, D. (2010). Lidar observations of aircraft exhaust plumes. *Journal of Atmospheric and Oceanic Technology*, 27(10):1638–1651.

Bernardin, F., Bossy, M., Chauvin, C., Drobinski, P., Rousseau, A., and Salameh, T. (2009). Stochastic downscaling method: application to wind refinement. *Stochastic Environmental Research and Risk Assessment*, 23(6):851–859.

Bernardin, F., Bossy, M., Chauvin, C., Jabir, J.-F., and Rousseau, A. (2010). Stochastic lagrangian method for downscaling problems in computational fluid dynamics. *ESAIM: Mathematical Modelling and Numerical Analysis*, 44(05):885–920.

Bettonvil, B. and Kleijnen, J. P. (1997). Searching for important factors in simulation models with many factors: Sequential bifurcation. *European Journal of Operational Research*, 96(1):180–194.

Borgonovo, E. (2007). A new uncertainty importance measure. *Reliability Engineering & System Safety*, 92(6):771–784.

Bougeault, P. and Lacarrere, P. (1989). Parameterization of orography-induced turbulence in a mesobeta–scale model. *Monthly Weather Review*, 117(8):1872–1890.

Box, G. E., Muller, M. E., et al. (1958). A note on the generation of random normal deviates. *The annals of mathematical statistics*, 29(2):610–611.

Breiman, L. (1995). Better subset regression using the nonnegative garrote. *Technometrics*, 37(4):373–384.

Bromiley, P. (2003). Products and convolutions of gaussian probability density functions. *Tina-Vision Memo*, 3.

Burgers, G., Jan van Leeuwen, P., and Evensen, G. (1998). Analysis scheme in the ensemble kalman filter. *Monthly weather review*, 126(6):1719–1724.

Cariou, J.-P., Sauvage, L., Thobois, L., Gorju, G., Machta, M., Lea, G., and Duboué, M. (2011). Long range scanning pulsed coherent lidar for real time wind monitoring in the planetary boundary layer. *16th CLRC*.

Chan, P. (2011). Generation of an eddy dissipation rate map at the hong kong international airport based on doppler lidar data. *Journal of atmospheric and oceanic technology*, 28(1):37–49.

Chan, P., Shun, C., and Wu, K. (2006). Operational lidar-based system for automatic windshear alerting at the hong kong international airport. In *12th Conference on Aviation, Range, and Aerospace Meteorology*.

Chan, P. W. and Shao, A. M. (2007). Depiction of complex airflow near hong kong international airport using a doppler lidar with a two-dimensional wind retrieval technique. *Meteorologische Zeitschrift*, 16(5):491–504.

Chassaing, P. (2000). *Turbulence en mécanique des fluides*.

Chastaing, G. (2013). *Indices de Sobol généralisés pour variables dépendantes*. PhD thesis, Université de Grenoble.

Chastaing, G., Gamboa, F., and Prieur, C. (2015). Generalized sobol sensitivity indices for dependent variables: numerical methods. *Journal of Statistical Computation and Simulation*, 85(7):1306–1333.

Chastaing, G., Gamboa, F., Prieur, C., et al. (2012). Generalized hoeffding-sobol decomposition for dependent variables-application to sensitivity analysis. *Electronic Journal of Statistics*, 6:2420–2448.

Cohn, S. A. (1995). Radar measurements of turbulent eddy dissipation rate in the troposphere: A comparison of techniques. *Journal of Atmospheric and Oceanic Technology*, 12(1):85–95.

Cukier, R., Levine, H., and Shuler, K. (1978). Nonlinear sensitivity analysis of multiparameter model systems. *Journal of computational physics*, 26(1):1–42.

Da Veiga, S. (2015). Global sensitivity analysis with dependence measures. *Journal of Statistical Computation and Simulation*, 85(7):1283–1305.

Dabas, A. (1999). Semiempirical model for the reliability of a matched filter frequency estimator for doppler lidar. *Journal of Atmospheric and Oceanic Technology*, 16(1):19–28.

Dabas, A. M., Drobinski, P., and Flamant, P. H. (1998). Chirp-induced bias in velocity measurements by a coherent doppler co2 lidar. *Journal of Atmospheric and Oceanic Technology*, 15(2):407–415.

Dabas, A. M., Drobinski, P., and Flamant, P. H. (1999). Adaptive filters for frequency estimate of heterodyne doppler lidar returns: Recursive implementation and quality control. *Journal of Atmospheric and Oceanic Technology*, 16(3):361–372.

Dabas, A. M., Drobinski, P., and Flamant, P. H. (2000). Velocity biases of adaptive filter estimates in heterodyne doppler lidar measurements. *Journal of Atmospheric and Oceanic Technology*, 17(9):1189–1202.

Darbieu, C., Lohou, F., Lothon, M., Vilà-Guerau de Arellano, J., Couvreux, F., Durand, P., Pino, D., Patton, E. G., Nilsson, E., Blay-Carreras, E., et al. (2015). Turbulence vertical structure of the boundary layer during the afternoon transition. *Atmospheric Chemistry and Physics*, 15(17):10071–10086.

Das, S. and Durbin, P. (2005). A lagrangian stochastic model for dispersion in stratified turbulence. *Physics of Fluids (1994-present)*, 17(2):025109.

de Moor, G. (2006). *Couche limite atmospherique et turbulence*. Ministère des transports Direction de la météorologie.

Del Moral, P. (2004). *Feynman-Kac Formulae*. Springer.

Doucet, A., Godsill, S., and Andrieu, C. (2000). On sequential monte carlo sampling methods for bayesian filtering. *Statistics and computing*, 10(3):197–208.

DU, S. (1997). Universality of the lagrangian velocity structure function constant (c0) across different kinds of turbulence. *Boundary-Layer Meteorology*, 83(2):207–219.

Du, S., Sawford, B. L., Wilson, J. D., and Wilson, D. J. (1995). Estimation of the kolmogorov constant (c0) for the lagrangian structure function, using a second-order lagrangian model of grid turbulence. *Physics of Fluids (1994-present)*, 7(12):3083–3090.

Einstein, A. (1905). Un the movement of small particles suspended in statiunary liquids required by the molecular-kinetic theory 0f heat. *Ann. d. Phys*, 17:549–560.

Evensen, G. (1994). Sequential data assimilation with a nonlinear quasi-geostrophic model using monte carlo methods to forecast error statistics. *Journal of Geophysical Research: Oceans*, 99(C5):10143–10162.

Evensen, G. (2003). The ensemble kalman filter: Theoretical formulation and practical implementation. *Ocean dynamics*, 53(4):343–367.

Fong, W., Godsill, S. J., Doucet, A., and West, M. (2002). Monte carlo smoothing with application to audio signal enhancement. *Signal Processing, IEEE Transactions on*, 50(2):438–449.

Frehlich, R. (1997). Effects of wind turbulence on coherent doppler lidar performance. *Journal of Atmospheric and Oceanic Technology*, 14(1):54–75.

Frehlich, R. (2001). Estimation of velocity error for doppler lidar measurements. *Journal of Atmospheric and Oceanic Technology*, 18(10):1628–1639.

Frehlich, R. and Yadlowsky, M. (1994). Performance of mean-frequency estimators for doppler radar and lidar. *Journal of atmospheric and oceanic technology*, 11(5):1217–1230.

Frisch, U. (1995). *Turbulence: the legacy of AN Kolmogorov*. Cambridge university press.

Frisch, U., Sulem, P.-L., and Nelkin, M. (1978). A simple dynamical model of intermittent fully developed turbulence. *Journal of Fluid Mechanics*, 87(04):719–736.

Fruth, J., Roustant, O., and Kuhnt, S. (2011). Total interaction indices for the decomposition of functions with high complexity. *HAL: http://hal. archives-ouvertes. fr/hal-00631066/en*.

Fruth, J., Roustant, O., and Kuhnt, S. (2014). Total interaction index: A variance-based sensitivity index for second-order interaction screening. *Journal of Statistical Planning and Inference*, 147:212–223.

Fruth, J., Roustant, O., and Muehlenstaedt, T. (2013). The fanovagraph package: Visualization of interaction structures and construction of block-additive kriging models.

Furnival, G. M. and Wilson, R. W. (1974). Regressions by leaps and bounds. *Technometrics*, 16(4):499–511.

Gamboa, F., Janon, A., Klein, T., Lagnoux, A., et al. (2014). Sensitivity analysis for multidimensional and functional outputs. *Electronic Journal of Statistics*, 8(1):575–603.

Gardiner, C. (2009). *Stochastic methods*. Number ISBN 978-3-540-70712-7. Springer Berlin, 4th edition.

Germano, M. (1992). Turbulence: the filtering approach. *Journal of Fluid Mechanics*, 238:325–336.

Ginsbourger, D. (2009). *Multiples metamodeles pour l'approximation et l'optimisation de fonctions numeriques multivariables*. PhD thesis, Ecole Nationale Supérieure des Mines de Saint-Etienne.

Grund, C. J., Banta, R. M., George, J. L., Howell, J. N., Post, M. J., Richter, R. A., and Weickmann, A. M. (2001). High-resolution doppler lidar for boundary layer and cloud research. *Journal of Atmospheric and Oceanic Technology*, 18(3):376–393.

Gryning, S.-E., Mikkelsen, T., Baehr, C., Dabas, A., Gómez, P., O'Connor, E., Rottner, L., Sjöholm, M., Suomi, I., and Vasiljevi, N. (2017). *Renewable Energy Forecasting*. Number ISBN 978-0-08-100504-0. Elsevier.

Gustafsson, F., Gunnarsson, F., Bergman, N., Forssell, U., Jansson, J., Karlsson, R., and Nordlund, P.-J. (2002). Particle filters for positioning, navigation, and tracking. *Signal Processing, IEEE Transactions on*, 50(2):425–437.

Gustafsson, F. and Hendeby, G. (2012). Some relations between extended and unscented kalman filters. *IEEE Transactions on Signal Processing*, 60(2):545–555.

Hall, F. F., Huffaker, R. M., Hardesty, R. M., Jackson, M., Lawrence, T. R., Post, M. J., Richter, R., and Weber, B. (1984). Wind measurement accuracy of the noaa pulsed infrared doppler lidar. *Applied optics*, 23(15):2503–2506.

Hamby, D. (1994). A review of techniques for parameter sensitivity analysis of environmental models. *Environmental monitoring and assessment*, 32(2):135–154.

Hesterberg, T., Choi, N. H., Meier, L., Fraley, C., et al. (2008). Least angle and l1 penalized regression: A review. *Statistics Surveys*, 2:61–93.

Hinton, D. A., Charnock, J. K., and Bagwell, D. R. (2000). Design of an aircraft vortex spacing system for airport capacity improvement.

Holton, J. R. and Hakim, G. J. (2012). *An introduction to dynamic meteorology*, volume 88. Academic press.

Homma, T. and Saltelli, A. (1996). Importance measures in global sensitivity analysis of nonlinear models. *Reliability Engineering & System Safety*, 52(1):1–17.

Hull, T. E. and Dobell, A. R. (1962). Random number generators. *SIAM review*, 4(3):230–254.

Iooss, B. and Lemaître, P. (2015). A review on global sensitivity analysis methods. In *Uncertainty Management in Simulation-Optimization of Complex Systems*, pages 101–122. Springer.

Jacques, J. (2005). *Contributions à l'analyse de sensibilité et à l'analyse discriminante généralisée*. PhD thesis, Université Joseph-Fourier-Grenoble I.

Jacques, J., Lavergne, C., and Devictor, N. (2006). Sensitivity analysis in presence of model uncertainty and correlated inputs. *Reliability Engineering & System Safety*, 91(10):1126–1134.

Janon, A. (2012). *Réduction de dimension et Analyse de sensibilité*. PhD thesis, Université de Grenoble.

Janon, A., Klein, T., Lagnoux, A., Nodet, M., and Prieur, C. (2014). Asymptotic normality and efficiency of two sobol index estimators. *ESAIM: Probability and Statistics*, 18:342–364.

Javaheri, A., Lautier, D., and Galli, A. (2003). Filtering in finance. *Wilmott*, 3:67–83.

Jennings, S. (1988). The mean free path in air. *Journal of Aerosol Science*, 19(2):159–166.

Julier, S. J. (2002). The scaled unscented transformation. In *American Control Conference, 2002. Proceedings of the 2002*, volume 6, pages 4555–4559. IEEE.

Julier, S. J. and Uhlmann, J. K. (1997). A new extension of the kalman filter to nonlinear systems. In *Int. symp. aerospace/defense sensing, simul. and controls*, volume 3, pages 3–2. Orlando, FL.

Julier, S. J. and Uhlmann, J. K. (2004). Unscented filtering and nonlinear estimation. *Proceedings of the IEEE*, 92(3):401–422.

Kalman, R. E. et al. (1960). A new approach to linear filtering and prediction problems. *Journal of basic Engineering*, 82(1):35–45.

Kolmogorov, A. N. (1941). The local structure of turbulence in incompressible viscous fluid for very large reynolds numbers. In *Dokl. Akad. Nauk SSSR*, volume 30, pages 299–303.

Köpp, F., Schwiesow, R., and Werner, C. (1983). Remote measurements of boundary-layer wind profiles using a cw doppler lidar. *Journal of climate and applied meteorology*, 23(1):148–154.

Kouznetsov, R., Kramar, V., Beyrich, F., and Engelbart, D. (2004). Sodar-based estimation of tke and momentum flux profiles in the atmospheric boundary layer: Test of a parameterization model. *Meteorology and Atmospheric Physics*, 85(1):93–99.

Kurowicka, D. and Cooke, R. M. (2006). *Uncertainty analysis with high dimensional dependence modelling*. John Wiley & Sons.

Kusiak, A. and Song, Z. (2010). Design of wind farm layout for maximum wind energy capture. *Renewable Energy*, 35(3):685–694.

Launder, B. E. and Spalding, D. (1974). The numerical computation of turbulent flows. *Computer methods in applied mechanics and engineering*, 3(2):269–289.

Le Gland, F. (2009). Introduction au filtrage en temps discret-filtre de kalman, filtrage particulaire, modeles de markov cachés. *Ecole Nationale Supérieure de Techniques Avancées*.

Le Gland, F., Monbet, V., Tran, V.-D., et al. (2009). Large sample asymptotics for the ensemble kalman filter.

Lenschow, D., Mann, J., and Kristensen, L. (1994). How long is long enough when measuring fluxes and other turbulence statistics? *Journal of Atmospheric and Oceanic Technology*, 11(3):661–673.

Levin, M. (1965). Power spectrum parameter estimation. *IEEE Transactions on Information Theory*, 11(1):100–107.

Lin, D., Foster, D. P., and Ungar, L. H. (2010). A risk ratio comparison of l0 and l1 penalized regressions. *University of Pennsylvania, techical report*.

Lin, D., Pitler, E., Foster, D. P., and Ungar, L. H. (2008). In defense of l0. In *Workshop on Feature Selection,(ICML 2008)*.

Lopes, H. F. and Tsay, R. S. (2011). Particle filters and bayesian inference in financial econometrics. *Journal of Forecasting*, 30(1):168–209.

Lothon, M., Lohou, F., Pino, D., Couvreux, F., Pardyjak, E., Reuder, J., Vilà-Guerau de Arellano, J., Durand, P., Hartogensis, O., Legain, D., et al. (2014). The bllast field experiment: Boundary-layer late afternoon and sunset turbulence. *Atmospheric chemistry and physics*, 14(20):10931–10960.

Maalouf, C. B. (2010). *Etude des phénomenes tourbillonnaires dans le sillage éolien*. PhD thesis, Arts et Métiers ParisTech.

Mahmoud, M. S. and Khalid, H. M. (2013). Distributed kalman filtering: a bibliographic review. *IET Control Theory & Applications*, 7(4):483–501.

Malardel, S. (2005). *Fondamentaux de Météorologie)*. Cépaduès Éditions. ISBN 2.85428.851.3.

Mandel, J., Cobb, L., and Beezley, J. D. (2011). On the convergence of the ensemble kalman filter. *Applications of Mathematics*, 56(6):533–541.

Marrel, A., Iooss, B., Da Veiga, S., and Ribatet, M. (2012). Global sensitivity analysis of stochastic computer models with joint metamodels. *Statistics and Computing*, 22(3):833–847.

Marrel, A., Iooss, B., Laurent, B., and Roustant, O. (2009). Calculations of sobol indices for the gaussian process metamodel. *Reliability Engineering & System Safety*, 94(3):742–751.

Marsaglia, G. et al. (2003). Xorshift rngs. *Journal of Statistical Software*, 8(14):1–6.

Maskell, S. and Gordon, N. (2001). A tutorial on particle filters for on-line nonlinear/non-gaussian bayesian tracking. In *Target tracking: algorithms and applications (Ref. No. 2001/174), IEE*, pages 2–1. IET.

Meneveau, C. and Sreenivasan, K. (1987). Simple multifractal cascade model for fully developed turbulence. *Physical review letters*, 59(13):1424.

Menzies, R. T. and Hardesty, R. M. (1989). Coherent doppler lidar for measurements of wind fields. *Proceedings of the IEEE*, 77(3):449–462.

Miller, S. and Childers, D. (2012). *Probability and random processes: With applications to signal processing and communications*. Academic Press.

Monin, A. S. and Yaglom, A. M. (1963). On the laws of small-scale turbulent flow of liquids and gases. *Russian Mathematical Surveys*, 18(5):89–109.

Mordant, N., Metz, P., Michel, O., and Pinton, J.-F. (2001). Measurement of lagrangian velocity in fully developed turbulence. *Physical Review Letters*, 87(21):214501.

Morris, M. D. (1991). Factorial sampling plans for preliminary computational experiments. *Technometrics*, 33(2):161–174.

Natarajan, B. K. (1995). Sparse approximate solutions to linear systems. *SIAM journal on computing*, 24(2):227–234.

Neiman, P. J., Hardesty, R., Shapiro, M., and Cupp, R. (1988). Doppler lidar observations of a downslope windstorm. *Monthly weather review*, 116(11):2265–2275.

O'Connor, E. J., Illingworth, A. J., Brooks, I. M., Westbrook, C. D., Hogan, R. J., Davies, F., and Brooks, B. J. (2010). A method for estimating the turbulent kinetic energy dissipation rate from a vertically pointing doppler lidar, and independent evaluation from balloon-borne in situ measurements. *Journal of atmospheric and oceanic technology*, 27(10):1652–1664.

Øksendal, B. (2013). *Stochastic differential equations: an introduction with applications*. Number ISBN 3-540-60243-7. Springer Science & Business Media, 4th edition.

Owen, A. B. (2013). Better estimation of small sobol' sensitivity indices. *ACM Transactions on Modeling and Computer Simulation (TOMACS)*, 23(2):11.

Pedregosa, F., Varoquaux, G., Gramfort, A., Michel, V., Thirion, B., Grisel, O., Blondel, M., Prettenhofer, P., Weiss, R., Dubourg, V., Vanderplas, J., Passos, A., Cournapeau, D., Brucher, M., Perrot, M., and Duchesnay, E. (2011). Scikit-learn: Machine learning in Python. *Journal of Machine Learning Research*, 12:2825–2830.

Pham, D. T. (2001). Stochastic methods for sequential data assimilation in strongly nonlinear systems. *Monthly weather review*, 129(5):1194–1207.

Pichugina, Y. L., Banta, R. M., Brewer, W. A., Sandberg, S. P., and Hardesty, R. M. (2011). Doppler lidar-based wind-profile measurement system for offshore wind-energy and other marine boundary layer applications. *Journal of Applied Meteorology and Climatology*, 51(2):327–349.

Pichugina, Y. L., Tucker, S. C., Banta, R. M., Brewer, W. A., Kelley, N. D., Jonkman, B. J., and Newsom, R. K. (2008). Horizontal-velocity and variance measurements in the stable boundary layer using doppler lidar: Sensitivity to averaging procedures. *Journal of Atmospheric and Oceanic Technology*, 25(8):1307–1327.

Pope, S. (1985). Pdf methods for turbulent reactive flows. *Progress in Energy and Combustion Science*, 11(2):119–192.

Pope, S. (1994). Lagrangian pdf methods for turbulent flows. *Annual review of fluid mechanics*, 26(1):23–63.

Pope, S. B. (2000). *Turbulent flows*. Cambridge university press.

Priestley, M. B. (1981). *Spectral analysis and time series*. Academic press.

Reif, K., Gunther, S., Yaz, E., and Unbehauen, R. (1999). Stochastic stability of the discrete-time extended kalman filter. *IEEE Transactions on Automatic control*, 44(4):714–728.

Rieutord, T., Baehr, C., and Rottner, L. (2016). Doppler lidar based reconstruction for fast estimation of turbulence: contribution and validation. In *18th International Symposium for the Advancement of Boundary-Layer Remote Sensing*.

Rotach, M. W. (2001). Simulation of urban-scale dispersion using a lagrangian stochastic dispersion model. *Boundary-Layer Meteorology*, 99(3):379–410.

Rottner, L. (2015). *Reconstruction de l'atmosphère turbulente à patir d'un lidar Doppler 3D et étude du couplage avec Meso-NH.* PhD thesis, Université Paul Sabatier-Toulouse III.

Rottner, L. and Baehr, C. (2014). 3D wind reconstruction and turbulence estimation in the boundary layer from doppler lidar measurements using particle method. http://adsabs.harvard.edu/abs/2014AGUFMNG23B3806R.

Rottner, L. and Baehr, C. (2017). Stochastic method for turbulence estimation from doppler lidar measurements. *Atmospheric Measurement Techniques*. submitted.

Rottner, L., Baehr, C., Couvreux, F., Canut, G., and Rieutord, T. (2017). A new downscaling method for sub-grid turbulence modeling. *Atmospheric Chemistry and Physics*, 17(11):6531–6546.

Rottner, L., Suomi, I., Rieutord, T., Baehr, C., and Gryning, S.-E. (2016). Real time turbulence and wind gust estimation from wind lidar observations using the turbulence reconstruction method. In *18th International Symposium for the Advancement of Boundary-Layer Remote Sensing*.

Rousseau, A., Bernardin, F., Bossy, M., Salameh, T., and Drobinski, P. (2007). Stochastic particle method applied to local wind simulation. In *ICCEP'07-International Conference for Clean Electrical Power*, pages 526–528.

Roustant, O., Ginsbourger, D., and Deville, Y. (2012). Dicekriging, diceoptim: Two r packages for the analysis of computer experiments by kriging-based metamodeling and optimization.

Rubin, D. B. (1976). Inference and missing data. *Biometrika*, 63(3):581–592.

Saltelli, A. (2002a). Making best use of model evaluations to compute sensitivity indices. *Computer Physics Communications*, 145(2):280–297.

Saltelli, A. (2002b). Sensitivity analysis for importance assessment. *Risk Analysis*, 22(3):579–590.

Saltelli, A. and Annoni, P. (2010). How to avoid a perfunctory sensitivity analysis. *Environmental Modelling & Software*, 25(12):1508–1517.

Saltelli, A., Annoni, P., Azzini, I., Campolongo, F., Ratto, M., and Tarantola, S. (2010). Variance based sensitivity analysis of model output. design and estimator for the total sensitivity index. *Computer Physics Communications*, 181(2):259–270.

Saltelli, A., Tarantola, S., and Campolongo, F. (2000). Sensitivity analysis as an ingredient of modeling. *Statistical Science*, pages 377–395.

Saporta, G. (2006). *Probabilités, analyse des données et statistique*. Editions Technip.

Sathe, A. and Mann, J. (2013). A review of turbulence measurements using ground-based wind lidars. *Atmospheric Measurement Techniques*, 6.

Schafer, J. L. and Graham, J. W. (2002). Missing data: our view of the state of the art. *Psychological methods*, 7(2):147.

Schlipf, D. (2014). Lidar assisted control of wind turbines. *Struttgart Wind Energy. Universitat Stuttgart*.

Schmid, H. P. (2002). Footprint modeling for vegetation atmosphere exchange studies: a review and perspective. *Agricultural and Forest Meteorology*, 113(1):159–183.

Smalikho, I., Köpp, F., and Rahm, S. (2005). Measurement of atmospheric turbulence by 2-μ m doppler lidar. *Journal of Atmospheric and Oceanic Technology*, 22(11):1733–1747.

Smith, A., Doucet, A., de Freitas, N., and Gordon, N. (2013). *Sequential Monte Carlo methods in practice*. Springer Science & Business Media.

Snyder, C., Bengtsson, T., Bickel, P., and Anderson, J. (2008). Obstacles to high-dimensional particle filtering. *Monthly Weather Review*, 136(12):4629–4640.

Sobol, I. M. (1976). Uniformly distributed sequences with an additional uniform property. *USSR Computational Mathematics and Mathematical Physics*, 16(5):236–242.

Sobol', I. M. (1990). On sensitivity estimation for nonlinear mathematical models. *Matematicheskoe Modelirovanie*, 2(1):112–118.

Sobol, I. M. (1993). Sensitivity estimates for nonlinear mathematical models. *Mathematical Modelling and Computational Experiments*, 1(4):407–414.

Sobol, I. M. (2001). Global sensitivity indices for nonlinear mathematical models and their monte carlo estimates. *Mathematics and computers in simulation*, 55(1):271–280.

Sommerfeld, M. (2001). Validation of a stochastic lagrangian modelling approach for inter-particle collisions in homogeneous isotropic turbulence. *International Journal of Multiphase Flow*, 27(10):1829–1858.

Stull, R. B. (1988). *An introduction to boundary layer meteorology*, volume 13. Springer.

Sudret, B. (2008). Global sensitivity analysis using polynomial chaos expansions. *Reliability Engineering & System Safety*, 93(7):964–979.

Sun, X., Huang, D., and Wu, G. (2012). The current state of offshore wind energy technology development. *Energy*, 41(1):298–312.

Suzat, F., Baehr, C., and Dabas, A. (2011). A fast atmospheric turbulent parameters estimation using particle filtering. application to lidar observations. In *Journal of Physics: Conference Series*, volume 318, page 072019. IOP Publishing.

Thomson, D. and Wilson, J. (2013). History of lagrangian stochastic models for turbulent dispersion. *Lagrangian Modeling of the Atmosphere*, pages 19–36.

Tibshirani, R. (1996). Regression shrinkage and selection via the lasso. *Journal of the Royal Statistical Society. Series B (Methodological)*, pages 267–288.

Tucker, S. C., Senff, C. J., Weickmann, A. M., Brewer, W. A., Banta, R. M., Sandberg, S. P., Law, D. C., and Hardesty, R. M. (2009). Doppler lidar estimation of mixing height using turbulence, shear, and aerosol profiles. *Journal of Atmospheric and Oceanic Technology*, 26(4):673–688.

van de Geer, S. A. (2016). *Estimation and testing under sparsity*. Springer.

van Leeuwen, P. J. (2003). A variance-minimizing filter for large-scale applications. *Monthly Weather Review*, 131(9):2071–2084.

van Leeuwen, P. J. (2009). Particle filtering in geophysical systems. *Monthly Weather Review*, 137(12).

Welch, G. and Bishop, G. (1995). An introduction to the kalman filter.

Wharton, S. and Lundquist, J. K. (2012). Atmospheric stability affects wind turbine power collection. *Environmental Research Letters*, 7(1):014005.

Wilson, J. D. and Sawford, B. L. (1996). Review of lagrangian stochastic models for trajectories in the turbulent atmosphere. *Boundary-layer meteorology*, 78(1-2):191–210.

Yakhot, V. (2008). Lagrangian structure functions in turbulence: Scaling exponents and universality. *arXiv preprint arXiv:0810.2955*.

List of figures

List of tables

List of definitions

List of theorems

Sensitivity analysis of a filtering algorithm for wind lidar measurements

Thomas Rieutord

Centre National de Recherches Météorologiques (UMR 3589)
Météo-France, CNRS
42 avenue Gaspard Coriolis, Toulouse, France.

Abstract — Wind energy industry and airport safety are in need of atmospheric observations. Remote sensors, such as lidars, are well proven and common technology to provide wind measurements in the first hundreds of meters of altitude. However, acquisition abilities of lidars are polluted by measurement noise. Using non-linear filtering techniques, we took part at the development of an algorithm improving wind and turbulence estimations. The process is based on a representation of the atmosphere with fluid particles. It uses a stochastic Lagrangian model of turbulence and a genetic selection filtering technique. Its efficiency depends of the setting of various parameters. Their values were fixed experimentally during the development phase. But their influence has never been assessed. This work addresses this question with a variance-based sensitivity analysis. New estimators of Sobol indices, using penalized regression have been tested. These estimators ensure the lowest Sobol indices automatically go to zero so the overall interpretation is simplified. The sensitivity analysis allows to reduce the system from 5 outputs and 9 inputs to 3 inputs (number of particles, real observation noise, observation noise given to the filter) and 2 outputs (wind spectrum slope, root-mean-squared error on wind). With this reduced system we determined a procedure to correctly set the most important parameters. The observation noise given to the filter is well set when the wind spectrum slope has the expected value of -5/3. Once it is set correctly, the error on wind is minimum and its expression is known.

Keywords — *sensitivity analysis, non-linear filtrering, Doppler lidar, turbulence*

PhD delivered by Toulouse INP in November 2017

PhD supervisors – Fabrice Gamboa, Alain Dabas
Speciality – Applied mathematics

Analyse de sensibilité d'un algorithme de filtrage pour les mesures de vent par lidar

Thomas Rieutord

Centre National de Recherches Météorologiques (UMR 3589)
Météo-France, CNRS
42 avenue Gaspard Coriolis, Toulouse, France.

Résumé — L'industrie éolienne et l'aéronautique ont des besoins importants en matière de mesure de vent dans les premières centaines de mètres de l'atmosphère. Les lidars sont des instruments répandus et éprouvés pour ce type de mesure. Cependant, leurs qualités d'acquisition sont atténuées par un bruit de mesure systématique. En utilisant des techniques sur le filtrage non-linéaire nous avons participé au développement d'un algorithme qui améliore l'estimation du vent et de la turbulence. Cet algorithme est basé sur une représentation de l'atmosphère par des particules fluides. Il utilise un modèle lagrangien stochastique de turbulence et un filtrage par sélection génétique. Son efficacité dépend du réglage de certains paramètres, fixés à une valeur acceptable à l'issue de la phase de développement. Mais l'influence de ces paramètres n'a jamais été étudiée. Ce travail de thèse répond à cette question par une analyse de sensibilité basée sur la décomposition de variance. De nouveaux estimateurs pour les indices de Sobol, utilisant des régression pénalisées, ont été testés. Ces estimateurs mettent les indices de Sobol les plus petits automatiquement à zéro pour faciliter l'interprétation globale. L'analyse de sensibilité permet de réduire le système à 9 entrées et 5 sorties à un système de 3 entrées (le nombre de particules, le bruit d'observation réel et le bruit d'observation donné au filtre) et 2 sorties (la pente du spectre de vent et l'erreur sur le vent). Grâce à ce système réduit, nous mettons en évidence une méthode de réglage des paramètres d'entrée les plus importants. Le bruit d'observation donné au filtre est bien réglé lorsque la pente du spectre est à la valeur cible de -5/3. Une fois ce bruit réglé, l'erreur sur le vent est minimale avec une expression connue.

Mots clés — *analyse de sensibilité, filtrage non-linéaire, lidar Doppler, turbulence.*

Doctorat délivré par Toulouse INP en novembre 2017

Directeurs de thèse – Fabrice Gamboa, Alain Dabas
Discipline – Mathématiques appliquées